THE UNIVERSITY *of* EDINBURGH

Determining the role of mononuclear phagocyte cell subsets in scrapie transmission from the skin

Gwennaëlle CLJJ Wathne

A thesis submitted in partial fulfilment of the requirements of the University of Edinburgh for the degree of Doctor of Philosophy.

The programme of research was carried out at the Neurobiology Division
The Roslin Institute and R(D)SVS, University of Edinburgh.

December 2011

Declaration

I declare that the work presented in this thesis is my own, except where stated. All experiments were designed by myself in collaboration with my supervisors Professor John Hopkins and Dr Neil Mabbott. No part of this work has been or will be submitted for any other degree or professional qualification.

Gwennaëlle CLJJ Wathne

December 2011

TABLE OF CONTENTS

ACKNOWLEDGEMENTS

I would like to express my thanks to my supervisors **Dr Neil Mabbott** and **Professor John Hopkins**, for their help and guidance throughout this PhD, for giving me the opportunity to explore my ideas, the possibility to visit foreign labs, and present my work at international conferences. I also want to thank **Neil** for always having his 'door open'.

I would like to thank the following people for provision of mouse lines, information or advice, and welcoming me to their laboratories:
Dr Steffen Jung (Weizmann Institute of Science, Rehovot, Israel) for provision of the CD11c-GFP-DTR mouse line
Dr Bernard Malissen (INSERM-CNRS Université de la Méditerranée, Marseille, France) for making the langerin-EGFP-DTR mouse line available through **EMMA**, and useful discussions at exotic conference locations
Dr Adrian Kissenpfennig (Queen's University, Belfast) for advice on epidermal sheet separation and genotyping
Dr Chiara Zurzolo (Institut Pasteur, Paris), for welcoming me to her lab, and **Dr Duncan Browman** and **Dr Anna Caputo** for teaching me the art of fluorescently tagging PrP
Dr Keisuke Nagao (Keio University, Tokyo, Japan) for taking the time to answer my questions about mouse ears and about Japan, and for allowing me to visit his laboratory
Dr Akiharo Kubo (Keio University, Tokyo, Japan) for showing me how to separate epdidermal sheets for tight junction staining
Dr Liv Eidsmo and **Dr Robert Wallin** (Karolinska Institutt, Stockholm, Sweden) for hosting my visit to Stockholm, to learn more about skin-related matters
Dr Andy Gill for helping me carry out fluorescent tagging back in Edinburgh, and for being a sounding board for all things Western blot related
Dr Pip Beard, for her sheer enthusiasm and helping me to determine the pathology of scarification, and for providing the best quote ever about science
Robert Flemming for his help and assistance with microscopy-related matters
Christine Farquhar for provision of the 1B3 antibody
Dr Mikio Furuse (Kobe University, Japan) for provision of the anti-ZO-1 antibody

I would like to thank all the animal house staff for the patience, help, and support without which I would not have been able to complete this project. Special thanks go to **Shona Faichney**, **Lorraine Gray**, and **Fraser Laing** for monitoring of infected and unifected animals and numerous culls, at various stages of the project, **Mary Brady** and **Irene McConnell** for numerous scarifications, and **Simon Cumming** for bone marrow transfers, DTX injections, and culls.

I would like to thank **Gillian McGregor**, **Sandra Mack**, **Aileen Boyle**, and **Anne Coghill**, for, vacuolation scoring, answering my questions and assisting with histology-related matters, and helping with my strange requests.

I would like to thank **Alison Downing** and **ARK-Genomics** for helping me with the RNA work and producing the microarrays.

Thank you to **Dr Darren Shaw** for guidance with statistical analysis.

I would like to thank everyone in the Immunopathogenesis group and the whole Neurobiology Division for their help and support throughout my time in the division. Special thanks go to:
Dr Karen Brown for having time to answer questions, our lab discussions, helping me with irradiations, and introducing me to the field of prions when I first started
Dr Laura McCulloch for being my PhD buddy, and letting me be the crazy tour guide
Professor Nora Hunter for taking the time to read parts of my thesis as a non-immunologist
Dawn Drummond for her wise words, always listening, and most importantly for having a smile for me at 7 AM in the darkest of winter
Charmaine Love for volunteering to proofread chapters of this thesis

I would also like to express my thanks to everyone else at the Roslin Institute, be it during those long waits at the bus stop, in the lab, or cracking a joke in the corridor. Thank you to all who have helped along the way, especially **Stores,** and **Lily Gray** for her permanent smile and cheery greetings. Thank you also to:
Liz Archibald, for always being available to listen to all things non-PhD related but that sometimes make completing the PhD that much more difficult
Tricia Hart, for always having a couple of minutes in her busy schedule and her willingness to point me in the right direction
Joni Macdonald for our insightful discussions in the car, in the gym, anywhere
Clare Pridans, for cheering up my bus stop waits, introducing me to the art of macaroons and fermentation, Happy Friday!

Thank you to **Jaclyn Schmidt**, my personal point of contact to several hunters in Alberta, and for her friends for taking the time to answer my question about gloves

Kristen Cairns, what would I have done without those mittens? Thank you for everything.

All my other friends for helping me train for those crazy challenges, listening, giving advice, and just being my friends.

To all my **family** for all their help in support during the hardest of times, made even harder during a PhD. For always being there at the other end of the phone or to meet me at the airport, and always having arms and doors open. Tusen hjertelig takk, jeg føler meg altid hjemme, et puis un gros merci!

Og pappa, synd du aldri fikk sett alle de fine bildene av cellene som jeg har ‘malt’.

Et puis, last but not least, mon PDC, tu sais tout ce que tu as fait pour moi.

ABBREVIATIONS

APC	antigen presenting cell
BSA	bovine serum albumin
BSE	bovine spongiform encephalopathy
CD	cluster of differentiation
CD40L	CD40 ligand
CJD	Creutzfeldt-Jacob Disease
CNS	central nervous system
CWD	chronic wasting disease
DC	dendritic cell
ddH_2O	double distilled water
dH_2O	distilled water
d.p.i.	days post infection
DTR	Diphtheria toxin receptor
DTX	Diphtheria toxin
EGFP	enhanced green fluorescent protein
FCS	foetal calf serum
FDC	follicular dendritic cell
GFP	green fluorescent protein
Hbegf	heparin binding EGF-like growth factor
H & E	haematoxylin and eosin
i.c.	intra-cerebral
i.p.	intra-peritoneal
iLN	inguinal lymph node
hr	hours
Kbp	kilobase pairs
kDa	kiloDaltons
LC	Langerhans cell
LN	lymph node
LRS	lymphoreticular system
mAb	monoclonal antibody
min	minutes
MNP	mononuclear phagocyte
NB	normal brain
PAT	perinodal adipose tissue
pAb	polyclonal antibody
PB	phosphate buffer
PBS	phosphate buffered saline
PET	paraffin embedded tissue
PFA	paraformaldehyde
PK	proteinase K
pLN	popliteal lymph node
PLP	periodate-lysine-paraformaldehyde
PMCA	protein misfolding cyclic amplification
PMN	polymorphonuclear leukocytes
PP	Peyer's patch
Prnp	murine PrP gene

PrP	prion protein
PrP^{c}	cellular (normal) form of the prion protein
PrP^{d}	disease-associated form of the prion protein
PrP^{Sc}	scrapie-specific form of the prion protein
RT	room temperature
s	seconds
SAF	scrapie associated fibril
SCS	subcapsular sinus
SEM	standard error of the mean
TME	transmissible mink encephalopathy
TSE	transmissible spongiform encephalopathy
vCJD	variant Creutzfeldt-Jacob disease
QUIC	quaking-induced conversion

Abstract

Transmissible spongiform encephalopathies (TSEs), or prion diseases, are fatal neurodegenerative diseases that affect several species, such as scrapie in sheep or goats and CJD in humans. In several species, neurological disease is preceded by TSE agent accumulation in lymphoid tissues prior to neuroinvasion. While oral transmission is considered the most common route for scrapie, transmission can also occur through lesions to the skin or mucosa, for example in the mouth or gastrointestinal tract due to rough feed, or birth associated skin damage. Scrapie has also been experimentally transmitted through skin scarification in mice. Following scrapie infection via skin scarification, PrP^{Sc} accumulates in the draining lymph node (LN) before spreading to other organs in the lymphoreticular system. It is not yet known by what means the scrapie agent is transported from the skin to the draining LN. Dendritic cells (DCs) in the skin have been found to transport viruses, such as HIV or Dengue, from the skin, thereby raising the question whether DCs or Langerhans cells (LCs), located within the epidermis, play a role in the uptake and transport of the TSE agent from the skin to the draining LN.

CD11c is a cell surface marker traditionally used to identify or isolate DCs from other cell types. Mice and rats are naturally resistant to Diphtheria toxin (DTX). A transgenic mouse line was created where the Diphtheria toxin receptor (DTR) was expressed on $CD11c^+$ cells. The presence of this receptor on $CD11c^+$ cells allowed for the temporary conditional depletion of $CD11c^+$ cells following a single injection of DTX. The cells repopulate the tissues within a time frame specific to the tissues the cells are located in. These mice were used to determine whether the absence of $CD11c^+$ cells at the time of scrapie infection via the skin had an effect on the early accumulation of PrP^{Sc} within the lymphoid tissues and on disease progression. Immunohistochemical analysis demonstrated that early PrP^{Sc} accumulation in the draining LNs was delayed following depletion of $CD11c^+$ cells, indicating that their potential role in the transport of the scrapie agent from the skin. Scrapie incubation period was not affected by the absence of the $CD11c^+$ cells at the time of infection.

Recent findings show that CD11c is not exclusive to DCs and is also expressed on macrophage populations. Following DTX-mediated depletion, DCs repopulate the tissues much faster than $CD11c^+$ macrophages. Scrapie infection was carried out in the skin in DTX treated mice after DCs had repopulated the tissues but before macrophage numbers had returned, to determine whether macrophages rather than DCs played a role in the early accumulation of PrP^{Sc} in the draining LNs. No differences in PrP^{Sc} accumulation were observed in mice depleted of macrophages compared to controls and there was no effect on disease incubation period.

Another transgenic mouse line was used, where DTX expression on $langerin^+$ cells (LCs and $langerin^+$ DCs in the dermis), allowed for their temporary depletion through DTX treatment. Following $langerin^+$ cell depletion, increased PrP^{Sc} accumulation was observed in the draining LNs 7 weeks post infection, but did not affect the incubation period of disease. These results indicate that the absence of LCs somehow accelerated PrP^{Sc} accumulation, and that LCs might play a preventative role in early stages after infection.

Histopathological analysis was used to complement microarray studies aimed to determine what immune responses were associated with scarification and DTX-mediated depletion of cells within the skin and whether these responses might be linked to disease transmission.

DCs and LCs in the skin appear to play different roles in the early stages following scrapie infection via the skin, but the lack of effect on incubation period does not rule out the involvement of other cell types or cell-free mechanisms of scrapie agent spread from the skin.

1

INTRODUCTION

1.1. Transmissible spongiform encephalopathies (TSEs)

1.1.1. What are TSEs?

The TSEs are a group of fatal neurodegenerative diseases that affect both humans and animals. These diseases can occur under several different forms: spontaneous, genetic, or acquired through various routes of exposure. Examples of the main disease forms and the species they affect are listed in Table 1.1. Some forms of disease, such as scrapie, have been around for centuries (McGowan, 1922), while other forms such as bovine spongiform encephalopathy (BSE) (Taylor, 1993; Taylor and Woodgate, 1997) emerged in the 1980s, and have caused the emergence of vCJD (Bruce *et al.*, 1997; Will *et al.*, 1996), as well as being linked to the emergence of feline spongiform encephalopathy (FSE) in non-domestic cats (Sigurdson and Miller, 2003). Chronic wasting disease (CWD) is a growing problem in North America, as it spreads between farmed as well as wild deer, elk and moose (Angers *et al.*, 2009; Keane *et al.*, 2009; Keane *et al.*, 2008; Mathiason *et al.*, 2006; Sigurdson *et al.*, 1999; Spraker *et al.*, 2004; Spraker *et al.*, 2009). TSE disease is characteristically associated with vacuolation in the brain (spongiform pathology), neuronal loss, glial cell activation and amyloid deposits of the disease-associated form of prion protein (PrP), and lead to neurodegeneration and death.

Despite being a neurodegenerative disease, natural transmission often occurs via the periphery before spreading to the central nervous system (CNS). In some experimental and natural TSEs, such as natural sheep scrapie, disease is characterised by early TSE agent accumulation in the peripheral lymphoid system (Brown *et al.*, 2000; Bruce *et al.*, 2000). It is worth noting that even within a single species such as sheep, the strain of the TSE agent or the *PRNP* genotype (which encodes the cellular

Table 1.1. TSE diseases.

TSE Disease	Affected Species	Route of Transmission
Iatrogenic Creutzfeldt-Jacob Disease	Human	Accidental medical exposure to CJD-contaminated tissues or tissue products
Sporadic Creutzfeldt-Jacob Disease (sCJD)	Human	Unknown. Somatic mutation or spontaneous conversion of PrP^{c} to PrP^{Sc}?
Variant Creutzfeldt-Jacob Disease (vCJD)	Human	Ingestion of BSE-contaminated food or blood transfusion from CJD-infected blood donor
Familial Creutzfeldt-Jacob Disease	Human	Germline mutations of the *PRNP* gene
Gerstmann-Straussler-Scheinker syndrome	Human	Germline mutations of the *PRNP* gene
Kuru	Human	Ritualistic cannibalism
Fatal familial insomnia	Human	Germline mutations of the *PRNP* gene
Bovine Spongiform encephalopathy	Cattle	Ingested feed
Scrapie	Sheep, Goats	Acquired, ingestion, horizontal transmission, vertical transmission unclear
Chronic wasting disease	Deer, Elk, Moose	Acquired, ingestion, horizontal transmission, vertical transmission unclear
Transmissible mink encephalopathy	Mink	Acquired (ingestion) source unknown
Feline spongiform encephalopathy	Domestic and zoological cats	Ingestion of BSE-contaminated food
Exotic ungulate encephalopathy	Nyala, Kudu,	Ingestion of BSE-contaminated food

prion protein, PrP^{c}) of the animal can significantly influence disease pathogenesis (Andréoletti *et al.*, 2000; Heggebø *et al.*, 2002), and some sheep genotypes are completely devoid of lymphoreticular system (LRS) involvement (Schreuder *et al.*, 1998). Other forms of the disease, such as BSE in cattle, appear not to be associated with early TSE agent replication in the peripheral lymphoid tissue of cattle (Somerville *et al.*, 1997), but PrP^{Sc} and/or infectivity have been detected in the gut of

experimentally and naturally infected cattle (Buschmann and Groschup, 2005; Hoffmann *et al.*, 2011; Iwata *et al.*, 2006; Terry *et al.*, 2003; Wells *et al.*, 1994). This difference between TSE agent strain targeting in host tissues is interesting since when BSE is transmitted to humans, agent accumulation in the lymphoid tissues is a key feature of variant Creutzfeldt-Jakob disease (Foster *et al.*, 2001; Hill *et al.*, 1997).

1.1.2. PrP^c

PrP is a 253 amino acid (Riesner, 2003) glycolipid-anchored surface protein (Bolton *et al.*, 1985; Shyng *et al.*, 1995). PrP arises in two different forms: the host encoded protease sensitive form, PrP^c, and the relatively protease resistant, disease-associated isoform, PrP^d, or PrP^{Sc} found in tissues of TSE-affected hosts (Lawson *et al.*, 2005). The normal cellular form of PrP, PrP^c, has a mainly α-helical structure (Pan *et al.*, 1993) and is protease sensitive. PrP^c is a 30-35 kDa glycoprotein which is anchored to the outer layer of the cell membrane through a glycosylphosphatidylinositol (GPI) anchor (Stahl *et al.*, 1987).

The replication of TSE agents by host cells is critically dependent upon the expression of the host encoded, cellular isoform of the prion protein, PrP^c (Büeler *et al.*, 1993). PrP^c is endogenous and is expressed on a large range of different cell types in many organs throughout the body (Brown *et al.*, 1999; Horiuchi *et al.*, 1995; Mabbott *et al.*, 1998). Some examples are Langerhans cells (LCs) and keratinocytes in the skin (Sugaya *et al.*, 2002), dendritic cells (DCs) (Burthem *et al.*, 2001), B lymphocytes (Li *et al.*, 2001), T lymphocytes (Mabbott *et al.*, 1997), FDCs (Brown *et al.*, 1999), or neurons (Kretzschmar *et al.*, 1986).

The protein has been associated with normal physiological functions of the nervous system (Martins *et al.*, 2010), including amongst other things, normal synaptic function, memory and maintenance of circadian rhythms and sleep patterns (Mabbott *et al.*, 1998). Although early studies determined that PrP^c deficient mice do not appear to be adversely affected by the absence of the protein (Bueler *et al.*, 1992), are not wholly immunodeficient (Isaacs *et al.*, 2006), and are developmentally normal (Manson *et al.*, 1994), more recent studies have used PrP-deficient mice to determine, for example, that PrP^c is associated with suppression of cognitive function caused by brain-derived amyloid-β in Alzheimer's disease (Gimbel *et al.*, 2010), as well as blocking pain receptors (Gadotti and Zamponi, 2011). The protein's protective function is also associated with epilepsy (Martins *et al.*, 2010; Walz *et al.*, 1999), and Martins *et al* present the view that as well as playing a role in 'loss-of-function components' in prion diseases, PrP^c might also be a component in the pathogenesis of other neurodegenerative disease (Martins *et al.*, 2010). In addition there has been some speculation about the function of PrP^c in the immune system. For example, PrP^c may provide cell survival signals in certain circumstances such as rapid memory cell expansion (Isaacs *et al.*, 2006), and T lymphocyte activation (Li *et al.*, 2001; Mabbott *et al.*, 1997; Mattei *et al.*, 2004).

1.1.3. Nature of the TSE agent

Many different hypotheses were made about the causal agent of TSEs. Prusiner coined the term "Prion", for *pro*teinaceous *in*fectious particles (Prusiner, 1982) arguing that the scrapie causing agent was of protein rather than viral origin. In the

past, TSEs have been referred to as a slow virus (Gajdusek, 1967). Some speculation existed about whether nucleic acids were also a part of the infectious agent, although experiments conducted to determine the structure and composition of the infectious agent had found it to be resistant to inactivation by most procedures that inactivate nucleic acids (Prusiner, 1982). Bolton *et al*, identified a protein in the brains of scrapie-infected animals which copurified with the infectious scrapie agent. This protein was absent in brains of uninoculated hamsters (Bolton *et al.*, 1982). It was later determined that this protein, which they designated as Prion protein, PrP, was, in fact, a component of the scrapie prion (McKinley *et al.*, 1983). Quaking-induced conversion (QUIC) (Atarashi *et al.*, 2008) and protein misfolding cyclic amplification (PMCA) (Saborio *et al.*, 2001) are methods which allow for the amplification of protein, in a similar manner to DNA amplification by polymerase chain reaction (PCR) (Soto *et al.*, 2002). These techniques have enabled propagation of infectious PrP using infected brain-derived or recombinant PrP. As well as studying PrP conversion, these techniques have allowed for the detection of infectious TSE agents in various tissues at dilutions previously undetected by other methods. This had only been carried out in the presence of additional cofactors such as nucleic acids and lipids, but recently, infectious prions were generated by PMCA from recombinant hamster prion protein without any apparent cofactors (other than buffer salts and detergent) (Kim *et al.*, 2010). The results generated by using these two techniques lend further weight to the argument of a protein hypothesis in disease transmission (Kim *et al.*, 2010).

TSE diseases are characteristically associated with the accumulation of insoluble aggregates of the disease-specific, abnormal form of PrP within the CNS and, in some cases, within the LRS. This abnormal form of the protein is a relatively protease resistant, predominantly β-pleated sheet isoform, termed PrP^{Sc} (Pan *et al.*, 1993). Fourier transform infrared microspectroscopy was used to study protein conformational changes within the dorsal root ganglia at various stage of disease development. This allowed for *in situ* observation of the increase in β-sheet protein content as disease progressed, some, but not all of which was associated with PrP^{Sc} (Kretlow *et al.*, 2008). Both the host-encoded and disease associated forms of the protein are associated with 3 different isoforms that are glycosylated at one, both, or neither of the protein's two possible glycosylation sites. These sites are situated at residues 181 and 197 of human PrP, while on murine PrP these sites are at residues 180 and 196 (Lawson *et al.*, 2005).

1.1.4. Scrapie agent strains

The earliest recorded evidence of scrapie in Britain goes as far back as 1732 (McGowan, 1922). Back in the 18^{th} century the disease was known under several different names, representative of the symptoms observed, such as 'goggles', 'rubbers', or 'shakings', but 'scrapie' was the name that prevailed (McGowan, 1922). Cuillé and Chelle successfully carried out experimental scrapie transmission in sheep for the first time in 1936 (Cuillé and Chelle, 1936). They suspected previous attempts had failed due to the short duration of experiments, and that the long incubation period in naturally infected animals (1.5 to 2 years) was key. Longer experimental times (Cuillé and Chelle, 1936) resulted in sheep that succumbed to symptoms

characteristic of scrapie 16 and 22 months post-inoculation. Serial passage of scrapie in goats (Pattison *et al.*, 1959), revealed different symptoms in some goats compared to others. These symptoms were separated into two distinct categories: the scratching syndrome and the nervous syndrome (Pattison and Millson, 1961).

Chandler was the first to carry out experimental transmission of scrapie in laboratory mice (Chandler, 1961). Having dubbed the nervous form of goat scrapie as 'drowsy', C.57black, C.B.A brindle, and Swiss white mice were inoculated with brain material from either the 'scratching' or the 'drowsy' goat (Chandler, 1961). Only the Swiss white mice inoculated from the 'drowsy' inoculum went on to show nervous symptoms 7.5 to 9 months post inoculation. The symptoms were not identical to those observed in sheep and goats, but they concluded that the similarities were close enough to prove a link, and that scrapie had been successfully transmitted to mice. The two distinct disease manifestations are the first indication of strain variation in scrapie. The fact that only one mouse strain developed disease, also indicates that mouse strains have varying susceptibility to the scrapie agent. For example, serial mouse passage of material from the 'drowsy' goat source has led to the isolation of the 139A strain of scrapie (Dickinson *et al.*, 1984).

The ME7 strain of scrapie, as it is used in this study, was originally isolated in a series of experiments studying experimental transmission of scrapie in mice (Zlotnik and Rennie, 1963). The ME.$_7$ strain, was isolated from **m**ouse **e**xperiment **7**, where mice were intragastrically inoculated with a spleen pool prepared from Suffolk sheep infected with natural scrapie. These mice had not developed clinical symptoms by 13

months post-inoculation. Yet, creating a brain pool from these mice, to transmit to a second group of mice resulted in clinical symptoms after 5 months. ME7 has since been repeatedly isolated at The Roslin Institute, Neurobiology Division (formerly the Neuropathogenesis Unit) in Edinburgh, by passaging scrapie material from Suffolk sheep through the C57BL mouse strain (s^7).

Dickinson *et al* (Dickinson *et al.*, 1968) identified a single gene which was responsible for the incubation period of scrapie in mice, which they designated as *Sinc* (***s***crapie ***inc***ubation). They suggested that *Sinc* was an autosomal gene with a single pair of alleles, without obvious dominance, and with very little evidence that any other genes are involved in controlling incubation time (Dickinson *et al.*, 1968). The two alleles were designated as s7 for the allele that shortens incubation time, and p7 for the allele that prolongs incubation time. As such, there are three different possibilities for mouse genotypes: s7s7, p7p7, or s7p7, which helps explain why some mouse strains succumb to scrapie much faster than others.

It has since been determined that the *Sinc* gene is linked to *Prnp*, the gene which encodes for PrP, where *Prnp* alleles 'express two distinct PrP protein variants, PrP A and PrP B which arise from codon 108L/F and 189T/V dimorphisms' (Moore *et al.*, 1998). Moore *et al* went on to show that the *Sinc* and *Prnp* genes were congruent (Moore *et al.*, 1998). The *Sinc* alleles have therefore since been renamed as $Prnp^a$ ($Sinc^{s7}$) and $Prnp^b$ ($Sinc^{p7}$).

In addition to the presence of this gene, which regulates scrapie incubation period in mice, each individual scrapie strain that has been isolated has its own distinct incubation period between different mouse lines. Each scrapie strain has a different incubation period within the one mouse line. For example, intracerebrally inoculated (i.c.) ME7 has an incubation period of approximately 180 days in C57BL mice, which are *Prnp*^{a} (*Sinc*^{s7}), whereas in VM mice, *Prnp*^{b} (*Sinc*^{p7}), the incubation period is approximately 330 days (Bruce, 1993). In the C57BLxVM cross *Prnp*^{a}*Prnp*^{b} (*Sinc*^{s7}*Sinc*^{p7}), the incubation period is almost right in the middle of the two incubation periods, at 250 days (Bruce, 1993).

1.1.5. Routes of transmission

As was mentioned earlier, TSEs have several identified routes of transmission. TSE studies have been carried out in mice since Chandler successfully transmitted scrapie to mice in 1961 (Chandler, 1961), but prior to this sheep were successfully experimentally infected with scrapie (Cuillé and Chelle, 1936). Since then experimental transmission has been successful in animals through different injection routes, for example intraperitoneal (Brown *et al.*, 2000), intracerebral (Taylor *et al.*, 1996) or intravenous (Taylor *et al.*, 1996) or via blood transfusion in sheep (Halliday *et al.*, 2005; Houston *et al.*, 2000; Houston *et al.*, 2008; McCutcheon *et al.*, 2011). Accidental transmission of vCJD in humans has occurred via blood transfusion (Llewelyn *et al.*, 2004; Peden *et al.*, 2004; Wroe *et al.*, 2006), or ingestion of BSE-contaminated meat (Bruce *et al.*, 1997; Will *et al.*, 1996), which is also linked to feline spongiform encephalopathy (Sigurdson and Miller, 2003). BSE is equally thought to develop from ingestion of contaminated food (Taylor, 1993; Taylor and

Woodgate, 1997). Oral TSE transmission has therefore been experimentally studied at length both in sheep and mice (Andréoletti *et al.*, 2000; Glaysher and Mabbott, 2007b; Huang *et al.*, 2002; Prinz *et al.*, 2003; Raymond *et al.*, 2007).

TSE agents can be readily experimentally transmitted via lesions to the skin (Glaysher and Mabbott, 2007a; Mohan *et al.*, 2004; Mohan *et al.*, 2005b; Taylor *et al.*, 1996) and oral mucosa (Bartz *et al.*, 2003; Carp, 1982; Denkers *et al.*, 2011). Thus, natural TSE infections might also occur via lesions in the mouth and gastrointestinal tract through consumption of rough feed or birth-associated lesions to the skin or mucus membranes. Furthermore, TSE agents have also been identified in the skin (Cunningham *et al.*, 2004; Notari *et al.*, 2010; Thomzig *et al.*, 2007), as well as in antler velvet (Angers *et al.*, 2009), as determined by Western blotting or bioassays from the target sites.

Disease may also be transmitted horizontally, in CWD or scrapie (Gough and Maddison, 2010; Saunders *et al.*, 2008). For example, infectivity has been detected in several excreta of CWD-infected cervids (Haley *et al.*, 2011; Haley *et al.*, 2009; Mathiason *et al.*, 2006), nasal secretions from both experimentally and naturally infected animals (Gough and Maddison, 2010), milk from scrapie infected sheep (Ligios *et al.*, 2011), as well as in the urine of scrapie-infected mice (Seeger *et al.*, 2005) or hamsters (Kariv-Inbal *et al.*, 2006). PrP^{Sc} was also detected in urine (Murayama *et al.*, 2007) and faeces (Krüger *et al.*, 2009) of hamsters orally infected with scrapie in the days following infection. PrP^{Sc} was identified in the urine at the terminal stage of disease (Murayama *et al.*, 2007) but was only identified in faeces at

the terminal stage following PMCA amplification (Krüger *et al.*, 2009). The fact that TSEs can be transmitted through wounds in the skin or through the gastro-intestinal tract are therefore of importance when taking into consideration the presence of infectivity in the environment. One of the symptoms of scrapie-affected sheep or goats is the rubbing or scratching (Chelle, 1945). If this is occurring in the field, knowing that infectivity can be present in the skin or excreta and that scrapie can be transmitted through wounds, it is probable that some cases of horizontal transmission might occur through minor skin lesions. Added to this are also the presence of disease specific PrP in tissues such as muscle (Cardone *et al.*, 2009), or TSE agent infectivity in fat (Race *et al.*, 2008; Race *et al.*, 2009), both of which are regularly consumed by animals and humans. Especially in the case of CWD, where animals can be hunted in the wild, the meat is often consumed by the same group of people over an extended period (Race *et al.*, 2009). While personal protective equipment is worn by at risk groups during surgery, or in the laboratory when exposed to TSE-infected materials, it is not certain that the average hunter will take the same measures, and small cuts or abrasions may often occur on hands etc, highlighting another potential risk.

Scarification of the skin, as a route of pathogen exposure, has been used in many contexts. In the 1950's it was used for various diagnostic methods such as for malaria (van den Berghe and Chardome, 1951) or tuberculosis (Frappier and Guy, 1950). Skin scarification was first used as a method of TSE transmission by Carp *et al* (Carp, 1982) where gingival scarification was carried out in mice before application of inoculum, leading to the development of scrapie in these mice. Since then, Taylor

et al (Taylor *et al.*, 1996) developed a technique for TSE transmission, via scarification of the skin of the thigh. They established that scarification is as effective for transmitting scrapie to mice as other routes of peripheral transmission, with comparable incubation periods (dependent on volume and concentration of inoculum), and equally, different sites of scarification also give comparable results (Taylor *et al.*, 1996). This is the method of TSE agent infection which has been used and described in this thesis.

1.1.6. Prions and the immune system

PrP^{Sc} accumulation within the LRS occurs in a number of species. LRS involvement was determined through splenectomy in scrapie infected mice, which significantly delayed the development of disease (Fraser and Dickinson, 1978), suggesting that the spleen was essential for successful disease progression. Other lymphoid tissues have been associated with PrP^{Sc} accumulation, dependent on the route of transmission. Scrapie infection through skin scarification highlighted the role of the draining lymph nodes (LNs) in disease (Glaysher and Mabbott, 2007a). Lymphoid tissues in the gut, such as Peyer's patches (PP) have been implicated in disease through oral transmission (Andréoletti *et al.*, 2000; Glaysher and Mabbott, 2007b; Heggebø *et al.*, 2002; Prinz *et al.*, 2003; Raymond *et al.*, 2007; Sigurdson *et al.*, 1999).

An important question surrounding these diseases is how the TSE agent is transported from the site of infection to the LRS and onwards into the CNS, as this knowledge might provide targets for successful therapeutic intervention. Much speculation has surrounded the issue of whether the TSE agent is transported via cell-

associated or cell-free mechanisms. Studies in certain species show that when LRS involvement occurs during the early stages of TSE infection, PrP^{Sc} accumulates first on PrP^{C}-expressing follicular dendritic cells (FDCs) (Andréoletti *et al.*, 2000; Glaysher and Mabbott, 2007b; Hilton *et al.*, 1998; Mabbott *et al.*, 2003; Prinz *et al.*, 2003; Sigurdson *et al.*, 1999). FDCs are stromal-derived, tissue resident cells, found in the germinal centres of lymphoid follicles (Mabbott *et al.*, 2011). These cells express high levels of PrP^{C} on their surface, and are clearly associated with PrP^{Sc} accumulation in peripheral lymphoid tissues (Jeffrey *et al.*, 2000a). The FDC has since been identified as an important site of TSE agent accumulation and replication in the LRS (Brown *et al.*, 1999; Mabbott *et al.*, 2000; McCulloch *et al.*, 2011; Montrasio *et al.*, 2000). Furthermore, in the absence of FDCs, TSE agent neuroinvasion is impaired and disease susceptibility reduced. FDCs are considered to amplify TSE agents above the threshold required for neuroinvasion.

TSE transmission studies in severe combined immunodeficient (SCID) mice highlighted the need for a functional immune system in order to successfully transmit the disease (Fraser *et al.*, 1996; Lasmézas *et al.*, 1996; O'Rourke *et al.*, 1994). So, in contrast to other pathogens, which exploit the lack of a fully functioning immune system, TSEs that feature a replicative stage in the LRS, require a functioning immune system to establish disease. However, traditional immune responses, such as antibody production are not associated with this infection, possibly due to immune tolerance to host PrP^{C} (Isaacs *et al.*, 2006). There is growing evidence for localised immune responses occurring within the lymphoid tissues, for example through changes in the germinal centers of the spleen, as detected by electron microscopy

(McGovern *et al.*, 2004). Following SSBP/1 scrapie infection in sheep, transcriptional analysis identified downregulation of genes linked to inflammation and oxidative stress, and the up-regulation of genes related to apoptosis in lymphoid tissues (Gossner *et al.*, 2011). These data suggest that TSE agent accumulation affects the local environment in the LRS.

1.2. Cells of the immune system and their influence on TSE pathogenesis

1.2.1. DCs vs Macrophages

Even though peripheral lymphoid tissues, and the FDCs within them, have been identified as important sites of TSE agent replication prior to neuroinvasion, little is known of how TSE agents are transported to these sites or what, if any, cells are involved. Mononuclear phagocytes (MNPs) are a diverse group of haematopoietically-derived phagocytic cells which includes classical DCs and macrophages, but also LCs in the epidermis of the skin and microglia in the brain. The distribution of these cells at the body's surfaces (intestine, skin, mucosa etc.) and their ability to phagocytose antigens and deliver them to draining lymphoid tissues suggests MNPs may either destroy TSE agents or transport them within the host.

The precise ontogeny of classical DCs and macrophages is the subject of much debate. Indeed, there is growing evidence that these two cells types are not as distinct from each other as was once thought (Bradford *et al.*, 2011; Hume, 2008; Mabbott *et al.*, 2010). These cells are often identified or isolated based solely on the expression of a small set of cell surface markers, such as CD11c/*Itgax* for DCs (Austin, 1999). and CD207/langerin (*Cd207*) for LCs (Takahara *et al.*, 2002; Valladeau *et al.*, 2002; Valladeau *et al.*, 1999; Valladeau *et al.*, 2000). Even under the traditional 'umbrella

terms' of DCs and macrophages, more distinct cellular subsets have been described based on the expression of a long list of different markers. However, the expression of these and other markers has been shown to be less specific than was originally considered (Bradford *et al.*, 2011; Probst *et al.*, 2005). For example, the temporary depletion of $CD11c^+$ cells in CD11c-DTR transgenic mice, originally considered to specifically deplete DCs (Jung *et al.*, 2002), has been shown to also deplete many other macrophage subsets, such as the $CD169^+$ macrophages in the spleen and LNs (Bradford *et al.*, 2011; Probst *et al.*, 2005). Much of the data described in this review was generated from *in vitro* experiments utilizing bone marrow-derived DCs. However, the recent meta-analysis of a large collection of gene expression data from a range of mouse leukocyte lineages shows bone marrow-DCs were clearly identified as phagocytes (macrophages) and were transcriptionally distinct from tissue classical DCs. Indeed, there are few mRNA markers that clearly distinguish classical DCs from macrophages other than low expression of those required for phagocytosis (Mabbott *et al.*, 2010). Clearly, without also testing their biological properties (phagocytosis, ability to stimulate naïve T cells etc.) it is difficult to accurately distinguish between classical DCs and macrophages based solely on the expression of a limited set of surface markers. This is especially true in immunohistochemistry-based studies. While it is important to highlight the ambiguity surrounding the discrimination of individual MNP populations, this thesis will stick to the traditional terms of macrophages or DCs to avoid further confusion.

1.2.2. CD11c

CD11c is an integrin (Lai *et al.*, 1998), also known as integrin alpha X (Itgax) and encoded by the *Itgax* gene. Integrins are heterodimeric integral membrane proteins composed of an alpha chain and a beta chain. CD11c combines with the beta 2 chain (ITGB2) to form a leukocyte-specific integrin referred to as inactivated-C3b (iC3b) receptor 4 (CR4). The Itgax complex appears to share the properties of Itgam (CD11b) that are involved in neutrophil and monocyte adherence to stimulated endothelial cells, as well as in the phagocytosis of complement coated particles (http://www.ncbi.nlm.nih.gov/gene/3687).

CD11c was thought to be a good marker for most if not all DCs in mouse lymphoid tissues (Austin, 1999), although in epidermal LCs it is only expressed as $CD11c^{negative\text{-}low}$, until it gets upregulated when they mature (Jung *et al.*, 2002) and migrate to the draining LNs. CD11c has been widely used as a marker for the identification and isolation of DC subsets. CD11c identification on a number of macrophage subsets means that this marker is not expressed exclusively on DCs (Fig. 1.1.), as was once thought (Hume, 2008). Therefore any research that targets $CD11c^{+}$ cells is targeting DCs as well as macrophages.

1.2.3. Langerin

CD207 or langerin (encoded by the *Cd207* gene) is a C-type lectin, originally thought to be specific to LCs (Kissenpfennig *et al.*, 2005a; Valladeau *et al.*, 1999; Valladeau *et al.*, 2000). It has been found to induce the formation of Birbeck granules (Valladeau *et al.*, 2000). These are tennis racquet-shaped, cytoplasmic

organelles specific to LCs (Birbeck *et al.*, 1961; Valladeau *et al.*, 2000; Wolff, 1967). Langerin is a C-type lectin, which plays a role in binding sulfated and mannosylated glycans via a single C-type carbohydrate recognition domain (Tateno *et al.*, 2010). The molecule appears to be internalised into the Birbeck granules, and langerin is thought to cause the internalisation of antigen into the Birbeck granules, which is believed to provide access to a non-classical antigen-processing pathway (Valladeau *et al.*, 2000). LCs appear to play an important role in the uptake of lectin-binding antibodies under vaccination conditions (Flacher *et al.*, 2009), further supporting the role of langerin in immune responses. Langerin expression was previously believed to be exclusive to LCs, and a useful tool for the identification or isolation of these cells (Valladeau *et al.*, 1999). It has since been identified on a number of other cell types both within the LRS and in other organs (Douillard *et al.*, 2005; Valladeau *et al.*, 2002) (Fig. 1.1.). Like CD11c, it is not an exclusive marker for cellular identification, but in the skin, it is useful for the identification of langerin^{+} cells.

LCs are the DCs of the skin. They are distinct from other DC subsets, as they are radioresistant (Merad *et al.*, 2002), have a much longer life-span than other DC subsets (Lucas and MacPherson, 2002), and only express CD11c at very low levels (Jung *et al.*, 2002). CD11c expression on LCs is upregulated as they migrate to the draining LNs. These cells function as the antigen presenting cells (APC) of the epidermis, and as such are considered to play a role in the immune response to foreign antigen in the skin, through their migration to the draining inguinal LNs (iLNs), even if their role in the primary immune response is being put into question.

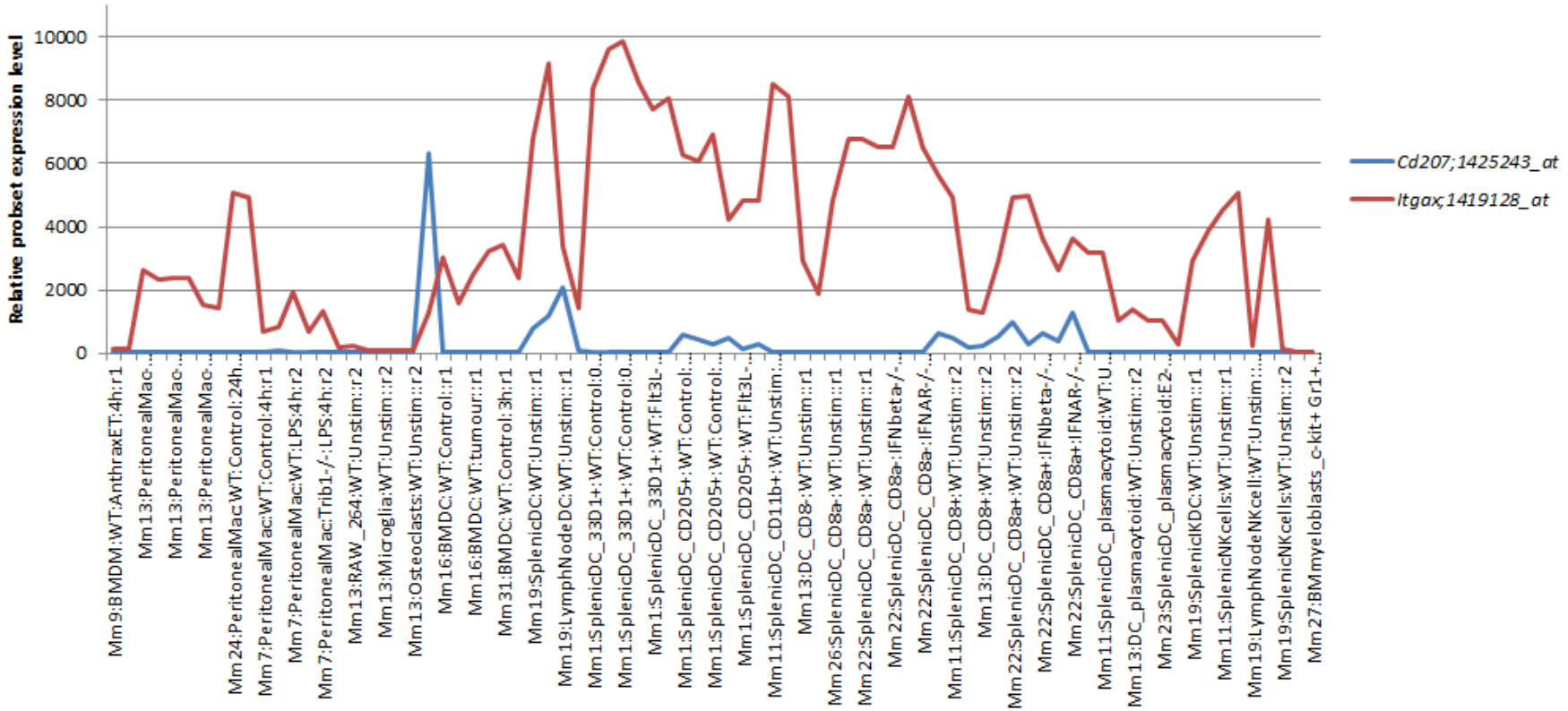

Figure 1.1. Comparison of *Itgax* and *Cd207* expression by mononuclear phagocyte subsets. Analysis of probeset expression across 81 individual microarray data sets (Affymetrix MOE430-2.0) representing peritoneal macrophages, splenic, and LN classical DC and plasmacytoid DCs. *Itgax* (CD11c) is expressed at varying levels across these cell populations; *Cd207* (langerin) is expressed on a few cell types, but highest on LCs. MmXX represents individual microarray sample ID. Full details of datasets are available in (Mabbott *et al.*, 2010).

1.2.4. MNPs and their role in TSEs

Haematopoietic, classical DCs are a distinct cell type from mesenchymal-derived FDCs (Mabbott *et al.*, 2011). Classical DCs are APCs and as such they sample their natural environment for foreign antigens, which they process and transport to the nearest lymphoid tissues to initiate a specific immune response. Classical DCs take up antigen through endocytosis or sometimes macropinocytosis (Sallusto *et al.*, 1995). Classical DCs travel via the lymphatic system to the secondary lymphoid organs in response to chemokine stimulation where they present antigen to lymphocytes (Steinman, 1991). Although the primary role of DCs is to present antigens to T-cells, they are also capable of presenting them to B-cells. This sometimes occurs in the form of intact antigen, in contrast to processed antigen, which is presented to T-cells (MacPherson *et al.*, 1999). Interestingly, recent studies have identified PrP^{Sc} associated with a subset of B cells in the blood of scrapie infected sheep (Edwards *et al.*, 2010). These characteristics therefore identify classical DCs as possible candidates for the transport of the intact TSE agents from the site of exposure to the peripheral lymphoid system. Studies show the retention of PrP^{Sc} within bone marrow derived DCs 72 hours after *in vitro* exposure to PrP^{Sc}-enriched scrapie associated fibrils (Huang *et al.*, 2002). However, another study has also suggested that bone marrow-derived DCs rapidly degrade PrP^{Sc} (Lai *et al.*, 1998; Luhr *et al.*, 2002). Whether these cells are a good representation of tissue classical DCs is uncertain. Meta-analysis of their transcriptomes shows bone marrow-derived DC closely resemble macrophages, not classical DCs.

Classical DCs could influence TSE pathogenesis at a variety of stages in the disease process: transport from the site of infection to the LRS in the case of LRS involvement; transport between cells within the lymphoid tissues; or the transfer between the lymphoid tissues and the nervous system (neuroinvasion). The argument for a DC-related role in TSE pathogenesis is strengthened by the evidence that the prion protein fragment 106-126 functions as a chemoattractant to immature monocyte-derived DCs (Kaneider *et al.*, 2003). Evidence for a possible role of DCs in the delivery of TSE agents to lymphoid tissues was provided by using a transgenic mouse model in which $CD11c^+$ cells (Cordier-Dirikoc and Chabry, 2008) or $CD8^+CD11c^+$ (Sethi *et al.*, 2007) cells were significantly reduced. The absence of these cells at the time of intraperitoneal scrapie infection significantly prolonged the incubation period of the disease when compared to wildtype controls (Cordier-Dirikoc and Chabry, 2008; Sethi *et al.*, 2007).

1.3. The skin

1.3.1. DC subsets within the skin

As has been previously mentioned, TSE agents can be readily transmitted via lesions to the skin (Glaysher and Mabbott, 2007a; Mohan *et al.*, 2004; Mohan *et al.*, 2005b; Taylor *et al.*, 1996) and oral mucosa (Bartz *et al.*, 2003; Carp, 1982; Denkers *et al.*, 2011), and TSE agent infectivity has been identified within in skin (Cunningham *et al.*, 2004; Notari *et al.*, 2010; Thomzig *et al.*, 2007) and antler velvet (Angers *et al.*, 2009). These findings further highlight the skin or oral and reproductive mucosa as possible sites of natural TSE transmission/infection.

The skin provides a first line of defence against infection and is therefore the primary site of residence for a number of MNPs that help to maintain this barrier. These MNPs include LCs in the epidermis and classical DCs and macrophages in the dermis (Fig. 1.2. and Fig. 1.3.). Classical DCs have been suggested to transport viruses such as HIV (de Jong and Geijtenbeek, 2010), Dengue (Palucka, 2000; Wu *et al.*, 2000), or Influenza virus following infection, from the skin, which raises the question whether skin-derived MNPs also play a role in the uptake and transport of the TSE agent from the skin to the LRS.

Following scrapie infection via skin scarification in the mouse, agent infectivity and PrP^{Sc} accumulation occurs first in the skin draining LN soon after exposure (Glaysher and Mabbott, 2007a; Mohan *et al.*, 2005a; Mohan *et al.*, 2005b). Experimental scrapie transmission in sheep via the skin failed to find a conclusive link between DCs and the transport of PrP^{Sc} (Gossner *et al.*, 2006). Neutrophils were found to associate with PrP^{Sc}. Definite involvement of skin resident MNPs in TSE agent transmission from the skin remains to be determined. Early research in mice also implied the lack of LC involvement (Mohan *et al.*, 2005b; Mohan *et al.*, 2005c).

The use of transgenic mouse models that allow for temporary depletion of LCs, $CD11c^{+}$ classical DCs or macrophages (Jung *et al.*, 2002; Kissenpfennig *et al.*, 2005b) prior to scrapie infection will help determine which, if any, of these cell populations play a role in TSE transmission from the skin as suggested after oral exposure (Andréoletti *et al.*, 2000; Glaysher and Mabbott, 2007b; Huang *et al.*, 2002; Prinz *et al.*, 2003; Raymond *et al.*, 2007). Any research studying the role of skin DCs

or macrophages in TSE transmission needs to be put into the context of the LC paradigm (Section 1.3.2.).

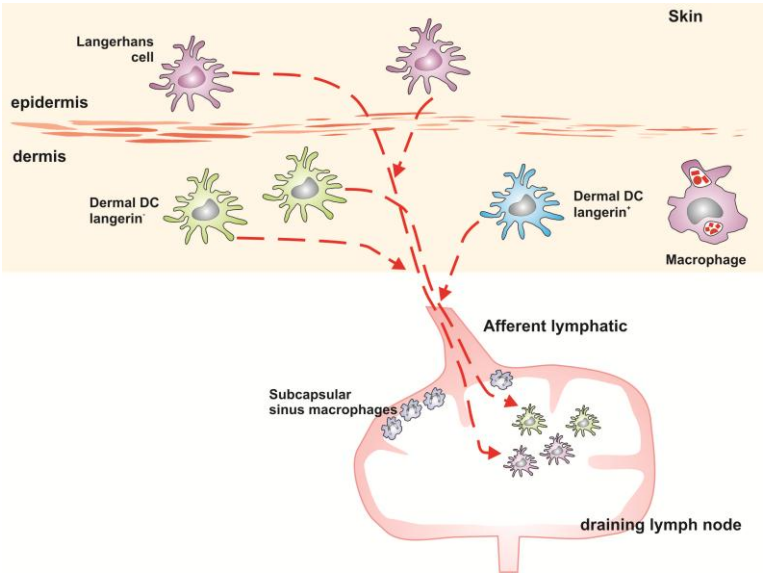

Figure 1.2. Schematic representation of the MNPs in the skin of the mouse. LCs are found in the epidermis. The dermis is situated below the epidermis and contains langerin$^+$ as well as langerin$^-$ DCs and various macrophage populations. These cells continually migrate through the skin and to the draining LN, and therefore may play a potential role in the transport of the TSE agent from the skin to the draining LN, where the agent replicates upon FDCs prior to neuroinvasion.

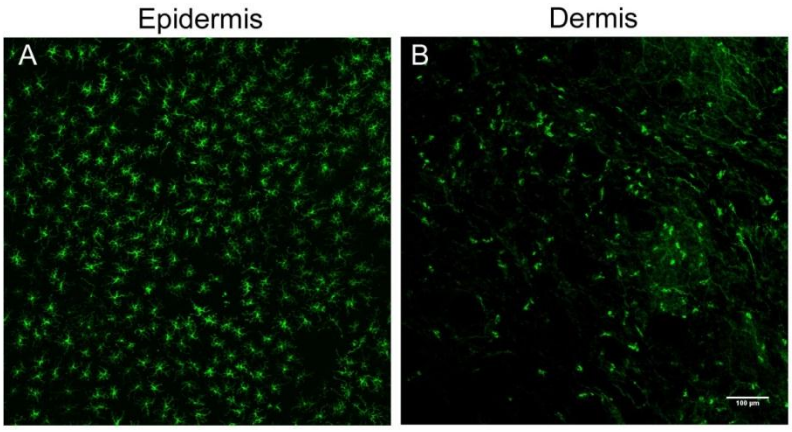

Figure 1.3. Distribution of LCs and langerin$^+$ dermal DCs (dDC) in the mouse ear. **A** LCs form a dense network of cells within the epidermis. **B** Langerin$^+$ dDCs are less frequent within the dermis than LCs in the epidermis. A small number of these cells may also be migrating LCs (modified from Chapter 7, Fig. 7.9.).

Substantial heterogeneity has been revealed between MNP subtypes in different inbred mouse stains (Flacher *et al.*, 2008). For example, LC density in the epidermis is much lower in C57BL/6 mice when compared to BALB/c, 129/Sv, and CBA mice. Such differences could significantly contribute to the differing results observed in many host species exposed to TSE agents.

1.3.2. The LC paradigm

The 'LC paradigm' arose from the often contradictory results generated by research in skin immunology. One explanation for this may be due to the heterogeneity between mouse strains, as described above (Flacher *et al.*, 2008). In addition to the difference observed in LC density between mouse strains, Flacher *et al* identified two different langerin expressing cellular subsets in the skin draining LN of BALB/c mice compared to mainly one subset in the C57BL/6. There may be further differences in the frequencies of different cell subsets. There are probably many further such differences between mouse lines, husbandry conditions in different animal units, and also between different animal species, which could help explain differing results in many diseases, including prion diseases.

In 2007 an important novel cell type was identified in the mouse dermis: the langerin$^+$ dermal DC (dDC) (Bursch *et al.*, 2007; Ginhoux *et al.*, 2007; Poulin *et al.*, 2007) (Fig. 1.2.). The use of a transgenic mouse model (langerin-EGFP-DTR mice) where langerin$^+$ cells were temporarily depleted through injection of Diphtheria toxin (DTX), identified langerin$^+$ cells that repopulated the skin draining LNs at different rates, without knowing why (Kissenpfennig *et al.*, 2005b). This discovery identified

two main DC subsets within the dermis of the skin, langerin^{+} dDCs and langerin^{-} dDCs, in addition to the LCs of the epidermis. These langerin^{+} dDCs have a much higher turnover rate than LCs and repopulate the skin several weeks faster than the epidermal LCs following DTX-mediated depletion (Bennett *et al.*, 2005; Kissenpfennig *et al.*, 2005b; Nagao *et al.*, 2009). Upon activation, for example by skin immunization, these dDCs migrate from the skin to the skin draining LNs faster than the LCs (Eidsmo *et al.*, 2009; Kissenpfennig *et al.*, 2005b).

Since the identification of langerin^{+} dDCs, a number of publications have questioned the role of LCs in skin immunity (Fukunaga *et al.*, 2008; Shklovskaya *et al.*, 2008), in particular the suggestion that they are the only APCs of the skin. Indeed, langerin^{+} dDCs have been shown to be fully capable of cross-presenting antigens regardless of whether LCs are present or not (Bedoui *et al.*, 2009; Henri *et al.*, 2010). Experiments where LC migration from the epidermis was blocked, in CD40L$^{-/-}$ mice or via caspase-1 inhibition, were previously used to determine whether LCs played a role in the transport of the scrapie agent from the skin to the draining LNs (Mohan *et al.*, 2005b). While the early accumulation of TSE agent infectivity was not affected in the draining LNs, the incubation period of disease was significantly shortened in the CD40L$^{-/-}$ mice. These data implied that instead of aiding pathogenesis by transporting TSE agents from the skin, LCs may impede pathogenesis by phagocytosing and degrading them (Mohan *et al.*, 2005b; Mohan *et al.*, 2005c). In light of recent findings, further experiments are necessary to distinguish the influence of LCs and langerin^{+} dermal DC in this process.

Closer examination of the cellular subsets within the skin, have identified no fewer than 5 DC subsets in the dermis, in addition to the epidermal LCs (Heath and Carbone, 2009; Henri *et al.*, 2010) through their differing expression levels of markers such as langerin, CD11b, and CD103. Efficient isolation and identification of these different cell populations requires careful cell sorting. However, the research in this thesis focuses on the epidermal LCs, and the two dDC populations that can be distinguished by their expression of langerin.

1.4. Other possible mechanisms in TSE pathogenesis

1.4.1. Subcapsular sinus (SCS) macrophages

FDCs trap and retain antigen on their surfaces (Kosco-Vilbois, 2003) in the form of immune complexes (Mabbott, 2004). Complement receptors on the FDCs bind these complexes in naïve mice, whereas in immunised mice they are also bound via antibody Fc receptors (van den Berg *et al.*, 1995). Complement receptors, as well as complement components C1q and C3 are considered to play an important role in TSE agent localisation to FDCs (Klein *et al.*, 2001; Mabbott *et al.*, 2001; Zabel *et al.*, 2007). $CD11c^{+}CD169^{+}$ SCS macrophages are a distinct, poorly endocytic and degradative macrophage subset (Phan *et al.*, 2009). These unique cells, located within the SCS of LNs, capture antigen-containing immune complexes arriving in the LN via their cell processes that they extend into the lumen of the SCS (Carrasco and Batista, 2007; Junt *et al.*, 2007; Phan *et al.*, 2009; Phan *et al.*, 2007; Roozendaal *et al.*, 2009). In contrast to other macrophage subsets, SCS macrophages retain immune complexes on their surfaces for rapid translocation through the floor of the SCS to underlying, non-cognate (non-specific) follicular B cells (Phan *et al.*, 2009). These B cells then acquire the immune complexes via their complement receptors

and deliver them to FDCs. The higher immune complex-binding affinities of FDCs most likely relieve the B cells of their cargo. Thus, the SCS macrophage-B cell immune complex relay represents an efficient route through which antigens are delivered to FDCs (Carrasco and Batista, 2007; Junt *et al.*, 2007; Phan *et al.*, 2009; Phan *et al.*, 2007; Roozendaal *et al.*, 2009). The demonstration that SCS macrophages in LNs (and their spleen counterparts) play a key role in the delivery of complement-bound immune complexes to FDCs raises the possibility that these cells also play an important role in the transport of complement-opsonized TSE agents to FDCs within lymphoid tissues. PrP^{d} has been detected within the SCS macrophages of intestinally-exposed sheep (Jeffrey *et al.*, 2006). Furthermore, $CD11c^{+}CD169^{+}$ SCS macrophages directly cross-present antigen captured from subcutaneous injection, after it arrives into the draining LN via the lymph (Asano *et al.*, 2011).

1.4.2. Other macrophages populations involved in TSEs

As well as the SCS macrophages mentioned above, there is evidence for the involvement of other macrophage subsets in TSE disease. However, it is not yet clear whether these cells might play a preventative role in disease, or whether, like DCs, they might play a role in disease progression. Macrophages typically phagocytose and degrade protein antigens more rapidly than classical DCs (Bergtold *et al.*, 2005; Delamarre *et al.*, 2005), which can retain some protein antigens in their native form up to 36 hours after exposure (Wykes *et al.*, 1998). Data from *in vitro* studies likewise suggest that macrophages also phagocytose and degrade TSE agents including scrapie and BSE (Carp and Callahan, 1981; Carp and Callahan, 1982; Sassa *et al.*, 2010a). Furthermore, the depletion of macrophages before scrapie

infection increased the accumulation of the scrapie agent in the spleen and accelerated disease pathogenesis (Beringue *et al.*, 2000). Within the macrophage, PrP^{Sc} was also found to colocalize with lysosomal and proteasomal proteins (Sassa *et al.*, 2010b), implying that, consistent with their biological characteristics, macrophages might play a preventative role in TSE disease when compared to classical DCs. However, data also imply that macrophages might transport orally acquired TSE agents within the gut associated lymphoid tissues (Takakura *et al.*, 2011). Whether the cells described are macrophages or classical DCs is uncertain. As highlighted earlier, it is difficult to classify these cells by immunohistochemistry based on the expression of cell surface markers alone.

Tingible body macrophages are found in close association with FDCs within the germinal centers of follicles within lymphoid tissues, where they clear proteins and apoptotic lymphocytes (tingible bodies) (Swartzendruber and Congdon, 1963). Data from ultrastructural studies show high levels of PrP^{Sc} within tingible body macrophages in lymphoid tissues of scrapie-affected mice and sheep (Jeffrey *et al.*, 2001b; Jeffrey *et al.*, 2000b; Ryder *et al.*, 2009). Deposition of PrP^{d} within tingible body macrophages in lymphoid tissues of patients with vCJD have also been described (Hilton *et al.*, 2004). Recent data suggests tingible body macrophages scavenge and degrade PrP^{Sc} following synthesis on other infected cells such as FDCs (McCulloch *et al.*, 2011).

Microglia are the macrophages of the CNS. Gliosis, involving astrocytes and microglia, is one of the neuropathological characteristics of terminal TSE disease.

Microglia are the main source of the inflammatory response that is associated with TSE disease, and microglial activation is directly linked to the patterns of PrP^{Sc} deposition in the brain, and precedes neuronal cell death (Perry *et al.*, 2002; Rezaie and Lantos, 2001). Significant vacuolar degeneration has been detected in the microglia/macrophages of two vCJD patients (Rezaie and Al-Sarraj, 2007). Microglia and astrocytes have been associated with granular PrP^{d} deposits, leading speculation that these cells play a role in processing, degrading or removing PrP^{Sc} (Kovács *et al.*, 2005). The *in vitro* exposure of microglia to murine scrapie brain homogenate or $PrP_{(106-126)}$ severely affected their phagocytic activity (Ciesielski-Treska *et al.*, 2004). In contrast, microglia from ME7-scrapie affected mice were capable of phagocytosis, but were not able to clear PrP^{Sc} (Hughes *et al.*, 2010). Within TSE-affected brains the pro-inflammatory activity of microglia is specifically modulated by the anti-inflammatory cytokine TGFβ1. This cytokine appears to play a critical role in the down-regulation of pro-inflammatory microglial responses minimizing brain inflammation and thus avoiding exacerbation of brain damage (Boche *et al.*, 2006). Whether systemic infections and inflammation lead to the dis-regulation of this control and the exacerbation of neurodegeneration remains to be determined (Perry *et al.*, 2007).

A recently identified brain DC population, morphologically similar to microglia is considered to be a new member of the heterogeneous microglia population (Bulloch *et al.*, 2008). However, it is uncertain whether these cells are a unique subset of classical DCs. These data indicate that, as in the other tissues discussed in this thesis, there are a number of different MNP populations that could influence TSE

pathogenesis in the brain depending on the circumstances. Some data might relate to a particular subset of cells, rather than to the entirety of MNPs within the brain.

1.4.3. Dissemination of TSE agents from the LRS

As well as being involved in the transport of the TSE agent from the periphery to the LRS, classical DCs may have a role in the act of neuroinvasion within the lymphoid tissues, for example, the transport of TSE agents to peripheral nerves. Studies show evidence of the intercellular transport of PrP^{Sc} through tunnelling nanotubules from DCs to cultured neuronal cells (Gousset *et al.*, 2009). In some TSE diseases where there appears to be little or no LRS involvement (such as BSE in cattle, or sheep of certain *PRNP* genotypes infected with scrapie) neuroinvasion occurs by an unidentified process. Whether classical DCs fulfil this role as implied in the Gousset study (Gousset *et al.*, 2009) is uncertain. However, studies carried out in scrapie infected, FDC-deficient, $TNFR1^{-/-}$ mice, determined that MNPs were unlikely to have directly infected peripheral nerves within lymphoid tissues, as these mice failed to develop disease when injected with scrapie-infected $CD11c^{+}$ cells (classical DCs) (Raymond and Mabbott, 2007). These results were in contrast to previous studies in FDC-deficient $RAG^{-/-}$ mice, where scrapie disease was successfully transmitted (Aucouturier *et al.*, 2001). The discrepancies between these two studies may possibly be due to much higher levels of innervation in the $RAG^{-/-}$ mouse spleens when compared to those from $TNFR1^{-/-}$ mice (Raymond and Mabbott, 2007).

1.4.4. A possible cell-free mechanism of transport?

Current data suggest MNPs may exhibit a diverse range of roles in TSE disease from the transport or destruction of TSE agents in lymphoid tissues, to mediators or

protectors of neuropathology in the brain. Much of the research described above studies the influence of MNPs on TSE pathogenesis during steady-state conditions. However, under inflammatory conditions MNPs may exacerbate TSE pathogenesis for example through the release of neurotoxic mediators in the brain (Perry *et al.*, 2007). While some MNPs may play important roles in TSE pathogenesis, it is equally likely that in some circumstances their involvement is minimal. The route of TSE infection, strain of TSE agent and host species may all influence the role of MNPs in disease pathogenesis. Indeed, it is equally probable that in some instances TSE agents reach the draining lymphoid tissues via a cell-free mechanism such as in a complement-bound immune complex or via the conduit system (Roozendaal *et al.*, 2009). Equally the transport of the TSE agent from the site of infection to the CNS may well also occur through cell-free mechanisms, for example in species where the LRS does not play a role in TSE pathogenesis.

1.5. DTX-mediated conditional cell depletion

DTX is an extracellular protein produced by the organism *Corynebacterium diphtheria*, which inhibits protein synthesis and kills susceptible cells (Holmes, 2000). The toxin is composed of two distinct fragments. The N-terminal fragment A specifically inhibits protein synthesis within the cell, whereas the C-terminal fragment B is required for the recognition of surface markers on the membranes of cells susceptible to infection (Pappenheimer, 1977). Most mammals, such as humans, monkey, and rabbit (Gabliks and Falconer, 1966), are sensitive to diphtheria toxin, except for mice and rats (Morris and Saelinger, 1983). These animals tolerate doses 100,000 higher than those used for sensitive animals (Gabliks and Falconer, 1966)

because surface markers on murine and rat cells do not bind fragment B (Mitamura *et al.*, 1995).

This phenomenon was utilised to establish murine models for the conditional depletion of a specific cell type. This work was first carried out by Saito *et al* (Saito *et al.*, 2001). They established several transgenic mouse models where the diphtheria toxin receptor (DTR) was expressed on the surface of hepatocytes. They tested a wide range of DTX doses. They found that low-dose injections into the mouse caused hepatocyte-specific cell death, without adversely affecting other cells or tissues (Saito *et al.*, 2001).

1.6. Transgenic mouse lines

DTX-mediated ablation has proved a popular method for targeted cell depletion because of its lack of effect on the mouse, it suffers no infection, inflammation etc. Following on from Saito *et al* a number of different transgenic mouse lines have been established using similar techniques. Two different such transgenic mouse lines were used in this thesis, they are described below.

1.6.1. The CD11c-GFP-DTR mouse line

As described above, the mouse's natural resistance to DTX, through their lack of expression of a DTR, has been employed to create transgenic mouse lines, where specific, targeted, cells can be transiently depleted, using a simian DTR transgene, coupled to a gene, whose expression is specific to the target cells. Jung *et al* (Jung *et al.*, 2002) used the CD11c gene, *Itgax*, as a target promoter. By coupling the

transgene encoding the simian DTR-green fluorescent protein (GFP) fusion protein to a CD11c vector, they were able to produce the CD11c-GFP-DTR transgenic mouse line (Fig. 1.4.) (Jung *et al.*, 2002). CD11c is a marker that was previously used to identify DCs, and the presence of the DTR transgene on $CD11c^+$ cells was intended to deplete $CD11c^+$ DCs. However, as CD11c is expressed on a number of different cell subsets, targeted depletion in these mice affects more than just DCs (Table 1.2) (Bradford *et al.*, 2011; Probst *et al.*, 2005).

The CD11c-DTR model has previously been used to study the effect of $CD11c^+$ cell depletion on scrapie uptake from the gut (Raymond *et al.*, 2007), providing a useful reference for the time course of depletion and repopulation of the cells. However, this model has not yet been used with regards to the skin, and the effect of depletion needed to be analysed in the skin and the skin draining LNs. The study highlighted the depletion of other cell types such as MOMA-2-binding cells in the sub-epithelial domes of PPs (Raymond *et al.*, 2007), marginal zone and metallophillic macrophages in the spleen (Probst *et al.*, 2005), as well as colony stimulating factor 1 receptor $(Csf1r)^+$ cells within the small intestine (Bradford *et al.*, 2011). These characteristics need to be taken into account in the studies using CD11c-DTR mice.

LCs, in contrast to other MNPs, are radioresistant and will remain of host origin up to 18 months after bone marrow reconstitution in lethally γ-irradiated mice (Merad *et al.*, 2002). Lethal γ-irradiation of C57BL/6 wildtype mice prior to reconstitution with bone marrow from CD11c-GFP-DTR mice (CD11c-GFP-DTR→WT) yields bone marrow chimeric mice where host-derived LCs do not express the DTR transgene.

Table 1.2. Summary table of transgenic mouse lines and depletion status of cell types described within the thesis.

			Depletion status					
Host genotype	**Donor genotype**	**DTX**	**CD11c$^+$/CD169$^+$ macrophages**	**CD11c$^+$/CD169$^-$ /langerin$^-$ cells (LN)**	**CD11c$^+$/CD169$^-$ /langerin$^+$ cells (LN)**	**langerin$^-$ dermal DCs**	**langerin$^+$ dermal DCs**	**LCs**
WT	WT	yes d2	no	no	no	no	no	no
WT	CD11c-DTR	yes d2	yes	yes	yes	yes	yes	no
WT	CD11c-DTR	no	no	no	no	no	no	no
WT	CD11c-DTR	yes d6	yes	cell numbers increase	cell numbers increase	cell numbers increase	cell numbers increase	no
WT	CD11c-DTR	no	no	no	no	no	no	no
WT	n/a	yes d2	no	no	no	no	no	no
langerin-DTR	n/a	yes d2	no	no	yes	no	yes	yes
langerin-DTR	n/a	no	no	no	no	no	no	no
WT	langerin-DTR	yes d2	no	no	yes	no	yes	no
WT	langerin-DTR	no	no	no	no	no	no	no
langerin-DTR	WT	yes d2	no	no	no	no	no	yes
langerin-DTR	WT	no	no	no	no	no	no	no

The other $CD11c^+$ cellular subsets are donor derived, and express the DTR transgene. DTX injection depleted $CD11c^+$, donor-derived cells, without affecting LCs (Table 1.2. and Fig. 1.5.). Both CD11c-DTR transgenic mice, and CD11c-DTR bone marrow chimeric mice (Table 1.2) were used in this thesis to characterise the depletion of $CD11c^+$ cells, and to determine whether depletion of $CD11c^+$ cells prior to scrapie infection via skin scarification would affect disease progression.

1.6.2. The langerin-EGFP-DTR mouse line

Based on the method used by Jung *et al*, another DTR-transgenic mouse line was created, the langerin-EGFP-DTR mouse. Here, Kissenpfennig *et al* (Kissenpfennig *et al.*, 2005b) used a human DTR and enhanced green fluorescent protein (EGFP) to create the transgene, which was coupled to langerin (*Cd207* gene) (Fig. 1.4.).

Langerin is expressed on LCs in the epidermis and $langerin^+$ dDCs in the dermis, but there also exists a $langerin^-$ dDC subset. Both these cellular subsets migrate from the skin to the skin draining LNs, where they can still be identified through their langerin expression. A number of other cell types have also been found to express langerin outside of skin draining lymphoid tissues, such as the spleen and thymus (Douillard *et al.*, 2005), or the lung, and liver (Valladeau *et al.*, 2002). This mouse line, therefore allowed for the transient conditional depletion of $langerin^+$ cells within the skin and skin draining LNs (Table 1.2 and Fig.1.6.), in addition to other relevant tissues.

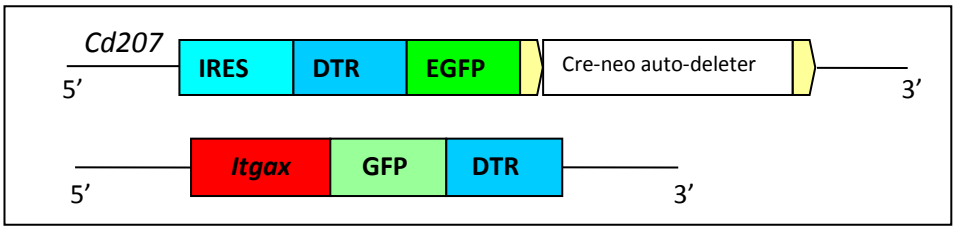

Figure 1.4. Diagram of transgene constructs, modified from Kissenpfennig *et al*, 2005; and Jung *et al*, 2002. The EGFP-DTR transgene was coupled to the *Cd207* (langerin) gene creating the langerin-EGFP-DTR transgene (Kissenpfennig *et al.*, 2005b). The GFP-DTR transgene was coupled to the *Itgax* gene (CD11c) creating the CD11c-GFP-DTR transgene (Jung *et al.*, 2002).

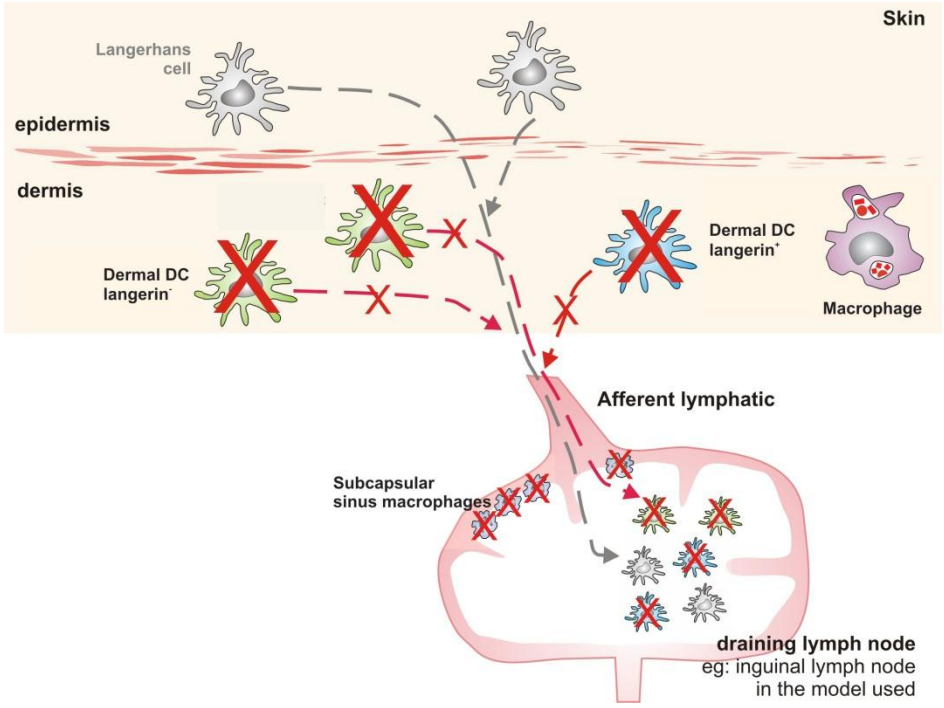

Figure 1.5. CD11c$^+$ cells targeted by DTX in the C57BL/6 wildtype mouse reconstituted with CD11c-DTR bone marrow. CD11c$^+$ cells within the skin and the skin draining LNs, including subcapsular sinus macrophages are temporarily depleted following DTX treatment in the CD11c-GFP-DTR→WT mouse. LCs are unaffected by DTX treatment.

As was mentioned above (section 1.2.3.), LCs are radioresistant, and will remain of host origin following irradiation and bone marrow reconstitution, in contrast to other DC subsets. By lethally γ-irradiating C57BL/6 wildtype mice prior to reconstitution with langerin-EGFP-DTR bone marrow, it is possible to generate a mouse where

only the langerin$^+$ dDCs express the DTR in the skin (Table 1.2). Inversely, reconstitution of lethally γ-irradiated langerin-EGFP-DTR mice with C57BL/6 wildtype bone marrow creates a mouse where only the epidermal LCs express DTR (Table 1.2), and are susceptible to DTX-mediated conditional depletion. These sets of mice were used in this thesis to characterise the depletion of langerin$^+$ cells (Table 1.2), and to determine whether depletion of langerin$^+$ cells prior to scrapie infection via skin scarification would affect disease progression.

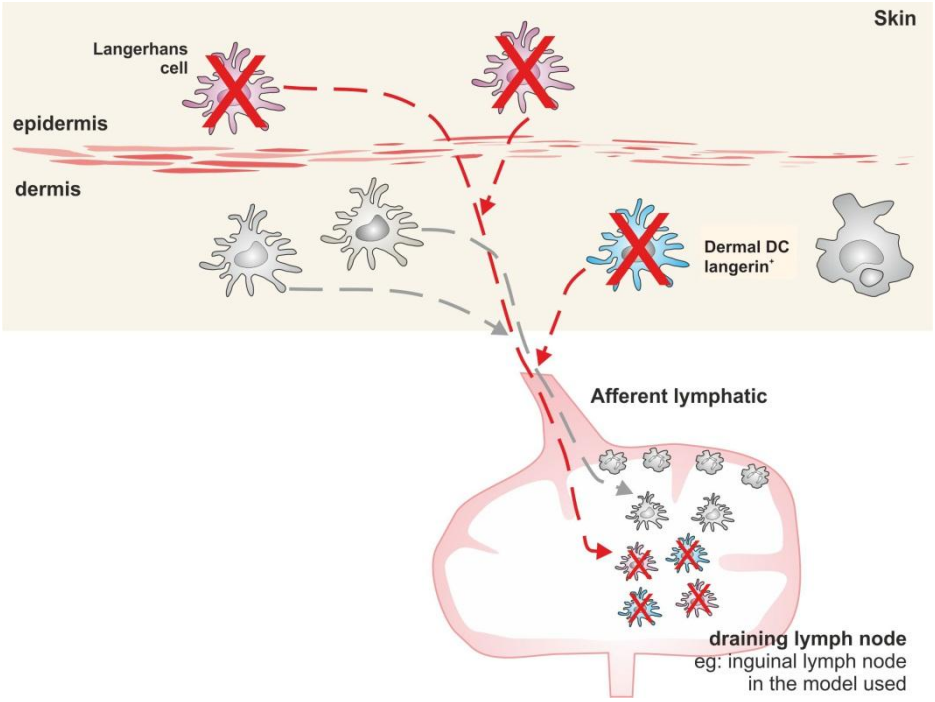

Figure 1.6. Langerin$^+$ cells targeted by DTX in the langerin-DTR mouse. Langerin$^+$ cells within the skin and skin draining LNs are temporarily depleted following DTX treatment in the langerin-EGFP-DTR mouse.

1.7. Thesis aims

Studies addressing the MNPs that influence TSE transmission from the skin have previously been carried out using an *in vitro* model of mature LCs (Mohan *et al.*,

2005c) or by blocking LC migration from the skin through the absence of CD40L ($CD40L^{-/-}$ mice) or caspase-1 inhibition (Mohan *et al.*, 2005b). CD40L is expressed on B lymphocytes, macrophages, DCs and endothelial cells, so therefore CD40L deficiency is likely to affect the activities of many cells other than LCs. The development of transgenic mice where it is possible to temporarily deplete individual MNP cell types provides a more useful tool for determining whether specific cell types play a role in the transport of the TSE agent from the skin to the draining iLN. By using lethal γ-irradiation and bone marrow reconstitution it is further possible to target individual cell types for DTX-mediated depletion.

The main aim of this thesis was to test the hypothesis that individual skin-resident MNP subsets play a role in the transport of the scrapie agent from the skin. To do so, experiments were designed where individual MNP subsets were temporarily depleted from the skin or skin draining LNs prior to scrapie infection via skin scarification, to determine whether the absence of the different cell types at time of infection had an effect on early scrapie agent transport from the skin to the draining iLN. The aim of this thesis was also to determine whether the absence of these cell types at the time of infection, via skin scarification, had an effect on the incubation period of disease. Further aims were to use histopathological and gene profile analysis to study how the effects of skin scarification or DTX-mediated cell depletion might influence scrapie disease. The thesis further aimed to determine whether fluorescent tagging of PrP^{Sc} would allow for *in vivo* visualisation of the PrP^{Sc} in the skin and draining iLN soon after exposure via scarification.

2

MATERIALS AND METHODS

2.1. Mice

All experiments were conducted under an appropriate home office project licence within the regulations of the Animals (Scientific Procedures) Act 1986. All individual experiments were scrutinised by the Neurobiology Division's ethical review process prior to commencement.

2.1.1. CD11c-GFP-DTR

The CD11c-green fluorescent protein-diphtheria toxin receptor (CD11c-GFP-DTR) transgenic mouse line, hereafter referred to as CD11c-DTR, were kindly gifted by S. Jung, Weizmann Institute of Science, Rehovot, Israel (Jung *et al.*, 2002). Mice were maintained on a C57BL/6 background. Age matched C57BL/6 were used as non-transgenic controls throughout the experiments.

2.1.2. Langerin-EGFP-DTR

The langerin-enhanced green fluorescent protein-diphtheria toxin receptor transgenic (langerin-EGFP-DTR) mouse line (Kissenpfennig *et al.*, 2005b), hereafter referred to as langerin-DTR, were maintained on a C57BL/6 background. Age matched C57BL/6 were used as non-transgenic controls throughout the experiments.

2.1.3. Housing

Mouse lines were maintained in a conventional animal facility with a 12 hour light and 12 hour dark cycle under specific pathogen free conditions at The Roslin Institute with access to food and water at all times.

2.2. Mouse genotype confirmation

Mice from both transgenic lines were routinely genotyped before inclusion into any experiment. DNA was extracted from tail or ear punches using the DNeasy kit (Qiagen, Crawley, UK) as indicated. Following PCR amplification, PCR products were viewed by running on a 1.5 % agarose gel, containing 0.001 % ethidium bromide (Sigma-Aldrich, Dorset, UK).

2.2.1. Determination of the CD11c-DTR genotype by PCR

PCR for the CD11c-DTR transgenic mice was carried out using the following DTR-specific oligonucleotides (Eurofins MWG/Operon, Ebersberg, Germany), which gave a band of 625 base pairs:

DTR 1: 5'- GCC ACC ATG AAG CTG CTG CCG - 3'

DTR 2: 5'- TCA GTG GGA ATT AGT CAT GCC - 3'

Using the following conditions: 1 cycle: 94 °C 5 min

39 cycles: 95 °C 1min

58 °C 1min

72 °C 1 min

1 cycle: 72 °C 5 min

hold at 4 °C

2.2.2. Determination of the langerin-DTR genotype by PCR

PCR for the langerin-DTR transgenic mice was carried out using the following DTR and langerin-EGFP oligonucleotides (Eurofins), which produced a band of 329 base

pairs for the wildtype *Cd207* gene (langerin), and 866 base pairs for the DTR transgene was coupled to the *Cd207* gene:

lang EGFP 1: 5'- GAA TGA CAG ATC TGG CCT GAG CTC G - 3'

lang EGFP 2: 5'- GTA GCT TTT ATA TGG TCA GCC AAG G - 3'

Dtox up4: 5'- TTC CAG CAG CTA GCC CTC TCC GAA - 3'

Using the following conditions: 1 cycle: 94 °C 3 min

30 cycles: 94 °C 45 s

63.5 °C 45 s

72 °C 1 min

1 cycle: 72 °C 5 min

hold at 10 °C

2.2.3. Determination of the PrP genotype by PCR

PCR for the *Prnp* gene was carried out on experimental bone marrow chimeric mice using the A044 and A045 oligonucleotides, which produced a PCR product with a band size of 765 base pairs:

A044: TCA TCC CAC GAT CAG GAA GAT GAG

A045: ATG GCG AAC CTT GGC TAC TGG CTG

Using the following conditions: 1 cycle: 94^{o}C for 3min

30 cycles: 94 ^{o}C for 30 s

62 ^{o}C for 30 s

72 ^{o}C for 1 min

1 cycle: 72 ^{o}C for 10 min

hold at 4 °C

2.3. Pre-scrapie inoculation treatments

2.3.1. Temporary conditional cell depletion

Diphtheria toxin receptor (DTR) (Sigma-Aldrich, Dorset, UK) was suspended in 5 % lactose in 10 mM phosphate buffer (PB). CD11c-DTR mice were given a single intraperitoneal (i.p.) injection of 100 ng/mouse DTX, to deplete their $CD11c^+$ cells. Langerin-DTR mice were injected i.p. with 1 μg/mouse DTX to deplete their $langerin^+$ cells. Some mice were injected with PB as a control.

2.3.2. Lethal γ-irradiation and bone marrow reconstitution

C57BL/6 wildtype mice were lethally γ-irradiated (1000 rad) with $caesium^{137}$ 24 hr prior to bone marrow reconstitution. Bone marrow single cell suspensions were prepared from the femurs of age and sex matched adult C57BL/6, and CD11c-DTR or langerin-DTR mice in Hank's balanced salt solution (HBSS; Invitrogen, Paisley, UK). Recipient mice were reconstituted with 100 μl bone marrow (3×10^7 - 4×10^7 cells/recipient mouse) injection into the tail vein. Mice were housed in individually ventilated cages, to prevent opportunistic infection, and used in subsequent experiments as described.

2.4. Inoculation with the scrapie agent

2.4.1. The ME7 scrapie agent strain

All scrapie pathogenesis studies described in this thesis were conducted using the ME7 scrapie agent strain (Zlotnik and Rennie, 1963). Mice were inoculated with brain homogenates prepared from terminally scrapie-affected mice or uninfected mice as described below. Two routes of inoculation were used in these experiments: intra-cerebral (i.c.) injection (section 2.4.3.); and skin scarification of the inner thigh

(section 2.4.4.). Mice were monitored following inoculation and any animals showing adverse reactions during the course of the experiment were killed using Schedule 1 procedure.

2.4.2. Purification of scrapie associated fibrils (SAF) for fluorescent labelling with Alexa-Fluor®546 succinimidyl ester

SAF Preparation: Brains from ME7 terminal mice were thawed, pooled, homogenised in Dounce homogenisers with 10 ml brain lysis buffer (0.01 M sodium phosphate pH 7.4, 10 % sarcosine), and topped up to 25 ml before transfer to Oak Ridge centrifuge tubes (Thermo Scientific Nalgene, Loughborough, UK). Tubes were centrifuged in the RC-5B centrifuge (Sorvall, DJB Labcare Ltd, Newport Pagnell, UK), using the SS34 rotor at 22,000 x *g* at 10 ºC for 30 min.

Supernatant was transferred into Beckman polycarbonate centrifuge bottles, with cap assembly (355618, Beckman Instruments, USA). Samples were centrifuged in the L8-60 Ultra centrifuge (Beckman), using the Ti70 rotor at 215,000 x *g* at 10 ºC for 2 hr 30. Supernatants were discarded and pellets suspended in 3 ml water, and incubated at room temperature (RT) for 1 hr. 6 ml iodide solution (0.9 M potassium iodide, 9 mM sodium thiosulphate, 15 mM sodium phosphate pH 8.5 with HCl, 1 % sarcosine) was added to samples and carefully layered onto a 3 ml sucrose cushion (20 % sucrose in iodide solution) in Beckman Ultraclear tubes (344059, Beckman) and centrifuged in the L8-60 Ultra centrifuge, in the SW41 rotor at 285,000 x *g* at 10 ºC for 90 min. Supernatants were carefully discarded, and tubes were left upside down overnight at RT on absorbent paper to dry off any excess fluid. Pellets were suspended in 1 ml 0.1 % Sarkosyl/ phosphate buffered saline (PBS) and centrifuged

in a benchtop microfuge at 16,000 x *g* at RT for 30 min. Pellets were suspended in 20 µl 0.1 % Sarkosyl/ PBS (approximately 1 µg/µl). To aid suspension, samples were sonicated (Sonicator, Ultrasonic Processor XL, Heat Systems) with 10 s bursts.

Fluorescent tagging of the SAF with Alexa-Fluor®546 succinimidyl ester: 2 µl Alexa-Fluor®546 succinimidyl ester (Invitrogen) was added to each sample (1 volume to 10 volumes of sample) and incubated at RT for 1 hr with constant agitation (in the dark). The reaction was quenched overnight at 4 ºC by adding 1 volume of 1.5 M hydroxylamine (pH 8.5) for 10 volumes of dye reaction. Labelled samples were washed in excess of 5 times in 0.1 % Sarkosyl/ PBS at RT for 10 min at 18,700 x *g*, ensuring that the supernatant of the final wash was clear and colourless. Pellets were suspended in 20 µl of 0.1 % Sarkosyl/ PBS, sonicated with 10 s bursts to aid suspension, and stored at - 20 ºC.

Preparation of the SAF-Alexa-Fluor®546 inoculum: Samples were thawed and sonicated with 10 s bursts, before separating into two aliquots. Proteinase K (Roche Diagnostics Ltd., UK) was diluted 1:10 to make a 2000 µg/ml solution. Proteinase K was added 1:20 to the samples to give a working concentration of 100 ng/ml. Samples were incubated at 37 ºC for 1 hr with agitation or 100 mM PMSF (phenylmethanesulfonylfluoride) (Sigma-Aldrich) was diluted 5-fold, and 2 µl (2 mM final concentration) was added to the other half of samples and incubated on ice for 1 hr, to block protein degradation. Proteinase K treated samples were treated with PMSF for 10 min, to inhibit proteinase K activity. Samples were topped up to 1 ml with 0.1 % Sarkosyl/ PBS, and washed 3 times at RT for 10 min at 18,700 x *g*.

Samples were diluted to a final volume of 760 µl, separated into two equal volumes of 380 µl and sonicated with 10 s bursts to aid suspension, and stored at - 20 ºC, ready for use.

Gel electrophoresis of SAF-Alexa-Fluor®546 inoculum: Alexa-Fluor®546-SAF samples were resuspended in 50 µl sample buffer, and denatured at 90 ºC for 10 min. Samples were loaded equally onto two pre-cast gels (Invitrogen) for electrophoresis according to manufacturer's instructions.

Fluorograph analysis and silver stain of the SAF-Alexa-Fluor®546 inoculum: Following electrophoresis, one gel was fixed in 'fluorofix' (40 % ethanol, 2 % acetic acid in double distilled water (ddH_2O)), prior to fluorescent imaging on a Typhoon Imager (GE Healthcare). Gel was fixed overnight with constant agitation, prior to sensitising (30 ml ethanol, 0.5 ml 25 % glutaraldehyde, 0.2 g sodium thiosulphate, 6.8 g sodium acetate, in 100 ml ddH_2O) for 1hr. The gel was washed 4 x 15 min in dH_2O, before adding silver solution (0.25 g silver nitrate, 40 µl 38 % formaldehyde, added just prior to use, in 100 ml ddH_2O) and incubating with constant agitation for 1 hr. Two 1 min washes preceded developing (2.5 g sodium carbonate, 80 µl 38 % formaldehyde, added just prior to use, in 100 ml ddH_2O) until desired intensity was reached. Developing was stopped by addition of 1.46 g EDTA sodium salt in 100 ml ddH_2O, prior to scanning.

Western blotting of the SAF-Alexa-Fluor®546 inoculum: One gel was transferred onto PVDF membrane (Table 2.4.), which had been fixed in methanol, using a semi-

dry blotter, according to manufacturer's instructions. The blot was washed in Tris buffered saline (TBS)- 0.05 % Tween and blocked in 5 % Marvel- TBS- 0.05 % Tween for 1 hr, prior to probing with mouse anti-PrP monoclonal antibody (mAb), 8H4 1/4000 (Abcam, UK) in 1 % Marvel- TBS- 0.05 % Tween overnight at RT. Blot received 3 x 10 min TBS- 0.05 % Tween, and 2 x 10 min 5 % Marvel- TBS- 0.05 % Tween block before probing with goat anti mouse-HRP antibody (Sigma-Aldrich) for 1 hr. The blot received four 15 min washes before addition of Pierce (Thermo scientific) enhanced chemiluminescence (ECL) substrate (Table 2.4.). Detection film was exposed to blots for predetermined lengths of time and developed using a medical film processor (Konica Minolta SRX-101A).

2.4.3. Intra-cerebral inoculation

For i.c. injection, mice were anaesthetised with 3 % fluorothane gas (delivered in oxygen) prior to inoculation. 20 µl brain homogenate from C57BL/Dk mice terminally affected with the ME7 scrapie agent strain was injected into the right mid-temporal cortex using a 1 ml syringe with a 26 gauge needle. To ensure accuracy the needle was sheathed to expose 2 mm length for injection. Scrapie-affected brain homogenate was used at 1 % dilution in physiological saline.

2.4.4. Inoculation through skin scarification

Mice were scarified on the medial surface of the left inner thigh as previously described, (Glaysher and Mabbott, 2007a; Mohan *et al.*, 2004; Mohan *et al.*, 2005a; Taylor *et al.*, 1996). 24 hours prior to inoculation, a 1 cm^2 area of hair was shaved from the inner left thigh. A 23 gauge needle was used to create an approximately 0.3 cm long abrasion in the epidermis of the skin; care was taken to avoid bleeding. One

drop (approximately 6 µl) of 1 % scrapie inoculum was dropped onto the scarification site by means of a 26 gauge needle and carefully worked into the site with sweeping strokes. The wound was sealed with Op-Site (Smith and Nephew Medical Limited, Hull, UK).

2.4.5. Determination of scrapie incubation period

The scrapie incubation period is defined as the time elapsed (in days) between the day of inoculation and the clinical endpoint of the disease, incubation period was only confirmed when both clinical and pathological scores were positive. All mice were clinically monitored by experienced animal technicians. Mice were assessed weekly on the same day and given a rating as follows: 'unaffected', 'possibly affected', or 'definitely affected'.

The clinical endpoint is defined in one of four ways:

1. The day on which the mouse receives a third consecutive 'definite' rating;

2. The day on which the mouse is culled *in extremis*, or;

3. The mouse is found dead in its cage after receiving a 'definite' rating at the time of scoring the previous week.

Once the clinical end-point had been defined animals were culled humanely and tissues collected for further analysis. This system has been used for many years at The Roslin Institute and has been applied to a wide range of TSE experiments.

2.4.6. Assessment of scrapie pathology in the brain by lesion profiles

Whole brains were cut into five defined areas (Fraser and Dickinson, 1968), fixed in 2% periodate-lysine-paraformaldehyde (PLP) (0.1 M periodate; 0.075 M D-L Lysine; 2% PFA in 0.05 M phosphate buffer pH 7.4) and processed in a tissue

processor before embedding in paraffin wax. 6 µm sections were cut using a microtome and stained with Harris haematoxylin and eosin. Sections were examined by experienced staff to determine the degree of scrapie-specific vacuolation in the neuropil. Vacuolation in the brain was scored on a scale of 0-5 in the following grey matter (G1-G9) areas (Bruce and Fraser, 1982): G1, dorsal medulla; G2, cerebellar cortex; G3, superior colliculus; G4, hypothalamus; G5, thalamus; G6, hippocampus; G7, septum; G8, retrosplenial and adjacent motor cortex; G9, cingulate and adjacent motor cortex (Fraser and Dickinson, 1967; Fraser and Dickinson, 1968).

2.4.7. Histological analysis of skin after scarification

Serial 8 µm sections were cut from snap-frozen tissues at - 20 ºC, using a Leica CM1900 cryostat machine (Leica). Sections were thawed and fixed in 10 % formal saline prior to staining with Harris haematoxylin and eosin (Surgipath).

Analysis was carried out with assistance of a board-certified pathologist. Tissues were examined for evidence of inflammatory infiltrate following scarification with or without scrapie inoculation, and compared alongside fluorescence microscopic analysis for cells indicative of inflammation or of SAF- Alexa-Fluor®546 inoculated tissues.

2.5. *Ex-vivo* analysis

2.5.1. Immunofluorescent histochemistry of epidermal and dermal sheets

Where indicated, ears were separated into dorsal and ventral halves. Subcutaneous fat and cartilage was removed. Skin was floated on 3.8 % ammonium thiocyanate (Sigma-Aldrich) in 100 mM sodium phosphate/100 mM potassium phosphate for 20

min at 37 °C. Epidermal and dermal sheets were separated before fixation in acetone at -20 °C for 15 min (Nagao *et al.*, 2009), before carrying out immunofluorescence histochemistry.

2.5.2. Epidermal sheet separation for tight junction analysis

Dorsal and ventral sides of the ear were separated as before. Ventral sides were floated out, cartilage side down, in PBS containing 0.7 mM Ca^{2+} (important for maintaining tight junction structure). Subcutaneous fat and cartilage were removed and tissues floated out in 95 % ethanol on ice and incubated for 30 min. Ears were dabbed lightly on the surface of PBS to rinse, before being floated out epidermis side up onto 3.8 % ammonium thiocyanate (as above) prewarmed to 37 °C, and incubated at 37 °C for 17-18 min. Tissues were floated out in PBS and transferred onto glass slides (Superfrost slides, Thermo Scientific, UK) to separate the epidermis from the dermis, and immunofluorescence histochemistry was carried out.

2.5.3. Immunohistochemistry and immunofluorescence histochemistry of frozen tissues

Tissue preparation: Thigh skin (hair shaved prior to analysis), ears, spleen, iLN and popliteal LN (Løvik *et al.*, 2007) were fixed in 3 % PFA for 3 hr, or snap frozen in liquid nitrogen and stored at - 150 °C. Following fixation, tissues were washed in PBS, transferred to a 30 % sucrose solution and stored at 4 ºC overnight. Tissues were embedded in Tissue-Tek® OCT Compound™ (Bayer Plc., Newbury, UK), rapidly frozen using isopentane and stored at - 80 ºC. Snap-frozen tissues were embedded in Tissue-Tek® OCT Compound™ prior to sectioning. Serial 8 μm frozen

sections were cut from snap-frozen and PFA-fixed tissues at - 20 ºC, using a Leica CM1900 cryostat machine.

Intracellular labelling: Snap-frozen and PFA-fixed tissue sections were thawed for 30 min, permeabilised for 15 min in 0.1 % saponin, 5 % FCS in PBS, incubated with antibody (Table 2.1.) diluted in the above buffer for 30 min, and washed with the same buffer. Antibodies were detected with appropriate fluorescence-labelled secondary antibodies (Table 2.2.). Sections were mounted using fluorescent mounting medium (Dako, Cambridgeshire, UK).

Immunohistochemistry and Immunofluorescence histochemistry: Snap-frozen tissues were thawed for 30 min, acetone fixed for 10 min and air dried for 15 min. Sections were blocked with appropriate non-specific serum. Antibody was diluted in PBS/ 1 % bovine serum albumin (BSA) (Sigma-Aldrich). For fluorescence labelling, sections were washed with PBS/BSA and antibodies were detected with fluorescence-labelled secondary antibodies (Table 2.2.) and mounted as above. A TSA tyramide amplification kit (Invitrogen) was used to enhance CD11c immunolabelling in skin. For light level imaging, sections were washed in TBS/BSA, labelled with biotinylated secondary antibody (Table 2.2.), VECTASTAIN ABC-AP KIT (Standard*) (Vector Labs, UK) as a tertiary step, followed by VECTOR® Red Alkaline Phosphatase Substrate Kit (Vector Labs). Sections were counterstained with haematoxylin Z to distinguish cell nuclei, and mounted using VectaMount™ AQ Mounting Medium (Vector Labs). Tissues from animals scarified with SAF-Alexa-Fluor®546 was fixed and denatured as previously described (Gousset *et al.*, 2009).

2.5.4. Immunohistochemistry of paraffin embedded tissue (PET) blots

Spleen, LN, or brain were fixed in 2 % PLP and embedded in paraffin wax. 6 µm sections were cut on a microtome and mounted onto Superfrost® Plus slides. Tissue sections were deparaffinised before immunolabelling with primary antibody (Table 2.3). Sections were washed in TBS/BSA, labelled with biotinylated secondary antibody (Table 2.2.), VECTASTAIN ABC-AP KIT (Standard*) as a tertiary step, followed by VECTOR® Red Alkaline Phosphatase Substrate Kit. Alternatively, sections were washed in PBS/BSA, labelled with biotinylated secondary antibody (Table 2.2.), VECTASTAIN Elite ABC Kit (Standard*) as a tertiary step**,** followed by diaminobenzidine (DAB) (Sigma-Aldrich). Sections were counterstained and mounted using VectaMount™ AQ Mounting Medium or Pertex mounting medium (CellPath, UK).

2.5.5. Detection of PrP^{Sc} by PET blotting

Spleen, LN, or brain were fixed in 2 % PLP and embedded in paraffin wax. 6 µm sections were cut on a microtome and mounted onto a nitrocellulose membrane (Bio-Rad Laboratories Ltd., Hertfordshire, UK). Sections were deparaffinised before treatment with Proteinase K 20 µg/ml (Sigma-Aldrich) overnight at 55 ˚C. 3 mol/L guanidine isothiocyanate treatment was carried out prior to blocking with 2 % casein in TBS (pH 7.8) - 0.05 % Tween and incubation with antibodies (Table 2.3). Alkaline phosphatase-conjugated secondary antibodies were used prior to developing with Nitro-blue tetrazolium chloride- 5-bromo, 4-chloro, 3’-indolyphosphate P-toluidine salt (NBT-BCIP®) solution (Sigma-Aldrich) at pH 9.0.

Table 2.1. Primary antibodies for immunohistochemical analysis of frozen sections and epidermal and dermal ear sheets.

Antigen	Clone	Dilution	Source	Catalogue no.
ZO-1 (tight junctions)	T8-754	1/10	M. Furuse, Kobe University (Itoh *et al.*, 1991)	n/a
CD207 (langerin)	929F3.01	5 μg/ml	Dendritics/ Cambridge Bioscience	DDX0362
CD207 (langerin)	929F3.01-Alexa-Fluor®488	20 μg/ml	Dendritics/ Cambridge Bioscience	DDX0362A488
CD11c (ITGAX)	HL3	1/100	BD Biosciences	550283
CD21/CD35 (CR2/CR1)	7G6	1/100	BD Biosciences	553817
CD45R (Ptprc)	RA3-6B2-Biotin	1/100	Caltag Laboratories/ Invitrogen	RM2615
CD11b (ITGAM)	M1/70.15	1/100	AbD Serotec	MCA74GA
CD169 (Siglec-1)	MOMA-1	1/10	AbD Serotec	MCA947
Ly-6B.2 (PMNs)	7/4	1/70	AbD Serotec	MCA771GA
CD35 (CR1)	8C12	1/100	BD Biosciences	558768
PrP^c	1B3	1/1000	Roslin Institute (Farquhar *et al.*, 1989)	n/a

Table 2.2. Secondary and tertiary antibodies for immunohistochemistry.

Antibody	Conjugate	Dilution	Source	Catalogue no.
AffiniPure Rabbit Anti-Mouse IgG (H+L)	biotin	1/500	Stratech scientific/ Jacksons	315-065-003
AffiniPure Goat Anti-Armenian Hamster IgG (H+L)	biotin	1/200	Stratech scientific/ Jacksons	127-065-160
AffiniPure Mouse Anti-Rat IgG (H+L)	biotin	1/500	Stratech scientific/ Jacksons	212-065-168
AffiniPure Goat Anti-Rabbit IgG (H+L)	biotin	1/500	Stratech scientific/ Jacksons	111-065-003
AffiniPure Goat Anti-Rabbit IgG (H+L)	alkaline phosphatase	1/4000	Stratech scientific/ Jacksons	111-055-003
goat anti-rat	Alexa-Fluor®488	15 µg/ml	Invitrogen	A11006
goat anti-rat	Alexa-Fluor®555	5 µg/ml	Invitrogen	A21434
goat anti-rabbit	Alexa-Fluor®647	1/200	Invitrogen	A21244
streptavidin	Alexa-Fluor®488	15 µg/ml	Invitrogen	S11223
streptavidin	Alexa-Fluor®647	1/200	Invitrogen	S21374
TO-PRO®-3 iodide		1 µM	Invitrogen	T3605

2.5.6. Microscopy and analysis

Confocal images were obtained by visualisation through a Zeiss LSM 5 Pascal Axioskop 2 microscope (Carl Zeiss Ltd, UK). Using the multitrack function of the confocal software, LSM5 Pascal version 3.2 SP2, images were captured using Helium Neon (HeNe) lasers 543 nm and 633 nm with LP560 and LP650 filters respectively (LASOS Lasertechnik GmbH, Germany) for Alexa Fluor® 546 or Alexa Fluor® 555 and Alexa Fluor® 647 or TO- PRO®-3 iodide, and an Argon-ion laser 488 nm with Bp filter 505-550 for Alexa Fluor® 488.

For light level microscopy, PET blot sections were examined using a Leica WLD MZ8 stereo light microscope and images were captured using Leica FireCam 3.0. Immunohistochemistry sections were examined using a Nikon Eclipse E800 (Nikon, UK) and captured using Image-Pro Plus version 6.2 (Media Cybernetics, Inc., USA).

2.5.7. Western Blot analysis

Spinal cord was dissected, snap frozen in liquid nitrogen, and stored at - 80 ºC. Samples were stored on ice throughout. Tissues were weighed, and a 10 % homogenate was made up with NP40 lysis buffer. Equal volumes of homogenate were transferred into two separate 1.5 ml screw top tubes. 100 ng/ml final concentration of Proteinase K was added to one of half of the tubes, and samples placed at 37 ºC for 1 hr with constant agitation. 1 µl PMSF was added to the other half of the samples and these were centrifuged at 16,100 *g* for 20 min at 4 ºC. Supernatants were split into 50 µl aliquots and snap frozen in liquid nitrogen before storage at - 80 ºC. 1 µl PMSF was added to proteinase K treated samples before the samples were centrifuged, aliquoted and frozen as above.

Table 2.3. Antibodies for immunohistochemical analysis of PET blot sections

Antigen	Clone	Dilution	Source	Catalogue no.
PrP	6H4	1/1000	Prionics	01-010
PrP	1B3	1/1000	Roslin Institute (Farquhar *et al.*, 1989)	
CD21/CD35 (CR2/CR1)	7G6	1/100	BD Biosciences	553817
CD45R	RA3-6B2-Biotin	1/100	Caltag Laboratories/ Invitrogen	RM2615
glial associated fibrillary protein (GFAP)		1/400	Dako	Z0334
Iba1		1/1000	Wako	019-19741

Table 2.4. Reagents used for Western blot analysis

Reagents	Source	Catalogue no.
NuPAGE® 4-12% Bis-Tris Gel 1.0mm x 15 well	Invitrogen	NP0323BOX
NuPAGE® MES SDS Running buffer (20X)	Invitrogen	NP0002
NuPAGE® Sample Reducing Agent (10X)	Invitrogen	NP0009
NuPAGE® LDS sample buffer (4x)	Invitrogen	NP0007
NuPAGE® Antioxidant	Invitrogen	NP0005
NuPAGE® Transfer Buffer (20X)	Invitrogen	NP0006-1
Invitrolon™ PVDF/Filter Paper Sandwiches	Invitrogen	LC2005
SeeBlue® Plus2 Pre-Stained Standard	Invitrogen	LC5925
BupH™ Tris Buffered Saline Pack	Thermo Scientific	28376
SuperSignal West Dura Chemiluminescent Substrate	Thermo Scientific	34075
Lumi-Film Chemiluminescent Detection Film	Roche	111 666 657001

Samples were thawed on ice, 40 % solutions were made up in NuPAGE® sample buffer, with sample reducing agent, diluted 1:10. Samples were denatured at 70 ºC for 15 min before centrifugation. 15 µl of sample were loaded onto NuPAGE® gels. Gels were electrophoresed and transferred onto PVDF membrane according to manufacturer's instructions.

The following steps were all carried out with constant agitation on The Belly Dancer® (Stovall Life Sciences, Inc., USA). PVDF membranes were fixed in methanol, washed in water, then TBS, prior to blocking overnight in 10 % Marvel/TBS 0.1% Tween at 4 ºC, to reduce background noise. Blots were probed with rabbit polyclonal anti-PrP antibody, 1B3, 1/8000 for 1 hr. Blots received three 15 min washes before probing with goat anti rabbit-IgG-HRP antibody (sc-2004, Santa Cruz Biotechnology, Inc.) for 1 hr. Blots received three 15 min washes before addition of Pierce enhanced chemiluminescence (ECL) substrate. Detection film was exposed to blots for predetermined lengths of time and developed using a medical film processor (Konica Minolta SRX-101A).

2.5.8. Microarray analysis

Tissues were collected into RNAlater (Ambion) and stored overnight at 4 ˚C before transfer to clean eppendorf tubes and storage at - 80 ˚C. RNA was extracted as follows. Tissues were added to 1 ml Tri Reagent in a Lysing Matrix D Tube (Fisher MBR-247-110Y), and homogenised in a FastPrep FP120 at 4 m/s for 20 s. Samples were incubated at RT for 5 min. 200 µl 1-bromo-3-chloropropane (BCP) (Sigma) was added and tubes vigorously shaken for 15 s before incubating at RT for 3 min.

Samples were centrifuged at 12,000 x *g* for 15 min at RT. Aqueous (upper) phase (approximately 500 µl) was transferred to a new tube. 500 µl propan-2-ol was added to each sample and vortexed before a 10 min incubation on ice. Samples were centrifuged at 12,000 x *g* for 30 min at RT. Supernatant was removed and pellets were washed with 1 ml 75 % ethanol. Samples were vortexed and centrifuged 12,000 x *g* for 15 min at RT. Supernatants were removed and pellets were air-dried for 5-10 min. Pellets were resuspended in 30 µl RNase-free water, vortexed and left on bench for 15 min, and stored at - 80 ºC. The following work was carried out by ARK-Genomics (Roslin Institute). A Bioanalyzer (Agilent Technologies) was used to check RNA quality. RNA was reverse transcribed to cDNA and amplified using GeneChip IVT Express Kit (Affymetrix, UK), and cDNA was hybridised to Mouse 430_2.0 Affymetrix™ chips for analysis on a GeneTitan®.

Normalisation of raw data, annotation of probe sets, and Pearson correlation were carried out by Dr Neil Mabbott. Raw data (.cel) files were normalised using RMA express (http://rmaexpress.bmbolstad.com/). Probe sets were annotated using the latest libraries available from Affymetrix (http://www.affymetrix.com) and samples were arranged according to cell-type grouping to ease interpretation of the data. Normalised, non-log transformed gene expression data were imported into BIOLAYOUT EXPRESS 3D, a tool specifically designed for the visualisation of large network graphs (Freeman *et al.*, 2007; Theocharidis *et al.*, 2009). A sample-to-sample correlation matrix was calculated and a graph was plotted using sample-to-sample relationships > 0.9. In this context nodes represent individual data sets (cells) and the edges between them Pearson correlation coefficients above the selected

threshold. Next, a pairwise transcript-to transcript Pearson correlation matrix was calculated based on each transcript's profile across all samples. A Pearson correlation coefficient cut-off threshold of r = 0.9 was selected and an undirected network graph of these data was generated. In this context nodes represent individual probe sets (genes/transcripts) and the edges between them Pearson correlation coefficients above the selected threshold. The network was clustered into groups of genes sharing similar profiles using the built-in Markov Clustering (MCL) algorithm at an MCL inflation value (which controls the granularity of clustering) (Freeman *et al.*, 2007) set to 2.2. The graph of these combined data sets was explored to understand the significance of the gene clusters and functional relationships between the cell populations investigated.

2.6. Statistical analysis

Statistical analysis was carried out with guidance from Dr Darren Shaw (R(D)SVS, University of Edinburgh). Prior to consideration of results, normality of residuals was established. When samples were normally distributed, they were analysed using a one way analysis of variants. Samples that were not normally distributed were analysed using a non-parametric test, the Kruskal-Wallis test was used on sample medians. Tests on power and sample size were carried out using one way analysis of variants to determine how many mice would have been required in each group for statistical significance.

3

CHARACTERISATION OF DIPHTHERIA TOXIN INDUCED CELL DEPLETION IN THE CD11c-DTR MOUSE

3.1. Abstract

Mice are naturally resistant to DTX. This has permitted the creation of a transgenic mouse line where DTRs are expressed on the surface of target cells, allowing for the temporary depletion of these cells after a single injection of DTX. The CD11c-DTR mouse line enables the temporary conditional depletion of $CD11c^+$ cells, traditionally believed to encompass DC subsets. CD11c is expressed on a number of different cellular subsets within the various tissues such as the skin and peripheral lymphoid organs. By carrying out an analysis of skin and lymphoid tissues following DTX-mediated depletion, it was possible to create a timeline for the depletion and repopulation of $CD11c^+$ cells within these tissues. It was also possible to determine that the temporary depletion of these cells did not adversely affect lymphoid tissue microarchitecture within the mice. Epidermal LCs are radioresistant and remain of host origin up to 18 months post irradiation and reconstitution. By creating bone marrow chimeric mice through reconstitution of lethally γ-irradiated wildtype mice with CD11c-DTR transgenic bone marrow it was possible to analyse depletion and repopulation of $CD11c^+$ cells with the exception of LCs. It is thereby possible to gain a better understanding of the different roles and functions of distinct skin resident DC subsets, through the targeted depletion of distinct cell populations.

3.2. Introduction

The CD11c-DTR transgenic mouse line (Jung *et al.*, 2002), allows for the temporary conditional depletion of $CD11c^+$ cells, which repopulate tissues within a tissue specific time frame. This technology has been used to study the function of $CD11c^+$ cells in a range of diseases, such as Herpes Simplex virus (Kassim *et al.*, 2006), Listeria (Waite *et al.*, 2011), or even scrapie (Raymond *et al.*, 2007). $CD11c^+$ cells are located in a range of different tissues. As cells of the immune system there is a large proportion of these cells within the peripheral lymphoid tissues (Probst *et al.*, 2005), as well as non-lymphoid organs, notably the skin (Jung *et al.*, 2002). It has been believed that the low level CD11c expression on LCs was not sufficient to deplete these cells in the CD11c-DTR mouse. This chapter will clearly demonstrate that LCs are depleted following DTX treatment in CD11c-DTR mice, but it is possible to circumvent this. LCs are radioresistant (Merad *et al.*, 2002), and will remain of host origin up to 18 months after lethal irradiation and bone marrow reconstitution. This is in contrast to other mononuclear phagocyte populations, which are radiosensitive, and are replenished from donor derived precursors following lethal irradiation and bone marrow reconstitution (Merad *et al.*, 2002).

While it was originally thought that CD11c was a marker exclusive to DCs (Hume, 2008), immunohistochemical analysis determined that DCs as well as several macrophage populations were depleted following DTX treatment in CD11c-DTR mice (Bradford *et al.*, 2011; Probst *et al.*, 2005). Probst *et al* also determined that the different $CD11c^+$ cellular subsets repopulated the tissues at varying rates. While traditional DCs have been shown to repopulate the spleen within a matter of days

(Jung *et al.*, 2002), other cell types, such as marginal zone or metallophillic macrophages remained absent for up to ten days post DTX treatment (Probst *et al.*, 2005).

The aim of this chapter is therefore to gain a better understanding of the depletion and repopulation of different $CD11c^+$ cell populations in various tissues following DTX treatment. In doing so, it is hoped that this knowledge will help to provide a better understanding of the potential involvement of $CD11c^+$ cells in scrapie pathogenesis, by using temporary conditional DTX-mediated depletion. Data from this chapter will determine depletion and repopulation dynamics of these different cell subsets after DTX treatment. These data will be utilised in Chapter 4 and Chapter 6 to determine the potential role of these different subsets in scrapie transmission from the skin.

3.3. Results

3.3.1. Detection of the DTR transgene

The presence of the DTR (Heparin binding EGF-like growth factor: *Hbegf*) transgene on the surface of $CD11c^+$ cells in CD11c-DTR mice allows for the temporary depletion of $CD11c^+$ cells through a single i.p. injection of DTX. These mice were utilised to study and determine a timeline for the depletion of $CD11c^+$ cells in the skin and lymphoid tissues. Genotyping was routinely carried out on all CD11c-DTR mice to confirm presence of the DTR transgene before inclusion in any experiment. The two DTR oligonucleotides used produced a PCR product with a band size of 625 base pairs, as shown in Fig. 3.1. The absence of the DTR transgene in a sample would have resulted in a complete absence of PCR product, a blank well (Fig. 3.1.).

3.3.2. Effect of DTX-mediated $CD11c^+$ cell depletion on epidermal LCs

To examine the effect of DTX on LCs of the epidermis, 3 CD11c-DTR mice from each of the following time points received a single i.p. injection of 100 ng DTX, or PB control, and tissues were collected for *ex vivo* analysis 0, 1, 2, 4, 6, 8, and 14 days post injection. Immunofluorescent analysis was carried out on epidermal sheets to determine the effect of DTX on LCs. Despite low level CD11c expression on LCs in the epidermis (Jung *et al.*, 2002), a partial depletion was observed from 2 days after DTX injection (Fig. 3.2.). Depletion was not complete, as a number of areas were detected that still contained LCs. The morphological difference detected in the LCs can be seen in Fig. 3.3. The network created by LCs in the epidermis under steady state conditions (without stimulus) was observed in the untreated control mice. The LCs presented long, thin branched dendrites. By contrast, following DTX injection, cell bodies were rounded and dendritic processes had been retracted. These

observations resemble morphological changes observed in LCs following mechanical stress of the skin (Kissenpfennig *et al.*, 2005b).

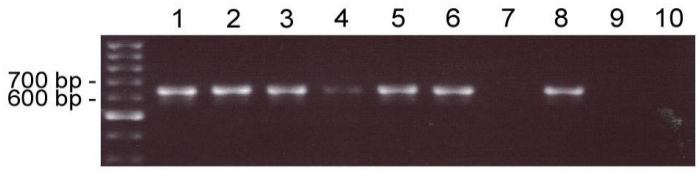

Figure 3.1. DTR PCR on CD11c-DTR mice. Lane 1: DNA ladder; lanes 1-6: samples from CD11c-DTR mice genotyped prior to inclusion in the experiment; lane 7: blank lane; 8: positive control, another CD11c-DTR sample from a previous PCR; 9: wildtype negative control; 10: dH_2O negative control.

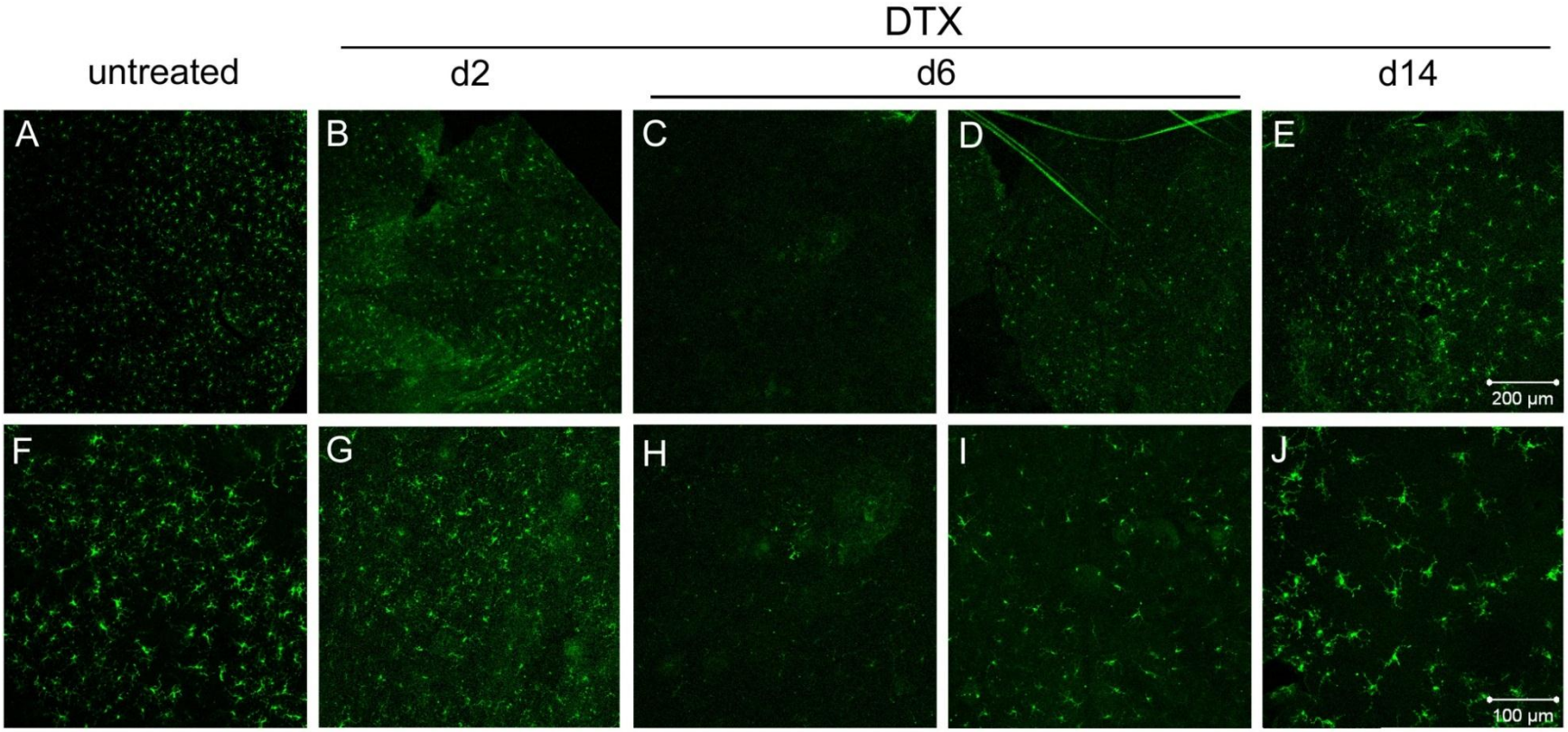

Figure 3.2. LC depletion timeline in ear epidermal sheets from CD11c-DTR mice. Mice received a single i.p. injection of DTX and epidermal ear sheets collected at the time points indicated were immunolabelled with the anti-langerin specific antibody (green). Only one field of view is represented, except for day 6 post injection, when two fields of view were selected to show the differences that were found in the same ear sheet. (**A**,**F**) Normal distribution of langerin^{+} cells within the epidermal sheets without DTX treatment. Two days after DTX injection, (**B**,**G**) a partial depletion of LCs was observed. By day 6 after DTX treatment (**C**,**H**,**D**,**I**), cells remained depleted, although this was not uniform throughout the tissues. **F-J** represent higher (2 x) magnification images of **A-E**, where it was clearer to distinguish the disruption to the morphology of the LCs. In mice treated with DTX there appeared to be more cellular debris and the cells' dendritic processes appeared less intact. The LC network appeared more disrupted, not as many cells were observed and they did not appear intact, compared to the animals that had not received DTX. Images are representative of observations in 3 animals/time point. top row, 200 µm; bottom row, 100 µm.

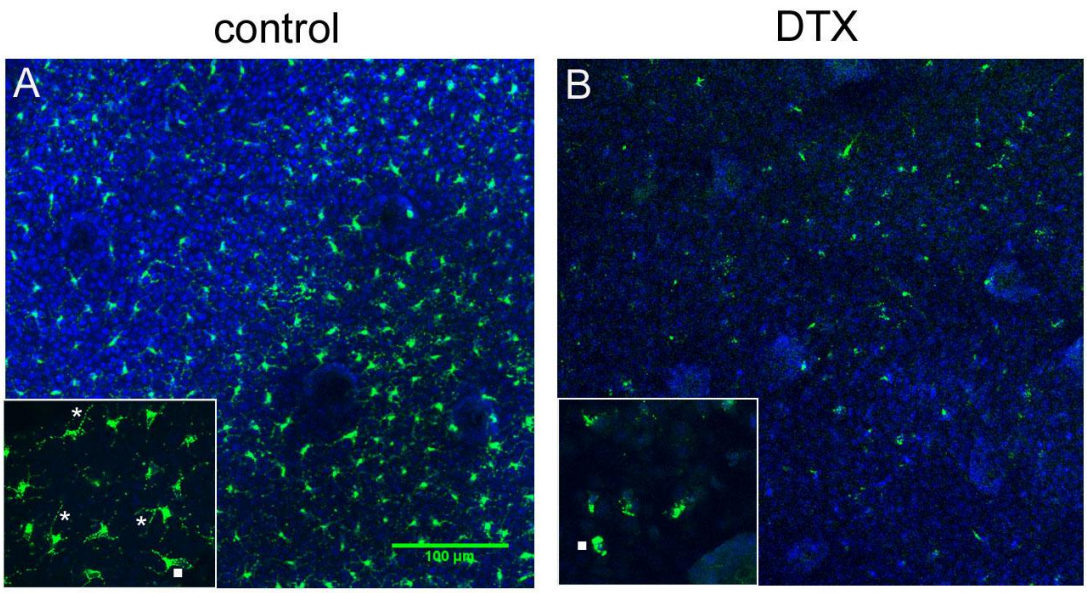

Figure 3.3. LC depletion in the epidermis of CD11c-DTR mice 4 days post DTX injection. CD11c-DTR mice were given a single i.p. injection of DTX, or PB control and epidermal ear sheets collected 4 days later. Immunofluorescent labelling of LCs with the anti-langerin specific antibody (green) and TO-PRO®-3 iodide nuclear counterstain (blue) revealed morphological changes of LCs in ear epidermal sheets following treatment with DTX or PB control. **A** shows healthy LCs, the cell bodies are elongated (▪ next to cell bodies), and long branched dendritic processes were observed (∗). **B** shows effect of DTX on LCs. Cell numbers were reduced, cell bodies (▪) appeared more rounded and lacked their dendritic processes (∗) compared to the LCs in untreated mice. Images are representative of observations in 3 different animals. **A** and **B** 200 x magnification. Inserts, 600 x magnification. Scale bar: 100 µm.

3.3.3. Depletion of CD11c$^+$ cells

To examine the depletion of CD11c$^+$ cells in the CD11c-DTR mice, animals were given a single i.p. injection of 100 ng DTX, or PB control, and tissues were collected from 3 mice in each group, for *ex vivo* analysis at 0, 1, 2, 4, 6, 8, and 14 days post injection. Immunofluorescence analysis carried out on ear cross sections confirmed a reduction in the number of CD11c$^+$ cells in both the epidermis and in the dermis following DTX injection (Fig. 3.4.). The CD11c$^+$ cells in the epidermis were most likely LCs, (as illustrated in Figs. 3.2. and 3.3.), and were still depleted 6 days post DTX injection. Dermal DCs are less abundant than the LCs in the epidermis, and not as uniformly distributed (Nagao *et al.*, 2009). This was evident in the untreated mice, panel A. A reduction in CD11c$^+$ cell numbers in the dermis was observed by day 2 post DTX injection; more cells appeared to be present in the dermis 6 days post DTX injection.

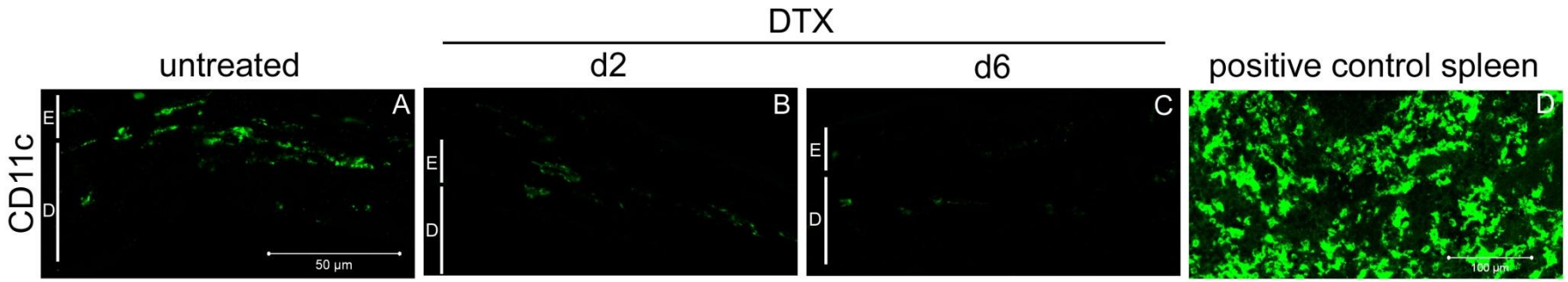

Figure 3.4. CD11c$^+$ cell depletion in the skin. Mice were given a single i.p. injection of DTX and tissues collected at the times indicated were analysed by immunofluorescence with the anti-CD11c specific antibody (green). E and D indicate the epidermis and dermis, respectively, of the skin of the ear. Normal CD11c$^+$ LCs of the epidermis and CD11c$^+$ DCs of the dermis can be visualised in **A**. **B** and **C** show reduced numbers of CD11c$^+$ cells in both the epidermis and the dermis, up to 6 days post DTX injection. **D**: positive control spleen showing abundance of CD11c$^+$ cells. Images are representative of observations in 3 different animals. Scale bar: skin, 50 µm; spleen, 500 µm.

In accordance with previous studies (Jung *et al.*, 2002; Probst *et al.*, 2005; Raymond *et al.*, 2007), immunohistochemical analysis of spleen, iLN and pLN shows that $CD11c^+$ cells were partially depleted in all three tissues, two days after DTX treatment (Fig. 3.5.). The effect of DTX treatment on $CD11c^+$ cells was transient, as cell numbers had started to increase by 6 days post injection.

3.3.4. Effect of DTX treatment on other cell types

To examine the effect of DTX on other cell types, spleen and iLN from DTX and PB injected animals were immunofluorescently analysed to determine any potential secondary effect of DTX on CD35 expressing FDCs and B lymphocytes. No differences were observed in the distribution of CD35 expression following DTX injection either 2 or 6 days post injection (Fig. 3.6.).

Further immunofluorescence analysis confirmed that $CD11c^+CD169^-$ cells were partially depleted in the spleen two days post DTX injection (Fig. 3.7.). By six days post DTX injection cell numbers had started to increase. Immunofluorescent analysis confirmed that $CD11c^+CD169^+$ cells, indicative of metallophilic marginal zone macrophages, were partially depleted and remained depleted for longer than the $CD11c^+CD169^-$ cells. Unlike the results observed with light microscopy ((Probst *et al.*, 2005), and not shown) this is not a complete depletion. CD11c expression is very low on the $CD11c^+CD169^+$ cells (Phan *et al.*, 2009) and there is no observable double labelling.

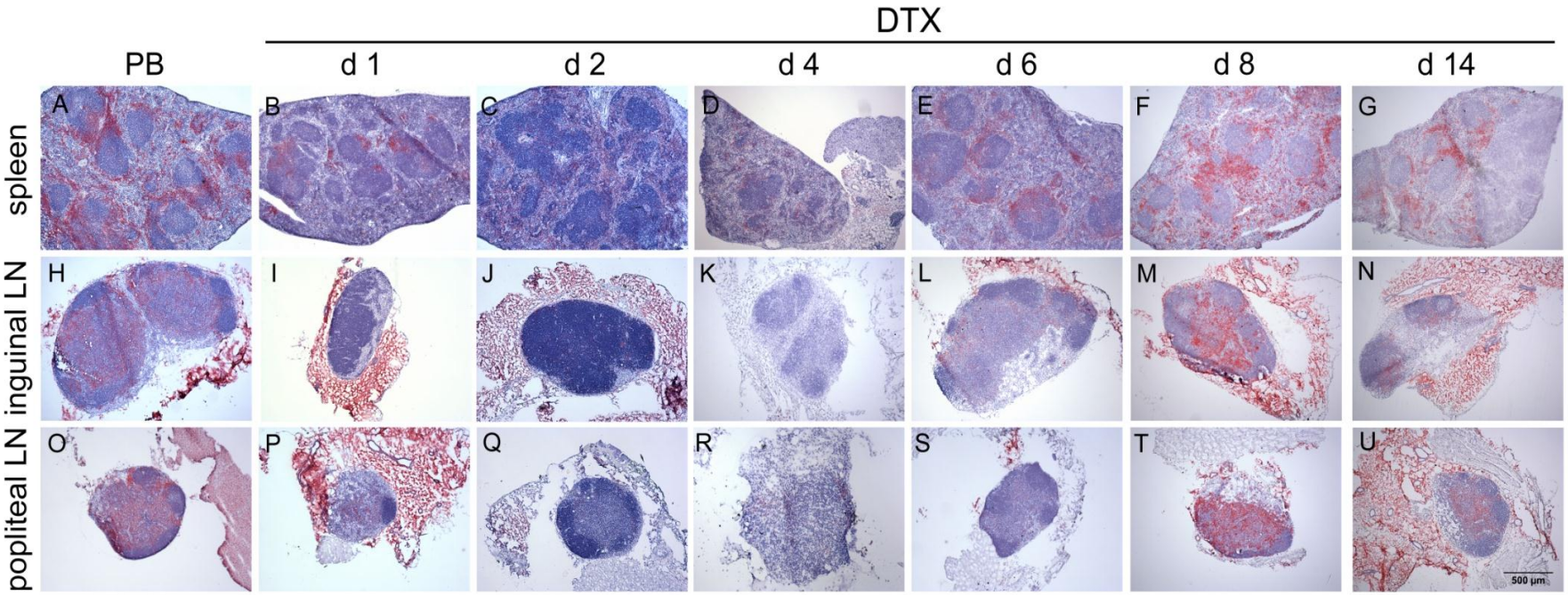

Figure 3.5. DTX-mediated depletion of CD11c$^+$ cells in the spleen, iLN and pLN of CD11c-DTR mice. Mice were given a single i.p. injection of DTX, or PB control, and tissues collected at the times indicated were analysed by immunohistochemistry using the anti-CD11c specific antibody (red). Sections were counterstained with haematoxylin Z (blue). (**A,H,O**) Normal distribution of CD11c$^+$ cells in the three lymphoid tissues in PB control treated mice. A partial depletion of CD11c$^+$ cells was observed from 1 day post DTX treatment (**B**,**I**,**P**). Cells numbers had started to increase by 6 days post DTX treatment (**E,L,S**), and had regained their pre-depleted distribution by 8 days post DTX treatment (**G**,**N**,**U**). Images are representative of observations in 3 different animals/time point. Scale bar: 500 µm.

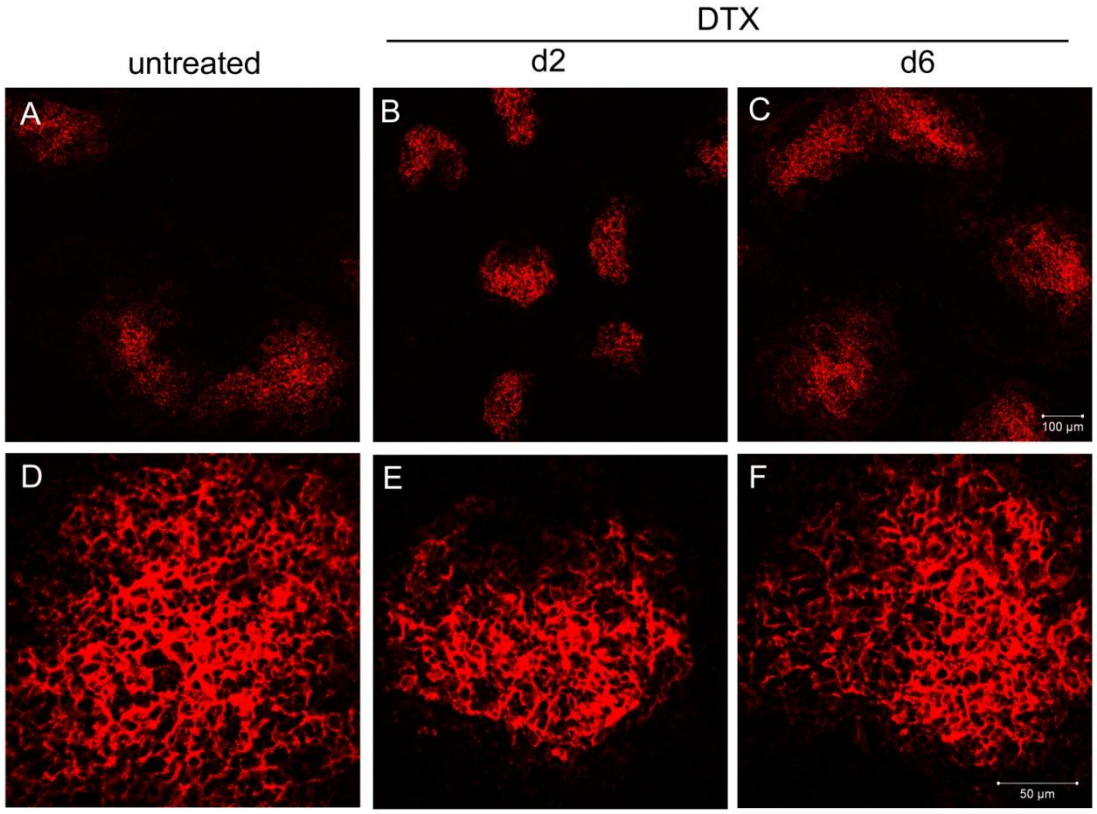

Figure 3.6. Effect of DTX injection on CD35 expression in the spleen. Mice were given a single i.p. injection of DTX and spleens collected at the times indicated were immunofluorescently labelled with the anti-CD35 specific antibody to detect FDCs and CD35-expressing B lymphocytes (red). **D-F** 400 x magnification of **A-C** (100 x magnification). Normal distribution of CD35 expressing cells were observed in the lymphoid follicles of the spleen both at 2 (**B,E**) and 6 (**C,F**) days post DTX injection. Images are representative of observations in 3 animals/time point. Scale bar: top, 100 µm; bottom, 50 µm.

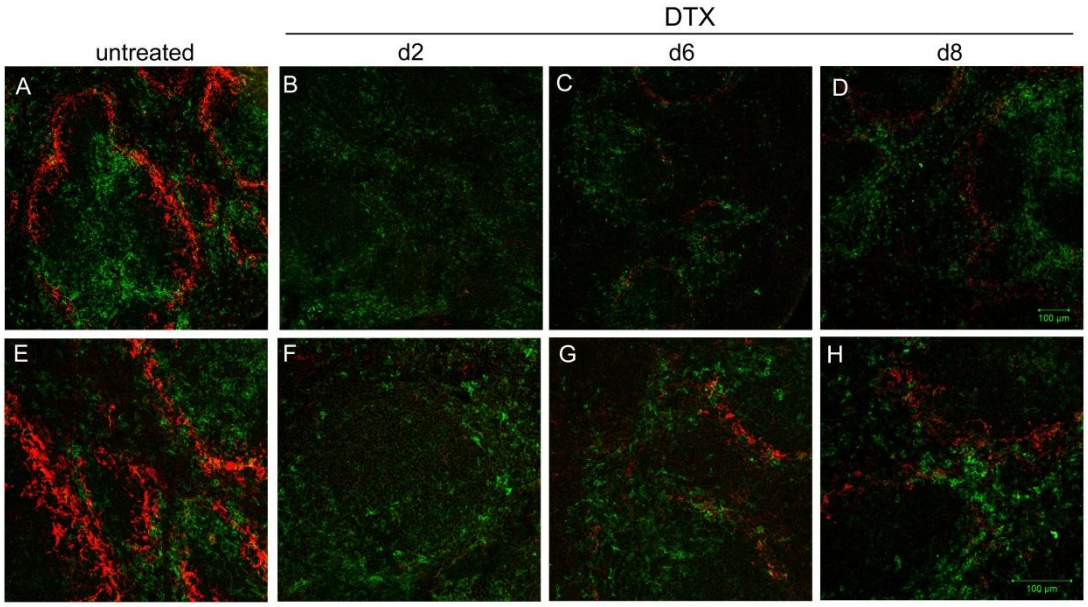

Figure 3.7. DTX-mediated depletion of CD11c$^+$ and CD169$^+$ cells in the spleens of CD11c-DTR mice. Mice were given a single i.p. injection of DTX and tissues collected at the time points indicated were immunolabelled with the anti-CD11c (HL3) specific (green) and the anti-CD169 (MOMA-1) specific (red) antibodies. **F-I** are higher magnification (200 x) images of the top row (100 x). (**A**,**F**) Normal distribution of the cell types (CD11c$^+$CD169$^-$ and CD11c$^+$CD169$^+$) within the spleen without DTX treatment. Two days after DTX treatment, (**B**,**G**) a partial depletion was observed for both cell types. By day 6 after DTX treatment, (**C**,**H**) CD11c$^+$CD169$^-$ cells numbers had started to increase, and appeared more abundant than the CD11c$^+$CD169$^+$ cells. Eight days after DTX treatment (**D**,**I**) CD11c$^+$CD169$^-$ cells appeared to have reached pre-depleted numbers; this was not the case for CD11c$^+$CD169$^+$ (**E**,**J**). Images are representative of observations in 3 animals/time point. Scale bar: 100 µm.

3.3.5. Depletion of langerin$^+$ cells in lymphoid tissues

Immunofluorescent analysis of iLNs and pLNs (not shown) indicated that langerin$^+$ cells were partially depleted in CD11c-DTR mice following DTX treatment (Fig. 3.8.). In contrast to the CD11c$^+$ cells shown in Fig. 3.5., the langerin$^+$ cells in the iLNs remained depleted for longer, and cell numbers appeared to have started to increase by 14 days post DTX injection.

3.3.6. CD11c-DTR bone marrow chimeric mice

C57BL/6 wildtype mice were lethally γ-irradiated 24 hr prior to receiving a full bone marrow reconstitution from CD11c-DTR transgenic mice, or C57BL/6 mice as a control. MNPs in the lymphoid tissues are radio sensitive and will be of donor origin 8 weeks after bone marrow reconstitution (Fig. 3.9.). LCs are radio resistant, and are host derived up to 18 months post irradiation (Merad *et al.*, 2002). LCs should, therefore, not express the DTR transgene as they are of host origin, while the other CD11c$^+$ cells are donor derived, express the DTR transgene, and are susceptible to depletion following DTX treatment (Table 3.1.). Three groups were established (Fig. 3.9. and Table 3.1.) and will hereafter be referred to as WT→WT+DTX (wildtype mouse reconstituted with wildtype bone marrow, injected with DTX); CD11c-DTR→WT+DTX (wildtype mouse reconstituted with CD11c-DTR transgenic bone marrow, injected with DTX); and CD11c-DTR→WT+PB (wildtype mouse reconstituted with CD11c-DTR transgenic bone marrow, injected with PB).

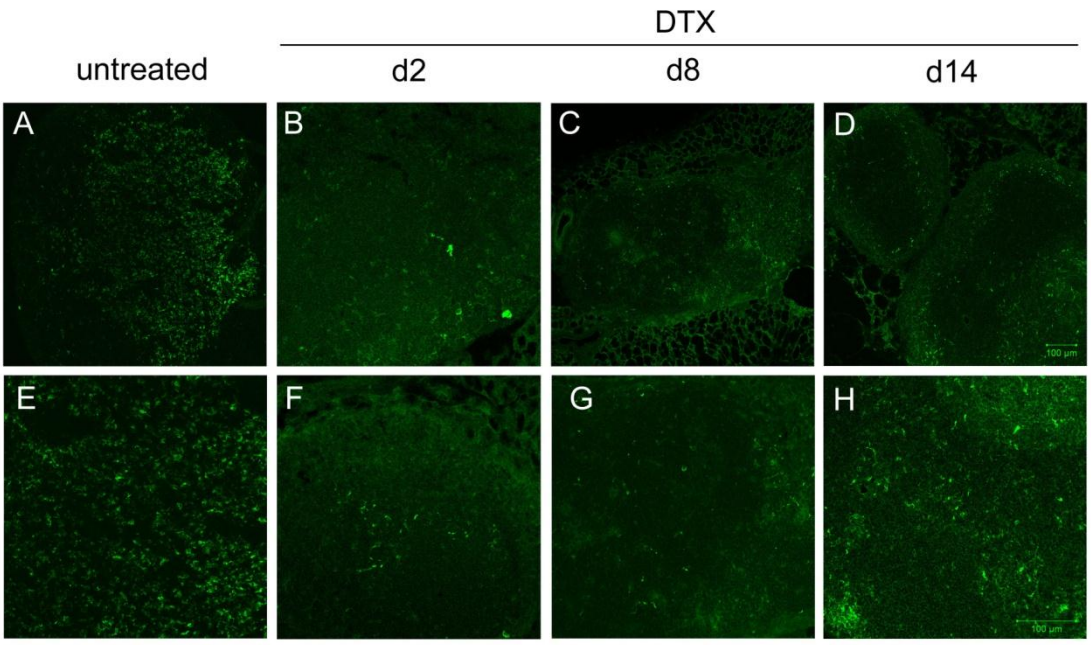

Figure 3.8. Langerin^{+} cell depletion in the iLN. Mice were given a single i.p. injection of DTX, or PB control, and tissues collected at the time points indicated were immunolabelled with the anti-langerin specific antibody (green). **F-J** represent higher magnification (200 x) images of **A-D** (100 x). (**A**,**E**) Normal distribution of the langerin^{+} cells within the iLN without DTX treatment. A partial depletion of langerin^{+} cells was observed in the iLN (**B**,**F**). By day 14 after DTX treatment, (**D**,**H**) cells had not reached pre-depleted numbers. Images are representative of observations in 3 animals/time point. Scale bar: 100 µm.

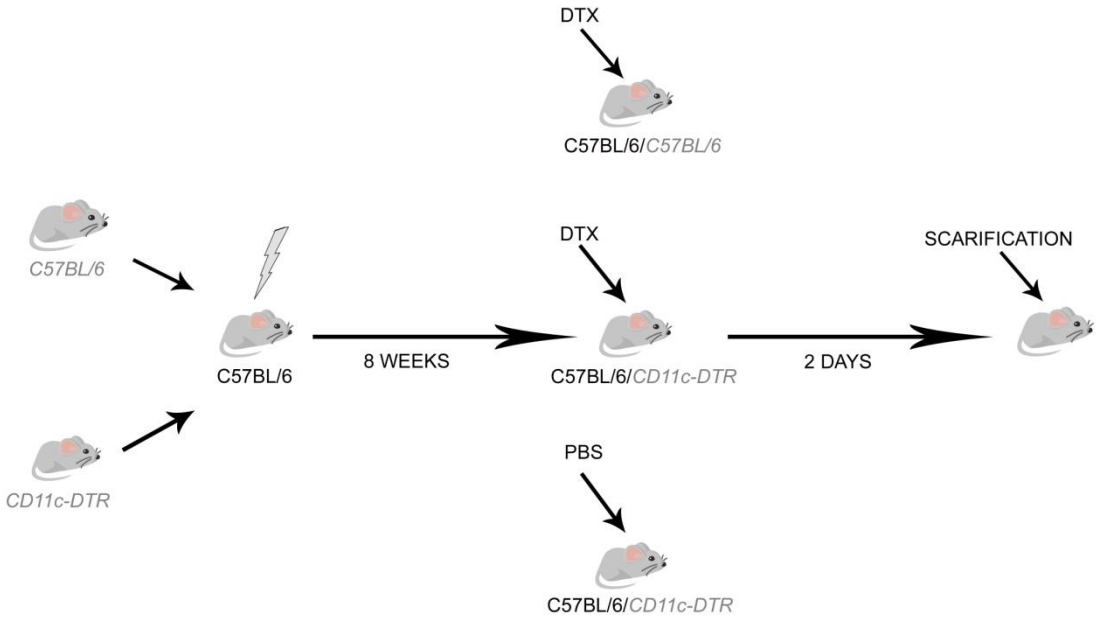

Figure 3.9. Model of irradiation and bone marrow reconstitution. C57BL/6 wildtype mice were lethally γ-irradiated 24 hr prior to receiving a bone marrow graft (grey) from either C57BL/6 mice, as a control, or CD11c-DTR mice. After 8 weeks mice were split into three groups. Mice that received wildtype bone marrow were injected with DTX as a control. Mice that received transgenic bone marrow were injected with DTX, or PB as a control.

Table 3.1. Depletion status of cells following lethal irradiation and reconstitution with CD11c-DTR or wildtype bone marrow.

			Depletion status			
Host genotype	**Donor genotype**	**DTX**	**$CD11c^+/CD169^+$ macrophages**	**$CD11c^+/CD169^-$ /$langerin^-$ cells**	**$langerin^+$ dermal DCs**	**LCs**
WT	WT	yes	no	no	no	no
WT	CD11c-DTR	yes	yes	yes	yes	no
WT	CD11c-DTR	No	no	no	no	no

3.3.7. Confirmation of successful CD11c-DTR bone marrow transplantation

To confirm presence of the DTR (*Hbegf*) transgene, and presence of the *Prnp* gene following lethal γ-irradiation and bone marrow reconstitution, frozen spleen and tail samples from mice in each group were analysed by PCR. The DTR transgene (625 bp) was detected in all animals reconstituted with CD11c-DTR bone marrow. The observed bands were stronger from the spleen samples, compared to tail samples, but this could be accounted for by the abundance of $CD11c^+$ cells in the spleen. The *Prnp* gene (765 bp) was detected in all the spleen and tail samples (Fig. 3.10.).

3.3.8. Effect of DTX injection on langerin$^+$ cells in CD11c-DTR bone marrow chimeric mice

Ear epidermal sheets and iLNs were analysed by immunofluorescent histochemistry using the anti-langerin specific antibody to determine the effect of DTX injection on langerin$^+$ cell status. A partial depletion of langerin$^+$ cells was confirmed in the iLN of DTX treated mice reconstituted with CD11c-DTR bone marrow, consistent with previous results in the CD11c-DTR mouse (Fig. 3.11.). No LC depletion was observed in the epidermis following DTX injection, regardless of whether the animals had been reconstituted with transgenic or wildtype bone marrow (Fig. 3.11.).

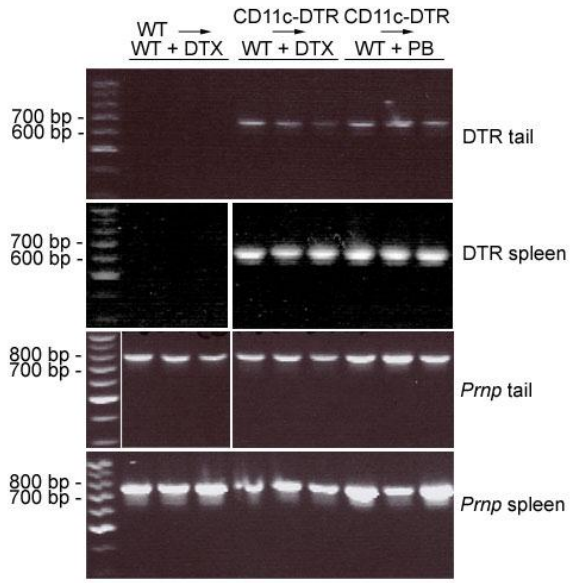

Figure 3.10. DTR and PrP PCR. The DTR transgene was detected in the spleen and tail of mice that had received CD11c-DTR transgenic bone marrow. The *Prnp* gene was detected in the spleen and tail of all animals.

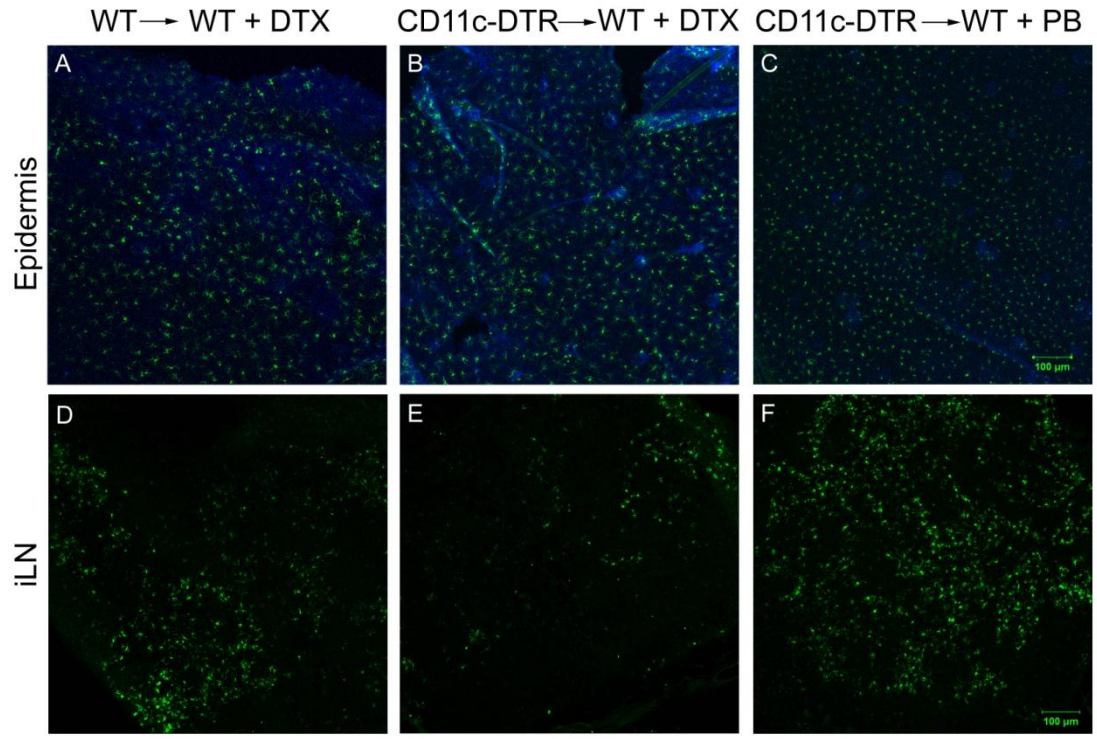

Figure 3.11. Langerin$^+$ cells in the iLN, but not LCs in the epidermis, were depleted in bone marrow chimeric mice following DTX treatment. Mice were given a single i.p. injection of DTX, or PB control, and epidermal sheets and iLNs collected two days later were immunolabelled with the anti-langerin specific antibody (green). Epidermal sheets were counterstained with TO-PRO®-3 iodide (blue). **A-C**: Normal distribution of langerin$^+$ LCs in all three groups. **E**: Partial depletion of langerin$^+$ cells in the iLN of CD11c-DTR→WT+DTX mice in comparison to both control groups (**D**, **E**). Images are representative of observations in 3 animals/group. Scale bar: 100 µm.

3.3.9. Effect of DTX treatment on $CD11c^+$ cell status in wildtype mice reconstituted with CD11c-DTR bone marrow

Immunofluorescent analysis confirmed that both $CD11c^+CD169^-$ and $CD11c^+CD169^+$ cells were partially depleted in the spleens and iLNs of CD11c-DTR→WT+DTX mice. No cellular depletion was observed in either of the control groups (Fig. 3.12.). In contrast with the CD11c-DTR mice (Fig. 3.7.), $CD11c^+$ cell depletion in these bone marrow chimeras did not appear to be as extensive, but $CD11c^+$ cell numbers were reduced 2 days post DTX injection, compared to the two control groups (Fig. 3.12.).

3.3.10. Lethal irradiation, bone marrow reconstitution, and DTX injection has no effect of FDC status

In order to verify that no changes had occurred to modify the lymphoid tissue microarchitecture following irradiation, bone marrow reconstitution, and DTX injection, further analysis was carried out on spleen and iLNs. Tissues from 3 mice in each of the groups outlined in Fig. 3.9. were collected for *ex vivo* analysis two days after DTX injection. The tissues were immunolabelled to detect B lymphocyte subsets and FDCs. Spleen and iLNs were also immunolabelled to detect PrP^c, to determine whether expression was influenced by DTX treatment. No differences were observed for the intensity or location of labelling for the FDCs and B lymphocytes in the CD11c-DTR→WT+DTX animals compared to the two control groups. Equally, the expression of PrP^c on FDC networks was not affected in the CD11c-DTR→WT+DTX mice, when compared to the control animals in either the spleen (Fig. 3.13.) or iLN (Fig. 3.14.).

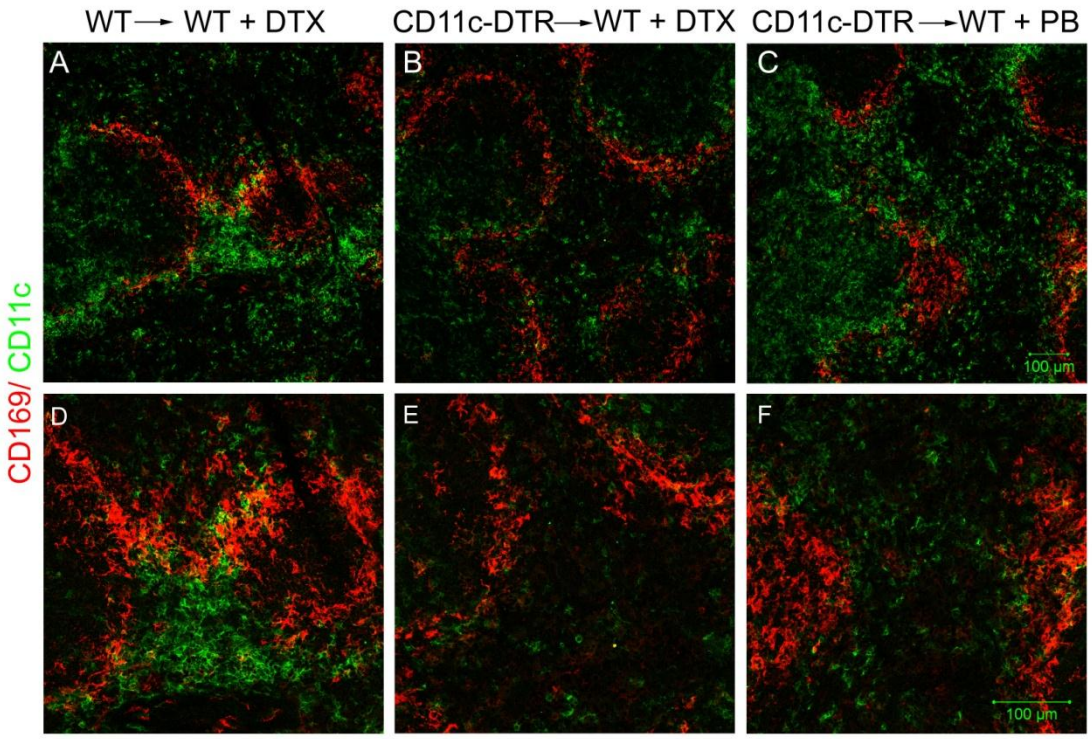

Figure 3.12. Confirmation of $CD11c^{+}CD169^{+}$ depletion two days post DTX injection. Mice were given a single i.p. injection of DTX and spleens collected two days later were immunolabelled with the anti-CD11c specific (green) and the anti-CD169 specific (red) antibodies. **D-F** represent higher magnification (200 x) images of the top row (100 x). WT→WT+DTX (**A**,**D**) and CD11c-DTR→WT+PB (**C**,**F**) control bone marrow chimeric mice showed distribution of $CD11c^{+}CD169^{-}$ and $CD11c^{+}CD169^{+}$ that correlates with previous controls. (**B**,**E**) CD11c-DTR→WT+DTX mice, both $CD11c^{+}CD169^{-}$ and $CD11c^{+}CD169^{+}$ cell subsets were partially depleted. Images are representative of observations in 3 animals/group. Scale bar: 100 µm.

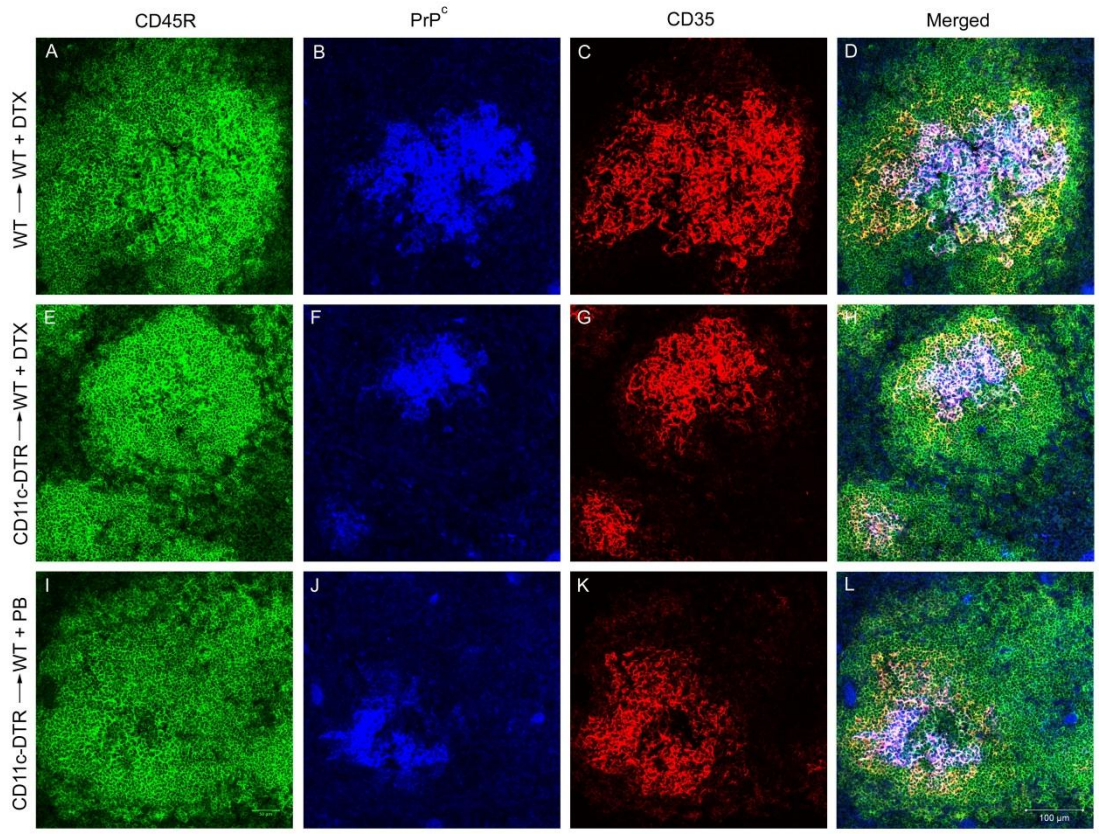

Figure 3.13. DTX treatment had no effect on FDC and B lymphocyte status in the spleen. Mice were given a single i.p. injection of DTX, and spleens collected two days later were immunolabelled with the anti-CD45R specific antibody to detect B lymphocytes (green, **A**,**E**,**I**); the anti-CD35 specific antibody to detect FDCs and CD35-expressing B lymphocytes (red, **C**,**G**,**K**); and the pAb 1B3 to detect PrP^c (blue, **B**,**F**,**J**). Comparison between the 3 groups indicated no effect of irradiation, bone marrow reconstitution, or DTX, or PB injection on presence of PrP^c on FDCs in the B cell zone of the spleen. **D**,**H**,**L** merged images of all three antibodies. Images are representative of observations in 3 animals/group. Scale bar: 100 µm.

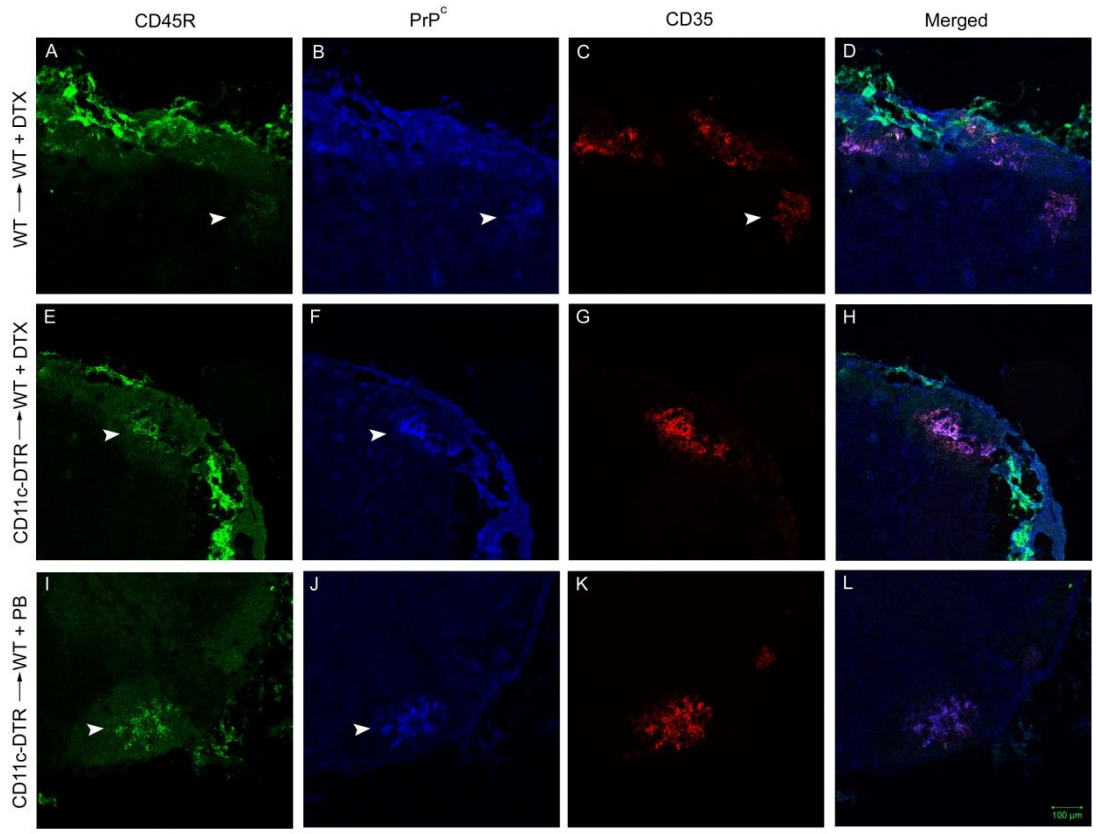

Figure 3.14. DTX treatment had no effect on FDC and B lymphocyte status in the iLN. Mice were given a single i.p. injection of DTX, and iLNs collected two days later were immunolabelled with with the anti-CD45R specific antibody to detect B lymphocytes (green, **A**,**E**,**I**);; the anti-CD35 specific antibody to detect FDCs and CD35-expressing B lymphocytes (red, **C**,**G**,**K**); and the pAb 1B3 to detect PrP^c (blue, **B**,**F**,**J**). Comparison between the 3 groups indicated no effect of irradiation, bone marrow reconstitution, or DTX, or PB injection on presence of PrP^c on FDCs in the B cell zone of the spleen. **D**,**H**,**L** merged images of all three antibodies. Images are representative of observations in 3 animals/group. Scale bar: 100 µm.

3.4. Discussion

In this chapter characterisation studies were carried out on the CD11c-DTR transgenic mouse line to determine a timeline for depletion and repopulation of $CD11c^{+}$ cells following DTX injection. This was achieved through collection of tissues for *ex vivo* analysis at various time points following a single i.p. injection of DTX, or PB control. Depletion and repopulation, as a result of DTX injection, was further analysed in mice following lethal irradiation and reconstitution with bone marrow from CD11c-DTR transgenic mice. Through this characterisation, it has been possible to determine that $CD11c^{+}$ cells were partially depleted in the skin and lymphoid tissues within 2 days of DTX injection until six days post injection.

Upon closer examination it is possible to confirm that different subsets of $CD11c^{+}$ cells exist in lymphoid tissues. Some $CD11c^{+/hi}$ cells, classically termed DCs, were observed to be repopulating tissues such as the spleen from six days post injection. Other, $CD11c^{low/med}$ cells such as the marginal zone and metallophillic macrophages, and subcapsular sinus macrophages in the LN, identified by their expression of CD169, were much slower to repopulate the tissues following DTX injection (Probst *et al.*, 2005). These cells were also depleted (to a lesser extent), following DTX injection in the lethally irradiated and reconstituted mice.

DTX as a toxin does not affect mice (Morris and Saelinger, 1983), but the mass depletion of cells, especially in the lymphoid tissues could have repercussions on other cell types especially those cells which are part of the immune system. Using the CD35 marker to identify FDCs and B lymphocytes within the lymphoid follicles, it

was possible to determine that FDC networks, within the B cell areas of lymphoid tissues were not adversely affected by DTX injection, or the resultant $CD11c^+$ cell depletion and repopulation.

Irradiation and reconstitution of wildtype mice with wildtype or CD11c-DTR transgenic bone marrow had no major effect on the depletion of $CD11c^+$ cells (excluding LCs), nor did it affect FDCs or B lymphocytes, located in the lymphoid follicles of the iLN or spleen. The animals were lethally γ-irradiated (1000 rad) and reconstituted with age and sex-matched bone marrow 24 hr later. Animals were maintained for 8 weeks post bone marrow transfer before DTX injection and tissues were collected for analysis. After 8 weeks the reconstitution and establishment of the CD11c-DTR transgenic cell population would be complete, with the exception of the LCs (Merad *et al.*, 2002). Following injection of DTX or PB into these animals there were no observable differences in the expression of PrP^c on the FDCs, or the structure of the FDC networks or the B-cell follicles. These results thereby indicate that injection of DTX into the lethally irradiated, bone marrow reconstituted mice, and the subsequent $CD11c^+$ cell depletion, did not have wide-ranging, non-specific effects in the affected tissues.

The presence of LCs in the epidermis makes them a likely candidate for the potential capture and transport of the scrapie agent from the skin (Mohan *et al.*, 2005c). Mohan *et al* found that XS106 cells, a DC cell line isolated from the mouse epidermis, with characteristics of mature LCs, degraded the scrapie agent following *in vitro* exposure. *In vitro* experiments may have forced extended exposure to the

scrapie agent, which might not replicate *in vivo* situations. More importantly, during scrapie infection via the skin, LCs in the epidermis are immature, and only mature as they migrate from the epidermis, and the added injury of scarification might trigger different maturation responses in the LCs at the time when they would encounter the scrapie agent in the skin. LCs have previously been linked to transport of pathogens, such as HIV (de Jong and Geijtenbeek, 2010) or Dengue virus (Wu *et al.*, 2000) from the skin. LCs express CD11c on their surface (Ginhoux *et al.*, 2007; Jung *et al.*, 2002) and are therefore potentially depleted following DTX injection in the CD11c-DTR mice. Epidermal sheets of the mouse ears were analysed for the depletion of LCs following DTX injection into these animals. Partial LC depletion was confirmed in these mice following DTX injection. In contrast, LCs were not depleted in the lethally irradiated mice following reconstitution and DTX injection, as the LCs are radioresistant and remain of host origin up to 18 months after lethal irradiation (Merad *et al.*, 2002). By isolating the epidermal LCs from depletion prior to scrapie infection via skin scarification, it will be possible to determine whether $CD11c^+$ cells other than LCs might play a role in the transport of the scrapie agent from the skin. Depletion of several different cellular subsets from the skin at the time of infection would simply obscure the results. LCs, and their potential role in scrapie infection via the skin will be fully investigated in Chapter 8.

As well as the LCs in the epidermis, low numbers of migratory LCs were found in the skin draining LNs. $Langerin^+$ DCs that have migrated from the dermis can also be found in the LNs. In the skin, LCs only express CD11c at a very low level, as they migrate and mature they upregulate MHC II and CD11c (Jung *et al.*, 2002).

Although langerin expression is down-regulated during migration and maturation, the marker can still be detected on the cells in the skin draining LNs (Kissenpfennig *et al.*, 2005b). Through their CD11c expression langerin$^+$ cells within the LNs were also affected by the DTX. As with other subtypes, shown above, only a partial depletion of langerin$^+$ cells was observed, but cell numbers are markedly reduced, and remain depleted for longer than other CD11c expressing cells.

In conclusion, these data indicate that CD11c$^+$ cells can be successfully depleted in lethally irradiated mice reconstituted with CD11c-DTR bone marrow. This temporary depletion confirms that these mice can serve as a useful model for investigating the role of CD11c$^+$ cells in the uptake and transport of the ME7 scrapie agent from the skin. Data in this chapter indicate that 2 days post DTX treatment is the most suitable time at which to infect the mice with scrapie via skin scarification. At this time, the majority of cells have been depleted and remain depleted for several days following scarification, before they start to repopulate the tissues. Furthermore, any potential effect on scrapie pathogenesis, observed following DTX treatment, will not be attributed to the LCs as they are unaffected by DTX in the irradiated mice.

4

EFFECTS OF CD11c$^+$ CELL DEPLETION ON SCRAPIE TRANSMISSION FOLLOWING INFECTION VIA SKIN SCARIFICATION

4.1. Abstract

Dendritic cells have been implicated in the transport of the scrapie agent from the gut lumen to the gut associated lymphoid tissues, as well as in other aspects of disease pathogenesis. TSEs can be readily experimentally transmitted via the skin or mucosa through the presence of small abrasions on the skin or within the mouth. Following infection via the skin, the scrapie agent, PrP^{Sc}, accumulates in the draining LNs. The skin is the body's first line of defence, and as such, there is an abundance of immune cells, including different DC subsets, within the skin. These cells could therefore play a potential role in the transport of the scrapie agent from the skin to the draining LN following infection via the skin. Temporary conditional depletion of DC subsets, excluding epidermal LCs, prior to scrapie infection via the skin delayed the accumulation of PrP^{Sc} in the draining iLN at the early time point following infection, when compared to control animals. PrP^{Sc} had not yet spread to non-draining lymphoid tissues at the early time point. Despite the delay in early PrP^{Sc} accumulation in mice depleted of DC subsets prior to scrapie infection via the skin, no differences were observed in the disease incubation period of these mice, when compared to the non-DC depleted control mice.

4.2. Introduction

In Chapter 3, CD11c-DTR animals (Jung *et al.*, 2002) and CD11c-DTR chimeric animals were analysed to determine a timeline for $CD11c^+$ cell depletion, and to determine whether injection of DTX or depletion of $CD11c^+$ cells had an adverse effect on the cellular environment within the skin or the secondary lymphoid system. Depletion of these $CD11c^+$ cells prior to oral scapie challenge has previously blocked early scrapie agent accumulation in the gut associated lymphoid tissues and reduced the susceptibility to disease (Raymond *et al.*, 2007). Equally, scrapie infection via the skin leads to the accumulation of PrP^{Sc} and infectivity in the draining LNs and spleen at early time points after infection (Glaysher and Mabbott, 2007a; Mohan *et al.*, 2004; Mohan *et al.*, 2005b). Three different bone marrow chimeric groups were created: WT→WT+DTX, CD11c-DTR→WT+DTX, and CD11c-DTR→WT+PB. These chimeric animals allowed for the depletion of DC subsets, without affecting epidermal LCs, which are radioresistant and would have remained of host origin (Merad *et al.*, 2002). The effect of LCs on scrapie infection via the skin will be discussed in Chapter 8. Chapter 4 will describe how these bone marrow chimeric groups were used to determine whether depletion of $CD11c^+$cells prior to infection with the ME7 scrapie agent by skin scarification affected the uptake and transport of the scrapie agent from the skin. The chapter will also look at whether the absence of these cells at the time of infection had an effect on the incubation period of disease. Experiments discussed in Chapter 3 demonstrated that the optimal time for scrapie infection was two days post DTX injection. In bone marrow chimeric animals, $CD11c^+$ cells (excluding LCs), had been depleted in the skin, iLN, pLN and spleen, and a window of several days existed before large numbers of cells returned to the

respective tissues. B cell follicles, FDCs and PrP^c expression in the lymphoid follicles of spleen, draining and non-draining LNs were not differently affected by injection of DTX in the bone marrow chimeric mice. In this chapter, mice were injected with DTX or PB control, and two days later mice were infected with the ME7 scrapie agent via scarification of the left inner thigh. In each of the three groups, 3 mice were sacrificed at each of the serial kill (SK) time points indicated in Fig. 4.1., and the remaining mice were maintained to reach disease endpoint. These results will allow us to determine whether $CD11c^+$ cells play a role in scrapie transmission from the skin.

4.3. Results

4.3.1. Effect of $CD11c^+$ cell depletion on early PrP^{Sc} accumulation

To determine the effect of $CD11c^+$ cell depletion on the early accumulation of the scrapie agent in the lymphoid tissues, mice received a single i.p. injection of DTX, or PB control, 2 days prior to scrapie infection via skin scarification. Draining (left) and non-draining (right) iLNs, pLNs, and spleens were collected from 3 mice from each of the groups outlined in Fig. 3.9., 3 and 5 weeks after scrapie infection. Immunohistochemical analysis with the anti-PrP mAb 6H4 determined that while disease specific PrP (PrP^d) deposition could be detected in the draining iLNs 5 weeks post infection (Fig. 4.2.), no PrP^d was detected in the non-draining (right) iLNs, left, or right pLNs, or the spleens (Table 4.1. and Table 4.2.).

Depletion of $CD11c^+$ cells prior to scrapie infection reduced the number of PrP^d positive follicles in the draining iLNs 5 weeks post infection. PrP^d was detected in two or more follicles in the draining iLNs of all 3 CD11c-DTR→WT+PB control mice (Fig. 4.2.), as well as 2 WT→WT+DTX mice (Fig. 4.2.). In the CD11c-DTR→WT+DTX mice, PrP^d was only detected in 1 follicle from 1 of 3 animals (Fig. 4.2.). Immunohistochemical analysis of the draining iLN confirmed that the PrP^d accumulated upon FDCs in the B cell follicles (Fig. 4.2.). Following PrP^d detection, adjacent draining iLNs sections were analysed via PET blots. Digestion of the blots with proteinase K confirmed that the PrP^d detected in draining iLNs was resistant to proteinase K digestion, and was the disease associated form of the protein, PrP^{Sc} (Fig. 4.3.). PET blot analysis was also carried out on spleen tissues to determine whether early low level PrP^{Sc} deposition, undetected by immunohistochemistry, was present. No PrP^{Sc} was detected in the spleen through PET blot analysis (Fig. 4.4.).

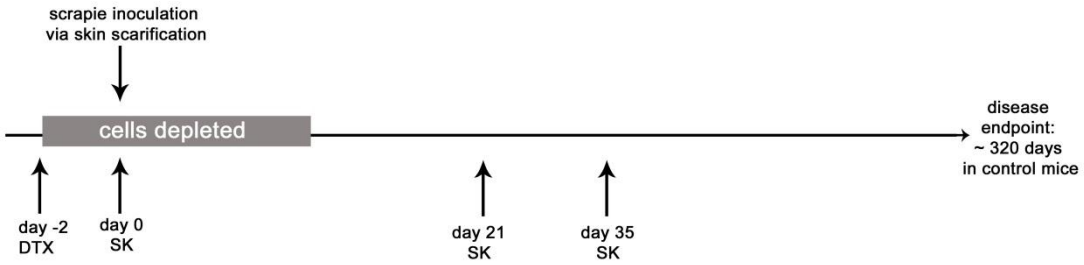

Figure 4.1. Experimental timeline. Mice were given a single injection of DTX, or PB, two days prior to inoculation via skin scarification. SK: serial kill. Tissues were collected from unscarified mice from each of the three groups, at day 0 (as a control), 21, and 35 days after scrapie infection. In each group 8 animals were left to reach disease endpoint.

Table 4.1. PrP^d deposition in peripheral lymphoid tissues 3 weeks post infection.

	WT →WT + DTX			CD11c-DTR→WT+DTX			CD11c-DTR→WT+PB		
	1	2	3	1	2	3	1	2	3
draining (left) iLN	–	–	–	–	–	–	–	–	–
right iLN	–	–	–	–	–	–	–	–	–
left pLN	–	–	–	–	–	–	–	–	–
right pLN	–	–	–	–	–	–	–	–	–
spleen	–	–	–	–	–	–	–	–	–

The numbers 1,2,3 represent animals in each group. PrP^d was not detected by immunohistochemistry in any of the peripheral lymphoid tissues from each group, collected 3 weeks post infection.

Table 4.2. PrP^d deposition in peripheral lymphoid tissues 5 weeks post scarification. Five weeks post scrapie infection PrP^d was only detected in the draining iLN, but had not spread to the non-draining LNs or spleens.

	WT →WT + DTX			CD11c-DTR→WT+DTX			CD11c-DTR→WT+PB		
	1	2	3	1	2	3	1	2	3
draining (left) iLN	–	+	+	–	+	–	+	+	+
non-draining iLN	–	–	–	–	–	–	–	–	–
draining pLN	–	–	–	–	–	–	–	–	–
non-draining pLN	–	–	–	–	–	–	–	–	–
spleen	–	–	–	–	–	–	–	–	–

The numbers 1,2,3 represent animals in each group. Five weeks post scrapie infection PrP^d was only detected in the draining iLN, but had not spread to the non-draining LNs or spleens.

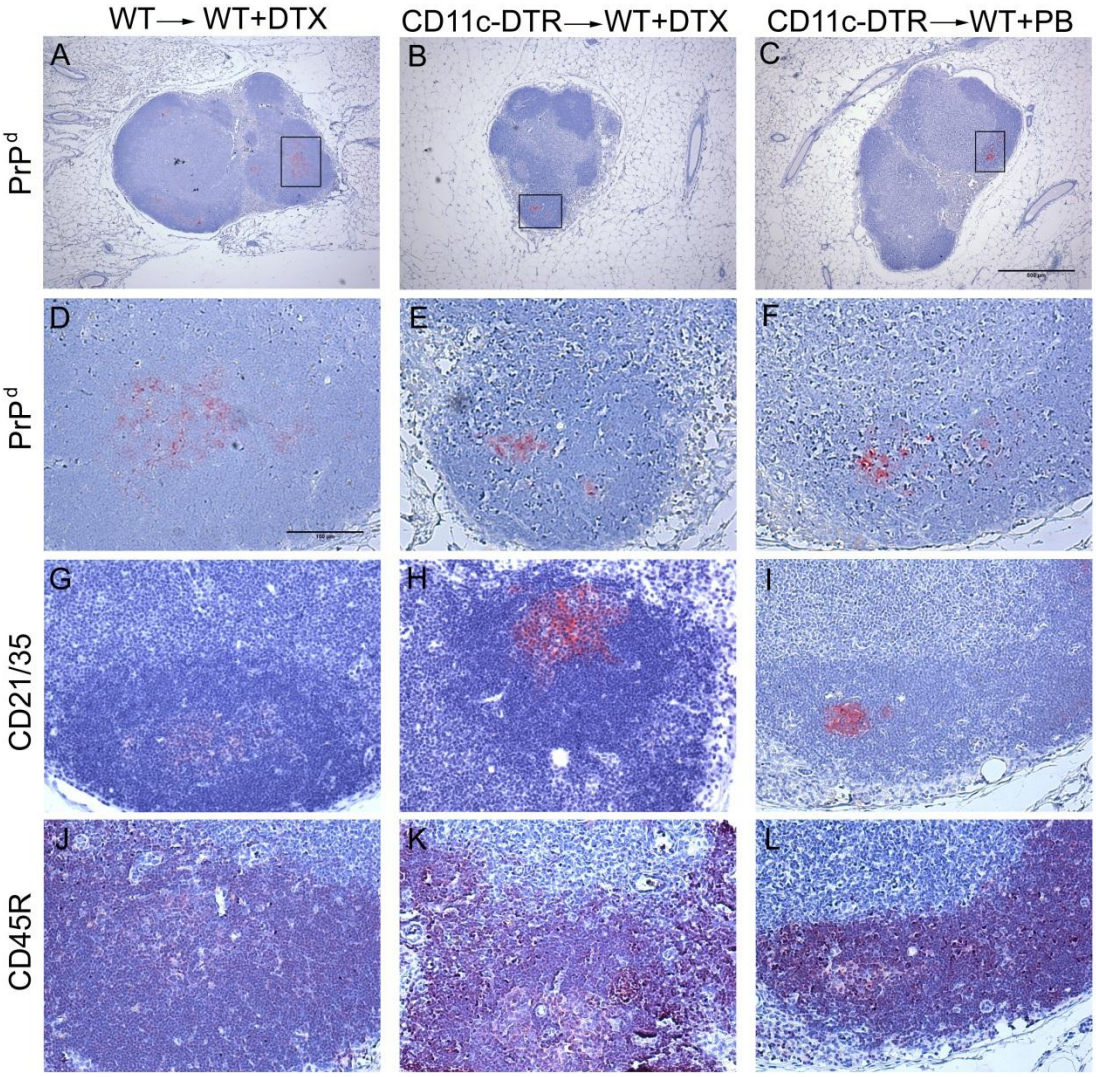

Figure 4.2. Delayed PrP^d accumulation in draining iLN of $CD11c^+$ cell-depleted mice is not due to lack of B cells and FDCs. Mice were inoculated with ME7 scrapie via skin scarification 2 days post DTX injection, or PB control. Draining iLNs were collected 5 weeks post scarification for immunohistochemical analysis. **A-C**: deposition of PrP^d (detected with 6H4 mAb) in all three groups (magnification 40 x). **D-F**: PrP^d (magnification 200 x). Detection of FDCs (CD21/35) (**G-I**) and B lymphocytes (CD45R) (**J-L**) in the draining iLNs confirmed that PrP^d accumulated upon FDCs in the B cell follicles. The lymphoid tissues were not lacking any cell populations that could have delayed PrP^d uptake from the skin and deposition in the iLN. Sections were counterstained with haematoxylin Z. Images are representative of observations in 3 animals. Scale bar: 100 µm.

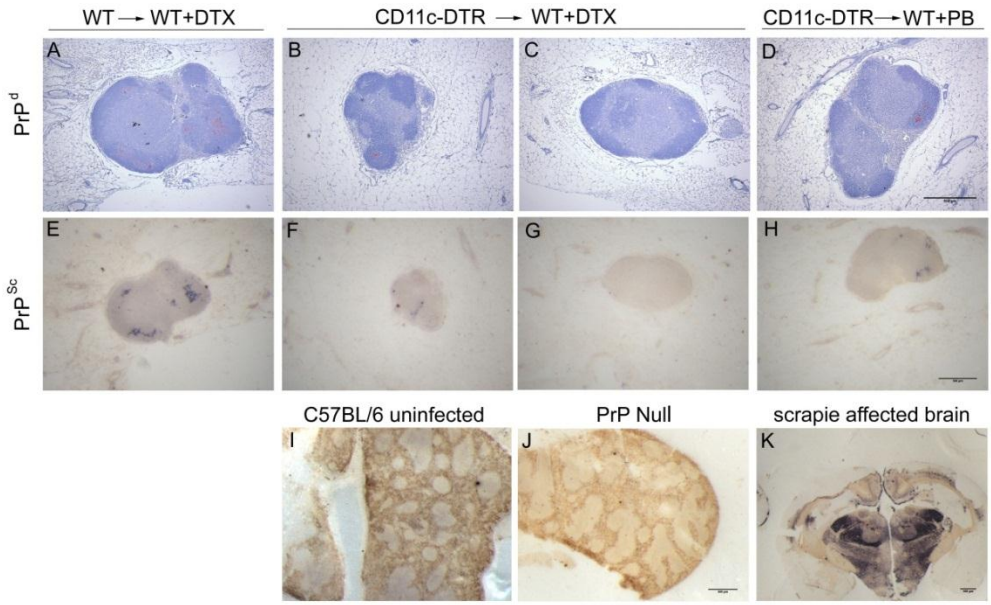

Figure 4.3. PrP^{Sc} accumulation in the draining iLN is impaired in the absence of $CD11c^+$ cells at the time of exposure. Mice were inoculated with ME7 scrapie via skin scarification 2 days post DTX-mediated $CD11c^+$ cell depletion. Draining iLNs were collected 5 weeks post scarification for immunohistochemical analysis. **A,B,D** Accumulation of PrP^d (mAb 6H4: red) in all three groups. In the CD11c-DTR→WT+DTX group only one of three mice showed PrP^d deposition; **C** is representative of the other two animals in the CD11c-DTR→WT+DTX group, where no PrP^d accumulation was observed. Sections were counterstained with haematoxylin Z. **E-H**: Adjacent PET blot sections confirmed that PrP^d was proteinase K resistant PrP^{Sc} (blue staining). **I:** uninfected wildtype mouse spleen, **J**: PrP deficient mouse spleen, **K:** scrapie affected brain positive control. Scale bar: 500 µm.

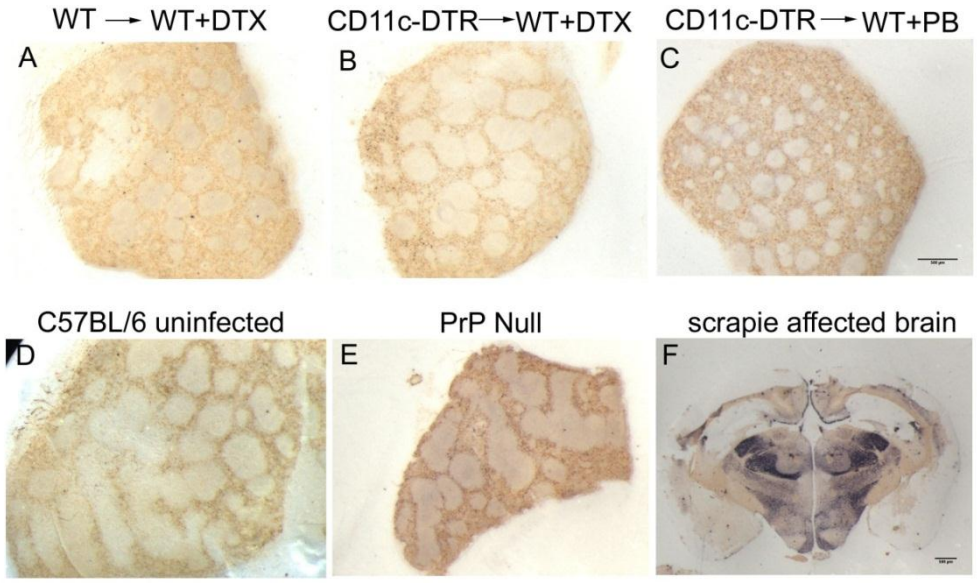

Figure 4.4. Absence of PrP^{Sc} deposition in mouse spleen 5 weeks post scarification. Mice were inoculated with ME7 scrapie via skin scarification 2 days post DTX injection, or PB control. Spleens were collected 5 weeks post scarification for immunohistochemical analysis. PET blot sections were labelled to detect proteinase K resistant PrP^{Sc}. **A-C**: immunohistochemical analysis with 1B3 antibody failed to show any PrP^{Sc} deposition in the PET Blot sections. **D**: uninfected control, **E**: PrP Null control, **F**: scrapie affected brain positive control. Images are representative of observations in 3 animals. Scale bar: 500 µm.

4.3.2. Effect of $CD11c^+$ cell depletion on the early accumulation of PrP^{Sc} in the spinal cord

In order to determine whether PrP^{Sc} had reached the spinal cord by at the early time points investigated, spinal cords collected 3 and 5 weeks post scrapie infection were analysed by Western blot alongside spinal cords from terminally scrapie infected animals. Spinal cords were analysed from WT→WT mice. As PrP^{Sc} accumulation was delayed following $CD11c^+$ cell depletion, PrP^{Sc} would be more likely to reach the spinal cords earlier in WT mice, (or CD11c-DTR→WT+PB mice). Samples were treated in the presence or absence of proteinase K, to determine the presence of proteinase K resistant, disease specific PrP^{Sc}. No PrP^{Sc} was detected in the spinal cords of any of these mice 7 weeks post scarification. Following proteinase K treatment, PrP^{Sc} was detected in the spinal cords of terminally scrapie affected mice (Fig. 4.5.). Proteinase K resistant samples exhibit the molecular weight shift of the di-, mono-, and unglycosylated proteins, characteristic of PrP^{Sc}, following proteinase K related cleavage of the N-terminal domain of the protein.

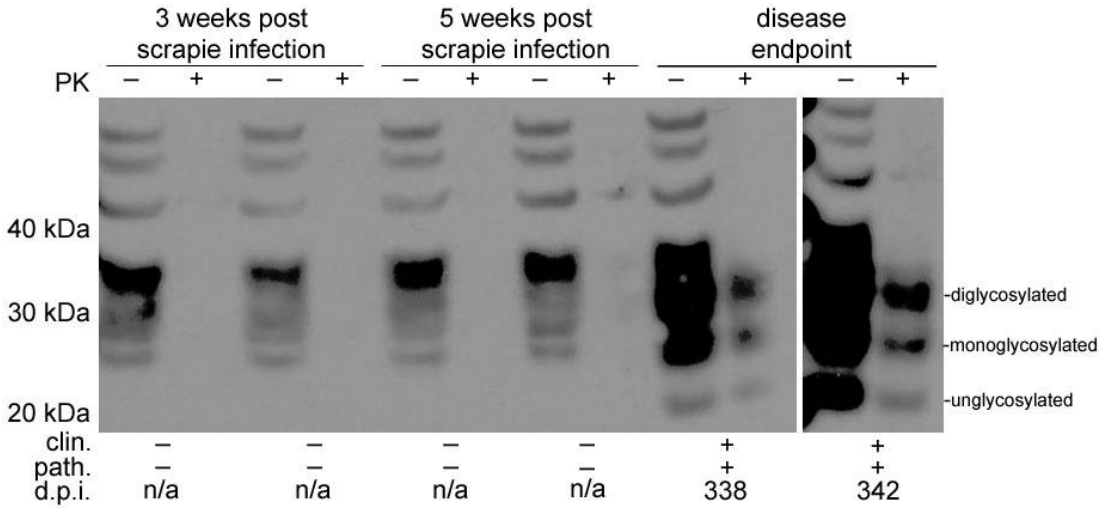

Figure 4.5. Absence of PrP^{Sc} in the spinal cord of WT→WT mice at early time points. Mice were infected with scrapie via the skin 2 days post DTX treatment. Spinal cord was collected from WT→WT animals 3 and 5 weeks post scrapie infection as well as at disease endpoint, and analysed by Western blot. Samples were treated in the presence (+) or absence (-) of proteinase K (PK) prior to electrophoresis. PrP^{c} was detected in all proteinase K untreated samples, using the 1B3 pAb, but proteinase K resistant, disease specific, PrP^{Sc} was only detected in the spinal cords terminally scrapie affected WT→WT animals. Proteinase K treatment cleaves the N-terminus of PrP, resulting in lighter protein isomers.

4.3.3. Effect of $CD11c^+$ cell depletion on scrapie incubation period following infection via skin scarification

To determine the effect of DTX injection and subsequent $CD11c^+$ cell depletion on the scrapie incubation period, 8 mice from each of the three bone marrow chimera groups were infected with the scrapie agent via skin scarification 2 days after injection with DTX, or PB control. Survival times were recorded as the incubation period of the disease; the time elapsed (in days) between the day of inoculation and the clinical endpoint of the disease. The mean incubation periods for the two control groups were 328 days (n=7) for WT→WT+DTX mice, and 324 days (n=7) for CD11c-DTR→WT+PB mice. In the CD11c-DTR→WT+DTX group, where PrP^{Sc} deposition in the draining iLN was delayed 5 weeks post scarification, the mean incubation period was 347 days (n=7).

Statistical analysis of the mean incubation periods determined that the residuals were not normally distributed. A one way analysis of variants was not possible, a non-parametric test is therefore required. The Kruskal-Wallis test used on sample medians, determined there to be no significant difference in incubation period between the three groups ($p = 0.099$, adjusted for ties). Despite an early delay in PrP^{Sc} accumulation in the draining iLN of CD11c-DTR→WT+DTX mice, this did not affect the incubation period of disease in these mice.

Characteristic spongiform encephalopathy, PrP^{d} accumulation, and reactive astrocytes and microglia were detected in the brains of all clinically scrapie affected animals from each group, consistent with terminal scrapie disease (Fig. 4.6.). PET blot analysis of adjacent sections confirmed the PrP^{d} accumulations detected were proteinase K resistant PrP^{Sc} (Fig. 4.6.). The targeted distribution of vacuolation in the brains of each clinically-scrapie affected mouse was consistent with an infection with the ME7 scrapie agent via the skin. No major variation was observed between the lesion profiles of each of the three groups (Fig. 4.7.).

Table 4.3. Effect of $CD11c^{+}$ cell depletion on scrapie incubation period after infection via the skin.

Group	Incidence	Median incubation period
WT → WT + DTX	7	335
CD11c-DTR→WT + DTX	7	329
CD11c-DTR→WT + PB	7	350

Median incubation periods.

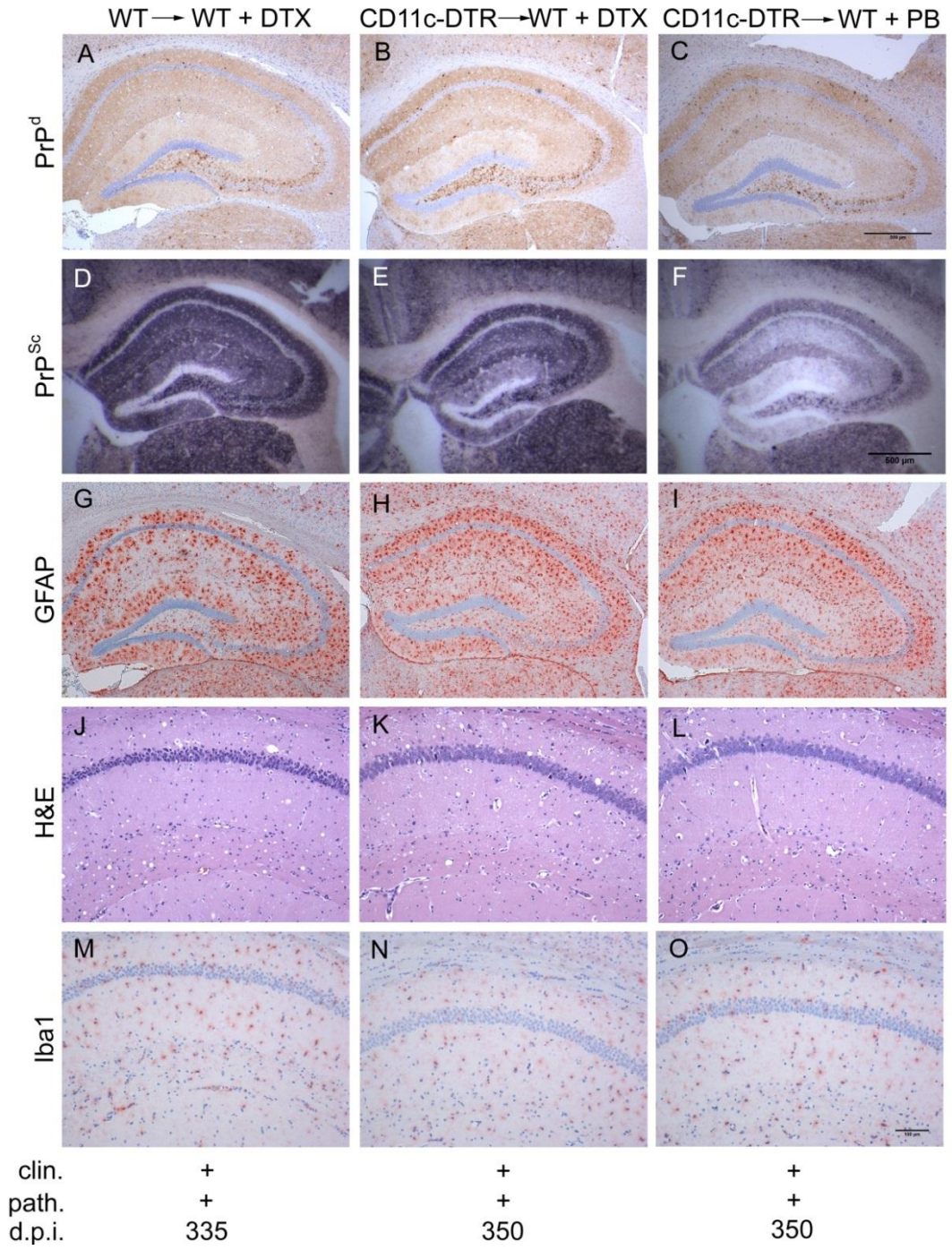

Figure 4.6. Histopathological analysis of brain tissues from terminally scrapie affected mice. Mice were inoculated with scrapie via skin scarification 2 days post DTX-mediated $CD11c^{+}$ cell depletion and brains from clinically scrapie-affected mice collected for immunohistochemical analysis. (**A-C**) Abundant PrP^{d} accumulations were detected in the hippocampi of mice from each group. (**D-F**) PET blot analysis confirmed the presence of proteinase K resistant PrP^{Sc}. Gliosis was confirmed through labelling with the GFAP antibody (astrocytes) (**G-I**), and the Iba1 antibody (microglia) (**M-O**). Sections were counterstained with haematoxylin Z. (**J-L**) Haematoxylin and eosin (H&E) staining revealed extensive vacuolation in the brains from all mice. Clin: clinical score; Path: pathological score, positive (+) or negative (-); d.p.i.: days post-inoculation on which tissues were taken for analysis. Images are representative of observations from 7 different animals. Scale bar: top 3 rows, 500 µm rows; and bottom two rows, 100 µm.

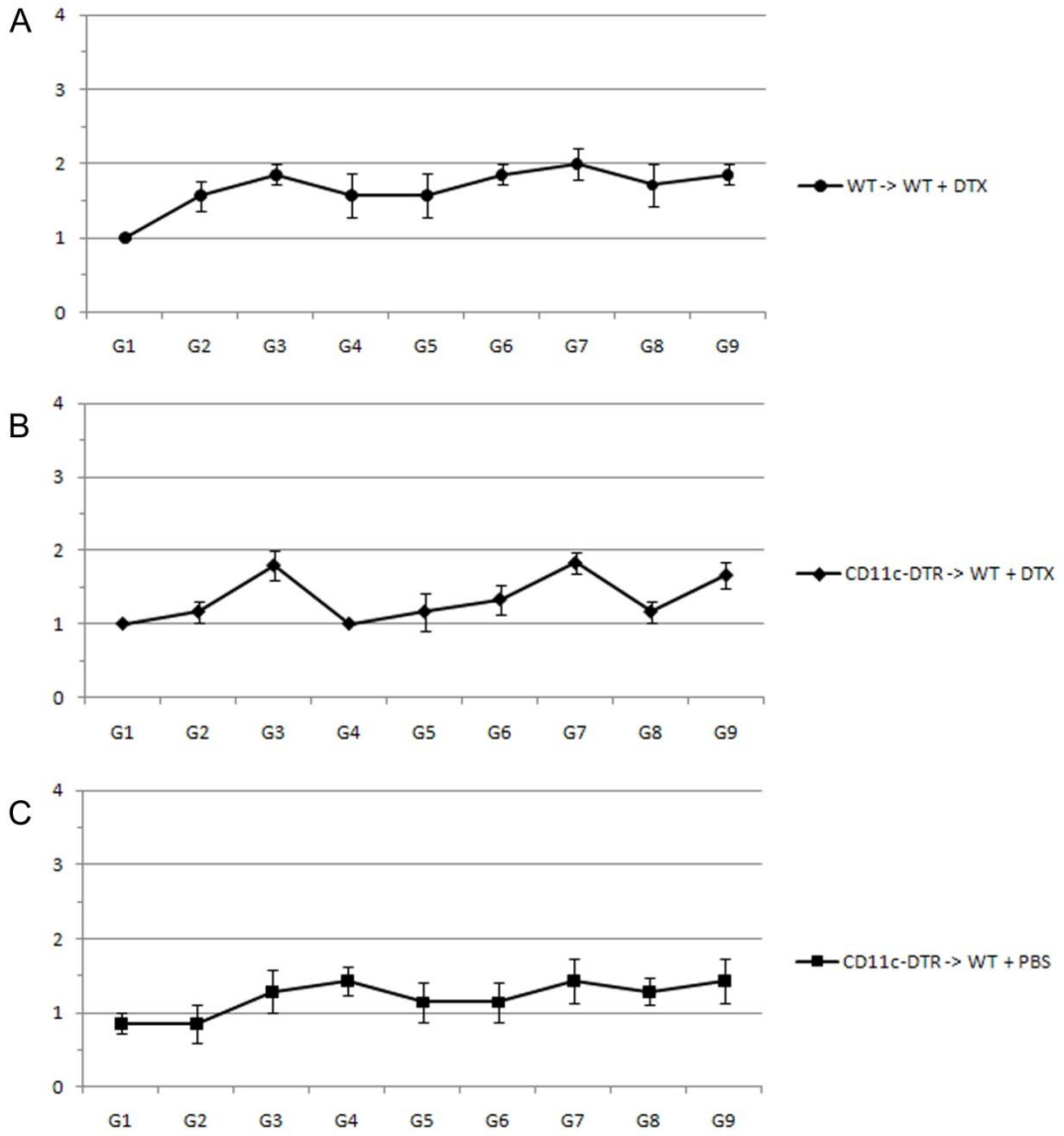

Figure 4.7. Pathological targeting of vacuolation in the brains of terminally scrapie affected mice. Mice were inoculated with scrapie via skin scarification 2 days post DTX-mediated $CD11c^{+}$ cell depletion and brains from each clinically scrapie affected mouse analysed by immunohistochemistry. **A**: WT→WT+DTX. **B**: CD11c-DTR→WT+DTX. **C**: CD11c-DTR→WT+PB. Vacuolation in the brain was scored on a scale of 0-5 in the following grey matter areas: G1, dorsal medulla; G2, cerebella cortex; G3, superior colliculus; G4, hypothalamus; G5, thalamus; G6, hippocampus; G7, septum; G8, retrosplenial and adjacent motor cortex; G9, cingulate and adjacent motor cortex. Each point represents mean vacuolation score ± S.E.M. for groups of 7 mice.

4.3.4. Effect of CD11c^{+} cell depletion on PrP^{Sc} accumulation in terminally scrapie affected mice

Following scrapie inoculation via the skin, PrP^{Sc} accumulation occurs first in the draining LNs before spreading to the non-draining LNs and the spleen. High levels of PrP^{Sc} are maintained in these tissues for the duration of the disease (Glaysher and Mabbott, 2007a; Mohan *et al.*, 2004). Immunohistochemical analysis of the spleens and draining iLNs from mice from all three groups further supported this. PrP^{d} accumulations were detected in all spleens from clinically affected mice and appeared comparable across the groups (Fig 4.8.). PrP^{d} deposition in the draining iLNs appeared to be greatly increased in the CD11c-DTR→WT+DTX animals when compared to the two control groups (Fig. 4.8.). PET blot analysis of adjacent sections confirmed this to be proteinase K resistant PrP^{Sc} (Fig. 4.8.). The iLNs were further analysed to determine whether this increased deposition of PrP^{Sc} was linked to increased activation or expansion of the FDC networks. Immunohistochemical analysis suggested no significant difference in CD21/35 immunolabelling in these tissues from each group (Fig. 4.8.).

Spinal cords were also collected from terminally scrapie-affected mice and PrP^{Sc} levels determined by Western blot analysis. Samples were treated in the presence or absence of proteinase K, to determine the presence of disease specific PrP^{Sc}. Spinal cords were found to contain large amounts of PrP^{Sc} in each of the three groups (Fig. 4.9.). The three bands found between approx. 50-60 kDa are most likely dimers of PrP^{Sc}.

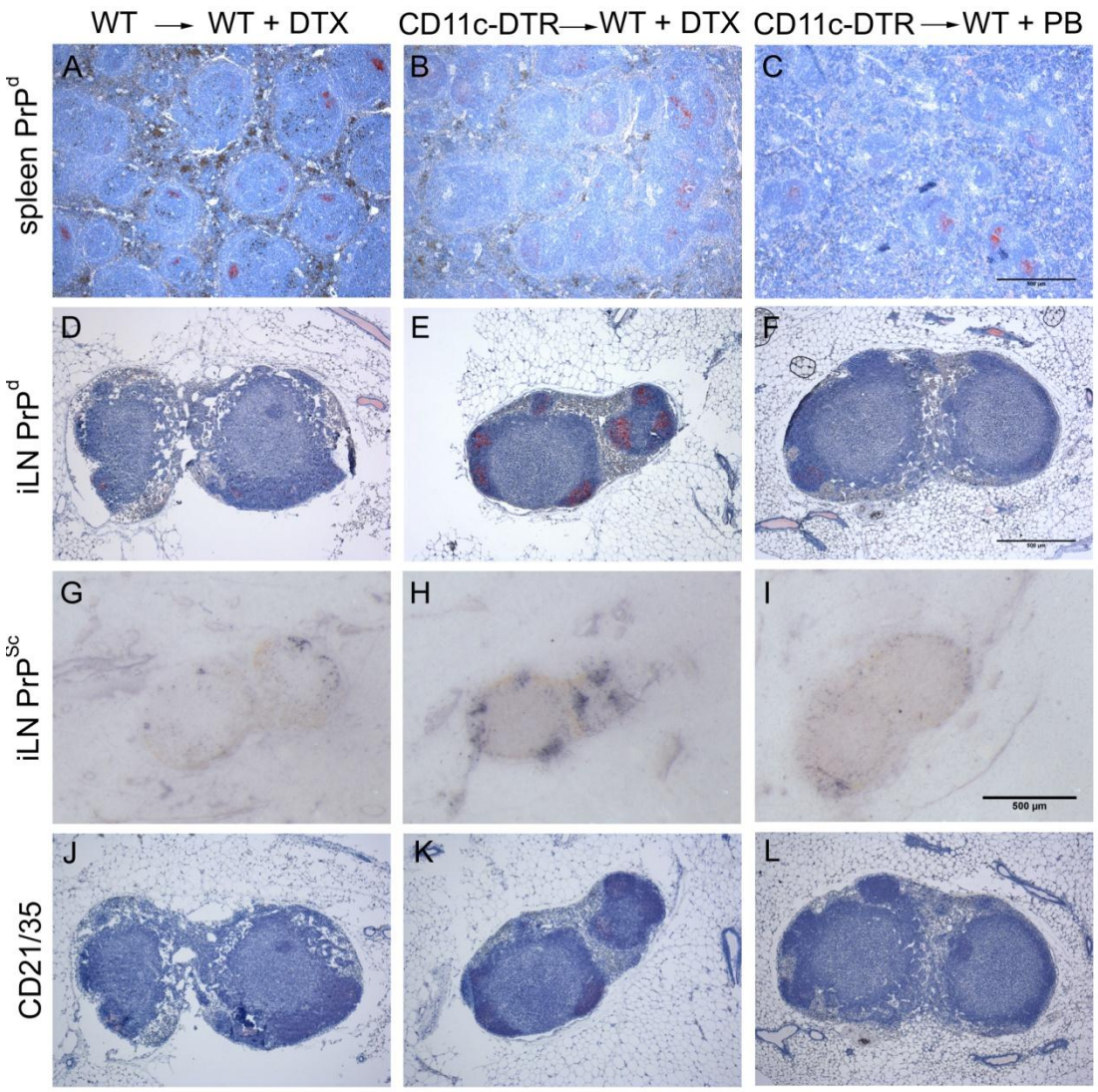

Figure 4.8. Histopathological analysis of peripheral lymphoid tissues from terminally scrapie affected mice. Mice were infected with scrapie via skin scarification 2 days post DTX injection, or PB control. Spleen and iLN were collected from clinically scrapie-affected animals and PrP^d and CD21/35 expression determined by immunohistochemistry. PrP^d expression was detected in the spleen of animals in all three groups (**A-C**). PrP^d expression was greatly increased in the draining iLN at the endpoint of disease in mice depleted of $CD11c^+$ cells (**D-F)**. PET blots analysis of adjacent sections confirmed the presence of proteinase K resistant PrP^{Sc}, which was increased in mice depleted of $CD11c^+$ cells at the time of infection (**G-H**). The expression of CD21/35 appeared to be unaffected (**J-L**). Sections were counterstained with haematoxylin Z. Images are representative of observations in 7 different animals. Scale bar: 500 µm.

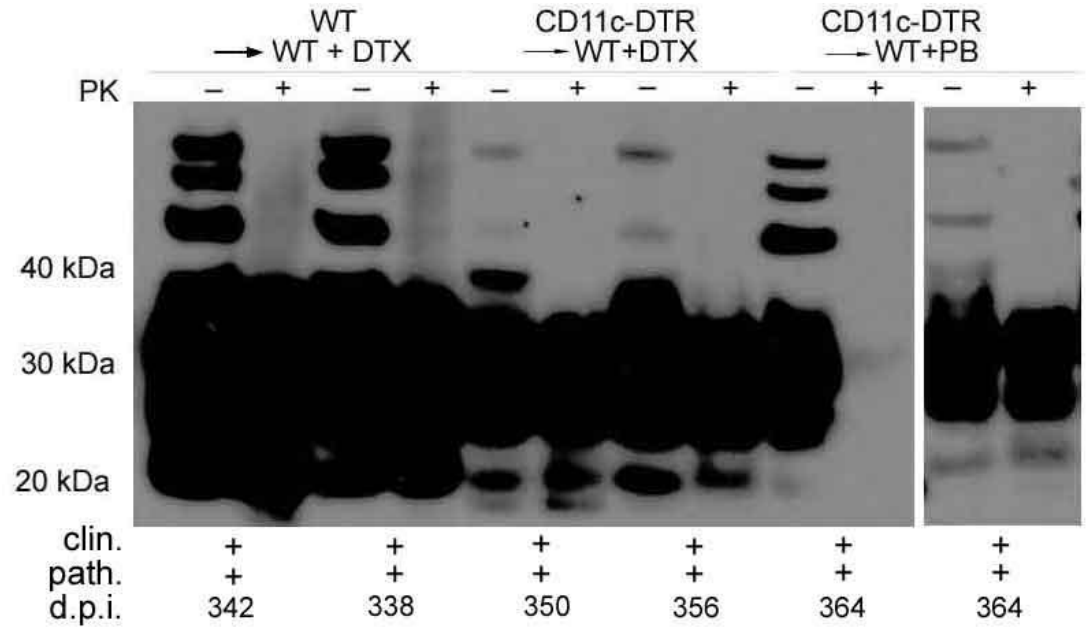

Figure 4.9. PrP^{Sc} accumulation in the spinal cord of terminally scrapie affected mice. Mice were inoculated with ME7 scrapie via skin scarification 2 days post DTX injection, or PB control. Spinal cord was collected from animals at the endpoint of disease and samples analysed via Western blot. Samples were treated in the presence (+) or absence (-) of proteinase K (PK) prior to electrophoresis. Proteinase K resistant, disease specific PrP^{Sc} was detected, using the 1B3 pAb, in the spinal cords of endpoint animals in all three groups. Clin: clinical score, positive (+) or negative (-); Path: pathological score, positive (+) or negative (-); d.p.i.: days post-inoculation on which tissues were taken for analysis.

4.4. Discussion

In this chapter, C57BL/6 wildtype mice were lethally γ-irradiated before reconstitution with either wildtype or CD11c-DTR bone marrow. These mice were subsequently injected with DTX, or PB control, to deplete their $CD11c^+$ cells (with the exception of LCs) 2 days prior to scrapie infection, via skin scarification of the inner thigh. Based on the timeline of depletion and repopulation of $CD11c^+$ cells established in Chapter 3, this protocol suggests a 4 day time-window, after infection, before the majority of cells have started to repopulate the tissues. Experiments demonstrated that the accumulation of PrP^{Sc} was delayed in the draining iLN of mice in which the $CD11c^+$ cells were depleted, when compared to controls. These results are consistent with previous work, where depletion of $CD11c^+$ cells prior to oral inoculation with the ME7 scrapie agent blocked the early accumulation of PrP^d in the PPs of the gut (Raymond *et al.*, 2007). Although DTX treatment of the mice used in this chapter did not completely deplete their $CD11c^+$ cells (Chapter 3, Fig. 3.5. and Fig. 3.12.), $CD11c^+$ cell numbers were diminished at the time of scarification with the ME7 scrapie agent. Despite, the difference in early stage PrP^{Sc} accumulation in the draining iLN, the incubation periods of the three groups all fit within the range of times established in previous models of scrapie infection via skin scarification (Glaysher and Mabbott, 2007a; Mohan *et al.*, 2004; Mohan *et al.*, 2005a; Mohan *et al.*, 2005b; Taylor *et al.*, 1996). The effects of treatment on scrapie pathogenesis were most likely related to effects on $CD11c^+$ cells, as DTX treatment of control mice did not significantly influence disease pathogenesis. The mean incubation periods for DTX injected mice reconstituted with wildtype bone marrow and PB

injected mice reconstituted with CD11c-DTR bone marrow were 328 days and 324 days respectively.

Following peripheral scrapie exposure in mice, PrP^{Sc} accumulates in the draining lymphoid tissues (spleen, LN, PP) before accumulation in the brain. Five weeks post scarification, PrP^{d} was not detected in any tissues other than the draining iLN either by immunohistochemistry or PET blot analysis regardless of whether $CD11c^{+}$ cells were depleted or not. This time point was too early for PrP^{d} detection in non-draining lymphoid tissues. However, large amounts of PrP^{Sc} were detected in the spinal cords and the brains of all terminally scrapie affected mice.

While accumulation of disease associated PrP in the spleens of terminally scrapie affected mice is found at similar levels throughout the three groups, PrP^{Sc} accumulation in the draining iLN was much greater in those mice where $CD11c^{+}$ cells were depleted prior to scrapie infection. As PrP^{Sc} accumulation was delayed in the draining iLNs of these mice at the early time points after exposure, it is possible that the return of the $CD11c^{+}$ cells (in the skin and lymphoid tissues) after DTX treatment triggered a 'second wave' of scrapie agent transport, or accelerated the accumulation process within the lymphoid tissues, for example, the sudden influx of $CD11c^{+}$ cells into an area abundant with PrP^{Sc} might cause the transport of the protein to the draining iLN. PrP^{d} accumulation (McGovern *et al.*, 2009) and disease infectivity (Kimberlin and Walker, 1979) reach a plateau between 7 and 10 weeks after which levels remain constant.

FDC networks and PrP^{c} expression was unchanged in the CD11c-DTR→WT+DTX animals at the time of scrapie agent exposure (Fig. 3.13. and 3.14.) or in those showing clinical signs of scrapie. These observations suggest it is unlikely that the effects observed on scrapie pathogenesis were due to a delayed immune reaction to the $CD11c^{+}$ cell repopulation increasing immune activity on the FDCs, and triggering greater PrP accumulation on their surfaces.

Despite a delay in early stage PrP^{Sc} accumulation in the draining iLN following $CD11c^{+}$ cell depletion, no significant differences were observed between the incubation periods of each group. All the mice succumbed to disease. No major differences were observed between the lesion profiles of each group, and exhibit similar trends to those observed in other cases of scrapie infection via skin scarification (unpublished). Based on previous evidence that $CD11c^{+}$ cell depletion reduced disease susceptibility (Raymond *et al.*, 2007), and the delayed early stage PrP^{Sc} accumulation observed in this chapter it is possible that if the number of mice in each group had been higher, then a significant difference might have been observed. However, power tests were conducted on using the data obtained from the animals that were used. These indicated that based on the trends observed, 29 mice would have been required for significant differences. Given the nature and duration of the experiment (> 380 days) this would not have been feasible.

The delay in PrP^{Sc} accumulation following $CD11c^{+}$ cell depletion points towards a possible role of the $CD11c^{+}$ cells in the skin (with the exception of LCs) in the transport of the scrapie agent from the skin to the peripheral lymphoid tissues. DCs

in the skin are perhaps not as abundant as they are in other tissues, but as they have been linked to the transport of other disease associated antigens from the skin (de Jong and Geijtenbeek, 2010; Palucka, 2000; Wu *et al.*, 2000), it is entirely possible that they also transport PrP^{Sc}. There is evidence that $langerin^{+}$ dDCs are able to cross-present antigens which they have picked up from keratinocytes, irrespective of the presence of LCs (Henri *et al.*, 2010). It was previously thought that LCs passed on antigen to dDCs, although this appears not to be the case (Henri *et al.*, 2010). This data supports earlier findings that dDCs rather than LCs play a role in antigen presentation (Henri *et al.*, 2007). The absence of dDCs in the skin at the time of scrapie infection via the skin could therefore be a possible cause for the delay in PrP^{Sc} accumulation. However, it is also possible that the scrapie agent is transported from the skin to the draining iLN via a cell-free mechanism, and that it is the absence of one of the $CD11c^{+}$ cell subsets in the LN that delays the accumulation of PrP^{Sc}.

As was demonstrated in Chapter 3, several $CD11c^{+}$ cell types, including, but not only, $CD11c^{+}langerin^{+}$ LCs, $CD11c^{+}CD169^{-}$ DCs, and $CD11c^{+}CD169^{+}$ macrophages are affected by DTX treatment. The $CD11c^{+}CD169^{+}$ macrophages, also termed SCS macrophages, in the LNs play a role in the presentation of immune complexes to non-cognate B cells which in turn present these complexes to FDCs. As PrP^{Sc} accumulation in lymphoid tissues occurs on FDCs (Brown *et al.*, 1999), there is a possibility that these macrophages play a role in the transport of PrP^{Sc} from the skin to the FDCs within LNs. By creating the CD11c-DTR/C57BL/6 bone marrow chimeric mice, LCs were not affected by DTX treatment. However, in these bone marrow chimeras several different $CD11c^{+}$ cell subsets had been depleted at the time

of scarification, two days post DTX treatment. The observed delays in PrP^{Sc} accumulation in the draining iLN, while it is as a result of $CD11c^{+}$ cell depletion, cannot be solely attributed to one specific cell type. The $CD11c^{+}CD169^{-}$ cells repopulate the tissues earlier than the $CD11c^{+}CD169^{+}$ cells (Probst *et al.*, 2005) and Chapter 3. In order to address the issue of different depleted cellular subsets, the different rates at which the cell types repopulate the tissues after depletion have been used to set up another study, where scarification occurs 6 days after DTX treatment, instead of 2; these results will be discussed in the following chapters.

5

CHARACTERISATION OF DIPHTHERIA TOXIN INDUCED CD11c^{+}CD169^{+} CELL DEPLETION IN THE CD11c-DTR MOUSE

5.1. Abstract

Transgenic mouse models where target cells express the DTR on their surface, allows for the temporary depletion of these cell types in order to further determine the role and function of the target cells in specific tissues or disease models. The CD11c-DTR transgenic mouse model allows for the temporary conditional depletion of $CD11c^+$ cells. CD11c was previously thought to be marker specific for DCs. It has been determined that CD11c is expressed on a number of different macrophage subsets, which are also depleted by DTX treatment in the CD11c-DTR mice. The different $CD11c^+$ cellular subsets exhibit independent repopulation dynamics, and several macrophage subsets repopulate tissues much later than DC subsets. By waiting 6 days after DTX-mediated depletion, it was possible to analyse the effect of macrophage depletion in various tissues after DCs had repopulated the tissues. By excluding DCs from the analysis, it is possible to gain further insight into the role and function of $CD11c^+$ macrophages within the target tissues.

5.2. Introduction

Data in this thesis (Chapter 3, section 3.3.4.) and elsewhere (Probst *et al.*, 2005) show that in addition to the depletion of $CD11c^+$ classic DCs, other macrophage populations, notably $CD11c^+CD169^+$ cells, are also depleted in CD11c-DTR after DTX treatment. CD169, or siaoladhesin, is a transmembrane receptor (Oetke *et al.*, 2006) and a prototypic member of the Siglec family of sialic acid binding immunoglobulin-like lectins (Crocker *et al.*, 1994). CD169 is expressed by marginal zone metallophillic macrophages in the spleen and the SCS macrophages in LNs (Phan *et al.*, 2007; Probst *et al.*, 2005). Probst *et al* observed complete depletion of $CD11c^+CD169^+$ cells in CD11c-DTR mice, along with the metallophillic macrophages, through the SIGNR1 receptor. Data in Chapter 3 (Chapter 3, section 3.3.10.) showed that following DTX-treatment of CD11c-DTR→WT mice, a partial depletion of $CD169^+$ cells was observed when compared to the CD11c-DTR mice. In the CD11c-DTR mice, the $CD11c^+CD169^+$ macrophages remained completely depleted until 6 days after DTX treatment. Although these $CD11c^+CD169^+$ cells were depleted at the same time as the $CD11c^+CD169^-$ cells in tissues from CD11c-DTR→WT and CD11c-DTR mice, the $CD11c^+CD169^+$ cells remained depleted for a longer period.

FDCs trap and retain antigen on their surfaces in the form of immune complexes (Kosco-Vilbois, 2003). These immune complexes are bound to FDCs via complement receptors and via antibody Fc receptors (van den Berg *et al.*, 1995). These complement receptors are considered to play an important role in TSE agent localisation to FDCs (Flores-Langarica *et al.*, 2009; Klein *et al.*, 2001; Mabbott and

Bruce, 2001; Zabel *et al.*, 2007). SCS macrophages are situated in a key location for B cell encounter with immune complexes (Phan *et al.*, 2007), and as these cells were depleted at the time of scrapie scarification, it is not possible to rule out their potential role in the uptake and transport of the scrapie agent from the skin. It was therefore important to determine whether the absence of the $CD11c^{+}CD169^{+}$ cells at the time of scrapie infection influenced the delay in scrapie agent accumulation to the draining lymphoid tissues in Chapter 4 (section 4.3.1.).

This chapter therefore determined whether the differences observed in scrapie pathogenesis in the DTX-treated CD11c-DTR→WT mice was due to the depletion of the $CD11c^{+}CD169^{-}$ classical DCs, or the depletion of $CD11c^{+}CD169^{+}$ cells.

5.3. Results

5.3.1. Characterisation

C57BL/6 wildtype mice were lethally γ-irradiated before reconstitution with CD11c-DTR bone marrow, as outlined in Chapter 3 (section 3.3.6.) (Fig. 5.1.).

5.3.2. DTX-mediated depletion of $CD11c^+CD169^+$ cells in CD11c-DTR→WT mice

Figure 3.7. demonstrated a partial depletion of $CD11c^+CD169^+$ cells from 2 days post DTX treatment. Cell numbers did not start to increase until after day 6 post DTX injection. In contrast, $CD11c^+CD169^-$ cell numbers had started to increase before day 6. This time point is therefore useful for studying the effect of a partial depletion of $CD11c^+CD169^+$ cells on scrapie pathogenesis without the absence of $CD11c^+CD169^-$ cells. DTX-mediated depletion of $CD11c^+$ cell types in CD11c-DTR→WT mice is outlined in Table 5.1.

Groups of 3 CD11c-DTR→WT mice received a single i.p. injection of DTX or PB control, spleen and iLN were collected for immunohistochemical analysis 6 days later. $CD11c^+CD169^+$ cells are located within the sinusoids and medullary cords of LNs or at the marginal sinus of the spleen, forming a ring around the periarteriolar lymphoid sheath and follicular areas at the inner side of the marginal zones. A partial DTX-mediated depletion of $CD11c^+CD169^+$ was confirmed. $CD169^+$ staining is disrupted within the SCS of the iLN (Fig. 5.2.). The distinctive 'rings' of staining around the marginal zones, characteristic of CD169 labelling, was very fragmented and much fewer $CD169^+$ cells were present in these areas (Fig.5.3.). No observable difference was detected in the density and distribution of the $CD11c^+CD169^-$ between DTX and the PB injected animals (Fig. 5.2. and Fig. 5.3.).

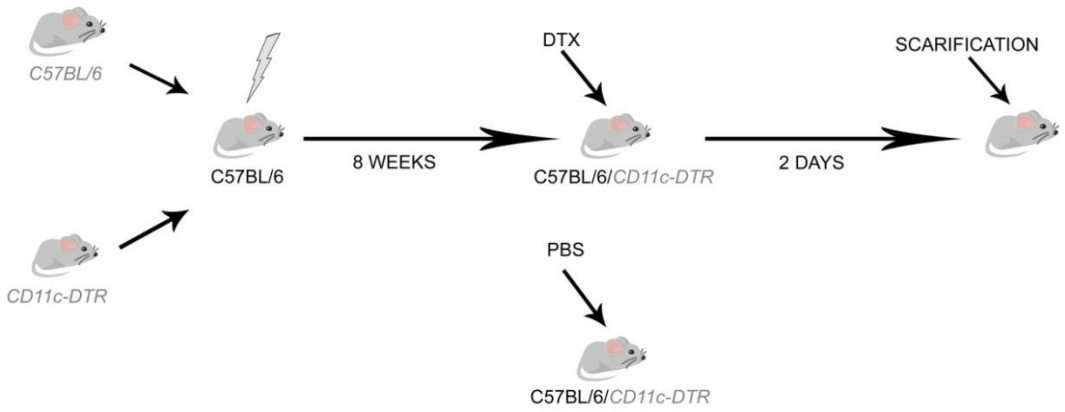

Figure 5.1. Model of irradiation and bone marrow reconstitution. C57BL/6 wildtype mice were lethally γ-irradiated 24 hr prior to receiving a bone marrow graft (grey) from CD11c-DTR mice. After 8 weeks mice were split into two groups. Mice were injected with DTX, or PB as a control.

Table 5.1. Depletion status of a range of CD11c$^+$ cell populations in the skin and lymphoid tissues of CD11c-DTR mice, six days post DTX injection.

			Depletion status			
Host genotype	**Donor genotype**	**DTX**	**CD11c$^+$/CD169$^+$ macrophages**	**CD11c$^+$/CD169$^-$ /langerin$^-$ cells**	**langerin$^+$ dermal DCs**	**LCs**
WT	CD11c-DTR	yes	yes	cell numbers increase	yes	no
WT	CD11c-DTR	no	no	no	no	no

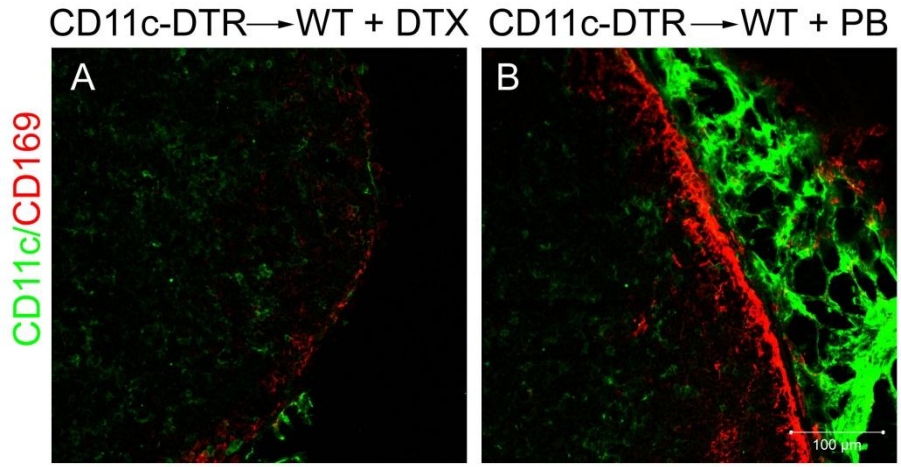

Figure 5.2. CD11c$^+$CD169$^+$ cell depletion in CD11c-DTR→WT six days after DTX treatment. Mice were given a single i.p. injection of DTX and iLNs collected six days later were immunolabelled with the anti-CD11c (HL3) specific (green) and the anti- CD169 (MOMA-1) specific (red) antibodies. (**A**), CD11c-DTR→WT+DTX mice. CD11c$^+$CD169$^+$ cells were partially depleted, whereas CD11c$^+$CD169$^-$ cells showed no depletion compared to the controls. CD11c-DTR→WT+PB control mice (**B**), normal distribution of CD11c$^+$CD169$^-$ and CD11c$^+$CD169$^+$ cells. Images are representative of observations in 3 animals/group. Scale bar: 100 µm.

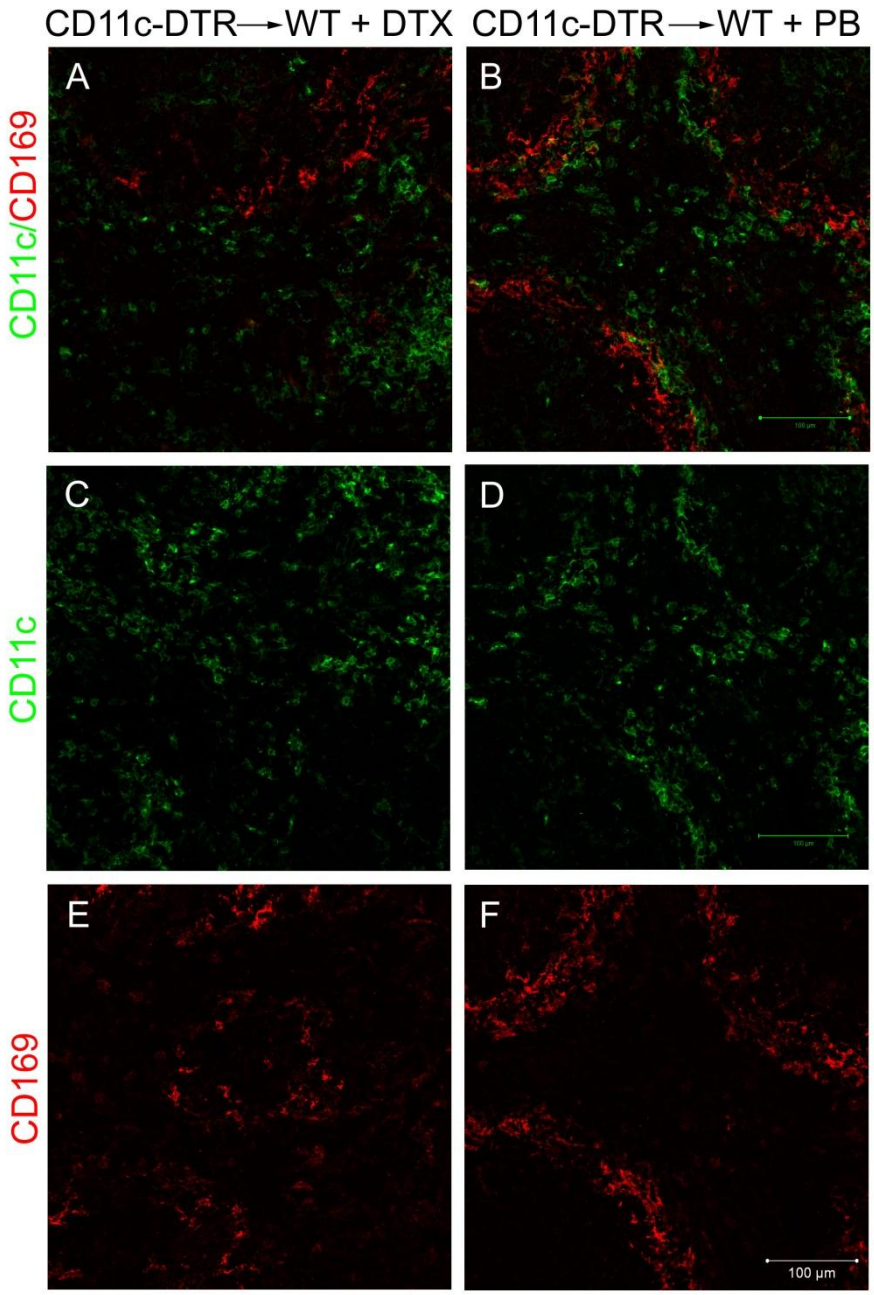

Figure 5.3. CD11c^{+}CD169^{+} cell depletion in CD11c-DTR→WT six days after DTX treatment. Mice were given a single i.p. injection of DTX and spleens collected six days later were immunolabelled with the anti-CD11c (HL3) specific (green) and the anti- CD169 (MOMA-1) specific (red) antibodies. CD11c-DTR→WT+PB control mice (**B**,**D**,**F**), normal distribution of CD11c^{+}CD169^{-} and CD11c^{+}CD169^{+} cells. (**A**,**C**,**E**), CD11c-DTR→WT+DTX mice. CD11c^{+}CD169^{+} cells were partially depleted, whereas CD11c^{+}CD169^{-} cells showed no depletion compared to the controls. Images are representative of observations in 3 animals/group. Scale bar: 100 µm.

5.3.3. Effect of DTX on langerin$^+$ cells

Section 3.3.8. confirmed that, as demonstrated in the literature, LCs present in the epidermis were unaffected by lethal irradiation and bone marrow reconstitution. As LCs are radioresistant, they were unaffected by DTX through their lack of transgene expression. To determine whether the LCs in the CD11c-DTR→WT+DTX mice were equally unaffected 6 days post DTX injection, immunohistochemical analysis was carried out on epidermal and dermal sheets from 3 CD11c-DTR→WT mice from each group. As anticipated, LCs in the epidermis were not depleted by DTX, since they derive from local wildtype precursors. Langerin$^+$ dermal DCs were partially depleted, as these were derived from the donor CD11c-DTR bone marrow. Immunohistochemical analysis of the draining iLN also confirmed a partial depletion of langerin$^+$ cells. These cells were likely to be LN-resident langerin$^+$ cells. The majority of the remaining langerin$^+$ cells in the iLN (Fig. 5.4.) would have migrated from the epidermis, and express lower levels of CD11c than tissue resident langerin$^+$ DCs (Kissenpfennig *et al.*, 2005b).

5.3.4. DTX treatment of CD11c-DTR→WT mice bone marrow does not affect FDC status

Immunofluorescence analysis was carried out to determine whether DTX-mediated CD11c$^+$ cell depletion in CD11c-DTR→WT had any effect on FDC status, or their expression of PrP^c. Analysis was carried out on spleen and iLN from 3 CD11c-DTR→WT+DTX or 3 CD11c-DTR→WT+PB mice six days post injection. The experiment confirmed DTX treatment of CD11c-DTR→WT mice had no observable effect on the status and distribution of FDCs in the lymphoid follicles of the spleen (Fig. 5.5.).

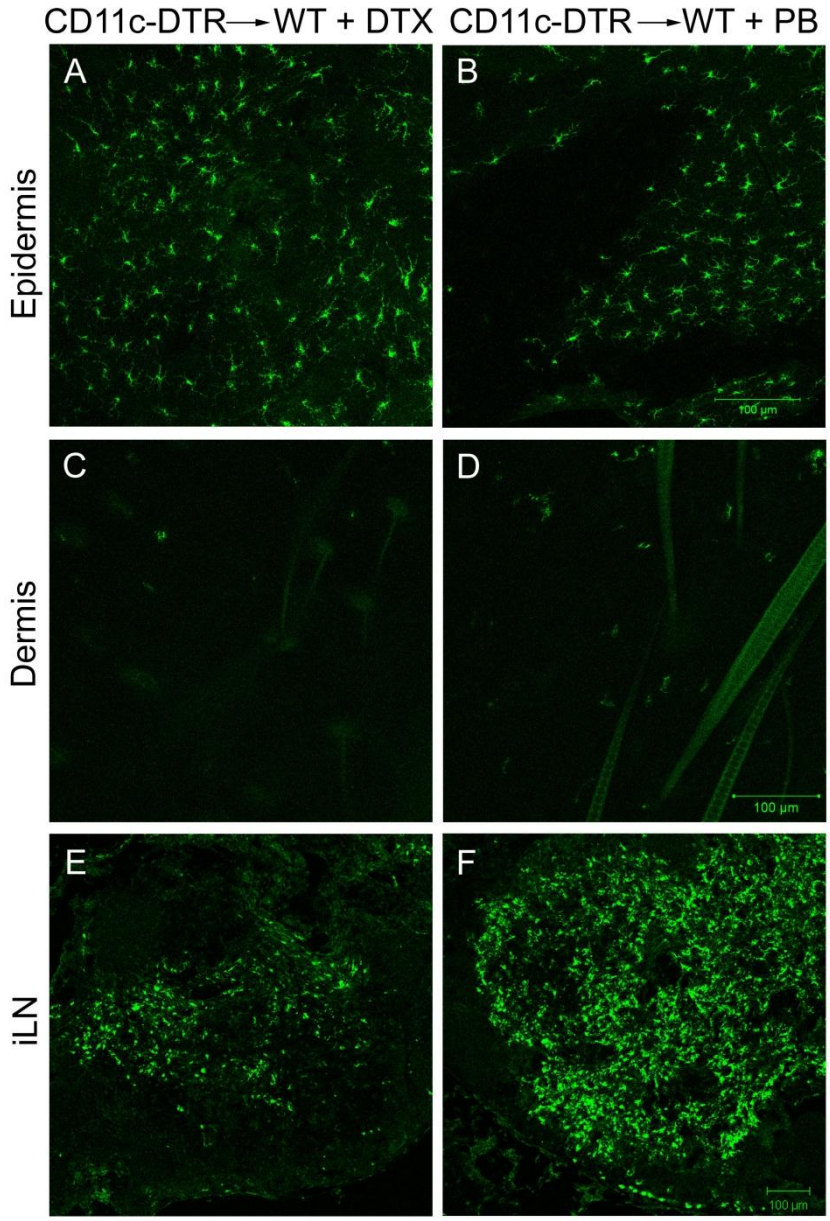

Figure 5.4. DTX-mediated langerin$^+$ cell depletion in the skin and LNs of CD11c-DTR→WT mice. CD11c-DTR→WT mice were given a single i.p. injection of DTX, or PB control, and tissues collected were immunolabelled with the anti-langerin antibody. (**A,B**) Normal distribution of langerin$^+$ LCs in the epidermis 6 days after injection with DTX or PB. **C**: Partial depletion of langerin$^+$ dermal DCs in CD11c-DTR→WT+DTX mice; **D**: normal distribution of langerin$^+$ dermal DCs in the dermis. **E**: Partial depletion of langerin$^+$ cells in the iLN following DTX injection. **F**: Normal distribution of langerin$^+$ cells in the iLN. Images as representative of observations in 3 animals/group. Scale bar: 100 µm.

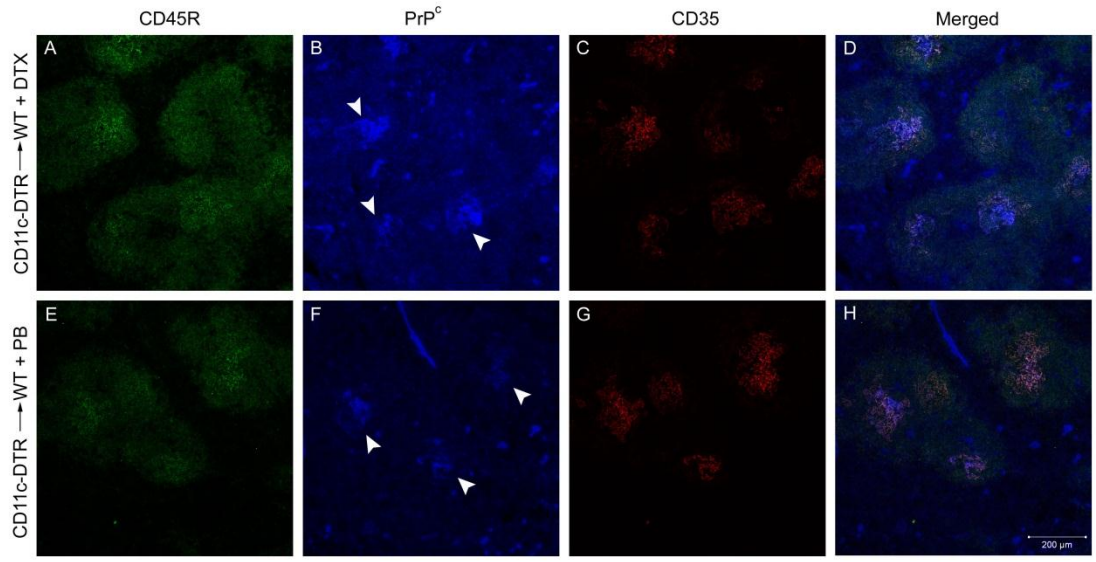

Fig. 5.5. DTX treatment had no effect on FDC and B cell status in the spleen. Mice were given a single i.p. injection of DTX and tissues collected six days later were immunolabelled with the anti-CD45R (green, **A**,**E**), anti-PrP (1B3) (blue, **B**,**F**), and anti-CD35 (red, **C**,**G**) antibodies. FDC and B cell status were unaffected in both animal groups; PrP^c expression was, equally, unaffected on the FDCs following DTX treatment. **D**, **H** merged images of all three antibodies. Images are representative of observations in 3 animals/group. Scale bar: 100 µm.

5.4. Discussion

In Chapter 3, characterisation studies were carried out on the CD11c-DTR transgenic mouse line to determine a timeline for depletion and repopulation of $CD11c^+$ cells following DTX injection. Data in that chapter also showed depletion of $CD11c^+CD169^+$ cells. In this chapter the effects of DTX treatment on the status of $CD11c^+CD169^+$ cells in CD11c-DTR→WT mice was also studied.

Analysis confirmed that in CD11c-DTR→WT mice, $CD11c^+CD169^+$ cells were partially depleted 6 days post DTX treatment, whereas the $CD11c^+CD169^-$ numbers had returned to similar numbers compared to those observed in control mice. These data confirm those observed in DTX-treated CD11c-DTR mice in Chapter 3 and Probst *et al* (Probst *et al.*, 2005). The delayed accumulation of the scrapie agent in the draining iLN following exposure via the skin, at the early time point observed in Chapter 4 could not be attributed to a single cell type, as both the classical $CD11c^+$ DCs and the $CD11c^+CD169^+$ SCS macrophages in the LNs (and marginal zone of the spleen) were depleted following DTX injection. In this chapter, data show that in the CD11c-DTR→WT mice the $CD11c^+CD169^+$ cells are partially depleted for a longer period than the classical DCs. This suggests it is possible to study the effects of a partial depletion of $CD11c^+CD169^+$ cells in the absence of any effects on the $CD11c^+CD169^+$ classical DCs. To do so, CD11c-DTR→WT mice could be exposed to the scrapie agent 6 days post DTX injection (when $CD11c^+CD169^-$ cells were restored, but $CD11c^+CD169^+$ cells remained partially depleted). This model could be used to determine whether the depletion of the $CD11c^+CD169^-$ or $CD11c^+CD169^+$ cells influence the accumulation of PrP^{Sc} in the draining LNs, thereby aiding to

determine whether the absence of either of these cells types, on their own, might be responsible for the delayed accumulation of PrP^{Sc} at the early time points.

As was previously confirmed in the epidermis of CD11c-DTR→WT mice were unaffected by DTX injection since they lacked expression of DTR, as the cells remained of host origin following lethal γ-irradiation (Merad *et al.*, 2002). In contrast, langerin$^+$ dDCs in the dermis, as well as langerin$^+$ cells in the LNs were partially depleted following DTX injection, as these cells are derived from the donor bone marrow (Merad *et al.*, 2002). These cells also took longer to repopulate than the CD11c$^+$ (CD169$^-$ langerin$^-$) DCs, and were still absent 6 days post DTX. These cells also need to be taken into consideration when assessing the effects of DTX treatment on the potential cell roles delaying the uptake and transport of the scrapie agent to the draining iLN. The potential role of these langerin$^+$ cells in scrapie pathogenesis will be examined further in Chapters 7 and 8.

Irradiation and reconstitution of wildtype mice with wildtype or CD11c-DTR transgenic bone marrow did not affect other cells such as the FDCs or B lymphocytes located in the lymphoid follicles of the iLN or spleen. The animals were lethally γ-irradiated (1000 rad) and reconstituted with age and sex-matched bone marrow 24 hr later. Animals were maintained for 8 weeks post bone marrow transfer before DTX injection and tissues were collected for analysis. After 8 weeks the reconstitution and establishment of the CD11c-DTR transgenic cell population would be complete, with the exception of the LCs (Merad *et al.*, 2002). Following injection of DTX or PBS into these animals there were no observable differences in the expression of PrP on

the FDCs, or the structure of the FDC networks or the B-cell follicles. These results thereby indicate that injection of DTX into CD11c-DTR→WT mice, did not have wide ranging, non-specific effects in the affected/target tissues.

6

THE ROLE OF SUBCAPSULAR SINUS MACROPHAGES IN SCRAPIE TRANSMISSION FROM THE SKIN

6.1. Abstract

Temporary DTX-mediated depletion of $CD11c^+$ cells prior to oral scrapie infection blocked early TSE agent accumulation in the gut-associated lymphoid tissues, and reduced susceptibility to disease. Similarly, DTX-mediated $CD11c^+$ cell depletion prior to scrapie infection via skin scarification delayed PrP^{Sc} accumulation in the draining iLN. Contrary to earlier belief, CD11c is not exclusively expressed on DCs, and various macrophage populations are also depleted following DTX treatment. The delays in PrP^{Sc} accumulation observed as a result of the absence of $CD11c^+$ cells at the time of infection can therefore not be specifically attributed to DCs. Different cell types repopulated tissues at varying times following DTX-mediated depletion, by waiting for $CD11c^+CD169^-$ cells (classical DCs) to repopulate tissues, it was possible to carry out scrapie infection via the skin when $CD11c^+CD169^+$ macrophages were still absent. The absence of these cells at the time of scarification did not affect early scrapie agent accumulation in the draining iLN. It was not possible to detect a difference in disease susceptibility, due to small sample size, but it is unlikely to have been the case. Therefore delays observed in early PrP^{Sc} accumulation in the draining iLNs is likely due to the absence of $CD11c^+CD169^-$ classical DCs.

6.2. Introduction

In Chapter 3 CD11c-DTR mice and CD11c-DTR chimeric mice were analysed to determine the effects of DTX injection on $CD11c^+$ cells in the lymphoid tissues and the skin. Chapter 4 looked to determine whether the depletion of $CD11c^+$ cells prior to scrapie infection via the skin had an effect on early scrapie agent accumulation in lymphoid tissues and the spread of disease to the brain. CD11c was previously thought to be a marker exclusive to DCs (Hume, 2008), and a great tool for identifying and isolating these cells. More recent evidence has shown that CD11c is not exclusive to DCs (Mabbott *et al.*, 2010), and that a number of other cell types are also depleted following DTX injection in the CD11c-DTR mice (Bradford *et al.*, 2011; Probst *et al.*, 2005). As such, the results obtained in Chapter 4 cannot be solely attributed to DCs. As other cell types remain depleted for longer than DCs, it is entirely possible that the results observed in Chapter 4 are due to the absence of other $CD11c^+$ cell types.

It was established, in Chapter 3, that $CD11c^+CD169^+$ SCS macrophages were also partially depleted following injection of DTX in CD11c-DTR mice and remained depleted for longer than $CD11c^+CD169^-$ cells (Fig. 3.7.). The lymphoid tissues of CD11c-DTR chimeric mice were analysed in Chapter 5 to determine the effect of DTX 6 days post injection. These results confirmed that while $CD11c^+CD169^+$ cells remained depleted, the $CD11c^+CD169^-$ cells had repopulated the tissues by this time point. LCs in the epidermis were not affected by DTX, as they were radioresistant and did not express the DTR (Fig. 5.3.). $Langerin^+$ cells in the dermis and iLN were

partially depleted (Fig. 5.3.). FDC status was also analysed and confirmed to be unaffected by DTX injection in the CD11c-DTR chimeric mice (Fig. 5.4.).

FDCs trap and retain antigen, in the form of immune complexes, which are stored on their surfaces for long periods (Kosco-Vilbois, 2003). These immune complexes are bound to FDCs via complement receptors in naïve mice, whereas in immunised mice they are also bound via antibody Fc receptors (van den Berg *et al.*, 1995). These complement receptors, as well as complement components C1q and C3 are considered to play an important role in TSE agent localisation to FDCs (Flores-Langarica *et al.*, 2009; Klein *et al.*, 2001; Mabbott and Bruce, 2001; Zabel *et al.*, 2007). $CD11c^{+}CD169^{+}$ cells are located within the marginal zones of the spleen, and also within the SCS of LNs. These $CD11c^{+}CD169^{+}$ SCS macrophages capture antigen-containing immune complexes arriving in the LN via their cell processes that they extend into the lumen of the SCS (Carrasco and Batista, 2007; Junt *et al.*, 2007; Phan *et al.*, 2009; Phan *et al.*, 2007; Roozendaal *et al.*, 2009). In contrast to other macrophage subsets, SCS macrophages retain immune complexes on their surfaces for rapid translocation through the floor of the SCS to underlying, non-cognate (non-specific) follicular B cells (Phan *et al.*, 2009). These B cells acquire the immune complexes via their complement receptors and deliver them to FDCs. The higher immune complex-binding affinities of FDCs most likely relieve the B cells of their cargo. Thus, the SCS macrophage-B cell immune complex relay represents an efficient route through which antigens are delivered to FDCs (Carrasco and Batista, 2007; Junt *et al.*, 2007; Phan *et al.*, 2009; Phan *et al.*, 2007; Roozendaal *et al.*, 2009). Reduced function of immune complex trapping together with decreased PrP^{c}

expression in aged mice, reduced the ability of aged FDCs to acquire and replicate TSE agents (Brown *et al.*, 2009). PrP^d has also been linked to FDC morphological changes during scrapie infection (McGovern *et al.*, 2009), where abnormal immune complexes colocalised with PrP^d accumulations. These data further support the idea that PrP^d reaches FDCs via immune complexes. These SCS macrophages could therefore play a potential role in the transport of the scrapie agent from the skin to the FDCs within the lymphoid follicles of the LRS.

By infecting CD11c-DTR chimeric mice with scrapie via skin scarification, 6 days after DTX injection (Fig. 6.1.), it is possible to determine whether the results obtained in Chapter 4 can be attributed to $CD11c^+CD169^-$ cells (typical of DCs), or whether these results are due to the absence of $CD11c^+CD169^+$ cells at the time of scrapie infection via the skin.

6.3. Results

6.3.1. Effect of $CD11c^{+}CD169^{+}$ cell depletion on early PrP^{Sc} accumulation

To determine the effect of $CD11c^{+}CD169^{+}$ cell depletion (after repopulation of $CD11c^{+}CD169^{-}$ cells) on the early accumulation of the scrapie agent in the lymphoid tissues, draining (left) and non-draining (right) iLNs, left and right pLNs, and spleen were collected from 3 mice from each group as outlined in Chapter 5 (Fig. 5.1.), 5 and 7 weeks post scrapie infection (Fig. 6.1.). Immunohistochemical analysis with the anti-PrP mAb 6H4 determined that accumulations of PrP^{d} could be detected in all the draining iLNs from CD11c-DTR→WT+DTX and from 2 of the 3 CD11c-DTR→WT+PB animals 5 weeks post scarification (Fig. 6.2.). The intensity of the immune-labelling appeared to be stronger in the CD11c-DTR→WT+DTX mice when compared to the controls. No PrP^{d} accumulations were detected in the non-draining iLN, left, or right pLN or spleen (Table 6.1.). Analysis of the 7 week time point tissues showed similar patterns of PrP^{d} deposition as in the 5 week time point draining iLNs (Fig. 6.2.). In addition, PrP^{d} was detected in the spleen and left pLN of one mouse CD11c-DTR→WT+DTX mouse and the non-draining (right) iLN of one CD11c-DTR→WT+PB mouse (Table 6.2.).

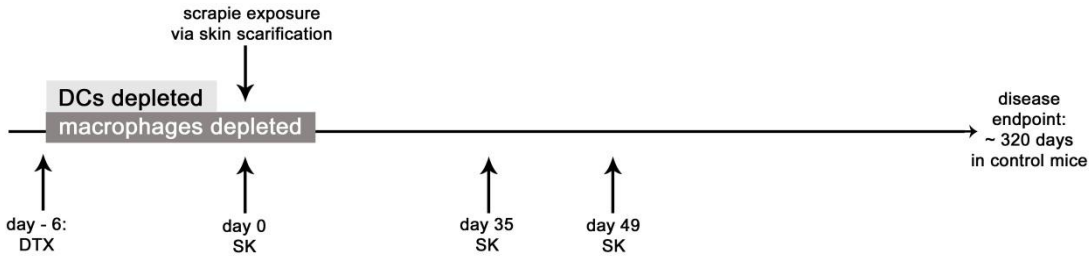

Figure 6.1. Experimental timeline following for scarification following DTX injection.
CD11c-DTR→WT mice were given a single injection of DTX, or PB, six days prior to scrapie infection via the skin. At this point the $CD11c^{+}CD169^{-}$ cells (typical of DCs) were no longer depleted but the $CD11c^{+}CD169^{-}$ cells remained depleted. Tissues were collected from 3 animals from each group at day 0 (with respect to TSE infection), 35, and 49 days after scrapie infection. In each group 8 animals were left to reach disease endpoint.

Table 6.1. PrP^{d} accumulation in peripheral lymphoid tissues 5 weeks post scrapie infection.

	CD11c-DTR→WT + DTX			CD11c-DTR→WT + PB		
	1	**2**	**3**	**1**	**2**	**3**
draining (left) iLN	+	+	+	–	+	+
right iLN	–	–	–	–	–	–
left pLN	–	–	–	–	–	–
right pLN	–	–	–	–	–	–
spleen	–	–	–	–	–	–

The numbers 1,2,3 represent individual animals in each group. PrP^{d} was detected by immunohistochemistry, only in the draining iLNs 5 weeks post infection. PrP^{d} was detected in all 3 CD11c-DTR→WT+DTX animals and 2 of 3 CD11c-DTR→ WT+PB animals.

Table 6.2. PrP^{d} accumulation in peripheral lymphoid tissues 7 weeks post scrapie infection.

	CD11c-DTR→WT + DTX			CD11c-DTR→WT + PB		
	1	**2**	**3**	**1**	**2**	**3**
draining (left) iLN	+	+	+	+	–	+
right iLN	–	–	–	–	–	+
left pLN	–	–	+	–	–	–
right pLN	–	–	–	–	–	–
spleen	–	–	+	–	–	–

The numbers 1,2,3 represent individual animals in each group. PrP^{d} was detected by immunohistochemistry, in the draining iLNs of animals in both groups, and also detected in the spleen and left pLN of one CD11c-DTR→WT+DTX mouse and non-draining (right) iLN of one CD11c-DTR→WT+PB mouse.

Depletion of $CD11c^{+}CD169^{+}$ cells prior to scrapie infection did not affect the number of PrP^{d} positive follicles in the draining iLN. PrP^{d} was detected in two or more follicles in the draining iLN of all three CD11c-DTR→WT+DTX mice, as well as two of the three CD11c-DTR→WT+PB mice (Fig. 6.2.).

Immunohistochemical analysis of the draining iLN confirmed that PrP^{d} accumulated upon FDCs in the B cell follicles (Fig. 6.2.). Observation of the labelling of PrP^{d} at a higher magnification (200 x, compared to 40 x), showed a 'punctate' pattern of labelling. PrP^{d} appeared to be associated with tingible body macrophages (*) as well as FDC networks (+). These results were comparable between the two groups, at both the 5 and 7 week time points (Fig. 6.2.).

The PrP^{d} accumulations observed in the draining iLNs were analysed by adjacent PET Blot sections of the same tissues. Digestion of the PET blots with proteinase K was used to confirm that the PrP^{d} detected in the draining iLNs was resistant to proteinase K digestion and was therefore the disease associated form of the protein, PrP^{Sc} (Fig. 6.3.). PET blot analysis was also carried out on spleen tissues to determine whether early low level PrP^{Sc} deposition, undetected by immunohistochemistry, was present. No PrP was detected in the spleen by PET blot analysis (Fig. 6.4.).

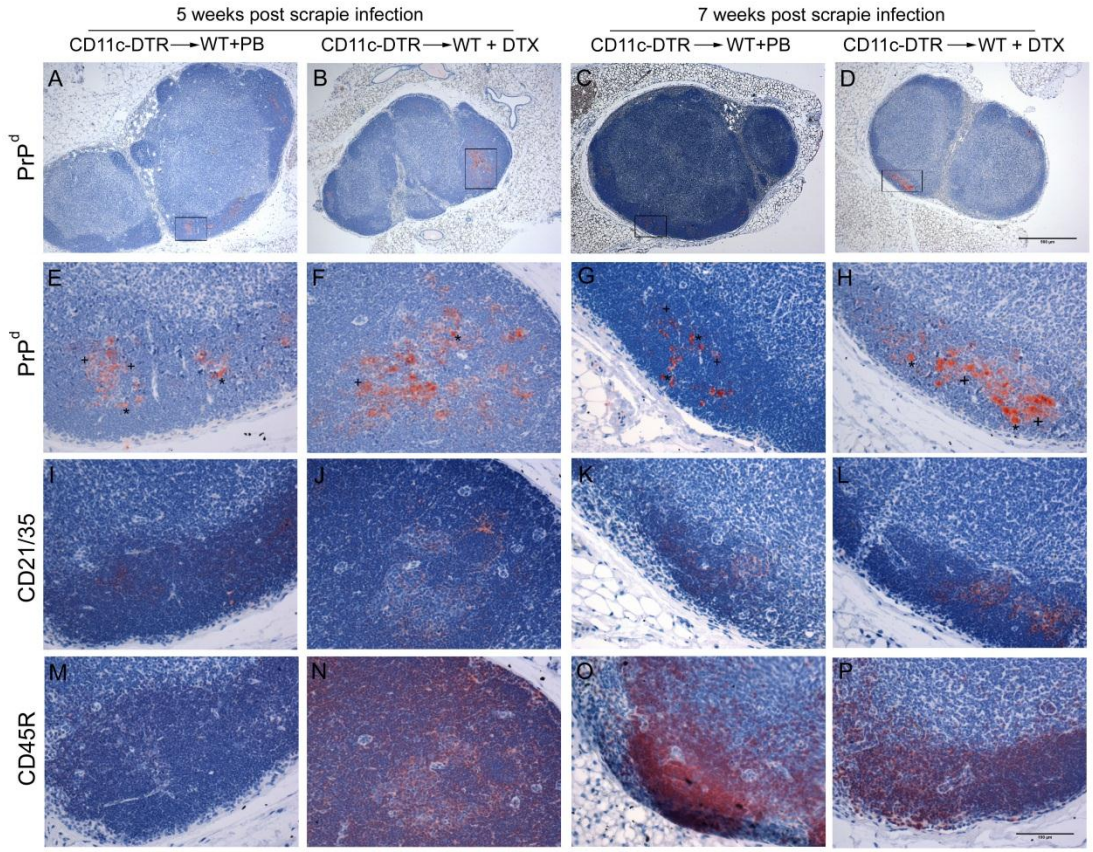

Figure 6.2. PrP^d accumulation in the draining iLN is unaffected by $CD11c^+/CD169^+$ cell depletion. Mice were infected with scrapie via skin scarification 6 days post DTX injection, or PB control. Draining iLNs were collected 5 and 7 weeks post scarification for immunohistochemical analysis. **A-D**: deposition of PrP^d (detected with 6H4 mAb) in both groups at both time points (magnification: 40 x). **E-H**: PrP^d accumulations (magnification: 200 x). Detection of FDCs (CD21/35) (**I-L**) and B lymphocytes (CD45R) (**M-P**) in the draining iLNs confirmed that PrP^d accumulated upon FDCs in the B cell follicles. PrP^d was detected both on FDC networks (+) and within tingible body macrophages (*). Sections were counterstained with haematoxylin Z (blue). Images are representative of observations in 3 animals/group. Scale bar: top row, 500 µm; bottom 3 rows, 100 µm.

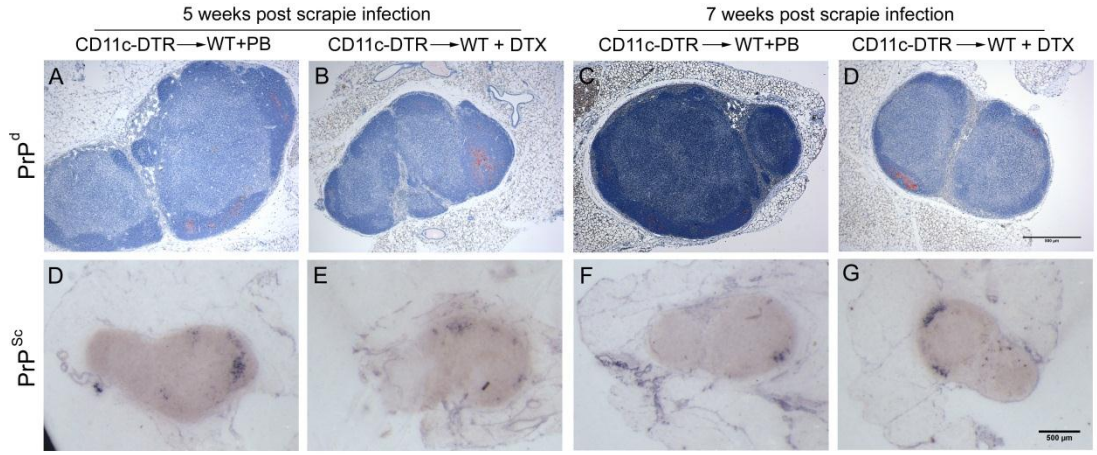

Figure 6.3. Confirmation of PrP^{Sc} accumulation in the draining iLN following scrapie infection via the skin. Mice were infected with scrapie via skin scarification 6 days post DTX injection, or PB control. Draining iLNs were collected 5 and 7 weeks post scarification for immunohistochemical analysis. **A-D**: deposition of PrP^{d} (detected with 6H4 mAb) in both groups at both time points. **E-H**: Adjacent PET blot sections confirmed that PrP detected by 6H4 was proteinase K resistant, disease-specific, PrP^{Sc}. Sections were counterstained with haematoxylin Z (blue). Images are representative of observations in 3 animals. Scale bar: 500 µm.

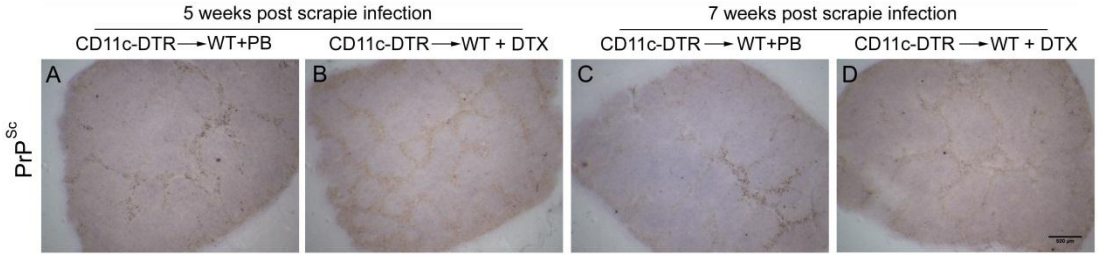

Figure 6.4. Absence of PrP^{Sc} deposition in spleen 5 and 7 weeks post scarification. Mice were infected with scrapie via skin scarification 6 days post DTX injection, or PB control. Spleens were collected 5 and 7 weeks post scarification for immunohistochemical analysis. PET blot sections were labelled to detect proteinase K resistant PrP^{Sc}. **A-D**: immunohistochemical analysis with 1B3 antibody failed to show any PrP^{Sc} deposition in the PET Blot sections. Images are representative of observations in 3 animals/group. Scale bar: 500 µm.

6.3.2. Effect of $CD11c^{+}CD169^{+}$ cell depletion on scrapie incubation period following inoculation via skin scarification

To determine the effect of DTX-mediated $CD11c^{+}$ cell depletion on scrapie incubation period following transmission through skin scarification, 8 mice from each bone marrow chimeric group were infected with the scrapie agent via skin scarification 6 days after injection with DTX, or PB control. Incubation period was determined on mice that were found to be both clinically and pathologically positive. In both groups a number of animals died or were culled before they reached disease endpoint. Several animals that were culled following two positive clinical scores were subsequently found to be pathologically negative for scrapie (via vacuolation). Mean group incubation periods could not be determined in this experiment, as only 1 and 3 clinically positive, pathologically positive animals were identified in the CD11c-DTR→WT+DTX and the CD11c-DTR→WT+PB groups, respectively. The incubation periods for the individual mice were 328 (CD11c-DTR→WT+DTX); 320, 335, and 335 days (CD11c-DTR→WT+PB).

Immunohistochemical analysis of the brain revealed characteristic spongiform encephalopathy and PrP^{d} accumulation in the hippocampi of mice which developed clinical signs of scrapie. Reactive astrocytes and microglia were detected in terminally scrapie affected mice, consistent with terminal scrapie disease (Fig. 6.5.). Reactive astrocytes and microglia were also detected to varying degrees in mice showing negative pathology for scrapie (Fig. 6.5.). PET blot analysis of adjacent sections confirmed PrP^{d} accumulation, to be proteinase K resistant PrP^{Sc} (Fig. 6.5.). The targeted distribution of vacuolation in the brains was consistent with ME7 scrapie agent infection in the terminally scrapie affected animals in both groups.

Immunohistochemical analysis of the non-terminally scrapie affected animals confirmed varying levels of PrP^{d} and PrP^{Sc} on brain sections from clinically negative, pathological negative animals as well as in the clinically positive, pathological negative animals (Fig. 6.5.). Analysis also confirmed varying degrees of reactive astrocytes and microglia in these animals (Fig. 6.5.).

Following scrapie inoculation via the skin, PrP^{Sc} accumulation occurs first in the draining LNs before spreading to the non-draining LNs and the spleen; high levels of PrP^{Sc} can still be detected in these tissues from mice terminally affected by scrapie (Glaysher and Mabbott, 2007a; Mohan *et al.*, 2004). Immunohistochemical analysis of the spleen and draining iLN of mice in both groups further supported this. Levels of PrP^{d} deposition in the spleen were comparable in both groups, regardless of whether animals had shown clinical or pathological signs of disease or not (Table 6.3.). PET blot analysis of adjacent sections confirmed this to be proteinase K resistant PrP^{Sc} (Table 6.3.). The iLNs were further analysed and no difference was observed in activation of CD21/35 (Table 6.3.).

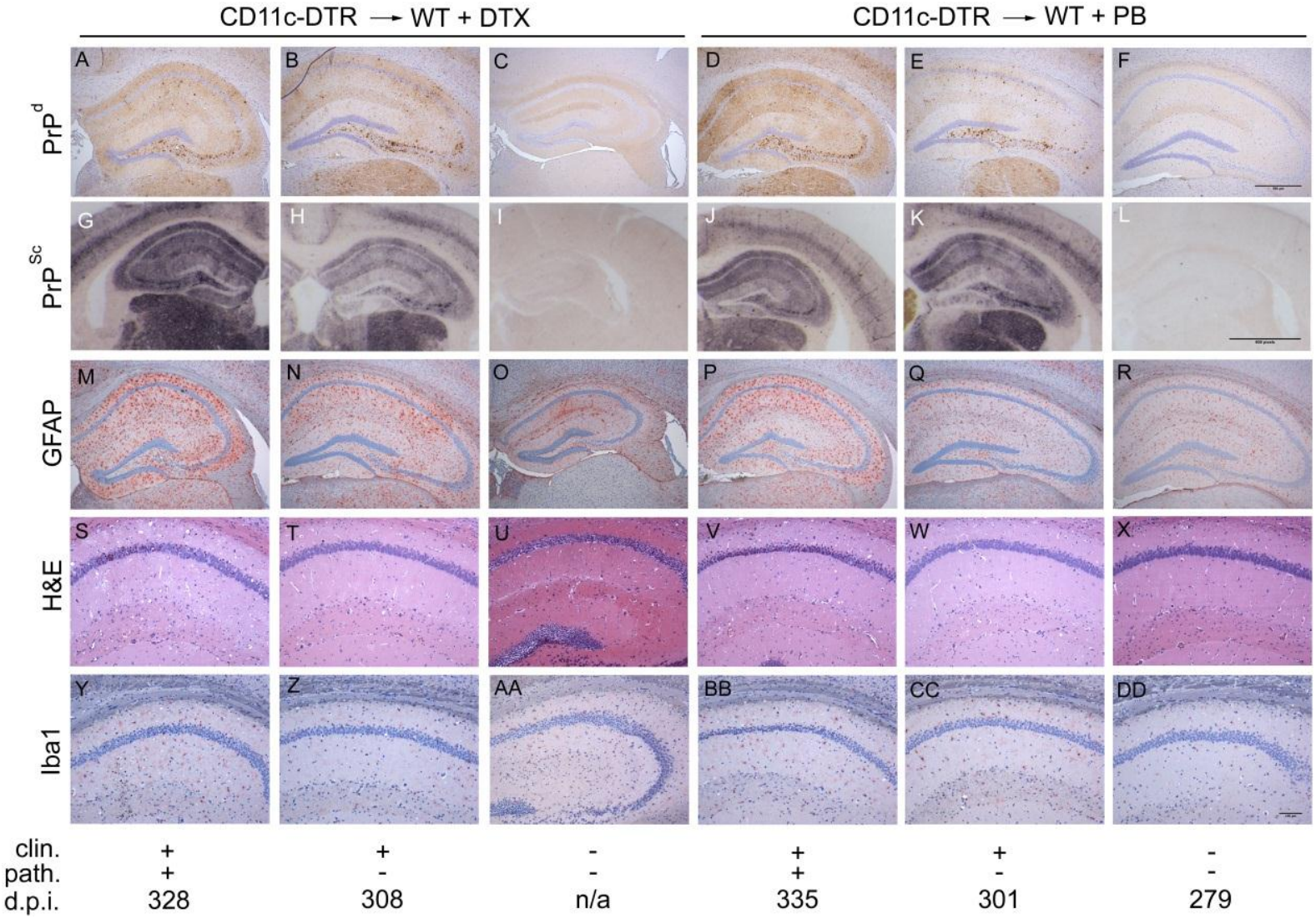
CD11c-DTR → WT + DTX
CD11c-DTR → WT + PB
PrP^d
PrP^Sc
GFAP
H&E
Iba1
A
B
C
D
E
F
G
H
I
J
K
L
M
N
O
P
Q
R
S
T
U
V
W
X
Y
Z
AA
BB
CC
DD
clin. + + - + + -
path. + - - + - -
d.p.i. 328 308 n/a 335 301 279

Figure 6.5. Histopathological analysis of brain tissues from terminally scrapie affected mice. Mice were inoculated with ME7 scrapie via skin scarification 6 days post DTX-mediated $CD11c^{+}CD169^{+}$ cell depletion and brains from each clinically scrapie affected mouse analysed by immunohistochemistry. Abundant PrP^{d} accumulations were detected in the hippocampi of clinically and pathologically positive mice from each group (**A**,**D)** and to a lesser extent in the clinically positive, pathologically negative mice (**B**,**E**). No PrP^{d} was detected in the clinically negative mice (**C**,**F**). (**G-L**) PET blot analysis confirmed the presence of proteinase K resistant PrP^{Sc} in tissues where PrP^{d} was detected. Varying degrees of gliosis were confirmed, consistent with PrP^{Sc} accumulation and clinical scores, through labelling with the GFAP antibody (astrocytes) (**M-R**), and the Iba1 antibody (microglia) (**Y-DD**). Sections were counterstained with haematoxylin Z. (**S-X**) Haematoxylin and eosin (H&E) staining revealed extensive vacuolation in the brains from clinically and pathologically positive mice. Clin: clinical score; path: pathological score, positive (+) or negative (-); d.p.i.: days post-inoculation on which tissues were taken for analysis. Images are representative of observations from 7 different animals. Scale bar: top 3 rows, 500 µm rows; and bottom two rows, 100 µm.

Table 6.3. PrP^{Sc} accumulation and disease pathogenesis in CD11c-DTR→WT mice following $CD11c^{+}CD169^{+}$ cell depletion

Group	Incubation period or *survival times* (days)	Clinical disease	Vacuolar pathology in brain	PrP^{Sc} in brain	PrP^{Sc} in lymphoid tissues
CD11c-DTR→WT+DTX	328	yes	yes	yes	yes
CD11c-DTR→WT+DTX	308	yes	no	yes	yes
CD11c-DTR→WT+DTX	n/a	no	no	no	yes
CD11c-DTR→WT+PB	335	yes	yes	yes	yes
CD11c-DTR→WT+PB	301	yes	no	yes	yes
CD11c-DTR→WT+PB	279	no	no	no	yes

6.3.3. Effect of $CD11c^{+}CD169^{+}$ cell depletion on PrP^{Sc} accumulation in the spinal cord

Several animals were unfortunately culled before manifestation of clinical signs or before reaching disease endpoint. Immunohistochemical analysis confirmed PrP^{Sc} deposition in the brains of some of these animals. Spinal cords collected from these animals were therefore analysed for the presence of PrP^{Sc} through Western blot analysis. Samples were treated in the presence or absence of proteinase K, to determine the presence of disease specific PrP^{Sc}. Spinal cords were found to contain varying amounts of PrP^{Sc} in both groups, dependant on their clinical and pathological score and the d.p.i. when the tissues were collected (Fig. 6.6.). The longer the mice survived after scrapie infection, the larger the quantities of PrP^{Sc} appeared to be present in their spinal cords. These results confirmed the presence of disease specific PrP^{Sc} in the CNS before a positive clinical score was determined. Disease specific PrP^{Sc} was also detected in the spinal cords of clinically positive mice that were found to be negative for scrapie pathology through vacuolation (Fig. 6.6). The three bands found between approx. 50-60 kDa are most likely dimers of PrP.

Spinal cords were collected from terminally scrapie affected mice and analysed by Western blot. Samples were treated in the presence or absence of proteinase K, to determine the presence of disease specific PrP^{Sc}. Spinal cords were found to contain large amounts of PrP^{Sc} in both groups (Fig. 6.7.).

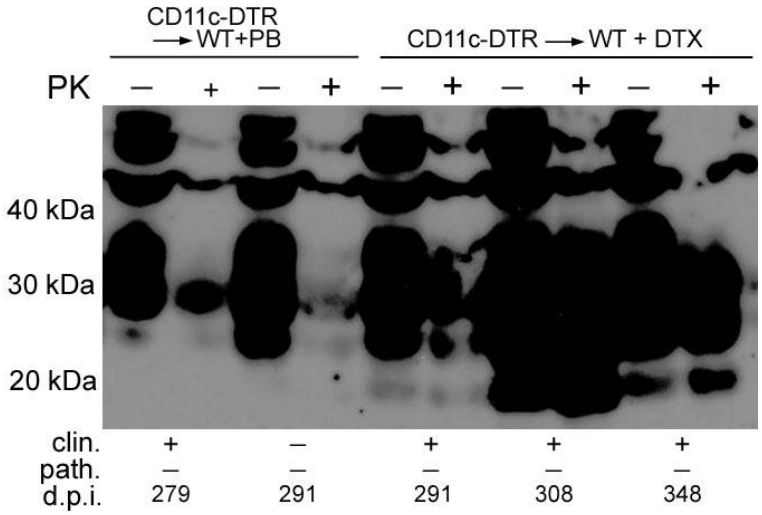

Figure 6.6. PrP^{Sc} accumulation in the spinal cord of mice suffering intercurrent deaths. Mice were infected with scrapie via the skin 6 days post DTX-mediated $CD11c^{+}CD169^{+}$ cell depletion. Spinal cord was collected from animals that died before reaching disease endpoint, and samples analysed via Western blot. Samples were treated in the presence (+) or absence (-) of PK prior to electrophoresis. Proteinase K resistant, scrapie specific, PrP^{Sc} was detected, with pAb 1B3, in varying levels in the spinal cords of animals in both groups. Clin, clinical score; path, pathological score, positive (+) or negative (-); d.p.i.: days post-inoculation on which tissues were taken for analysis.

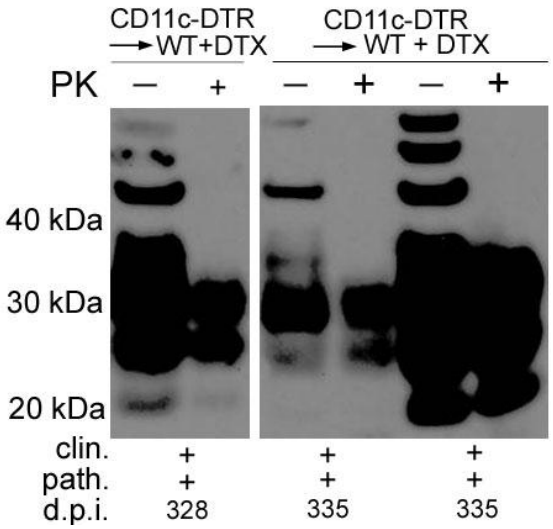

Figure 6.7. PrP^{Sc} accumulation in the spinal cord of terminally scrapie affected mice. Mice were inoculated with ME7 scrapie via skin scarification 6 days post DTX-mediated $CD11c^{+}CD169^{+}$ cell depletion. Spinal cords were collected from terminally scrapie affected animals and analysed via Western blot. Samples were treated in the presence (+) or absence (-) of PK prior to electrophoresis. Proteinase K resistant, disease specific, PrP^{Sc} was detected, with pAb 1B3, in the spinal cords of endpoint animals in both groups. Clin: clinical score; path: pathological score, positive (+) or negative (-); d.p.i.: days post-inoculation on which tissues were taken for analysis.

6.4. Discussion

In this chapter C57BL/6 wildtype mice were lethally γ-irradiated before reconstitution with CD11c-DTR bone marrow. The mice were subsequently injected with DTX, or PB control, to deplete $CD11c^+$ cells 6 days prior to scrapie exposure via skin scarification of the inner thigh. By scarifying the mice 6 days after DTX injection, $CD11c^+CD169^-$ cells (classical DCs) had repopulated the tissues. For other cell types, such as the $CD11c^+CD169^+$ cells, this had not occurred by 6 days post depletion, and these cells remained depleted at the time of scrapie infection.

Unlike the results observed in Chapter 4, this experiment indicated no difference in levels of PrP^{Sc} accumulation in the draining iLNs 5 and 7 weeks after scrapie exposure via the skin. Examination of tissues at higher magnification indicated the accumulation of PrP^{Sc} within tingible body macrophages, as well as on the FDC networks. These results were observed at both the early time points, and in both the groups, and therefore appear to be independent of $CD11c^+$ $CD169^+$ depletion.

The number of clinically and pathologically scrapie positive mice was too low, in each group, to determine mean incubation times for the groups. However, immunohistochemical and Western blot analysis of lymphoid tissues and CNS confirmed the presence of PrP^{Sc} accumulation in these animals consistent with development of scrapie in these mice. It is probable that these mice would have succumbed to the disease if they had lived for longer. The absence of a difference in PrP^{Sc} accumulations at the early time points implies that no significant difference

would have been observed between the mean incubation times of the two groups, if sufficient numbers of mice had succumbed to clinical disease.

In Chapter 4, the absence of $CD11c^+$ cells at the time of scrapie exposure via the skin, delayed PrP^{Sc} accumulation in the draining iLN, 5 weeks post infection. No significant differences were observed in the incubation times between the groups, but larger group numbers may have confirmed a lengthening of the incubation time. These results could not be attributed solely to the absence of cells classically termed DCs, because other cell types were also depleted by injection of DTX (Bradford *et al.*, 2011; Probst *et al.*, 2005). The absence of any change in PrP^{Sc} accumulation at the early time points following scrapie infection 6 days post DTX injection indicates that the differences observed in Chapter 4 were a result of the depletion of $CD11c^+CD169^-$ cells.

Complement receptors, as well as complement components C1q and C3 are considered to play an important role in TSE agent localisation to FDCs (Klein *et al.*, 2001; Mabbott *et al.*, 2001; Zabel *et al.*, 2007). Complement receptors on FDCs play a role in trapping immune complexes to the surface of FDCs (van den Berg *et al.*, 1995). It is therefore a possibility that PrP^{Sc} might reach the FDCs in lymphoid tissues via immune complexes. SCS macrophages have been linked to the transport of immune complexes from the SCS to the lymphoid follicles (Phan *et al.*, 2007). If these cells were, similarly, involved in the transport of the scrapie agent, for example through immune complexes, their depletion prior to scrapie infection via the scrapie agent would affect PrP^{Sc} accumulation in the draining iLN, and might subsequently

alter the expected incubation time for these mice. Depletion of these cells prior to scrapie exposure via the skin failed to affect accumulation of PrP^{Sc} in the draining iLNs.

While it is possible that the scrapie agent reaches the draining iLNs by first entering the SCS, the lack of effect on PrP^{Sc} accumulation in mice depleted of SCS macrophages, indicates that these cells do not play a role in the transport from the SCS to the lymphoid follicles. Alternatively, if this is a route of transport of the scrapie agent from the skin, then scrapie agent is not immediately transported from the skin. This possibility is ruled out based on the results in Chapter 4. Equally, Phan *et al*, described the appearance of antigen-immune complexes as early as 15 minutes after injection, thereby indicating that transport to the SCS is a rapid process. If the scrapie agent were not transported from the skin until after the SCS macrophage numbers had repopulated the tissues, then during the experiment from Chapter 4, the depleted $CD11c^{+}$ $CD169^{-}$ cells would have repopulated tissues earlier than the SCS macrophages (as shown in Chapter 3), and there would not have been a delay in PrP^{Sc} accumulation in the draining iLN after $CD11c^{+}$ cell depletion.

The results in this chapter therefore indicate that SCS macrophages do not play a direct role in the accumulation of PrP^{Sc} in the draining LNs of mice following scrapie infection via the skin.

7

CHARACTERISATION OF DIPHTHERIA TOXIN INDUCED CELL DEPLETION IN THE LANGERIN-DTR MOUSE

7.1. Abstract

The skin is the body's first line of defence against infection, as such there are a number of different immune cells resident within the layers of the skin. Langerin$^+$ epidermal LCs and langerin$^+$ dermal DCs are two such cell types. The use of a transgenic mouse line (langerin-DTR) where langerin$^+$ cells can be transiently depleted, by DTX injection, through their expression of DTR on their surfaces, allows for the characterisation of langerin$^+$ cell depletion and repopulation in the skin and lymphoid tissues. It was possible to establish a timeline for depletion and repopulation of langerin$^+$ cells in the skin. Following DTX treatment LCs were depleted and had not fully repopulated the epidermis by 7 weeks after treatment. In contrast, langerin$^+$ dDCs were depleted at the same time as LCs, but had repopulated the dermis much earlier than LCs. The creation of transgenic langerin-DTR/C56BL/6 wildtype chimeric mice, where transgenic mice were reconstituted with wildtype bone marrow, or wildtype mice reconstituted with transgenic bone marrow allowed for the targeted depletion of either LCs or langerin$^+$ dDCs, independently of each other. These findings can be further utilised to study the role of these two cellular subsets in desired models.

7.2. Introduction

Chapters 3 - 6 have dealt with the effects of the depletion of $CD11c^+$ cells in scrapie transmission from the skin. CD11c is expressed on a wide range of cell types, and following DTX-mediated depletion of in CD11c-DTR→WT mice, $CD11c^+$ cell subsets repopulate tissues at different rates. It was thereby possible to exclude $CD11c^+CD169^-$ classical DCs by waiting for these cells to repopulate tissues. Equally it was possible to exclude the influence of the epidermal LCs from those studies by using CD11c-DTR transgenic bone marrow in wildtype mice, where the LCs were not depleted. Chapter 7 (and subsequently Chapter 8) will focus on the $langerin^+$ cells by using the langerin-DTR mouse line (Kissenpfennig *et al.*, 2005b), which was created in a similar way to the CD11c-DTR mouse line (Jung *et al.*, 2002) described in previous chapters. The DTR transgene is expressed on $langerin^+$ cells and as a consequence, these cells are specifically depleted through a single i.p. injection of DTX.

Langerin is highly expressed by the LCs in the epidermis. The dermis contains two major DC subpopulations, one is $langerin^+$ and the second one is $langerin^-$ subpopulation. Both these dDC subsets were depleted in CD11c-DTR and CD11c-DTR→WT mice, but langerin expression, or lack thereof, will allow for experiments which differentiate between the two cell types and further expand knowledge of the potential differing roles between these subsets.

Until a few years ago, studies from different laboratories investigating the role and function of LCs often obtained contrasting results, this was dubbed the LC paradigm

(Kissenpfennig and Malissen, 2006). Some of these differences were attributed to the use of different inbred mouse strains, as a number of different cellular subsets were identified with differing langerin$^+$ expression observed between the mouse lines (Flacher *et al.*, 2008). Identification, in 2007, of langerin$^+$ dDC (Bursch *et al.*, 2007; Ginhoux *et al.*, 2007; Poulin *et al.*, 2007) unravelled the mystery of this 'paradigm'. The presence of a second langerin-expressing cell type in the skin, that migrated from the skin at a faster rate than LCs (Kissenpfennig *et al.*, 2005b; Nagao *et al.*, 2009), and repopulated their tissues of origin faster after DTX-mediated depletion (Bursch *et al.*, 2007; Ginhoux *et al.*, 2007; Nagao *et al.*, 2009), explains why research into the role of langerin$^+$ cells was sometimes contradictory. These langerin$^+$ dDCs also appear to carry out independent functions from epidermal LCs (Bennett *et al.*, 2005; Fukunaga *et al.*, 2008; Henri *et al.*, 2010; Nagao *et al.*, 2009; Poulin *et al.*, 2007; Shklovskaya *et al.*, 2008). These findings help to explain the discrepancy previously observed between different research laboratories; some data can be attributed to a role for the epidermal LC, while other results can be attributed to the langerin$^+$ dDCs.

This chapter aims to gain an understanding of the potential involvement of LC and langerin$^+$ dDCs in scrapie pathogenesis by using temporary conditional DTX-mediated depletion. Data from this chapter will determine depletion and repopulation dynamics of these different cell subsets after DTX treatment. These data will be utilised in Chapter 8 to determine the potential role of these different subsets in scrapie transmission from the skin.

7.3 Results

7.3.1. Detection of the DTR transgene

The presence of the DTR (Heparin binding EGF-like growth factor: *Hbegf*) transgene on the surface of langerin$^+$ cells in langerin-DTR mice allows for the temporary depletion of langerin$^+$ cells through a single i.p. injection of DTX. Genotyping was routinely carried on all langerin-DTR mice used to confirm presence of the DTR transgene before inclusion in any experiment. The DTR oligonucleotide, in combination with the two oligonucleotides for *Cd207* (langerin), produced a PCR product with a band size of 866 base pairs, was present on the *Cd207* gene (Fig. 7.1.). In the case of a wildtype animal, the two *Cd207* oligonucleotides produced a PCR product with a band size of 329 base pairs, consistent with the wildtype *Cd207* gene (Fig. 7.1.).

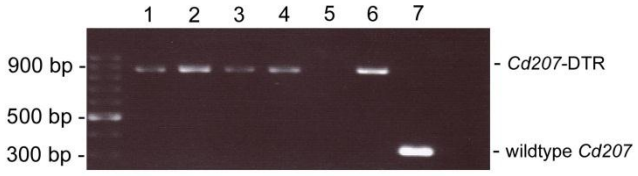

Figure 7.1. Confirmation of the presence of DTR and langerin in DNA from langerin-DTR mice Lanes 1-4: langerin-DTR samples, 5: blank, 6: langerin-DTR positive control from previous PCR, 7: wildtype control.

7.3.2. Effect of DTX treatment on langerin$^+$ cells in the skin and draining iLN

To examine the effect of DTX treatment on langerin$^+$ cells in the skin, langerin-DTR mice received a single i.p. injection of DTX, or PB control, and tissues were collected for *ex vivo* analysis from 4 mice/group at 0, 2, 7, 14, 22 days, and 7 weeks post injection. Immunofluorescent analysis of epidermal and dermal sheets with the anti-langerin specific antibody confirmed that LCs were completely depleted from the epidermis two days after DTX injection, and remained absent for at least 3 weeks (Fig. 7.2.). LCs started to reappear in large clusters by 7 weeks post DTX injection, but the tight LC network observed in untreated animals, was still disrupted (Fig. 7.2.). Langerin$^+$ cells in the dermis are not as uniformly distributed within the dermis (Nagao *et al.*, 2009), but are readily visualised in dermal sheets. These cells were also depleted 2 days after DTX injection, but in contrast to epidermal LCs, they appeared to have returned to a similar density to that observed in untreated mice by 14 days post treatment (Fig. 7.2.). These data are consistent with data from similar published studies (Bursch *et al.*, 2007; Ginhoux *et al.*, 2007; Nagao *et al.*, 2009).

Mice were injected according to the following groups 2 days prior to tissue collection for *ex vivo* analysis: WT+DTX; langerin-DTR+DTX, and langerin-DTR+PB (Table 7.1.). Immunofluorescent analysis of ear epidermal and dermal sheets confirmed normal langerin$^+$ cell distribution in WT+DTX or langerin-DTR+PB animals (not shown). LCs and langerin$^+$ dDCs were completely depleted (not shown), confirming that DTX-mediated langerin$^+$ cell depletion, is specific to DTR transgenic animals. Immunofluorescent analysis of iLNs confirmed a partial depletion of langerin$^+$ cells in the langerin-DTR+DTX group, compared to the control groups (Fig. 7.3.).

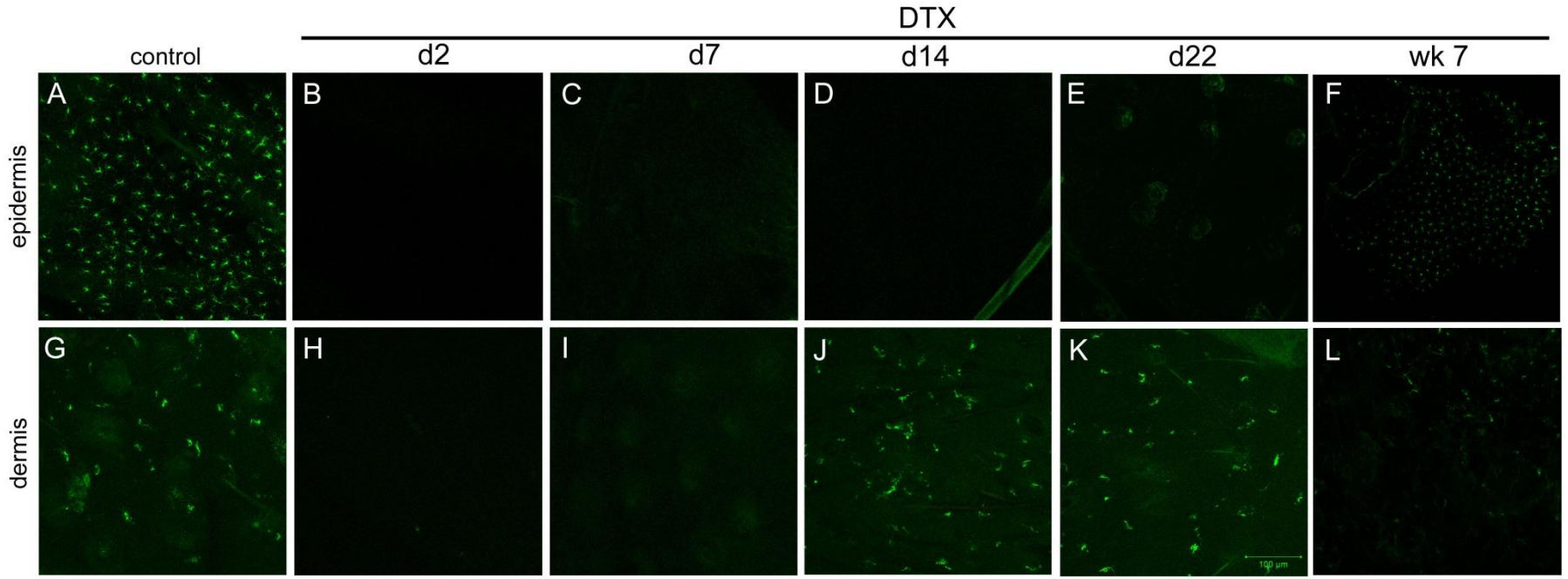

Figure 7.2. Timeline of DTX-mediated langerin$^+$ cell depletion in the skin of langerin-DTR mice. Mice received a single i.p. injection of DTX and epidermal and dermal ear sheets collected at the time points indicated were immunolabelled with the anti-langerin specific antibody (green). (**A**,**G**) Normal distribution of LCs and langerin$^+$ dDCs in the epidermis and dermis in DTX untreated mice. Two days after DTX injection, (**B**) a complete depletion of LCs was observed. Cells had not returned by day 22 post DTX (**E**). LCs had reappeared in the epidermis in small organised clusters 7 weeks post DTX injection, the whole surface of the epidermis was not covered (**F**). Two days after DTX injection, (**H**) depletion of langerin$^+$ dDCs was observed. Langerin$^+$ dDCs numbers resembled controls by day 14 post DTX (**K**). Images are representative of observations in 4 different animals. Scale bar: 100 µm.

Table 7.1. Depletion status of langerin$^+$ cells in the skin of langerin-DTR or wildtype mice.

			Depletion status	
Genotype	**DTX**	**LCs**	**langerin$^+$ dermal DCs**	**langerin$^-$ dermal DCs**
WT	yes	no	no	no
langerin-DTR	yes	yes	yes	no
langerin-DTR	no	no	no	no

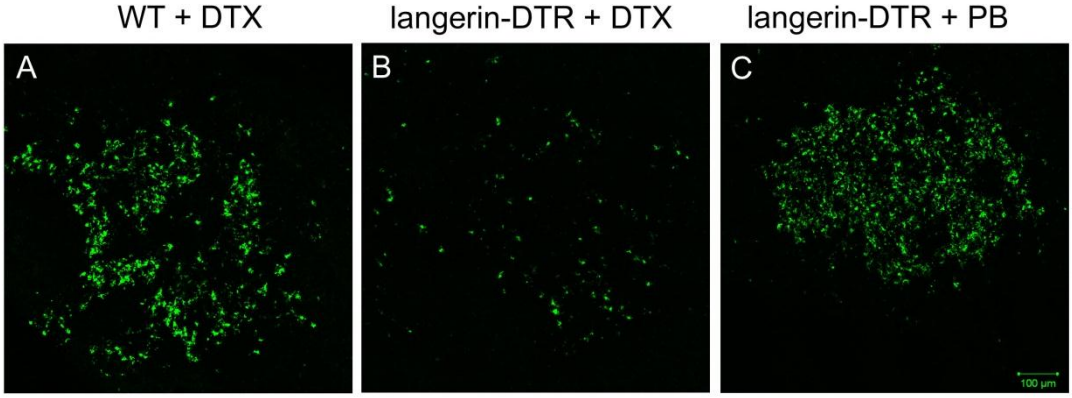

Figure 7.3. Langerin$^+$ cell depletion in the draining iLN following DTX injection. Mice were given a single i.p. injection of DTX, or PB control, and epidermal and dermal sheets collected two days later were immunolabelled with the anti-langerin specific antibody (green). **(A**,**C**) Normal distribution of langerin$^+$ cells in the iLN in control groups. Partial depletion of langerin$^+$ cells in the iLN of DTX treated mice, in comparison to control groups (**B**). Images are representative of observations in 3 animals/group. Scale bar: 100 µm.

7.3.3. Depletion of other cell types

As well as skin-resident and migratory LCs and DCs, other langerin$^+$ DC subsets in other organs are also depleted through DTX treatment in the langerin-DTR mouse. To determine a timeline for depletion of these cell populations, Lung, liver, heart, and kidney were also analysed. These subpopulations comprise a very small percentage of the cells in these tissues. Immunofluorescent analysis indicated that langerin$^+$ cells were rare in these tissues (Fig. 7.4.), although they were more abundant in the liver and lungs compared to in the heart and kidney (Fig. 7.4.). There did not appear to be a sufficient number of langerin$^+$ cells detected through immunofluorescence labelling to determine a potential effect of DTX on their status.

Further immunohistochemical anlaysis was carried out on spleen and iLN (not shown) from DTX treated and untreated animals. Immunofluorescence analysis was used to determine any potential secondary effect of DTX treatment on CD35 expressing FDCs and B lymphocytes. No differences were observed following DTX injection (Fig. 7.5.).

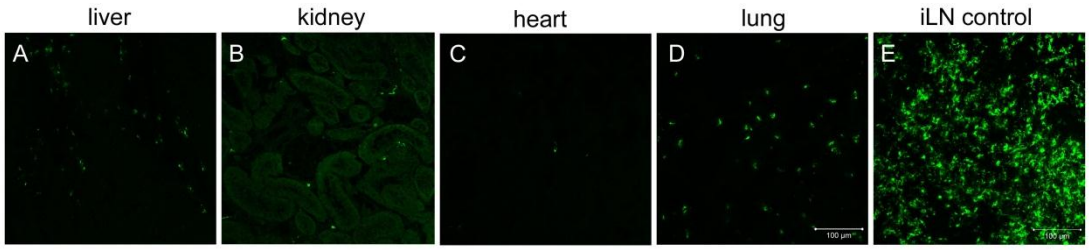

Figure 7.4. Langerin$^+$ cells in the liver, lung, kidney, and heart. Tissues were collected from untreated mice and immunolabelled with the anti-langerin specific antibody (green) to assess normal distribution of langerin$^+$ cells in non-lymphoid organs. Langerin expression on cells in the kidney (**B**) and heart (**C**) was very scarce. Langerin expression was more abundant in the liver (**A**) and lung (**D**). Images are representative of observation in 4 animals. Scale bar: 100 µm.

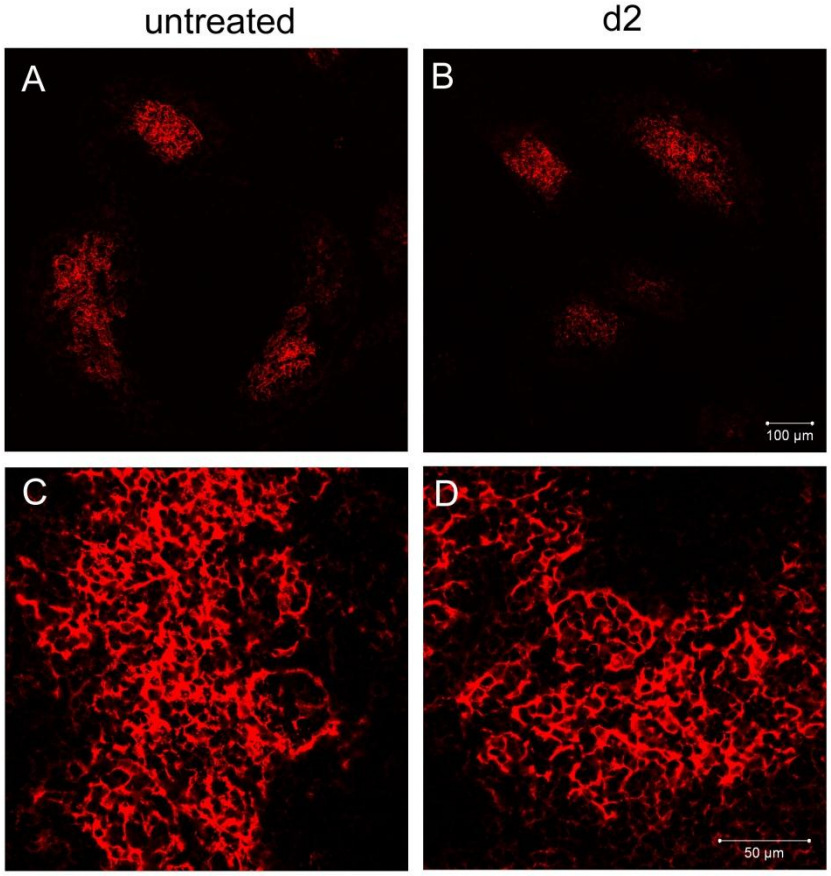

Figure 7.5. Effect of DTX injection on CD35-expressing cells in the langerin-DTR mouse. Mice were given a single i.p. injection of DTX and spleens collected at the times indicated were immunofluorescently labelled with the anti-CD35 specific antibody to detect FDCs and CD35-expressing B lymphocytes (red). **C** and **D** are higher magnification images of **A** and **B**. Normal distribution of CD35 expressing cells were observed in the lymphoid follicles of the spleen 2 days post DTX injection (**B**,**D**), compared to untreated controls (**A**, **C**). Images are representative of observations in 3 different animals. Scale bar: top, 100 µm; bottom, 50 µm.

7.3.4. Effect of DTX on FDC status

To determine whether injection of DTX and depletion of large numbers of langerin$^+$ cells had an effect on langerin$^-$ cell types such as FDCs, or their expression of PrP^c, in lymphoid follicles, immunofluorescence analysis was carried out on spleen and iLNs from mice in each treatment group. Mice were injected as outlined in Figure 7.6. and tissues were collected for *ex vivo* analysis two days post injection. Tissues were immunolabelled to detect B lymphocyte subsets and FDCs. Spleen and iLN were also immunolabelled to detect PrP^c, to determine whether expression was influenced by DTX treatment. Analysis confirmed no observable differences in labelling intensity or location of the FDCs and B lymphocytes in the langerin-DTR+DTX animals compared to the two control groups (Fig. 7.6. and Fig. 7.7.). Equally, the expression of PrP^c on FDC networks was not affected in the langerin-DTR+DTX mice, when compared to the control animals in either the spleen (Fig. 7.6.) or iLN (Fig. 7.7.).

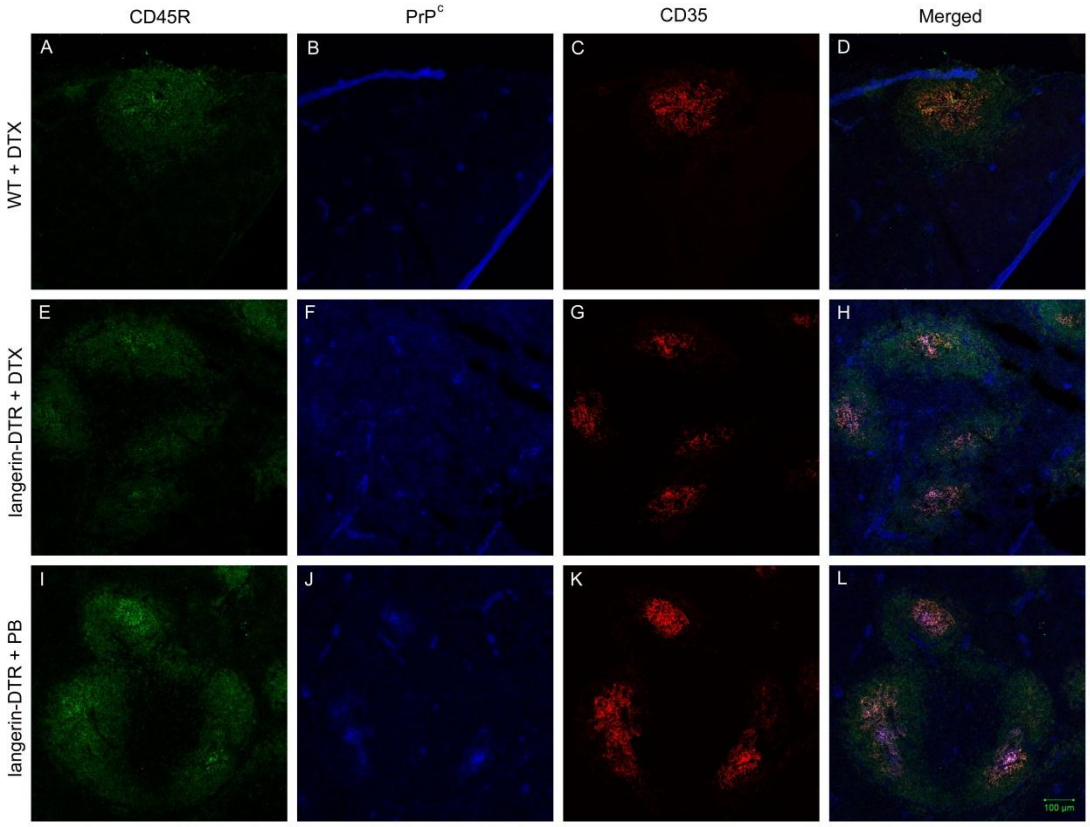

Figure 7.6. DTX treatment of langerin-DTR mice had no effect on FDC and B cell status in the spleen. Mice were given a single i.p. injection of DTX and spleens collected two days later were immunolabelled with the anti-CD45R (green, **A,E,I**); the anti-CD35 (red, **C,G,K**); and anti-PrP (1B3) (blue, **B,F,J**) specific antibodies. FDC and B cell status were unaffected in each group; PrP^c expression was, equally, unaffected on the FDCs, regardless of DTX or PB treatment **D, H, L** merged images of all three antibodies. Images are representative of observations in 3 animals/group. Scale bar: 100 µm.

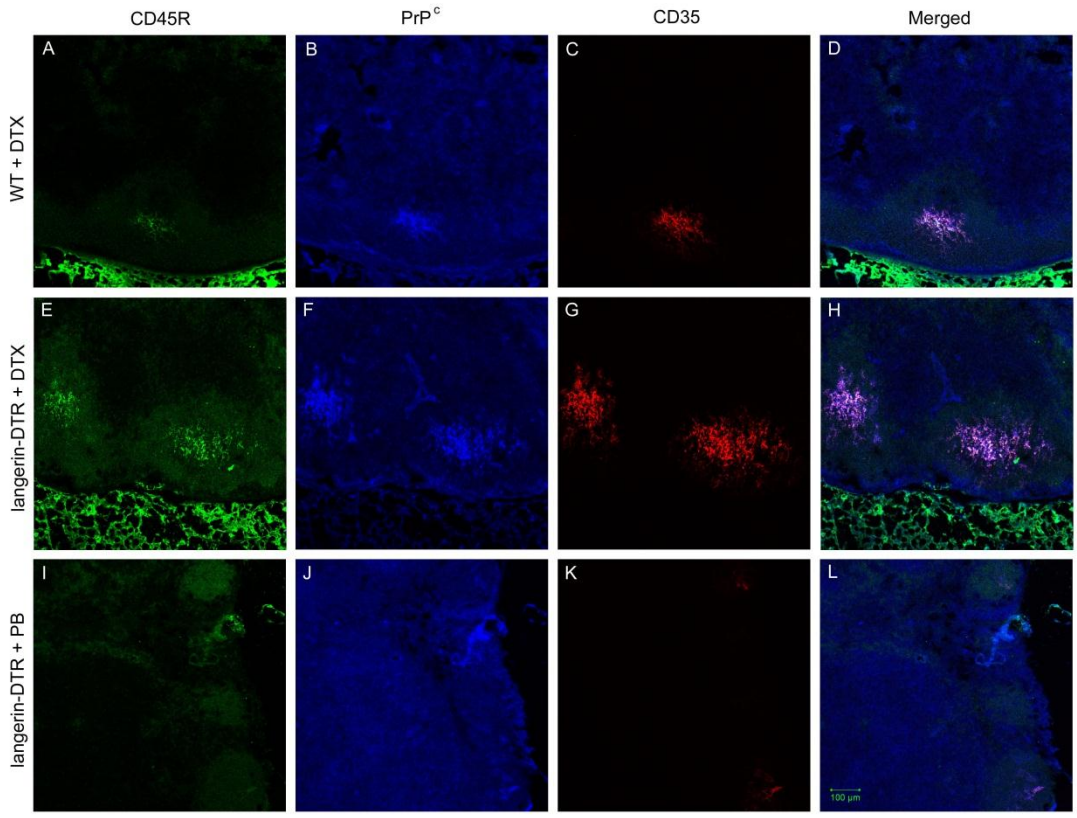

Figure 7.7. DTX treatment of langerin-DTR mice had no effect on FDC and B cell status in the draining iLN. Mice received a single i.p. injection of DTX and iLNs collected two days later were immunolabelled with the anti-CD45R (green, **A,E,I**); the anti-CD35 (red, **C,G,K**); and anti-PrP (1B3) (blue, **B,F,J**) specific antibodies. FDC and B cell status were unaffected in each group; PrP^c expression was, equally, unaffected on the FDCs, regardless of DTX or PB treatment **D, H, L** merged images of all three antibodies. Images are representative of observations in 3 animals/group. Scale bar: 100 µm.

7.3.5. Langerin-DTR bone marrow chimeric mice

A series of bone marrow reconstitution experiments were put in place to provide the opportunity to specifically deplete only the epidermal LCs or the langerin$^+$ dDCs following DTX treatment. C57BL/6 wildtype or langerin-DTR transgenic mice were lethally γ-irradiated 24 hr prior to receiving a full bone marrow reconstitution from langerin-DTR mice or C57BL/6 wildtype mice, respectively. Eight weeks after bone marrow reconstitution the mice were injected with DTX, or PB control, as indicated in Fig. 7.8.

Mononuclear phagocytes in the lymphoid tissues are radio sensitive and will be of donor origin 8 weeks after bone marrow reconstitution. LCs are relatively radio resistant, and are host derived up to 18 months post irradiation and bone marrow reconstitution (Merad *et al.*, 2002). In the wildtype mice reconstituted with langerin-DTR transgenic bone marrow (langerin-DTR→WT), the LCs, of host origin, did not express the DTR transgene. The other langerin$^+$ cells were donor derived, expressed the DTR transgene, and were susceptible to depletion following DTX treatment (Table 7.2.). The langerin-DTR mice reconstituted with wildtype bone marrow (WT→langerin-DTR) contained DTR-expressing LCs, being of host origin. The other langerin$^+$ cells were donor derived, did not express the transgene, and were not susceptible to depletion (Table 7.2.)

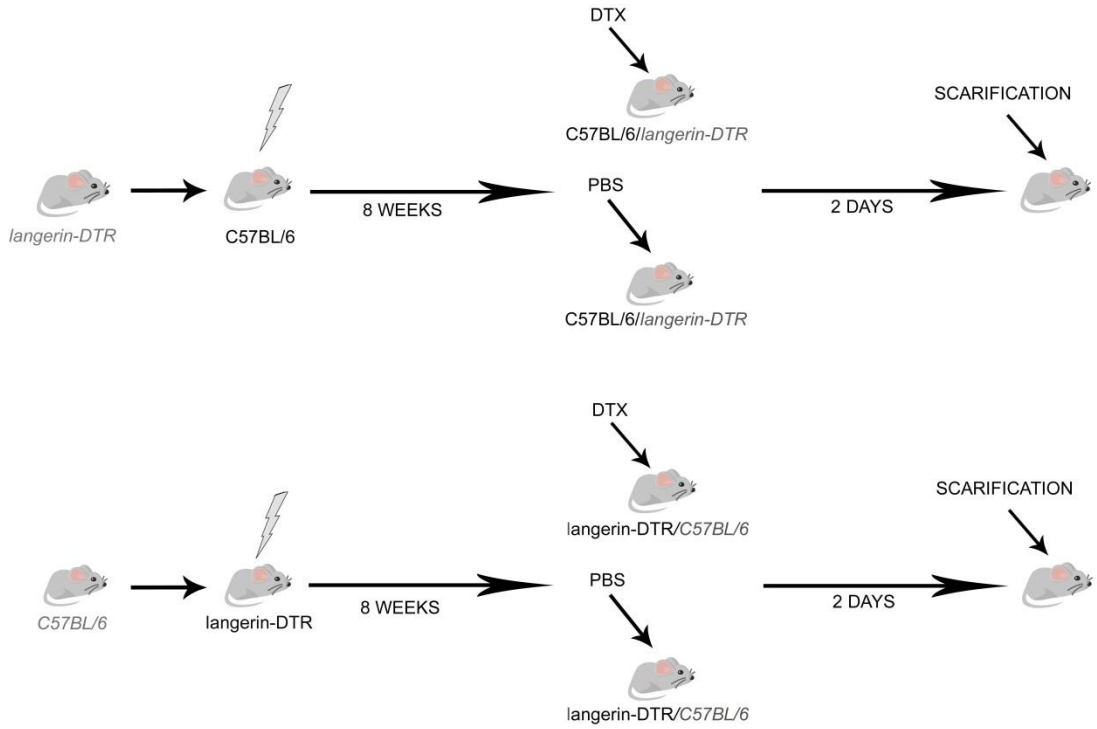

Figure 7.8. Model of irradiation and bone marrow reconstitution. C57BL/6 wildtype or langerin-DTR transgenic mice were lethally γ-irradiated 24 hr prior to receiving a bone marrow graft (grey) from langerin-DTR mice or C57BL/6 mice, respectively. After 8 weeks mice were split into four groups. Mice that received wildtype bone marrow were injected with DTX, or PB control. Mice that received transgenic bone marrow were injected with DTX, or PB control.

Table 7.2. Depletion status of langerin$^+$ cells in the skin following lethal irradiation and reconstitution.

			Depletion status		
Host genotype	**Donor genotype**	**DTX**	**LCs**	**langerin$^+$ dermal DCs**	**langerin$^-$ dermal DCs**
WT	langerin-DTR	yes	no	yes	no
WT	langerin-DTR	no	no	no	no
langerin-DTR	WT	yes	yes	no	no
langerin-DTR	WT	no	no	no	no

7.3.6. DTX-mediated langerin$^+$ cell depletion in bone marrow chimeric mice

To determine the effect of DTX injection on the status of langerin$^+$ cells in langerin-DTR bone marrow chimeric mice, 4 animals in each group described in Table 7.2. and Fig. 7.8. received a single i.p. injection of DTX and tissues collected for *ex vivo* analysis 2 days later. Immunofluorescent analysis was carried out on ear epidermal and dermal sheets with the anti-langerin specific antibody. As anticipated, LCs in the epidermis of langerin-DTR→WT+DTX were unaffected by DTX treatment, but the langerin$^+$ dDCs were almost completely depleted (Fig. 7.9.). In contrast, the LCs in the epidermis of WT→langerin-DTR+DTX mice were depleted but had started to repopulate in small clusters of 5 or 6 cells (Fig. 7.9.). Larger clusters of LCs could be found in the epidermal sheets of some of the mice (not shown), indicating that maybe a small number of LC progenitor cells were of donor origin. As anticipated, langerin$^+$ dDCs were unaffected by the DTX injection in these mice (Fig. 7.9.). Following DTX-mediated depletion, langerin$^+$ dDCs did not show a clustering effect of cells like that observed for the LCs. Immunofluorescent analysis of the iLN following DTX injection confirmed a partial depletion of langerin$^+$ cells in the langerin-DTR→WT+DTX mice (Fig. 7.10.). Langerin$^+$ cells in the iLN of WT→langerin-DTR+DTX mice were unaffected by DTX treatment (Fig. 7.10.). Further immunofluorescent analysis of the draining iLN, with the anti-langerin specific antibody confirmed a partial depletion langerin$^+$ cells in the langerin-DTR→WT animals following DTX injection (Fig. 7.10.).

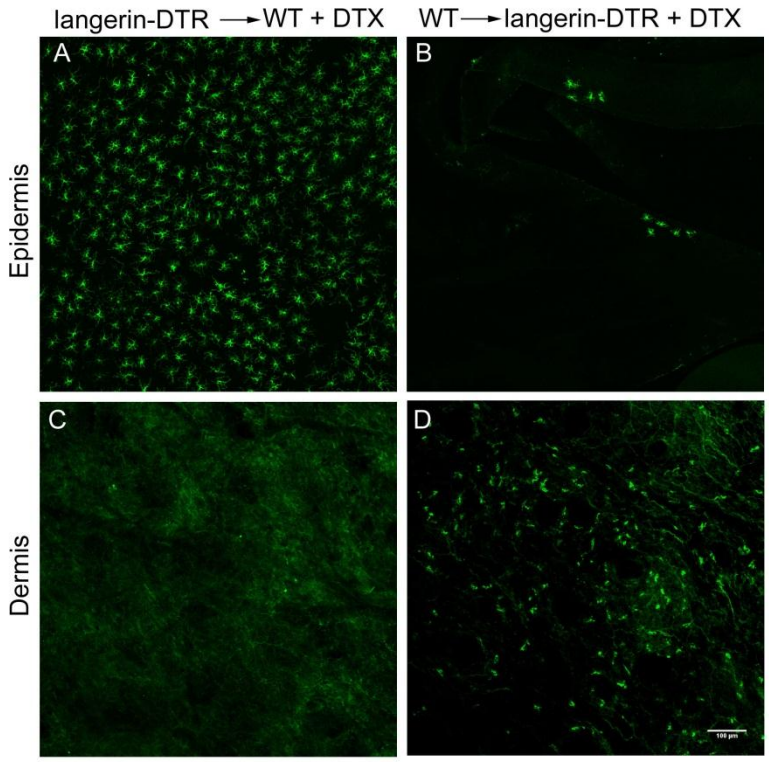

Figure 7.9. Langerin$^+$ cell depletion in the epidermis and dermis of bone marrow chimeric mice. Mice were given a single i.p. injection of DTX, and epidermal and dermal sheets collected two days later were immunolabelled with the anti-langerin specific antibody (green). (**A**) Normal distribution of LCs was observed in the epidermis of langerin-DTR→WT mice following DTX injection. Langerin$^+$ dDCs in the dermis were almost completely depleted (**C**). In the WT→langerin-DTR mice, LCs were depleted in the epidermis, except for a few small clusters of cells following DTX injection (**B**), whereas the langerin$^+$ dDCs in the dermis were unaffected by DTX (**D**). Images are representative of observations in 3 animals/group. Scale bar: 100 µm.

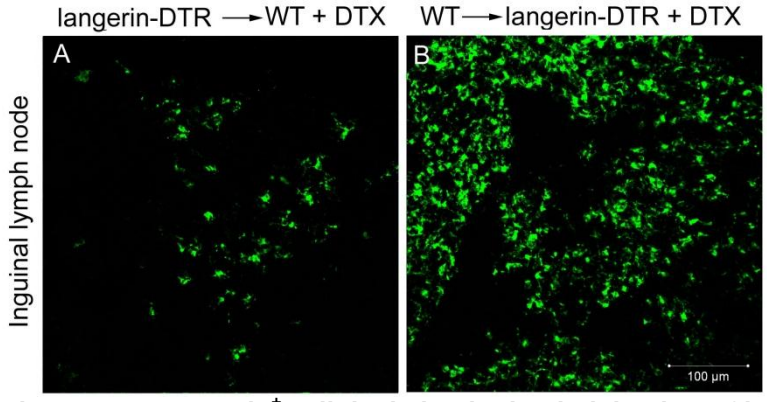

Figure 7.10. Langerin$^+$ cell depletion in the draining iLN of bone marrow chimeric mice following DTX treatment. Mice were given a single i.p. injection of DTX, and iLNs collected two days later were immunolabelled with the anti-langerin specific antibody (green). **A**: Partial depletion of langerin$^+$ cells in the iLN of WT→langerin-DTR mice following DTX injection. **B**: Normal distribution of langerin$^+$ in the iLN of langerin-DTR→WT mice following DTX treatment. Images as representative of observations in 3 animals/group. Scale bar: 100 µm.

7.3.7. DTX treatment of langerin-DTR bone marrow chimeric mice does not affect FDC status

Immunofluorescence analysis was carried out to determine whether DTX-mediated langerin^{+} cell depletion langerin-DTR→WT and WT→langerin-DTR mice had any effect on FDC status, or their expression of PrP^{c}. Analysis was carried out on spleen and iLNs from 4 mice from each group 2 days post DTX treatment. The experiment confirmed that DTX treatment of langerin-DTR→WT and WT→langerin-DTR mice had no observable effect on the status and distribution of FDCs in the lymphoid follicles in either the spleen (Fig. 7.11.) or the iLN (Fig. 7.12.). Equally, PrP^{c} expression on FDC networks was not affected in either of the chimeric mouse groups compared to the control animals in the spleen (Fig. 7.11.) or the iLN (Fig. 7.12.).

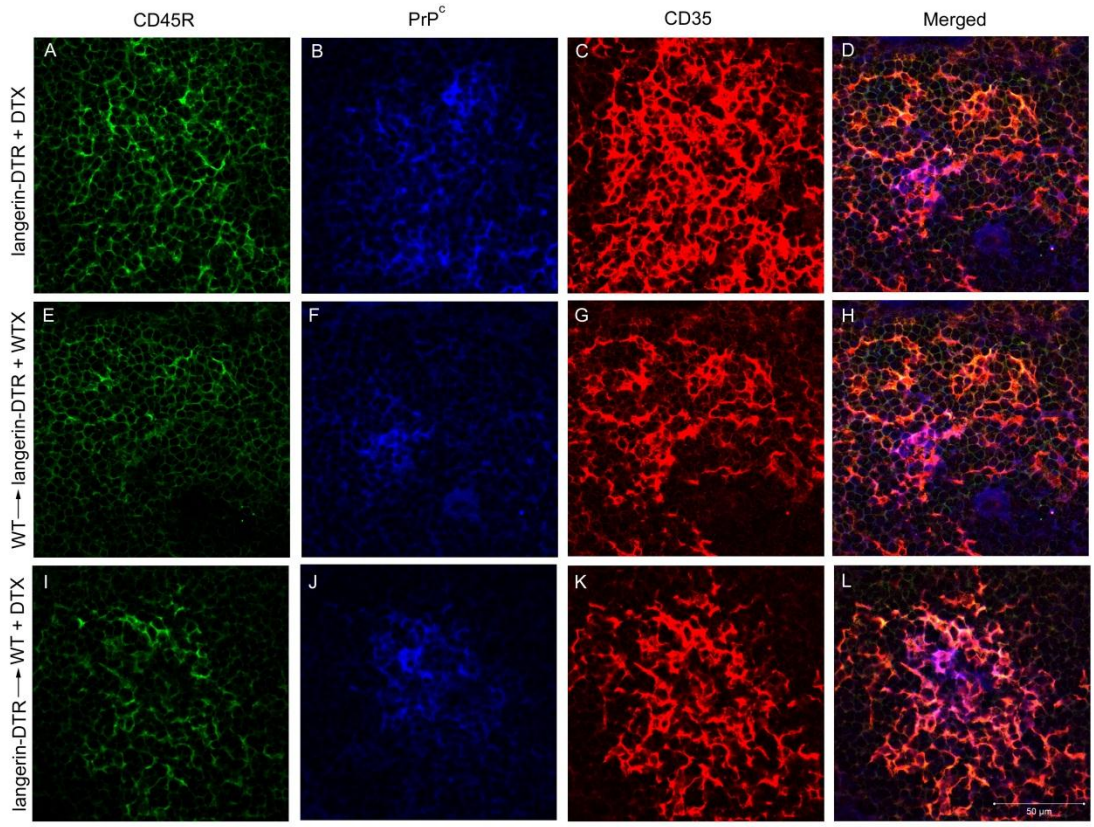

Figure 7.11. DTX treatment had no effect on FDC and B cell status in the spleens of bone marrow chimeric mice. Mice were given a single i.p. injection of DTX and spleens collected two days later were immunolabelled with the anti-CD45R (green, **A**,**E**), anti-PrP (1B3) (blue, **B**,**F**), and anti-CD35 (red, **C**,**G**) antibodies. FDC and B cell status were unaffected in both animal groups; PrP^c expression was, equally, unaffected on the FDCs following DTX treatment. **D**, **H** merged images of all three antibodies. Images are representative of observations in 3 animals. Scale bar: 100 µm.

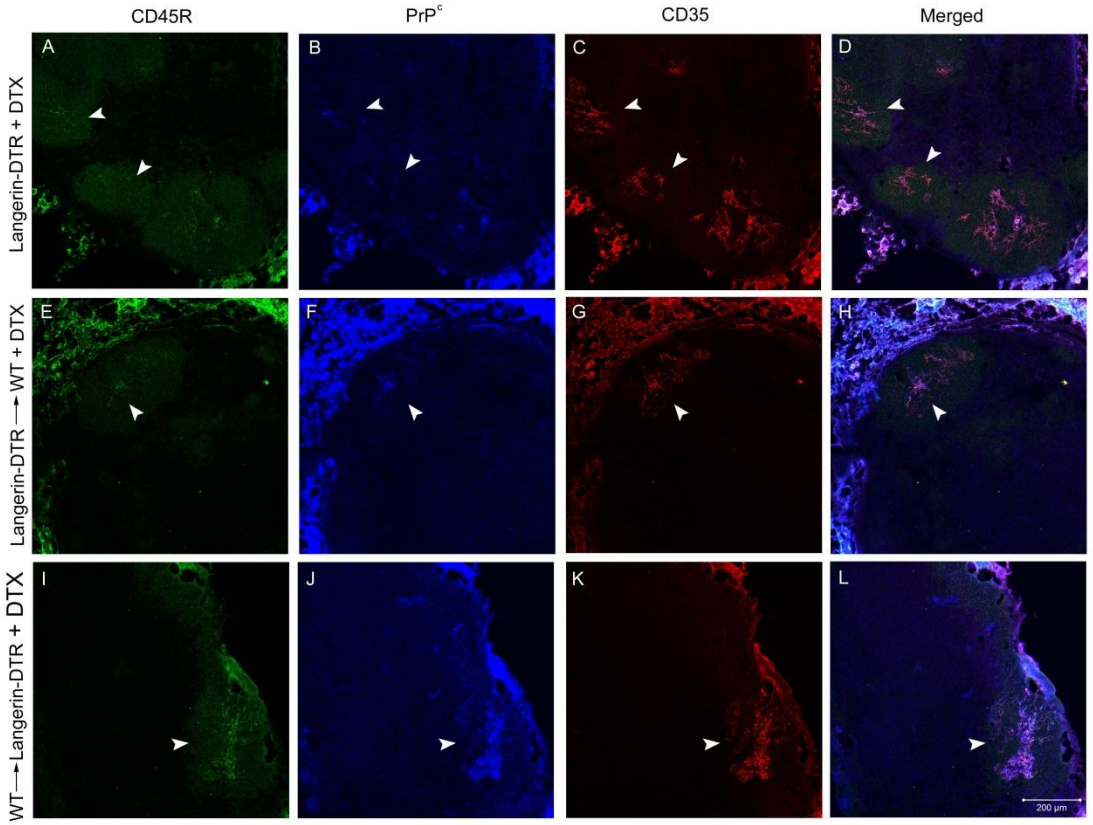

Figure 7.12. DTX treatment had no effect on FDC and B cell status in the iLNs of bone marrow chimeric mice. Mice were given a single i.p. injection of DTX and iLNs collected two days later were immunolabelled with anti-CD45R (green, **A**,**E**), anti-PrP (1B3) (blue, **B**,**F**), and anti-CD35 (red, **C**,**G**) antibodies. FDC and B cell status were unaffected in both animal groups; PrP^c expression was, equally, unaffected on the FDCs following DTX treatment. **D**, **H** merged images of all three antibodies. Images are representative of observations in 3 animals. Scale bar: 100 µm.

7.4. Discussion

In this chapter, characterisation studies were carried out on the langerin-DTR transgenic mouse line to determine a timeline for the depletion and repopulation of langerin$^+$ cells following DTX injection. Tissues were collected for *ex vivo* analysis at various time points following a single i.p. injection of DTX, or PB control. Epidermal and dermal sheet analysis confirmed depletion of LCs as well langerin$^+$ cells in both the dermis and the epidermis following treatment of langerin-DTR mice, in accordance with previous results (Bursch *et al.*, 2007; Ginhoux *et al.*, 2007; Kissenpfennig *et al.*, 2005b; Nagao *et al.*, 2009). As was described in previous studies, the two langerin$^+$ cell types within the skin display very different repopulation dynamics (Bursch *et al.*, 2007; Ginhoux *et al.*, 2007; Nagao *et al.*, 2009), highlighting how different these cells are, and how different their potential roles in skin immunity might be. LCs had not completely repopulated the epidermis by 7 weeks post DTX injection, further highlighting their slow turnover rate (Merad *et al.*, 2002), in comparison to other DC subsets, including the langerin$^+$ dDCs in the dermis, which repopulated the skin in under 2 weeks (Nagao *et al.*, 2009).

Langerin was also expressed on non-lymphoid tissues other than the skin (Douillard *et al.*, 2005; Valladeau *et al.*, 2002), and this was also reproduced in this chapter, although the cell numbers detected by immunofluorescent analysis were not sufficient to carry out a visual comparison of the effects of DTX treatment on their status. To confirm whether DTX-mediated depletion has a substantial impact on non-lymphoid tissues other than the skin, flow cytometric analysis might provide more accurate results.

The depletion of langerin$^+$ cells in the LNs was not complete, even though a large number of cells were depleted. The results resemble those observed in Chapters 3 and 5 in CD11c-DTR→WT mice, where these cells were depleted through their expression of CD11c. DTX-mediated depletion in the bone marrow chimeric mice further outlined the radiosensitive nature of the large proportion of LN-resident langerin$^+$ DCs compared to epidermal LCs. These cells were not depleted in langerin-DTR mice reconstituted with wildtype bone marrow and *vice versa*.

Data from the studies of the bone marrow chimeric mice did establish that it was possible to carry out DTX-mediated depletion of LCs independently of the langerin$^+$ dDCs and *vice versa*. LCs were clearly depleted in langerin-DTR mice reconstituted with wildtype bone marrow. In contrast to LC depletion described earlier in this chapter and in Chapter 3 (section 3.3.2.) small clusters of 5-10 LCs were observed in the epidermis only 2 days post DTX injection. This phenomenon has been previously observed in other studies (Nagao *et al.*, 2009). These results therefore indicate that a small number of LC precursors might be of donor origin, leading to the production of small numbers of donor derived LCs.

In parallel with Chapters 3 and 5, the distribution of other cell types within the lymphoid tissues was also analysed following DTX-mediated depletion or bone marrow reconstitution. CD35 expression within B cell follicles was unaffected by DTX injection in langerin-DTR mice when compared to controls. DTX-mediated depletion did not affect FDC status or their expression of PrP^c in either the langerin-

DTR mice, the langerin-DTR→WT or WT→ langerin-DTR mice. These results confirm that the depletion of langerin^{+} cells in the lymphoid tissues did not adversely affect FDC status in these mice.

Analysis of the langerin-DTR mice established a timeline for the depletion and repopulation of langerin^{+} cells in the epidermis and the dermis of langerin-DTR mice. Langerin^{+} cell depletion was also confirmed in the iLN. Bone marrow chimeric mice were used to show that LCs and langerin^{+} dDCs could be depleted independently of each other. These data will be used to provide a useful foundation to study the role of langerin^{+} and langerin^{-} skin DC subsets in scrapie pathogenesis in the subsequent chapter.

8

EFFECTS OF LANGERIN^{+} CELL DEPLETION ON SCRAPIE TRANSMISSION FOLLOWING INFECTION VIA SKIN SCARIFICATION

8.1. Abstract

Following scrapie infection via the skin scarification, PrP^{Sc} accumuluation occurs first in the draining LNs before spreading to the non-draining LNs and the spleen. DC subsets have been implicated in PrP^{Sc} transport following oral scrapie infection in mice. Chapter 4 demonstrated a delay in the accumulation of PrP^{Sc} in the draining iLN following scrapie infection via skin scarification in mice depleted of $CD11c^{+}$ cells. Bone marrow chimerism in these mice allowed for the temporary depletion of $CD11c^{+}$ cells, with the exception of epidermal LCs. A transgenic mouse model was used, which allows for the temporary depletion of $langerin^{+}$ epidermal LCs and dDCs. It was, thereby, possible to determine that the absence of these $langerin^{+}$ cells at the time of scrapie infection did not delay scrapie agent accumulation in the draining iLNs. In contrast to the results presented in Chapter 4, depletion of $langerin^{+}$ cells prior to scrapie infection increased PrP^{Sc} accumulation in the draining iLNs between 5 and 7 weeks post infection. By using bone marrow chimeric mice that contained the transgene for $langerin^{+}$ cell depletion, it was possible to attribute this increase in PrP^{Sc} accumulation to the absence of epidermal LCs, regardless of whether the $langerin^{+}$ dDCs were present or not. Scrapie incubation period was unaffected in these mice despite the increase in PrP^{Sc} accumulation, thereby indicating that the absence of LCs at the time of scrapie infection via the skin does not affect disease progression, and spread to the peripheral nervous system is likely to have occurred earlier than 7 weeks post infection.

8.2. Introduction

Langerin-DTR mice were analysed in Chapter 7 to characterise the depletion and repopulation of langerin$^+$ cells following DTX-mediated depletion. Chapters 4 and 6 studied the role of CD11c$^+$ dermal cells and SCS macrophages on scrapie transmission. The use of langerin-DTR mice in this chapter will allow for the identification of the potential role of langerin$^+$ dDC and also epidermal LCs cells in scrapie transmission from the skin. The radioresistant nature of LCs, compared to other mononuclear phagocytes lineages allows for the creation of bone marrow chimeras whereby the specific depletion of LCs in the epidermis or the langerin$^+$ dDCs of the dermis can be achieved. These mice were created by lethal γ-irradiation of C57BL/6 wildtype mice and reconstitution with bone marrow from langerin-DTR mice or *vice versa*, creating: langerin-DTR→WT or WT→langerin-DTR mice, respectively. These chimeras were used to attempt to determine the involvement of epidermal LCs or the langerin$^+$ dDCs in scrapie pathogenesis.

The role of LCs in scrapie transmission from the skin has previously been investigated through *in vitro* studies (Mohan *et al.*, 2005c), or by blocking their migration from the skin (Mohan *et al.*, 2005b). These studies were carried out before the identification of the langerin$^+$ dDCs (Bursch *et al.*, 2007; Ginhoux *et al.*, 2007; Poulin *et al.*, 2007). Since then a lot of work has highlighted the potential role of these langerin$^+$ cells in many functions previously attributed to LCs (Henri *et al.*, 2010; Henri *et al.*, 2007; Schröder *et al.*, 2006). In this chapter, by temporarily depleting each cell type independently of the other, it is possible to gain insight into the potential role of each of these langerin$^+$ cell subsets in scrapie transmission from

the skin. In Chapter 7, LCs were confirmed to be completely depleted in the epidermis following DTX injection in the langerin-DTR mice. Seven weeks post DTX injection these cells had not completely repopulated the epidermis (Fig. 7.2.). By contrast, the langerin^{+} cells of the dermis repopulated at a much more rapid rate than the LCs, and were present at similar levels to controls by 14 days post DTX injection (Fig. 7.2.).

Scrapie transmission to the langerin-DTR mice was carried out as outlined in previous chapters. Mice were injected with DTX, or PB control, to deplete the cell population of interest. Two days later mice were infected with scrapie via skin scarification (Fig. 8.1.). Draining and non-draining lymphoid tissues were collected at early time points from animals in each of the three groups outlined in Table 7.1. A number of animals in each group were maintained to reach disease endpoint, to study the effects of cell depletion on scrapie susceptibility. By infecting the langerin-DTR mice 2 days after DTX injection, it was possible to determine whether the absence of langerin^{+} cells at the time of infection affected the early accumulation of PrP^{Sc} in the draining iLNs and the subsequent transmission of disease to the brain.

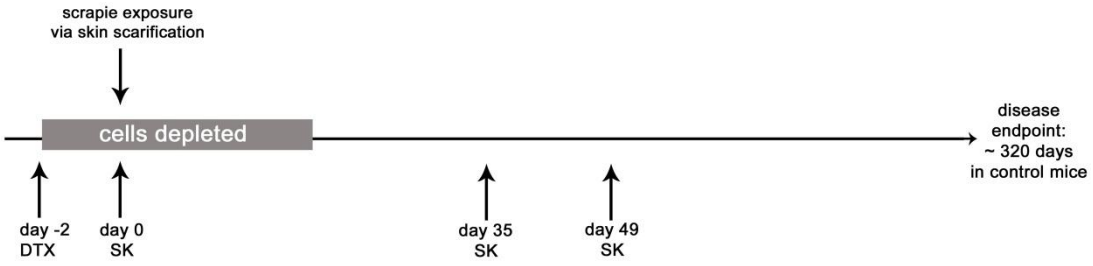

Figure 8.1. Experimental timeline. Mice were given a single injection of DTX, or PB, two days prior to inoculation with the scrapie agent via skin scarification. SK: serial kill. From each of the three groups tissues were collected from uninfected mice, at day 0 (with respect to TSE infection), 35, and 49 days after scrapie infection. In each group 8 animals were left to reach disease endpoint.

8.3. Results

Several studies were carried out to determine the role of the different langerin^{+} cells in the role of early scrapie accumulation and subsequent transmission. Sections 8.3.1.-8.3.3. describe the studies carried out in langerin-DTR mice. Section 8.3.4. describes the results obtained following scrapie infection via the skin of bone marrow chimeric mice (langerin-DTR→WT or WT→langerin-DTR), while sections 8.3.5 and 8.3.6. focus on the langerin-DTR mice at the end stage of disease.

8.3.1. Effect of langerin^{+} cell depletion on the early accumulation of PrP^{Sc} in lymphoid tissues

To determine the effect of langerin^{+} cell depletion (both LC and langerin^{+} dDCs) on the early accumulation of the scrapie agent in lymphoid tissues, langerin-DTR mice were injected with DTX, or PB control, and infected with the scrapie agent via skin scarification 2 days later. As an additional control, DTX-treated wildtype mice were also used. Draining (left) and non-draining (right) iLNs, left and right pLNs, and spleens were collected from 3 mice from each group as outlined in Chapter 7 (Table 7.1.) at 5 and 7 weeks post scrapie infection. Immunohistochemical analysis with the anti-PrP specific mAb 6H4 determined that accumulations of PrP^{d} could be detected in each of the 3 draining iLNs of all three groups 5 weeks post scrapie infection (Fig. 8.2.). PET blot analysis of adjacent sections confirmed that the detected protein was the proteinase K resistant, disease specific PrP^{Sc} (Fig. 8.2.). Labelling with the anti-CD21/35 specific antibody confirmed that PrP^{Sc} accumulation was occurring on FDCs within the lymphoid follicles (Fig. 8.2.). PrP^{d} was not detected in any other lymphoid tissues 5 weeks after infection (Table 8.1.). These data suggest that

langerin^{+} cell depletion did not impair the early accumulation of the TSE agent in the draining iLN.

By 7 weeks post scrapie infection, PrP^{d} had spread to the spleen in all the animals from each of the 3 groups. In addition, PrP^{d} was detected in the non-draining (right) iLNs of all three mice from the langerin^{+} cell-depleted (langerin-DTR+DTX) mice, as well as one left pLN from both the langerin-DTR+DTX and langerin-DTR+PB groups. Unfortunately a number of the pLN tissues were unavailable for analysis (Table 8.2.). While PrP^{Sc} was detected at a similar level throughout the draining iLNs 5 weeks post scarification, the intensity of labelling observed in the draining iLNs of the langerin-DTR+DTX mice 7 weeks after scrapie infection, appeared to be greatly increased when compared to the two control groups (Fig. 8.3.).

Further immunohistochemical analysis of the draining iLNs confirmed that PrP^{d} accumulated upon FDCs in the B cell follicles (Fig. 8.3.). Coincident with the increased accumulation of PrP^{d} in the draining iLNs of the langerin-DTR+DTX mice, increased activation of CR1 and CR2 (CD21/35) was detected upon FDCs in the iLNs of these mice, when compared to the two control groups. When observed at a higher magnification (magnification 200 x, compared to 40 x), the PrP^{d} showed a 'punctate' pattern. PrP^{d} appeared to be associated with tingible body macrophages (*) (Fig. 8.3.) as well as FDC networks (+) (Fig. 8.3.). These results were comparable between all 3 groups, at both the 5 (not shown) and 7 week time points (Fig. 8.3.). The increased intensity of PrP^{Sc} labelling in the langerin-DTR+DTX mice was also observed in adjacent PET blot sections of the iLNs. These data suggest increased

PrP^{Sc} accumulation in the iLNs of $langerin^{+}$ cell depleted mice 7 weeks after scrapie infection (Fig. 8.4).

Immunohistochemical analysis was also carried out on frozen sections from the draining iLN of day 0 (uninfected mice) to determine whether DTX treatment of langerin-DTR mice influenced any potential differences in CD21/35 expression by FDCs. No differences were observed in any of the three groups (Fig. 8.5.). Immunohistochemical analysis for CD21/35 expression in the non-draining (right) iLN 7 weeks post scarification, showed labelling indicative of slightly higher CD21/35 expression in langerin-DTR+DTX mice compared to the controls (Fig. 8.6.), where PrP^{d} accumulation had also been detected by 7 weeks post scarification. This difference was not as pronounced in the non-draining iLN.

Table 8.1. PrP^d accumulation in peripheral lymphoid tissues 5 weeks post scrapie infection.

	WT + DTX			langerin-DTR+DTX			langerin-DTR+PB		
	1	**2**	**3**	**1**	**2**	**3**	**1**	**2**	**3**
draining (left) iLN	+	+	+	+	+	+	+	+	+
right iLN	–	–	–	–	–	–	–	–	–
left pLN	–	–	–	–	–	–	–	–	–
right pLN	–	–	–	–	–	–	–	–	–
spleen	–	–	–	–	–	–	–	–	–

PrP^d was undetected in all but the draining iLNs 5 weeks after scrapie infection.

Table 8.2. PrP^d accumulation in peripheral lymphoid tissues 7 weeks post scrapie infection.

	WT + DTX			langerin-DTR+DTX			langerin-DTR+PB		
	1	**2**	**3**	**1**	**2**	**3**	**1**	**2**	**3**
draining (left) iLN	+	+	+	+	+	+	+	+	+
right iLN	–	–	–	+	+	+	–	–	+
left pLN	n/a	–	–	+	–	–	–	+	n/a
right pLN	–	–	–	–	–	n/a	–	n/a	n/a
spleen	+	+	+	+	+	+	+	+	+

PrP^d was detected in all draining iLNs and spleens 7 weeks after scarification. PrP^d was also detected in all non-draining (right) iLNs from langerin-DTR+DTX mice and one left pLN from each of the langerin-DTR groups (n/a: no tissue available).

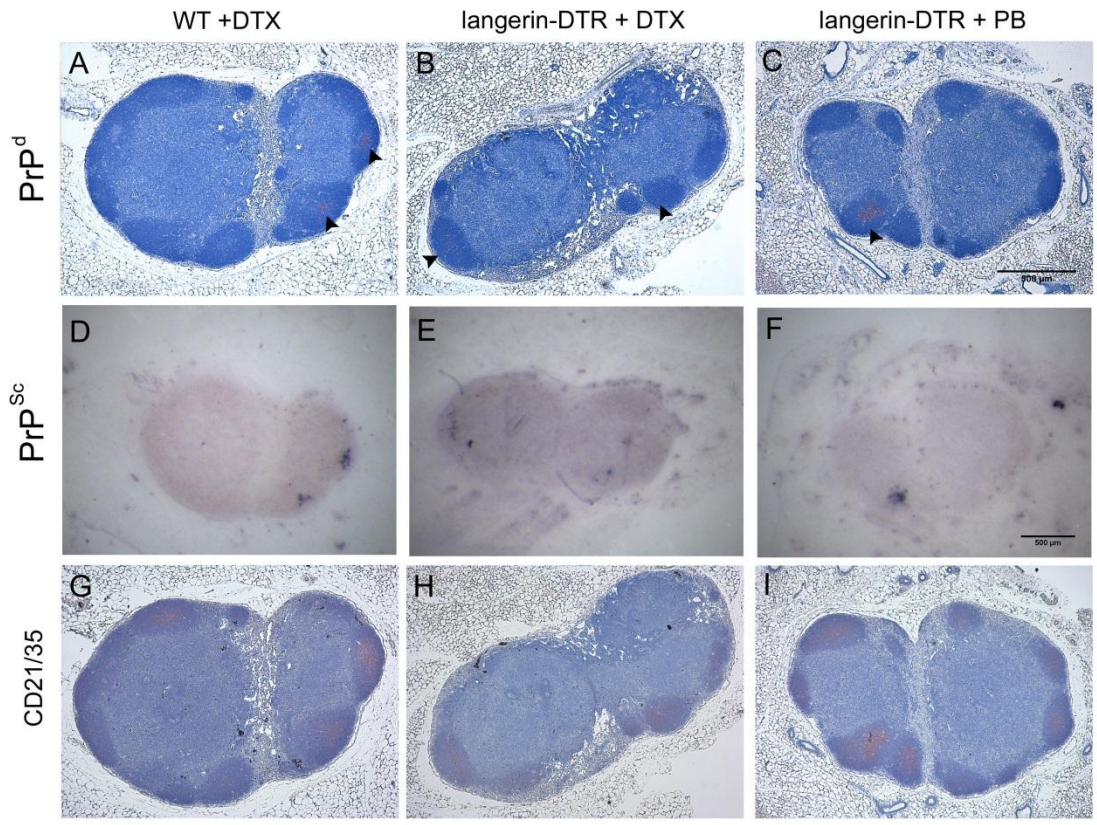

Figure 8.2. PrP^{Sc} accumulation in the draining iLN 5 weeks post scrapie infection was unaffected in langerin$^+$ cell depleted mice. Mice were infected with the scrapie agent via skin scarification 2 days post DTX injection, or PB control. Draining iLNs were collected 5 weeks post infection for immunohistochemical analysis. **A-C**: deposition of PrP^d (detected with 6H4 mAb) in all 3 groups. **D-F**: Adjacent PET blot sections confirmed that PrP^d was proteinase K resistant PrP^{Sc}. Detection of FDCs (CD21/35) (**G-I**) in the draining iLNs confirmed that PrP^{Sc} accumulated upon FDCs. Sections were counterstained with haematoxylin Z (blue). Images are representative of observations in 3 animals/group. Scale bar: top row, 500 µm; bottom 3 rows, 100 µm.

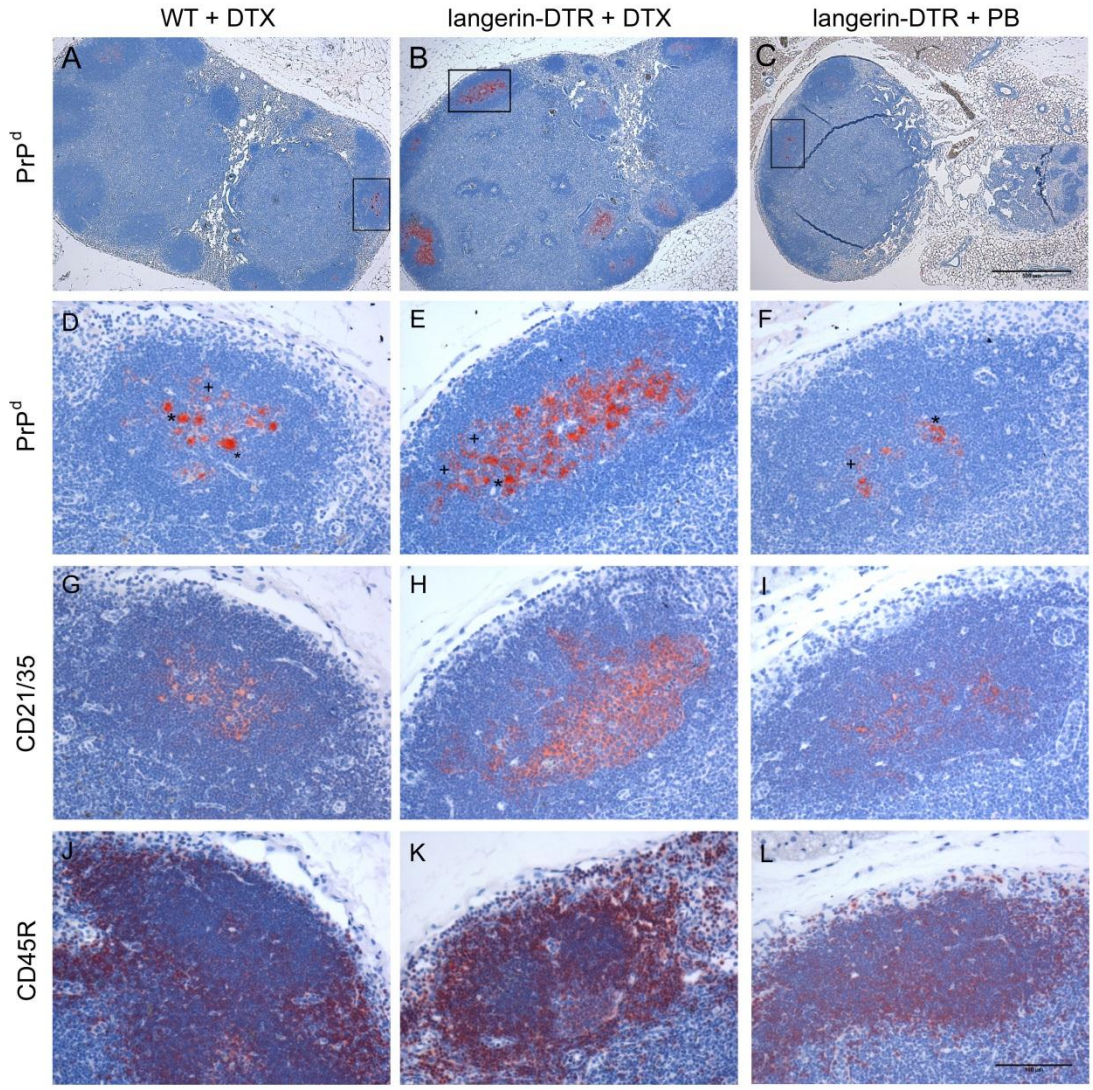

Figure 8.3. Increased PrP^d accumulation, 7 weeks post scrapie infection, in the draining iLN of mice depleted of langerin$^+$ cells at the time of exposure. Mice were infected with scrapie via skin scarification 2 days post DTX injection, or PB control. Draining iLNs were collected 7 weeks post scarification for immunohistochemical analysis. **A-C**: deposition of PrP^d (detected with 6H4 mAb) in all 3 groups. Labelling was much stronger in the langerin-DTR+DTX group compared to the two control groups (magnification: 40 x). **D-F**: PrP^d accumulations (magnification: 200 x). Detection of FDCs (CD21/35) (**G-I**) and B lymphocytes (CD45R) (**J-L**) in the draining iLNs confirmed that PrP^d accumulated upon FDCs in the B cell follicles. PrP^d was detected both on FDC networks (+) and within tingible body macrophages (*). Sections were counterstained with haematoxylin Z (blue). Images are representative of observations in 3 animals/group. Scale bar: top row, 500 µm; bottom 3 rows, 100 µm.

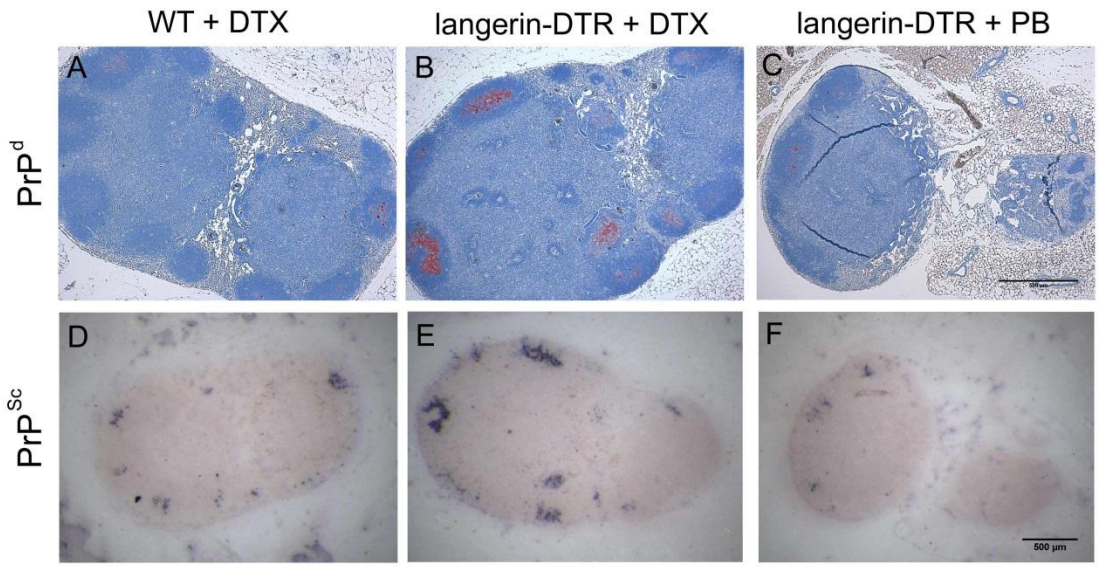

Figure 8.4. Increased PrP^{Sc} accumulation, 7 weeks post scrapie infection, in the draining iLN of mice depleted of langerin$^+$ cells at the time of exposure. Mice were infected with scrapie via skin scarification 2 days post DTX injection, or PB control. Draining iLNs were collected 7 weeks post scarification for immunohistochemical analysis. **A-C**: deposition of PrP^d (detected with 6H4 mAb) in all 3 groups. Labelling was much stronger in the langerin-DTR+DTX group compared to the two control groups. Sections were counterstained with haematoxylin Z (blue). **D-F**: Adjacent PET blot sections confirmed that PrP^d was proteinase K resistant, disease specific PrP^{Sc}. **E**: Increased PrP^{Sc} deposition was confirmed in the langerin-DTR+DTX mice. Images are representative of observations in 3 animals/group. Scale bar: 500 µm.

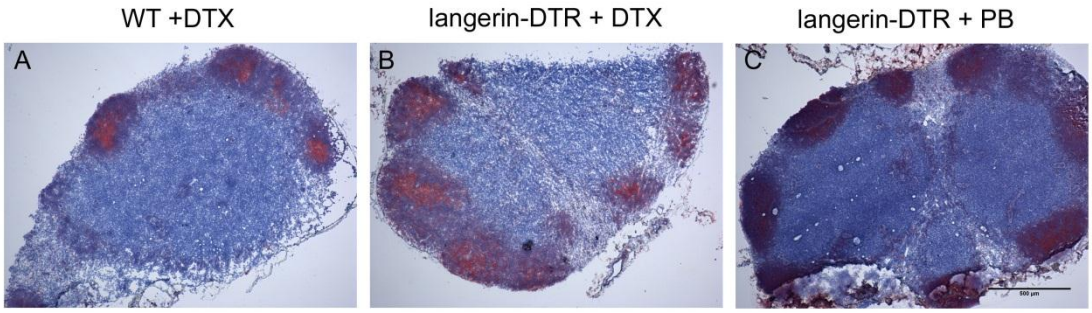

Figure 8.5. Effect of DTX-treatment on CD21/35 immunolabelling. Mice received a single i.p. injection of DTX, or PB control. Inguinal LNs were collected two days post injection and immunolabelled with the anti-CD21/35 specific antibody (red) (**A-C**). No differences were observed in the expression of CD21/35 between the 3 groups. Sections were counterstained with haematoxylin Z (blue). Images are representative of observations in 3 animals/group. Scale bar: 100 µm.

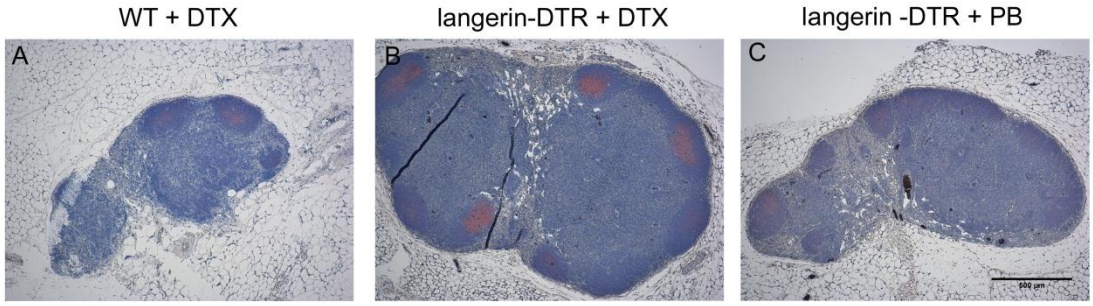

Fig. 8.6. Effect of DTX-treatment on CD21/35 immunolabelling in the right iLN 7 weeks post infection. Mice were infected with scrapie via skin scarification 2 days post DTX injection, or PB control. Non-draining (right) iLNs were collected 7 weeks post scarification and immunolabelled with the anti-CD21/35 specific antibody (red) (**A-C**). Labelling was stronger in 2 of the 3 langerin-DTR+DTX mice compared to the two control groups. Sections were counterstained with haematoxylin Z (blue). Images are representative of observations in 3 animals/group. Scale bar: 500 µm.

8.3.2. Effect of langerin^{+} cell depletion on the early accumulation of PrP^{Sc} in the spinal cord

In Chapter 4 (section 4.3.2.), it was shown that PrP^{Sc} had not reached the spinal cord by 5 weeks after scrapie infection. Earlier in this chapter (Fig. 8.3.) immunohistochemical analysis showed increased PrP^{Sc} accumulation in the langerin-DTR+DTX mice 7 weeks after scrapie infection. Spinal cords from these mice were analysed by Western blot to determine whether the increased PrP^{Sc} accumulation observed in the draining iLN of langerin-DTR+DTX after scrapie infection had accelerated the spread of PrP^{Sc} into the spinal cord. Samples were treated in the presence or absence of proteinase K, to determine the presence of proteinase K resistant, disease specific PrP^{Sc}. No PrP^{Sc} was detected in the spinal cords of any of these mice 7 weeks post scarification (Fig. 8.7.).

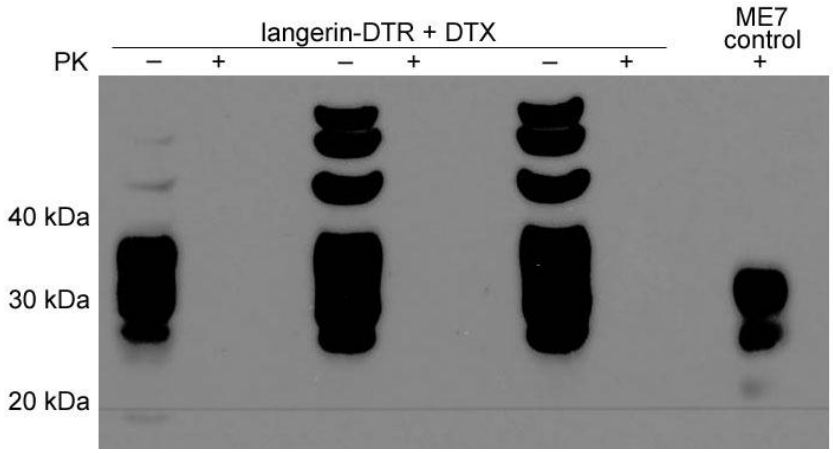

Figure 8.7. Absence of PrP^{Sc} in the spinal cord of langerin-DTR+DTX mice at early time points. Mice were infected with scrapie via the skin 2 days post DTX-mediated langerin^{+} cell depletion. Spinal cord was collected from langerin-DTR+DTX animals 7 weeks post scrapie infection and analysed by Western blot. Samples were treated in the presence (+) or absence (-) of proteinase K (PK) prior to electrophoresis. PrP^{c} was detected in all proteinase K untreated samples, using the 1B3 pAb, but no proteinase K resistant, disease specific, PrP^{Sc} was detected in the spinal cords of langerin-DTR+DTX animals 7 weeks post scarification. Successful detection of proteinase K resistant PrP^{Sc} was confirmed in the ME7 positive control sample.

8.3.3. Exposure of langerin^{+} cell-depleted mice to normal brain (NB) homogenate via skin scarification does not influence FDC status

A study was established to further investigate the cause of the apparent increase in PrP^{Sc} accumulation, and associated increased activation of complement receptors CR1 and CR2 in scrapie-exposed langerin^{+} cell-depleted mice. This experiment sought to determine whether the effects were caused by an immune response to skin scarification (injury), exposure to brain homogenate at the time of langerin^{+} cell depletion or whether PrP^{Sc} was accumulated faster due to the absence of cells that might normally process or degrade the scrapie agent. Groups of 4 langerin-DTR mice received a single i.p. injection of DTX, or PB control. Two days after DTX treatment, the mice were scarified with NB homogenate from an uninfected C57BL/Dk mouse. Tissues were collected for *ex vivo* analysis at day 0 (unscarified) and 7 weeks post scarification. Immunohistochemical analysis of epidermal and dermal sheets and iLN confirmed langerin^{+} cell depletion following DTX treatment of the langerin-DTR mice (not shown). Draining iLNs were immunolabelled with the anti-PrP pAb 1B3. Low levels of expression of PrP^{c} were detected, consistent with expression in uninfected tissues. These results were similar in both the DTX and PB treated groups (Fig. 8.8.). Immunohistochemical analysis with the anti-CD45R and anti-CD21/35 antibodies, confirmed PrP^{c} to be localised on FDCs within B cell follicles. In addition, no differences were observed in FDC status between the langerin-DTR+DTX and langerin-DTR+PB mice (Fig. 8.8.). These data suggest the increased PrP^{Sc} accumulation and CR2/CR1 activation observed following scrapie infection of langerin^{+} cell-depleted mice (Fig. 8.3), in langerin-DTR mice was not simply due a reaction to skin injury or exposure to brain homogenate.

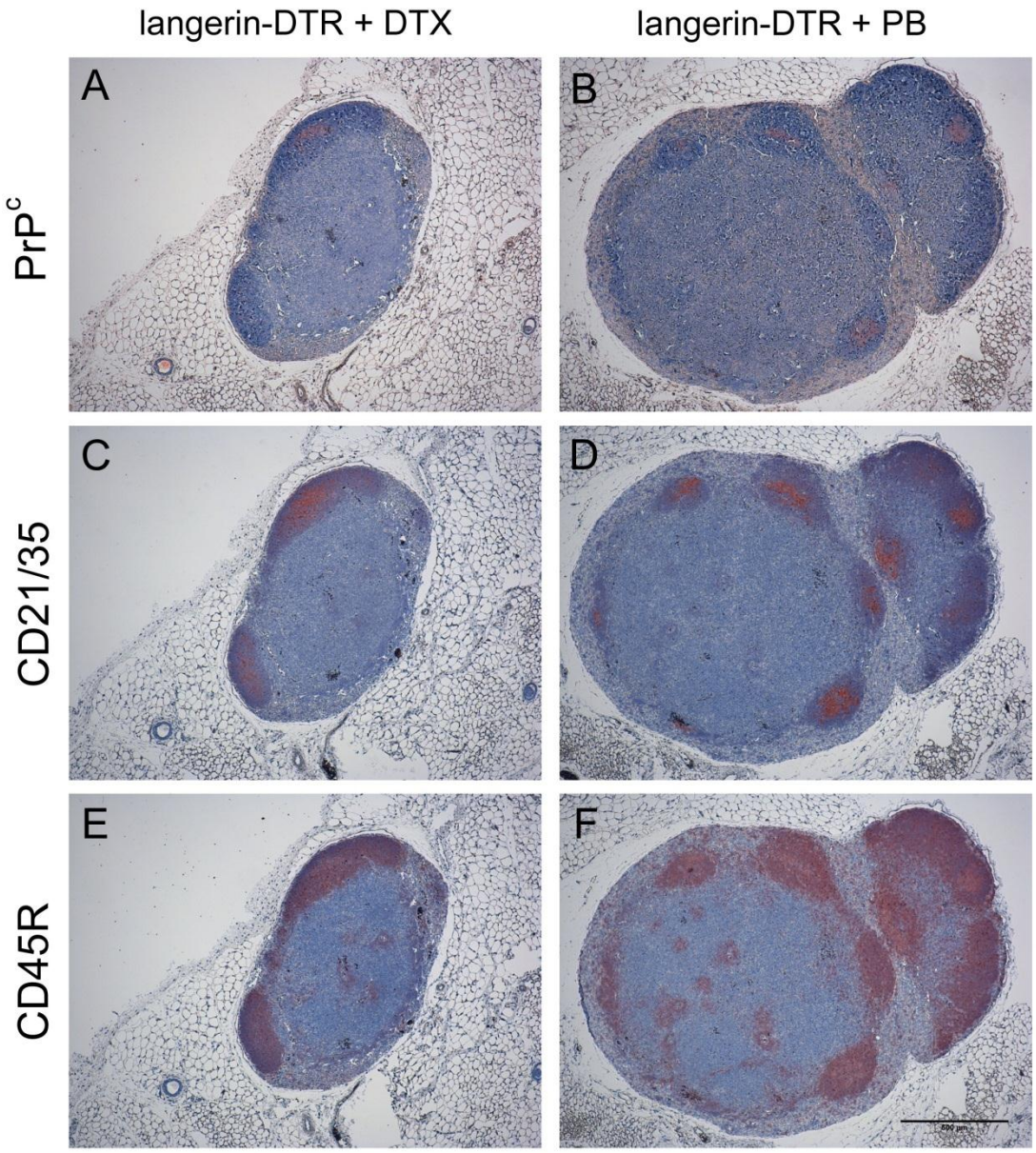

Figure 8.8. Normal distribution of PrP^c, FDCs and B cells in the draining iLN of NB-exposed langerin$^+$ cell-depleted mice. Mice were exposed to NB homogenate via skin scarification 2 days post DTX injection, or PB control. Draining iLNs were collected 7 weeks post scarification for immunohistochemical analysis. Detection of B lymphocytes and FDCs in the iLN showed no increased cell activation as a result of DTX injection, skin injury, or exposure to NB. **A**,**B**: Normal PrP^c distribution in the lymphoid follicles of uninfected mice, detected with the anti-PrP pAb 1B3 (red). Detection of FDCs (CD21/35) (**C-D**) and B lymphocytes (CD45R) (**E-F**) in the draining iLNs confirmed that PrP^c was located on the FDC networks in the B cell follicles. Sections were counterstained with haematoxylin Z (blue). Images are representative of observations in 4 animals/group. Scale bar: 500 µm.

8.3.4. Effect of LC or langerin$^+$ dDC depletion on early accumulation of PrP^{Sc} in lymphoid tissues

Experiments were performed to determine whether the increased accumulation of PrP^{Sc} in the draining iLN following scrapie infection via the skin could be attributed to depletion of a specific population of langerin$^+$ cells. C57BL/6 wildtype mice were lethally irradiated 24 hr prior to reconstitution with langerin-DTR bone marrow, or *vice versa*. The following bone marrow chimeras were produced as a result: langerin-DTR→WT and WT→langerin-DTR, where langerin$^+$ dDCs or LCs, respectively, were depleted independently of each other following DTX injection (Table 8.3.).

Groups of WT/langerin-DTR bone marrow chimeric mice were prepared as outlined in Table 8.3., 8 weeks after irradiation and bone marrow reconstitution. Specific depletion of LC or langerin$^+$ dDC was achieved in the bone marrow chimeric mice through a single i.p. injection of DTX, or PB control. Two days after DTX treatment, mice were infected with the scrapie agent via skin scarification. Tissues were collected for *ex vivo* analysis at day 0 (as a control) and 7 weeks post scrapie infection.

Table 8.3. Specific depletion of LCs or langerin$^+$ dDCs in langerin-DTR/WT bone marrow chimeric mice.

			Depletion status		
Host genotype	**Donor genotype**	**DTX**	**LCs**	**langerin$^+$ dermal DCs**	**langerin$^-$ dermal DCs**
WT	langerin-DTR	yes	no	yes	no
WT	langerin-DTR	no	no	no	no
langerin-DTR	WT	yes	yes	no	no
langerin-DTR	WT	no	no	no	no

As shown in Chapter 7 (Fig. 7.11.), by using these chimeric mice it was possible to selectively deplete epidermal LCs in the WT→langerin-DTR+DTX mice, and the langerin^{+} dDCs and langerin^{+} cells in the iLNs of the langerin-DTR→WT+DTX mice. Immunohistochemical detection of PrP^{d} in the draining iLNs of these mice 7 weeks post scrapie infection confirmed PrP^{d} accumulation in the draining iLNs of all the animals (Fig. 8.9.). Comparable to the observations in Fig. 8.2., PrP^{d} accumulation was increased following DTX injection, when compared to PB injected animals, in the LC-depleted WT→langerin-DTR mice. No differences in PrP^{d} accumulation were observed between the scrapie-infected DTX and PB treated animals in the langerin^{+} cell-depleted langerin-DTR→WT groups. The intensity of PrP^{d} labelling in the scrapie-infected langerin-DTR→WT mice was comparable to the WT→langerin-DTR+PB control mice. However, PrP^{d} labelling intensity was increased in WT→langerin-DTR+DTX mice when compared to the other 3 groups. These data suggest increased accumulation of PrP^{d} in the draining iLNs of the WT→langerin-DTR mice was a result of the absence of LCs, rather than the absence of langerin^{+} dDCs, or both. PET Blot analysis of these tissues confirmed that the PrP^{d} detected in the draining iLNs was resistant to proteinase K digestion and was therefore the disease-specific form, PrP^{Sc} (Fig. 8.10.). Taken together, these results suggest that the specific depletion of epidermal LCs prior to scrapie infection via the skin enhanced the early accumulation of PrP^{Sc} in the draining iLNs.

langerin-DTR → WT
WT → langerin - DTR
DTX
PB
DTX
PB
A
B
C
D
PrP^c
E
F
G
H
PrP^c
I
J
K
L
CD21/35
M
N
O
P
CD45R

Figure 8.9. Effect of specific LC or langerin$^+$ dDC depletion on PrP^d accumulation in the draining LN. Mice were infected with the scrapie agent via skin scarification 2 days post DTX injection, or PB control. Draining iLNs were collected 7 weeks post scarification for immunohistochemical analysis. **A-D**: deposition of PrP^d (detected with mAb 6H4) in all 4 groups. PrP^d immunolabelling appeared to be much stronger in the WT→langerin-DTR+DTX group when compared to the other 3 groups. Detection of FDCs (CD21/35) (**E-H**) and B lymphocytes (CD45R) (**I-L**) in the draining iLNs confirmed that PrP^d accumulated upon FDCs in the B cell follicles. Sections were counterstained with haematoxylin Z. Images are representative of observations in 4 animals/group. Scale bar: second row, 100 µm; other 3 rows, 500 µm.

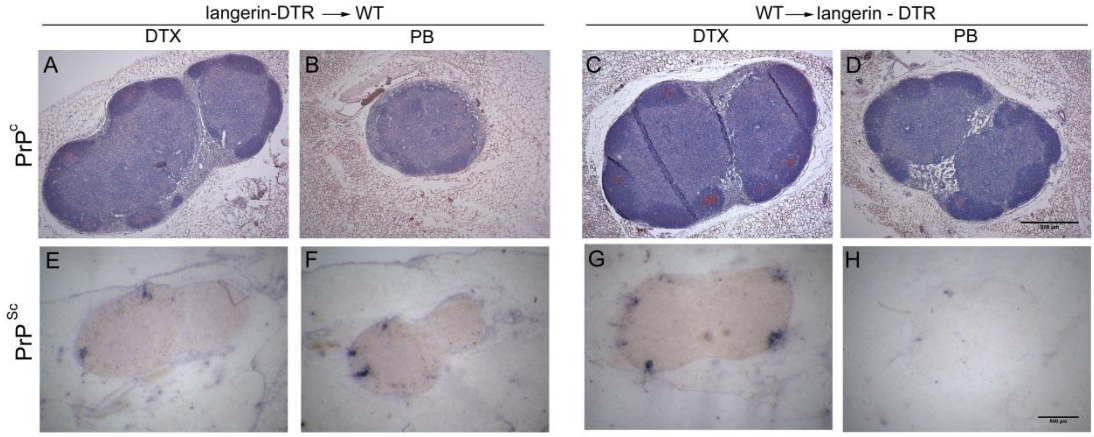

Figure 8.10. Effect of specific LC or langerin$^+$ dDC depletion on PrP^{Sc} accumulation in the draining LN. Langerin-DTR/C57BL/6 bone marrow chimeric mice were infected with scrapie via skin scarification 2 days post DTX injection, or PB control. Draining iLNs were collected 7 weeks post infection for immunohistochemical analysis. (**A**,**B**) Deposition of PrP^d (detected with 6H4 mAb) in the langerin-DTR→WT group, no major differences observed between the two groups. (**C**) PrP^d deposition in WT→langerin-DTR appeared to be much stronger following DTX treatment when compared to the other 3 groups. Sections were counterstained with haematoxylin Z (blue). (**E-H**) Adjacent PET blot sections confirmed that PrP^d detected by 6H4 was proteinase K resistant PrP^{Sc}. Images are representative of observations in 4 animals/group. Scale bar: 500 µm.

8.3.5. Effect of langerin$^+$ cell depletion on scrapie incubation period following infection via skin scarification

To determine the effect of langerin$^+$ cell depletion on the transmission of disease to the brain, groups of 8 langerin-DTR mice were treated with DTX, or PB as a control, and infected with the scrapie agent 2 days later. The disease incubation period was determined for mice that were found to be both clinically and pathologically positive for the signs of scrapie. All the animals in each group succumbed to clinical TSE disease, with mean incubation periods of 350 ± 35 days (WT+DTX), 347 ± 19 days (langerin-DTR+DTX), and 332 ±17 days (langerin-DTR+PB) (Table 8.4.). Statistical analysis of the mean incubation periods determined that the residuals were normally distributed ($p = 0.154$). A one way analysis of variants confirmed there was no significant difference between the disease incubation periods in each group ($p = 0.320$). Therefore, despite an early increase in PrP^{Sc} accumulation in the draining iLN of langerin-DTR+DTX mice, this did not affect the incubation period of disease in these mice.

Table 8.4. Effect of langerin$^+$ cell depletion on scrapie incubation period after infection via the skin.

Group	Incidence	Mean incubation period
WT + DTX	8	350 ± 35
langerin-DTR + DTX	7	347 ± 19
langerin-DTR + PB	8	332 ± 17

Mean incubation period listed as mean ± standard deviation.

Immunohistochemical analysis of the brain revealed characteristic spongiform encephalopathy, PrP^{d} accumulation, reactive astrocytes and microglia in all clinically scrapie affected animals from each group, consistent with development of terminal scrapie disease (Fig. 8.11.). PET blot analysis of adjacent sections confirmed the PrP^{d} accumulations detected were proteinase K resistant, PrP^{Sc} (Fig. 8.11.). The targeted distribution of vacuolation in the brains was consistent with an infection with the ME7 scrapie agent in each of the three groups. No major variation was observed between the lesion profiles of each of the two langerin-DTR groups. Small differences were detected in Area 4 and 9 of the WT+DTX mice compared to the langerin-DTR groups, probably a difference between the mouse strains (Fig. 8.12.).

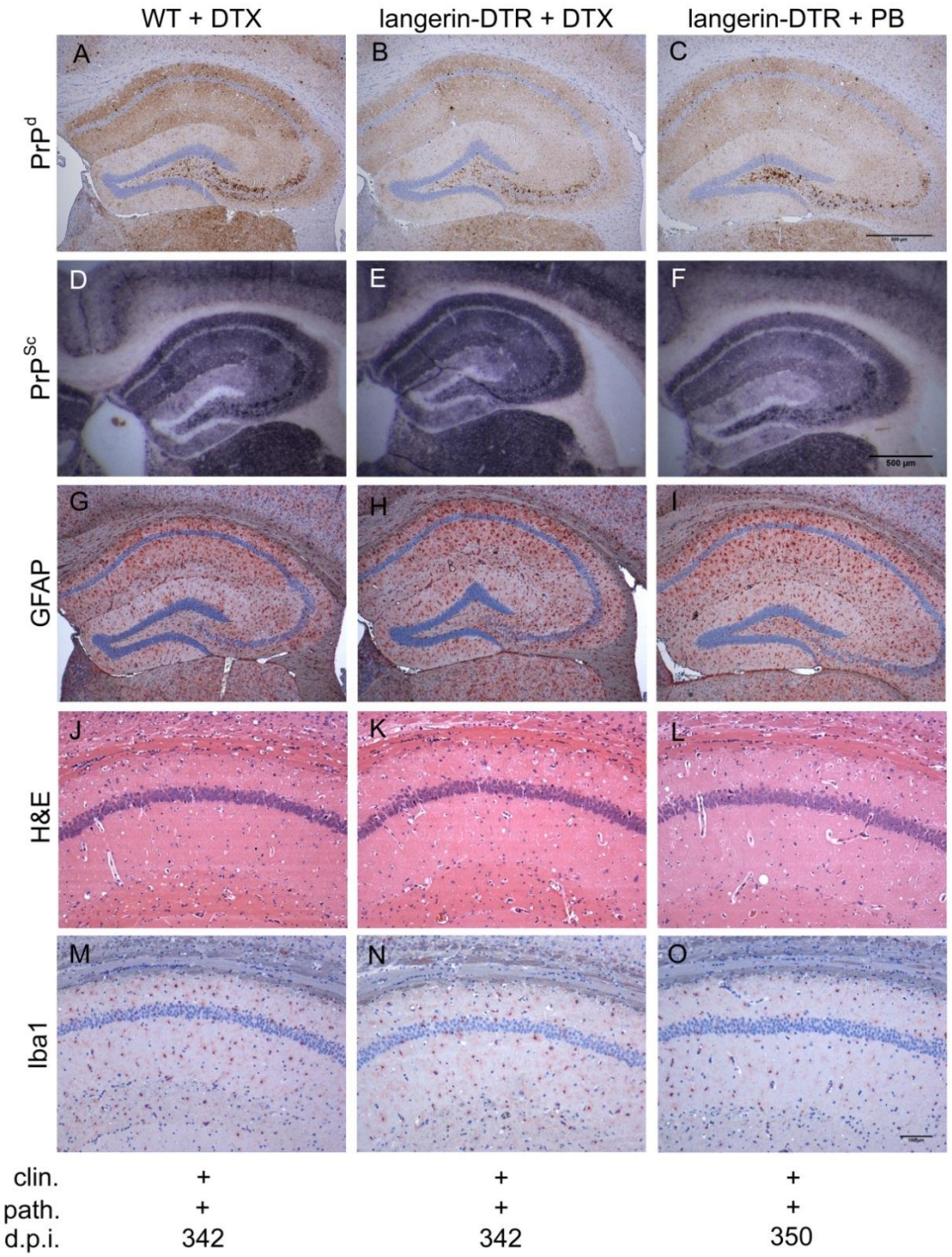

Figure 8.11. Histopathological analysis of brain tissues from terminally scrapie-affected mice. Mice were inoculated with ME7 scrapie via skin scarification 2 days post DTX-mediated langerin^{+} cell depletion and brains from each clinically scrapie affected mouse analysed by immunohistochemistry. Abundant PrP^{d} accumulations were detected in the hippocampi of clinically and pathologically positive mice from each group (**A**-**C**). (**D**-**F**) PET blot analysis confirmed the presence of proteinase K resistant PrP^{Sc}. Gliosis were confirmed through labelling with the GFAP antibody (astrocytes) (**G**-**I**), and the Iba1 antibody (microglia) (**M**-**O**). Sections were counterstained with haematoxylin Z (blue). (**J**-**L**) Haematoxylin and eosin (H&E) staining revealed extensive vacuolation in the brains from all mice. Clin: clinical score; path: pathological score, positive (+) or negative (-); d.p.i.: days post-inoculation on which tissues were taken for analysis. Images are representative of observations from 8 (7) different animals. Scale bar: top 3 rows, 500 µm rows; and bottom two rows, 100 µm.

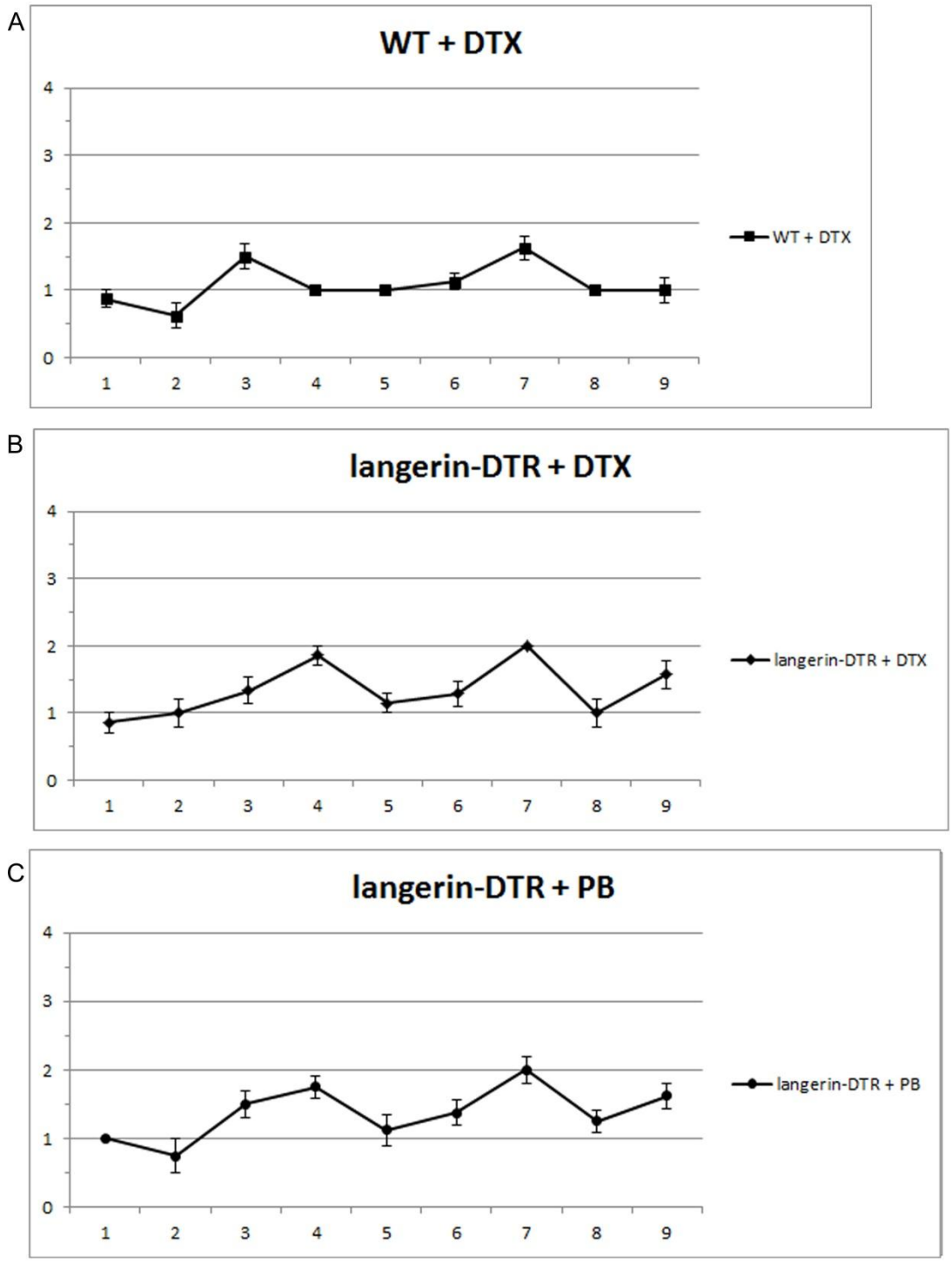

Figure 8.12. Pathological targeting of vacuolation in the brains of terminally scrapie-affected mice. Mice were inoculated with scrapie via skin scarification 2 days post DTX injection, or PB control. **A**: WT+DTX. **B**: langerin-DTR+DTX. **C**: langerin-DTR+PB. Vacuolation in the brain was scored on a scale of 0-5 in the following grey matter areas: G1, dorsal medulla; G2, cerebella cortex; G3, superior colliculus; G4, hypothalamus; G5, thalamus; G6, hippocampus; G7, septum; G8, retrosplenial and adjacent motor cortex; G9, cingulate and adjacent motor cortex. Each point represents mean vacuolation score ± S.E.M. for groups of 8 (7) mice.

8.3.6. Effect of langerin^{+} cell depletion on late PrP^{Sc} accumulation

Following scrapie inoculation via the skin, PrP^{Sc} accumulation occurs first in the draining LNs before spreading to the non-draining LNs and the spleen. High levels of PrP^{Sc} are maintained in these tissues until the terminal stages of disease (Glaysher and Mabbott, 2007a; Mohan *et al.*, 2004). Immunohistochemical analysis of the spleen and draining iLN of clinically scrapie-affected mice from all three groups further supported this. The levels of PrP^{d} deposition in the spleen were comparable across all the groups (Fig 8.13.). PrP^{d} deposition in the draining iLNs was likewise comparable across these groups (Fig. 8.13.). PET blot analysis of adjacent iLN sections confirmed this to be proteinase K resistant PrP^{Sc} (Fig. 8.13.). The iLNs were further analysed, to determine that no major differences were observed in CD21/35 labelling between the 3 groups (Fig. 8.13.).

Spinal cords were also collected from terminally scrapie affected mice and analysed through Western blot analysis. Samples were treated in the presence or absence of proteinase K, to determine the presence of disease specific PrP^{Sc}. As anticipated, spinal cords were found to contain large amounts of PrP^{Sc} in each of the three groups (Fig. 8.14.). The three bands found between approx. 50-60 kDa are most likely dimers of PrP^{Sc}.

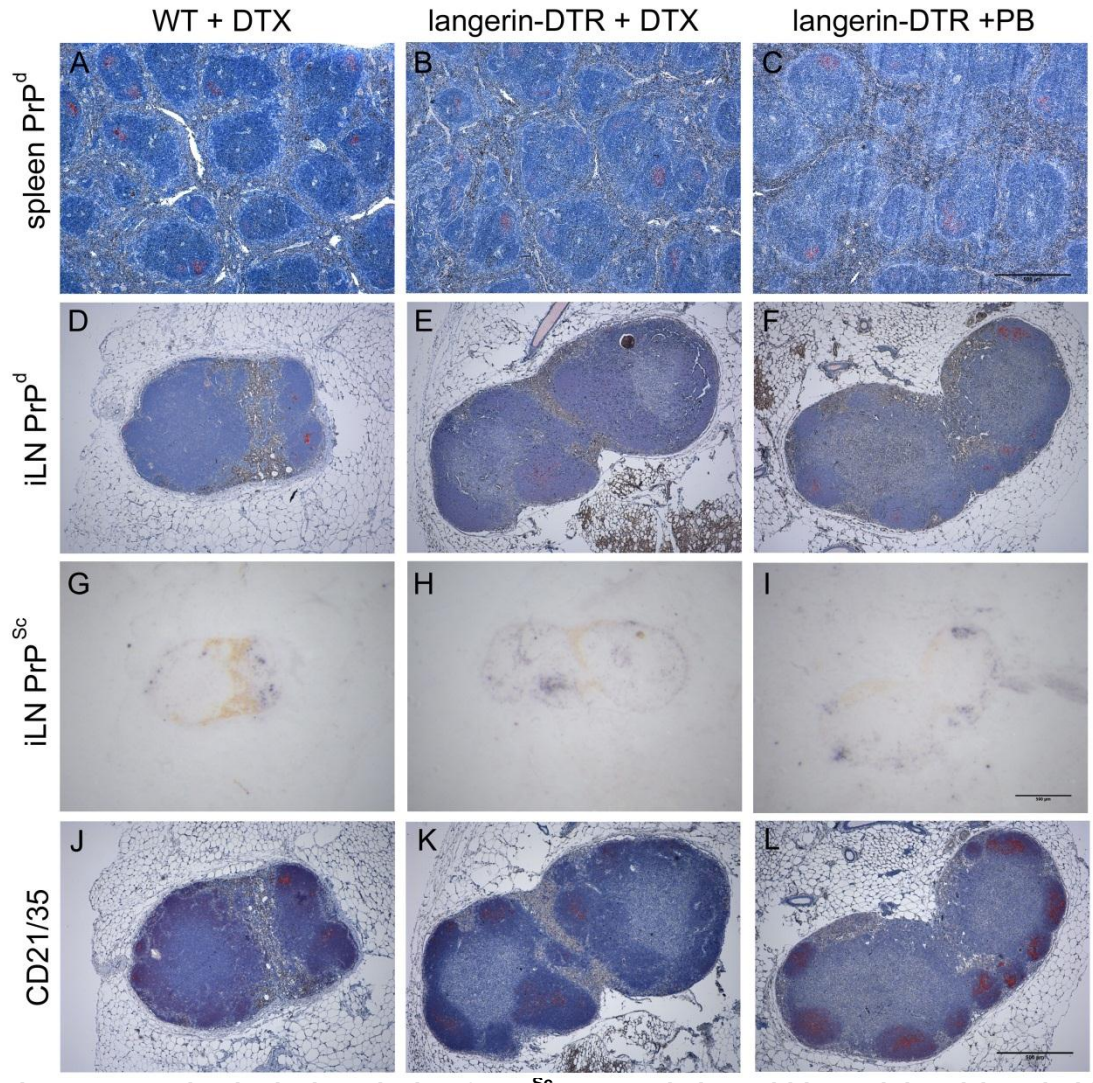

Figure 8.13. Histological analysis of PrP^{Sc} accumulation within peripheral lymphoid tissues from terminally scrapie-affected mice. Mice were inoculated with ME7 scrapie via skin scarification 2 days post DTX injection, or PB control. Spleen and iLN were collected from animals at the endpoint of disease, and immunohistochemical analysis was carried out for the detection of PrP and CD21/35. PrP expression was detected in the spleen of animals in all three groups (**A-C**). PrP expression was detected in the spleen of animals in all three groups (**D-F)**. Adjacent PET blot sections confirmed the presence of proteinase K resistant PrP^{Sc} (**G-H**). CD21/35 expression was consistent throughout the three groups at scrapie disease endpoint (**J-L**). Sections were counterstained with haematoxylin Z. Images are representative of observations in 8 (7) animals/group. Scale bar: 500 µm.

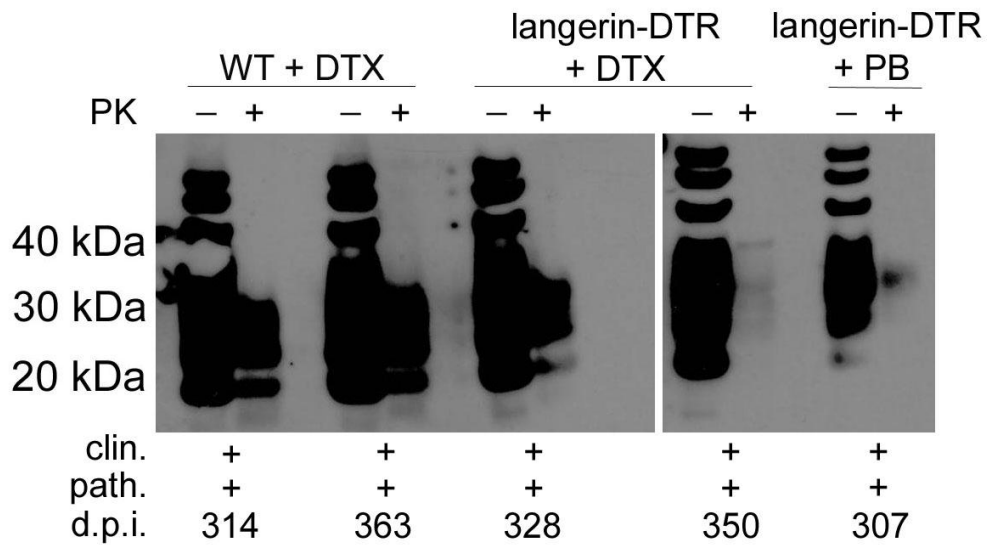

Figure 8.14. PrP^{Sc} accumulation in the spinal cord of terminally scrapie-affected mice. Mice were infected with scrapie via the skin 2 days post DTX-mediated langerin^{+} cell depletion. Spinal cords were collected from terminally scrapie-affected mice and analysed by Western blot. Samples were treated in the presence (+) or absence (-) of proteinase K (PK) prior to electrophoresis. Proteinase K resistant, disease specific, PrP^{Sc} was detected, using the 1B3 pAB, in the spinal cords of animals in all three groups.

8.4. Discussion

In this chapter langerin-DTR transgenic mice were injected with DTX to specifically deplete their langerin$^+$ cells prior to scrapie exposure via skin scarification of the inner thigh. In contrast to the delayed PrP^{Sc} accumulation observed following the depletion of CD11c$^+$ cells in Chapter 4, the depletion of langerin$^+$ cells in this chapter lead to the increased accumulation of PrP^{Sc} in the draining iLN 7 weeks post infection. No differences were observed in the level of PrP^{Sc} accumulation 5 weeks post infection, indicating that this was not a direct result of the absence of langerin$^+$ cells in the skin at the time of infection.

PrP^d accumulation in the spleen had occurred in all animals from all three groups by 7 weeks post scrapie infection, a phenomenon not observed in the CD11c-DTR→WT mice. In addition, PrP^d accumulation was detected in the non-draining (right) iLN of the langerin-DTR+DTX mice 7 weeks post scrapie infection. PrP^d was also detected in two left pLNs (langerin-DTR+DTX and langerin-DTR+PB).

The increased accumulation of PrP^{Sc} 7 weeks post infection, following depletion of langerin$^+$ cells, was accompanied by an increased expression of CR1 and CR2 in the follicles of the draining iLN. However, no differences in CR1 and CR2 expression were detected in the draining iLNs at earlier time points. Equally, depletion of langerin$^+$ cells prior to skin scarification with NB homogenate, did not affect CR1 and CR2 levels in the draining iLNs 7 weeks post scarification. Increased labelling intensity associated with CR1 and CR2 was also detected in a number of non-draining (right) iLNs 7 weeks post infection, these mice were the same ones where

PrP^{d} had spread to the non-draining iLN by 7 weeks post infection. No differences in labelling of CR1 and CR2 were observed in the bone marrow chimera groups 7 weeks post scrapie infection, although labelling was strong throughout all 4 groups, possibly a result of lethal γ-irradation and bone marrow reconstitution. By contrast, differences were observed in PrP^{Sc} labelling intensity in the draining iLN of bone marrow chimeric mice 7 weeks post scrapie infection. Increased PrP^{Sc} accumulation was restricted to the WT→langerin-DTR+DTX mice, where the radioresistant LCs were specifically depleted, but the donor-derived langerin^{+} dDCs were unaffected by DTX. These results indicate that the increased PrP^{Sc} accumulation in the draining iLN following scrapie infection via the skin was a specific consequence of the depletion of LCs.

The increased PrP^{Sc} accumulation and CR1/CR2 expression appeared to be linked. Both occurred as a result of the depletion of LCs prior to scrapie infection via skin scarification. Neither of these results were observed 5 weeks post infection, therefore an event is occurring between these two time points to trigger this effect. Following DTX-mediated depletion, LCs remain depleted for several weeks (Bennett *et al.*, 2005; Kissenpfennig *et al.*, 2005b; Nagao *et al.*, 2009) and Chapter 7. As the LCs repopulate the skin, it is plausible that residual traces of the scrapie inoculum left in the skin are being acquired by the repopulating LCs and transported to the draining iLN.

Previous *in vitro* work (Mohan *et al.*, 2005c) indicated that LCs degraded the scrapie agent and were an unlikely candidate for the transport of the scrapie agent from the

skin to the draining iLN. The blocking of LC transport from the skin prior to scrapie infection via skin scarification did not impair the accumulation of scrapie infectivity in the draining iLN or inhibit disease (Mohan *et al.*, 2005b). These results further support the findings from this chapter, that langerin^{+} cell depletion did not block TSE agent accumulation in the draining iLN, suggesting that LCs are not involved in the early delivery of the TSE agent from the skin to the draining iLN. LCs have also been shown to internalise antigen from the surface to the Birbeck granules, and degrades antigen such as HIV (Merad *et al.*, 2008). Therefore, LCs may likewise phagocytose and gradually destroy PrP^{Sc}. The absence of LCs following DTX-mediated depletion might therefore explain the increased PrP^{Sc} deposition in the draining iLN, as these degradatory cells were absent at the time of scarification.

It could be argued that the increase in PrP^{Sc} accumulation is a result of an immune-mediated response to DTX-mediated cell death in the lymphoid tissues, especially considering the increased expression of CR1/CR2. An increase in CR1/CR2 expression may lead to increased uptake of PrP^{Sc} by FDCs (Zabel *et al.*, 2007). However, the scarification study with NB homogenate showed no increase in CR1/CR2 activity despite langerin^{+} cell depletion prior to scarification. This suggests the effects observed were not simply due to an immunological response to DTX-mediated cellular depletion or injury caused by scarification.

Despite all the changes that have occurred in the draining iLN as a result of langerin^{+} cell depletion prior to scrapie infection, no differences were observed between the incubation periods of terminally scrapie-affected mice of all 3 groups. Previous

studies involving scrapie transmission via skin scarification indicate that infection may already have spread to the peripheral nervous system earlier than 42 days post infection (Mohan *et al.*, 2005a). This could explain why the differences observed at the early time points are not reflected in the terminally scrapie-affected animals. The differences in PrP^{Sc} accumulation observed in the draining iLN of mice where $langerin^{+}$ cells were depleted appear to occur between 5 and 7 weeks post scarification. The increased accumulation at 7 weeks post scarification therefore indicates a potential 'second wave' of PrP^{Sc} accumulating in the draining iLN, and also spreading to the non-draining LNs. If this is the case and neuroinvasion has already occurred, this could explain why the differences observed at the early time points are not reflected in the terminally-scrapie-affected animals.

This chapter has determined that DTX-mediated depletion of $langerin^{+}$ cells in the langerin-DTR transgenic mice prior to scrapie infection via skin scarification did not block TSE agent accumulation in the draining iLN. Between 5 and 7 weeks post PrP^{Sc} accumulation was increased in the draining iLNs of mice depleted of $langerin^{+}$ cells. Bone marrow chimerism determined that this difference can be attributed to the absence of LCs at the time of scrapie infection. Despite the increase in PrP^{Sc} accumulation, incubation period was not affected in these mice, thereby indicating that the increase in PrP^{Sc} accumulation followed initial neuroinvasion.

9

EFFECTS OF SCARIFICATION ON SKIN MICROARCHITECHTURE, GENE EXPRESSION, AND THE UPTAKE OF PrP^{Sc}

9.1. Abstract

The previous chapters have studied the effect of MNP depletion on scrapie transmission from the skin following scarification. Little is known of the fate of the TSE agent within the skin following infection. This chapter will aim to address this question through histopathological and gene expression analysis of scarified skin. Scarification was found to be associated with a local inflammatory response, identified both by histopathology and gene expression analysis. Analysis also determined there to be no major gene expression changes following DTX-mediated depletion in either the CD11c-DTR→WT or the langerin-DTR mice. Histopathology was also used to visualise the effects of scarification on the fate of fluorescently tagged PrP^{Sc} (from scrapie associated fibrils: SAFs) and to determine whether it was possible to track the inoculum *in vivo* following scarification. Alexa-PrP^{Sc} was detected on or below the skin, up to 72 hr post scarification. Small amounts were also detected in the perinodal adipose tissue (PAT) as early as 15 min post scarification.

9.2. Introduction

Technology is continually advancing and the use of fluorescent tags, for proteins or molecules of interest, has been around for a number of years. This technology has previously been used within the field of PrP research (Gossner *et al.*, 2006). The development of the 'very photostable' Alexa-Fluor® succinimidyl ester dyes, helps to eliminate issues concerning the photostability of the dye or the strength of the molecular bonds between the dye and target molecule, as the molecular bonds that are formed in this reaction are as stable as peptide bonds (Banks and Paquette, 1995). Gousset *et al* (Gousset *et al.*, 2009), fluorescently tagged PrP^{Sc} with Alexa-Fluor®546 and used this to track PrP^{Sc} in cells *in vitro*. The authors carried out extensive steps to ensure the stability of the bonds and that specific binding to the desired protein was in place. These steps included saving samples from each step of the PrP^{Sc} isolation/tagging process for comparative analysis, fluorography imaging of protein electrophoresis gels that were subsequently transferred to nitrocellulose membrane and probed with anti-PrP antibodies (Western blot), to confirm that the fluorescent dye did indeed bind to PrP^{Sc}. PrP^{Sc} was extracted from brains of scrapie affected mice.

There are numerous other proteins in the brain that the fluorescent dye could bind to, so it is of utmost importance to ensure that the target protein has been fluorescently labelled, and that samples do not contain a range of fluorescently tagged non-specific proteins. It was therefore decided that the work outlined in this chapter would describe Alexa Fluor®546 labelling of scrapie associated fibrils (SAF) (Merz *et al.*, 1981). Isolation of these SAFs directly eliminates a large percentage of non-specific

proteins. Alexa Fluor®546-PrP^{Sc} was used in this chapter to determine whether it was possible to track the movement of the PrP^{Sc} from the skin to the draining iLN. This approach also provided the opportunity to determine how long PrP^{Sc} is present in the skin following infection via scarification.

Little is known of the adipose tissue that surrounds lymphoid tissues (perinodal adipose tissue: PAT) and its potential role in immune responses, but the fatty acid content in PAT shows site-specific specialisation, which may influence inflammatory diseases (Knight, 2008). PAT contains a high number of DCs, in contrast to subcutaneous fat (Bedford *et al.*, 2006). It is suggested that maturation, function or even migration into LNs of these DCs might be modulated by their fatty acid environment (Knight, 2008). When LNs are removed from the carcass, excess PAT is removed and discarded. This is often the case for tissues collected for immunohistochemical analysis of frozen sections, since the fat from PAT can destroy the LN microarchitecture. As such the potential influence of the PAT is often overlooked. However, studies suggest the PAT may play an important role in the immune response by its ability to modulate inflammation, through adipokines, or fatty acids and their metabolites (Knight, 2008).

TSE agent accumulation within the fat of scrapie infected mice and CWD-infected deer has recently been reported (Race *et al.*, 2008; Race *et al.*, 2009). In light of these data, and the potential role for the PAT in immune responses, it would be important to investigate whether PrP^{Sc} was also detectable within the PAT after infection via

the skin. This has led to analysis of the PAT of mice infected with Alexa Fluor®546-PrP by skin scarification.

Microarray analysis permits the comparison of gene expression profiles from many different cell types or tissues, and the effects of treatments on those tissues. In this chapter, gene expression profiles were compared from animals in the different studies. Samples were taken from animals that were scarified in the ear (to examine the effect of scarification). Samples were also collected from CD11c-DTR and langerin-DTR mice two days post DTX-treatment (to examine the effect of DTX-mediated cell depletion in the skin). Using this approach it was therefore possible to determine what genes and/or cell types were affected by the different treatments that the mice have undergone, throughout this thesis. These results can be put into context of the previous chapters where mice had undergone DTX treatment to deplete specific cells, and where mice were scarified in order to transmit scrapie via the skin. These results aim to determine whether other factors might play a role in determining the outcome of various experiments that have been described in this thesis.

9.3. Results

9.3.1. Histopathological analysis of the effect of scarification on the skin

To determine the effect of scarification on the skin, the pinna of the ear was selected as an appropriately flat surface, as presence of cartilage within the ear prevents the skin from curling during analysis. Furthermore, the epidermis and dermis can be readily discriminated. Mice were scarified on the ventral side of the ear, and tissues were collected for analysis 15 min and 2 hr post scarification. Histopathological analysis confirmed peracute localised dermatitis at the site of scarification by 15 min (Fig. 9.1.), becoming more obvious at two hours post scarification when an inflammatory exudate was identified at the site (Fig. 9.1.). Immunofluorescence analysis confirmed localised infiltration of neutrophils and $CD11b^{+}$ cells (Fig. 9.1.), consistent with inflammation in the skin (Delavary *et al.*, 2011).

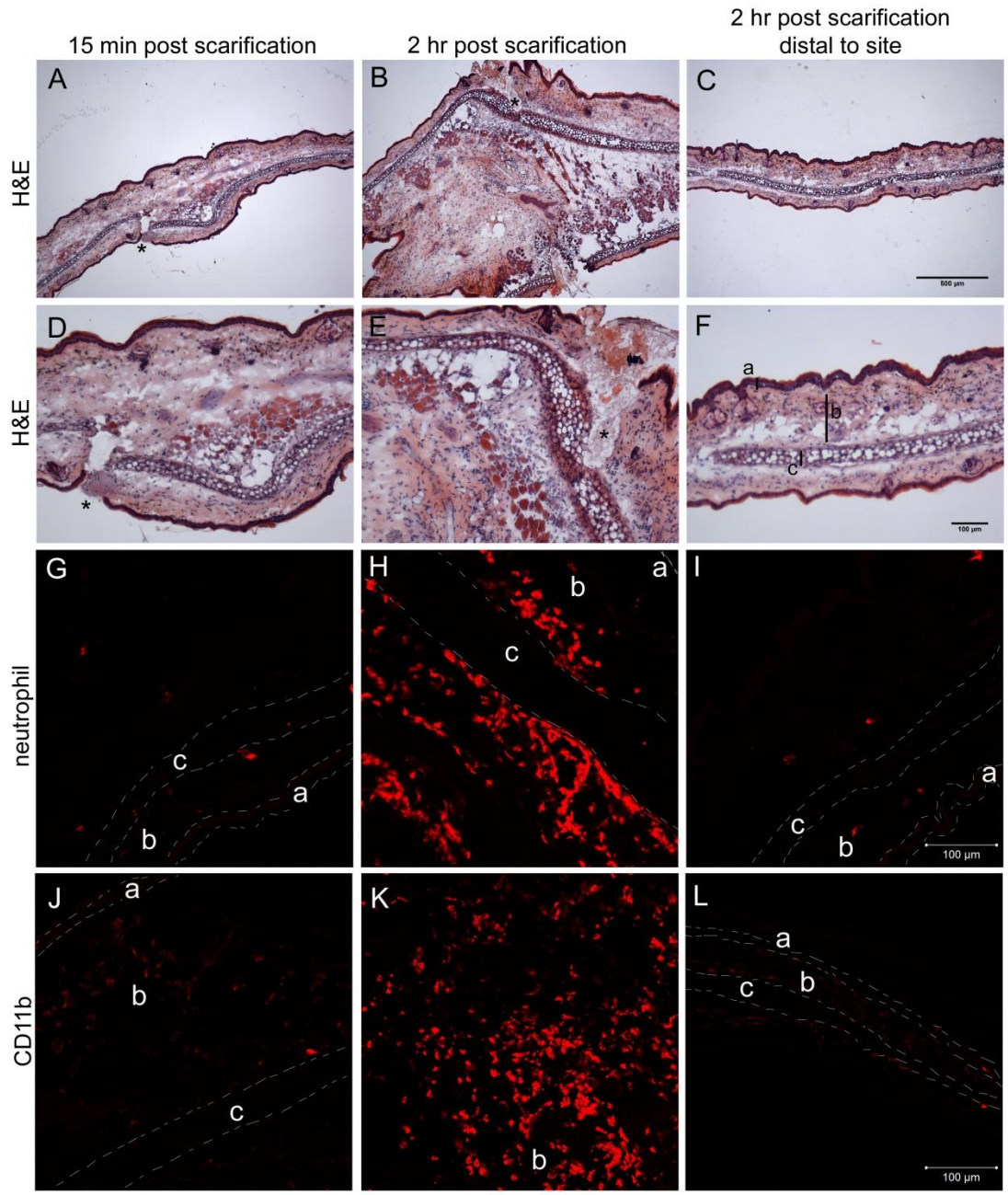

Figure 9.1. Histopathological effects of scarification on the inner surface of the ear. Mice were scarified on the ventral side of the ear, and tissues collected for histological analysis 15 min and 2 hr post scarification. Throughout the figure, **a** denotes the epidermis, **b** denotes dermis, and **c** denotes cartilage. Haematoxylin and eosin (H&E) staining revealed a localised inflammatory response to the scarification after 15 min (**A**,**D**). The site of scarification is marked by ∗. By 2 hr after scarification (**B**,**E**) inflammation was accompanied by the infiltration of neutrophils (red) (**H**) and $CD11b^{+}$ cells (red) (**K**). These inflammatory responses were localised to the site of scarification, images captured distal to the scarification site show no inflammatory changes or cellular infiltration (**C**,**F**,**I**,**L**). Images are representative of observations in 4 animals per time point. Scale bar: top row, 500 µm; bottom 3 rows, 100 µm.

9.3.2. Microarray analysis

To determine whether scarification or DTX-mediated depletion affected gene expression in the skin, ear samples were collected for mRNA extraction from langerin-DTR transgenic mice or CD11c-DTR→WT treated with DTX or PB, and from wildtype mice scarified on the ventral side of the ear (Table 9.1.). Gene expression within these samples was analysed on a single microarray platform (Affymetrix mouse genome 430-2 arrays).

9.3.3. Clustering of co-expressed genes in distinct cell lineages

Raw data sets (.cel files) were normalised during RMA and annotated using the latest libraries available from Affymetrix. A full probe set-to-probe set Pearson correlation matrix was calculated whereby the similarity in the expression profile of each transcript (probe set) represented on the array was compared across each of the 20 samples. The matrix was imported into BIOLAYOUT *EXPRESS*^{3D} (Freeman *et al.*, 2007; Theocharidis *et al.*, 2009), and a graph was created of the sample-to-sample correlations using relationships $r > 0.9$. to define edges (Fig. 9.2.). The network graph contained 8,792 nodes representing individual transcripts connected by 87,920 edges indicating Pearson correlation values above the selected threshold of $r = 0.90$. After clustering, 177 clusters containing at least 7 nodes were obtained and their contents are provided in the attached CD-ROM. The network graph's topology is complex and is derived from cliques of genes which are co-expressed (Fig. 9.2.). This analysis clearly shows that clusters containing genes with related expression patterns were localised within similar neighbourhoods within the graph.

The expression profile of the clusters helps to provide an indication of the biology they encode. Several, clusters, for example cluster 7 and 9, contained genes that were expressed in all 20 samples. These mostly contained genes involved in housekeeping functions, such as ribosome regulation (Table 9.2.).

Several cell-specific gene clusters were also identified (Table 9.2.), and examples of the gene expression profiles where these clusters vary between treatment groups can be found in Figure 9.3. For example, cluster 2 and 6 are enriched in genes related to the function of phagocytes, such as *Ccl21a, Cd163, Cd47, Cd209f, Cd209g, Ccl8, Ccr2, Cd200r4, Cd40, Cd48,* and *Cd68*. Cluster 12 is enriched in genes known to be associated with B lymphocytes, and antibody production, including *Bank1, Blk, Btla, Igh6, Ighg, Ighv14-2*. Clusters 8, 10, 18, and 44 contain genes that were only enriched in the samples from mice that had been scarified. These include genes associated with B cells, *Bcl-10, Btg2, Bcr*, and with inflammation, *Ccr1,Ccl3, Ccl4, Clec4e, Il1b,* and *Trem1*, but also contained genes associated with the regulation of inflammatory responses, including *Crem, Socs3, Tnfaip3*, and *Wsb2*. Clusters 19, 32, and 50 contain genes that were only enriched in langerin-DTR+DTX samples, and these genes appear to be associated with transcription. Equally, other clusters are only associated with genes enriched in the CD11c-DTR→WT samples. Scarification of the skin is associated with localised inflammation and cell proliferation. DTX-mediated langerin^{+} or CD11c^{+} cell depletion did not adversely affect gene expression profiles within the skin.

Table 9.1. Sources of ear skin samples where RNA was extracted for microarray analysis

Mouse line	treatment	time point	replicates
C57BL/6	scarification	2 hr	3
CD11c-DTR→WT	PB	2 d	3
CD11c-DTR→WT	DTX	2 d	3
CD11c-DTR→WT	DTX	6 d	3
langerin-DTR	PB	0 d	2
langerin-DTR	DTX	2 d	3
langerin-DTR	DTX	22 d	3

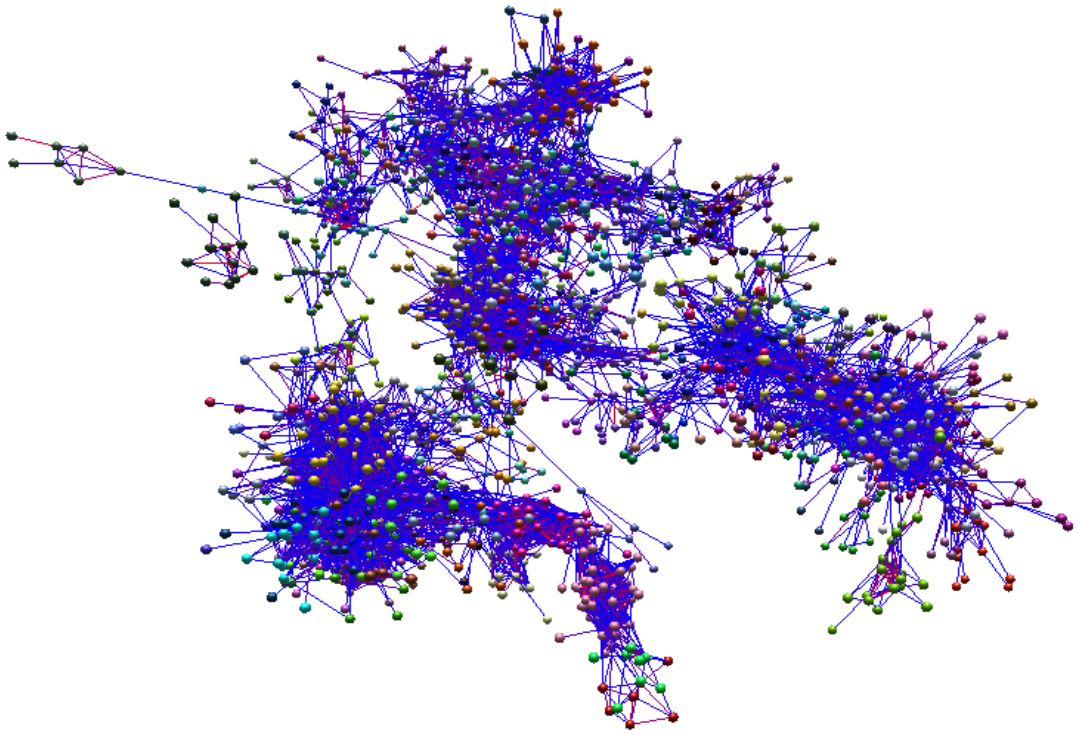

Figure 9.2. Network analysis of mouse skin transcriptomics data. A Pearson correlation matrix was prepared by comparing data derived from all 20 samples used in this study performed on Affymetrix mouse genome 430-2 arrays. A graph was constructed using probe set-to-probe set relationships greater than r = 0.9. Nodes represent samples (individual chips) and edges coloured according to the strength of the correlation (red, r = 1.0; blue, r = 0.9). The graph was then clustered using a Markov clustering (MCL) inflation value of 2.2 and each cluster of samples assigned a different colour. Full descriptions of the sources of each data set are given in Table 9.1.

Table 9.2. Annotation of cell-type specific co-expressed gene clusters.

Cluster ID number	Cluster profile description	Putative cluster function or cell lineage	Number annotated genes	Known markers present in cluster
2	CD11c-DTR→WT	Phagocyte-related	136	*C1qtnf2, C1ra, Ccl21a, Ccr2, CD163, Cd47, Cd209f, Cd209g, CD300, Clec10a, Csfr-1, Emr1, Grn, H2-Aa, H2-Ab1, IL10ra, Itgb2, Laptm5*
6	CD11c-DTR→WT	Phagocyte-related	72	*C1qa, C1qb, C1qc, Casp12, Ccl8, Ccr2, Cd200r4, Cd40, Cd48, Cd68, Clec4a2, Clec4a3, Clec4n, Ctsc, Ctss, Fcer1g, Fcgr2b*
7	All	Ribosome-associated	54	*Rpl10, Rpl11, Rpl15, Rpl19, Rpl23a, Rpl3, Rpl34, Rpl35, Rpl4, Rpl6*
8	Scarified samples	Phagocyte-related	54	*Atf3, Atf4, Btc, Crem, Nr4a1, Nr4a2, Socs3, Tnfaip3, Trib1, Wsb2*
9	All	Ribosome-associated	32	*Btf3, Rpl12, Rpl14, Rpl18, Rpl21, Rpl32, Rpl37*
10	Scarified samples	Pro-inflammatory		*Ccl3, Ccl4, Ccr1, Ccrl2, CD14, Clec4d, Clec4e, Csf2rb, Csf3r, Cxcl1, Cxcl2, Cxcl3, Il1b, Il6, Trem1, Trem3*
12	CD11c-DTR→WT+PB	B cell-associated	36	*Bank1, Blk, Btla, Cd5l, Cr2, Cxcr5, H2-Ob, Igh6, Ighg, Ighv14-2, Igj, Igl-V1, Ltb*
18	Scarified samples	Cell proliferation	23	*Arc, Arl5b, Chchd4, Clcf1, Cyr61, Ddx21, Dusp7, Fosl1, Gm16516, Itga5, Lrrfip5, Sgms2, Siah2, Skil, Stk40, Tnfrsf12a, Zc3h12c*
19	Langerin-DTR+DTX	Transcription-related	26	*Ctnnal1, Erbb2ip, Irak1, Nup107, Ofd1, Pdk1, Ppip5k1, Prpf39, Pxmp3, Rbak, Scyl3, Siah1a, Slc35b3, Srebf1, Stk24, Zfp280c*
32	Langerin-DTR+DTX	Transcription-related	14	*Dph5, Hnrnpr, Mapk14, Phf20l1, Sbf2, Cdc37l1, Cpsf7, Hlf, Ppil6, Ptbp2, Tmem181a, Ube2i*
42	Langerin-DTR+PB	B cell-associated	13	*Ccr6, Cd19, Cd22, Cd37, Cd79b, Fcer2a, Fcrl1, Ms4a1, Pla2g2d, sipa1, spib, Wipf1*
44	Scarified samples	B cell-associated	10	*Bcl-10, Btg2, Bcr*
50	Langerin-DTR+DTX	Transcription-related	10	*Dnm1l, Fam76b, Fbxl3, Lnp, Lypla1, Ncl, Rpa2, Slc25a46, Top2b*

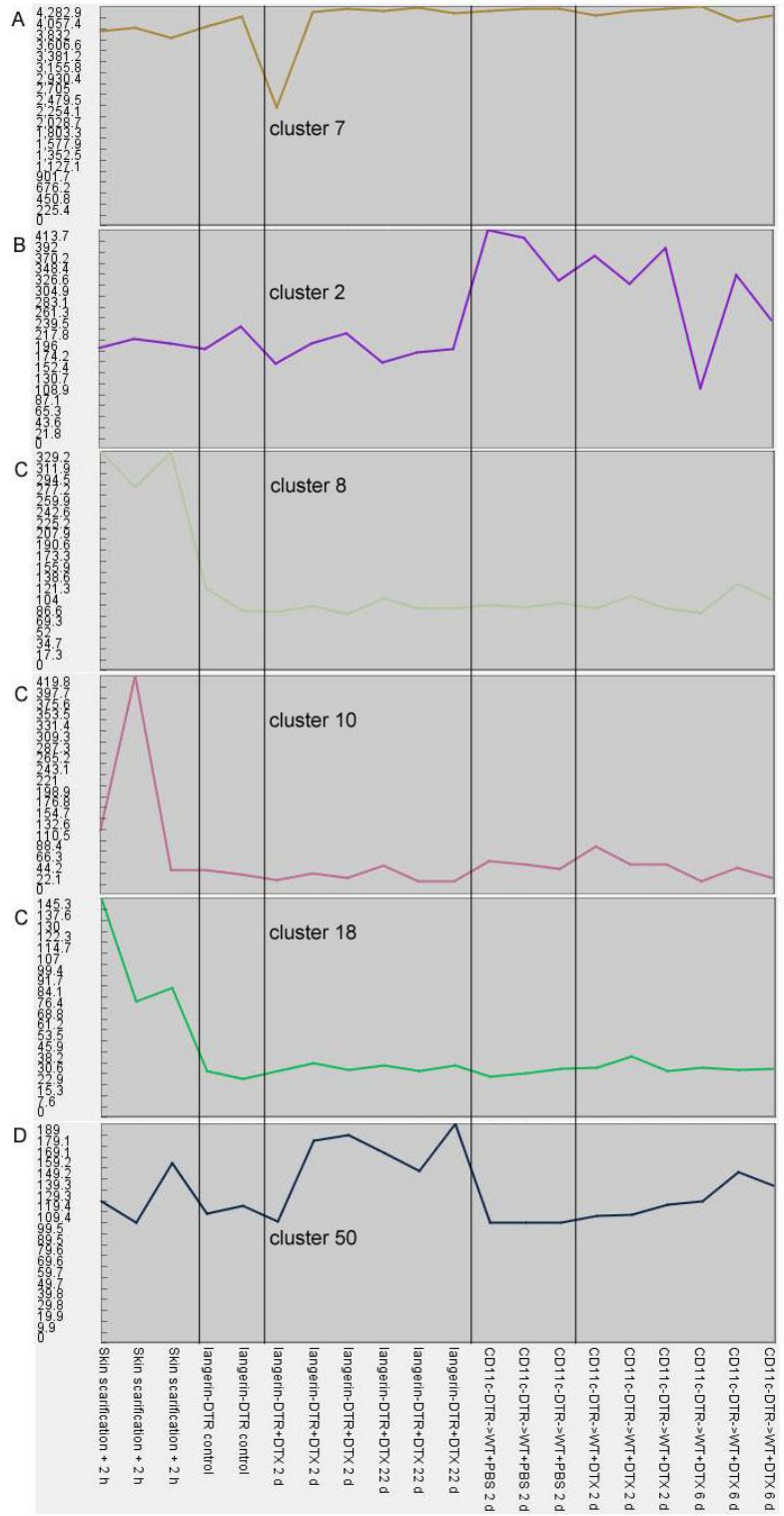

Figure 9.3. Gene expression profiles from distinct clusters. The gene expression profiles of a number of different clusters were selected for representation to cover the different types of clusters observed. The y-axis shows average expression for the cluster (intensity). **A** Expression profiles of one 'housekeeping' cluster: cluster 7. **B** Cluster 2: expression profile of a phagocyte-related gene cluster mainly enriched in the CD11c-DTR→WT samples. **C** Expression profiles of gene clusters enriched following scarification. **D** Expression profile of genes enriched in the langerin-DTR+DTX samples.

9.3.4. Fluorescent labelling of the ME7 scrapie agent SAFs

In order to gain further insight into how PrP^{Sc} reached the draining iLN following inoculation via the skin, PrP^{Sc} was fluorescently labelled prior to infection via the skin scarification, in order to determine whether it was possible to visually track the movement of PrP^{Sc} from the skin. Recent findings, using fluorescent labels, demonstrate the transport of immune complexes from the skin to the draining iLN as soon as 15 min after application or injection (Phan *et al.*, 2009; Phan *et al.*, 2007). By fluorescently tagging PrP^{Sc} prior to application via skin scarification, it may be possible to gain further insight into how PrP^{Sc} reaches the draining iLN. To determine whether it was possible to track the scrapie agent from the skin to the draining iLN, following infection via scarification, ME7 scrapie agent SAFs, extracted from pooled ME7 affected brain homogenates, were fluorescently tagged with Alexa-Fluor®546 to enable their visualisation in tissues *ex vivo* (Gousset *et al.*, 2009). Alexa- Fluor®546-PrP samples were treated in the presence or absence of proteinase K, to confirm the presence of disease specific PrP^{Sc} within the samples. Several tests were carried out to ensure that fluorescent labelling was bound to the SAFs. The samples were simultaneously separated by gel electrophoresis on two gels. One gel was further analysed via Western blot, with the anti-PrP mAb 8H4. Scrapie specific PrP^{Sc} was detected in both samples (Fig. 9.4.). The second gel was scanned on a fluorograph machine, to determine fluorescence within the electrophoresed samples. Fluorescence was detected in both samples, consistent with labelling of PrP^{Sc} with Alexa-Fluor®546 (Fig. 9.4.). Proteinase K untreated samples indicated some non-specific protein labelling (Fig. 9.4.), as well as 3 bands consistent with PrP^{c}. Protease sensitive proteins were digested by proteinase K,

leaving three bands consistent with proteinase K resistant PrP^{Sc} (Fig. 9.4.). A silver stain was also carried out on the second gel (Fig. 9.4.). A lot more protein was detected in these samples than through the other two staining methods, (confirming that the fluorescence emission is very specific). These data show that although a lot of non-PrP^{Sc} protein was present in the samples, these proteins did not emit fluorescence after proteinase K digestion, nor did they immmunostain with the anti-PrP mAb. Together, these data suggested that the proteinase K treated samples appeared to contain fluorescently labelled scrapie specific PrP^{Sc}, hereafter referred to as Alexa-PrP^{Sc}. This compound will be used to visualise spread of PrP^{Sc} from the skin, following inoculation via skin scarification.

9.3.5. Tracking of Alexa-PrP^{Sc} in the skin following exposure by skin scarification

To determine whether fluorescent tagging of PrP^{Sc} would enable visual tracking of the spread of PrP^{Sc} from the skin to the draining iLN, mice were infected with Alexa-PrP^{Sc} by skin scarification. Skin sections of the scarification site and draining iLNs, with associated PAT, were collected 15 min, 2, 6.5, 24, 48, and 72 hr after exposure. Early changes were observed in the epidermis 2 hr post infection by haematoxylin and eosin (H&E) labelling, and the appearance of a crust on the epidermal surface was observed from 6.5 hr post scarification (Fig. 9.5.). 48 hr post scarification, the scarification site was not captured on the section, but was most-likely on adjacent sections, as higher magnification images showed evidence of epidermal hyperplasia at the site of Alexa-PrP^{Sc} accumulation (Fig. 9.5. and most evident on Fig. 9.9. highest magnification). Alexa-PrP^{Sc} was detected in the skin at each of the above time points, until 72 hr post infection (Fig. 9.6., Fig 9.8., and Fig. 9.9.).

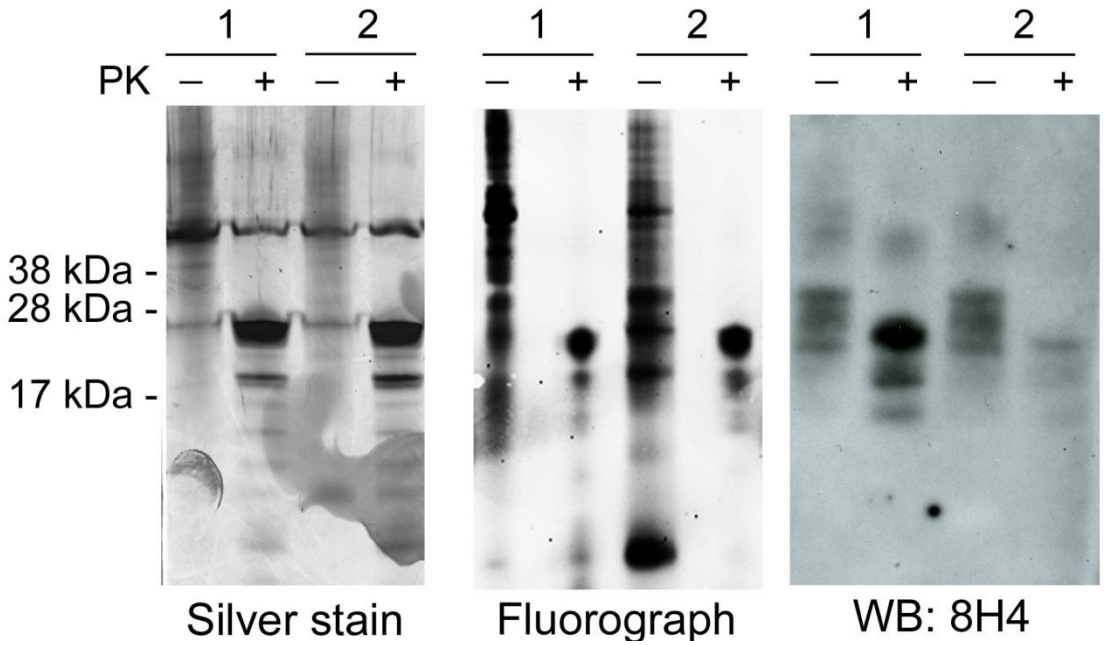

Figure 9.4. Confirmation of fluorescently labelled PrP^{Sc} in SAFs. SAFs were extracted from ME7 affected brain homogenates and fluorescently labelled. Samples underwent gel electrophoresis and were further analysed by Western blot with the anti-PrP mAb 8H4, fluorograph scanning, and silver staining to confirm that fluorescence was specific to PrP^{Sc} (following proteinase K treatment).

In the tissues collected 72 hr post infection the scarification site was identified by the presence of a crust on the skin surface (Fig. 9.5.), but unlike in the other time point tissues, Alexa-PrP^{Sc} was not detected at or adjacent to the scarification site. At this time, Alexa-PrP^{Sc} was detected below the epidermal surface of the skin, distal to the site of scarification (area denoted by a * in Fig. 9.5). These findings are further illustrated in Fig. 9.6., where immunofluorescent labelling of LCs highlights the location of the epidermis in respect to the Alexa-PrP^{Sc}.

Analysis of the draining iLN and the PAT yielded inconclusive evidence of Alexa-PrP^{Sc} transport from the skin via the fat. Some cells associated with inflammation, such as neutrophils, were detected in and around the iLNs but there was no clear effect of scarification or Alexa-PrP^{Sc} transport to the PAT or the iLNs, when compared to iLNs from unscarified mice (data not shown). Small specks of fluorescent labelling were detected in the PAT surrounding the draining iLN 15 min, 2, 6.5, and 24 hr post infection (Fig. 9.7.). These specks were difficult to capture images of, due to their small size, but these specks were brighter than non-specific, background staining when observed through the microscope.

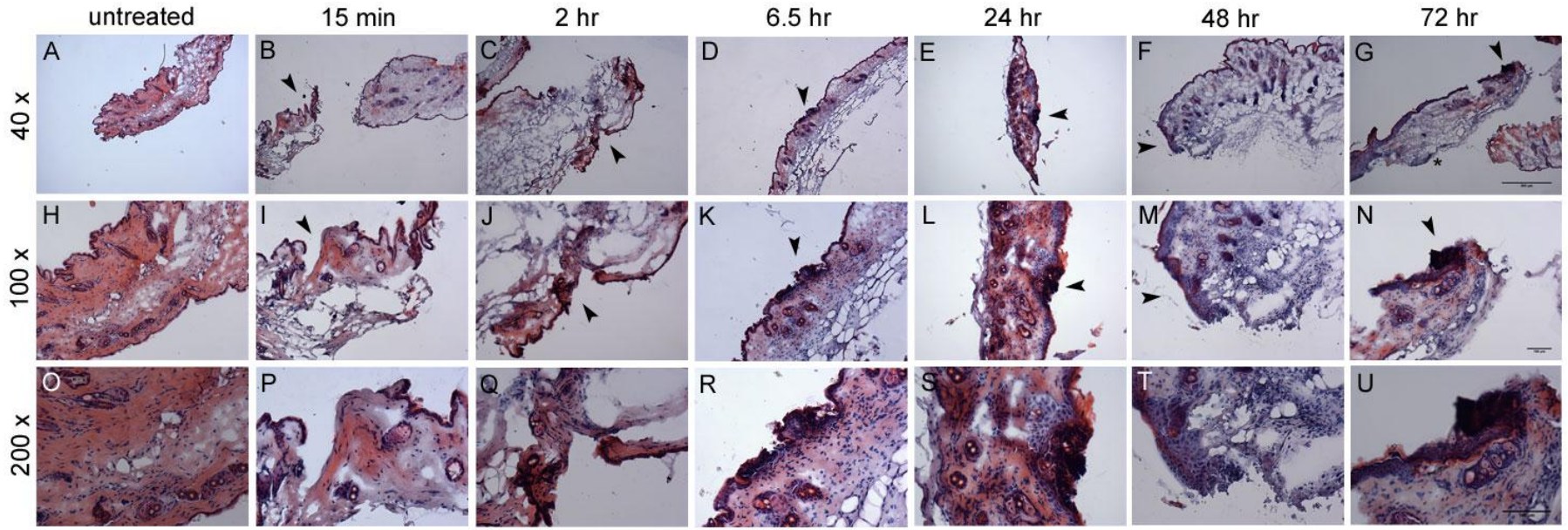

Figure 9.5. Histopathological analysis of skin sections following exposure to Alexa-PrP^{Sc} via scarification. Mice were infected with the Alexa-PrP^{Sc} via skin scarification and sections from the site of scarification were collected at the above time points for histopathological analysis. Scarification site or area near scarification is indicated by arrowheads. Haematoxylin and eosin (H&E) staining of the scarification sites revealed: by 2 hr post scarification changes in the epidermal layer were observed (**Q**). Epidermal hyperplasia was present by 6.5 hr post scarification, below a sero-cellular crust (**R**,**S**,**U**). In absence of a crust, 48 hr post scarification, a hyperplastic epidermis was detected. The ∗ in **G** denotes the location of Alexa-PrP^{Sc} which is distal to the scarification site (arrowhead), magnified in **N** and **U**. Images are representative of observations in 4 animals/group. Scale bar, left column: top row, 500 µm; bottom 2 rows, 100 µm.

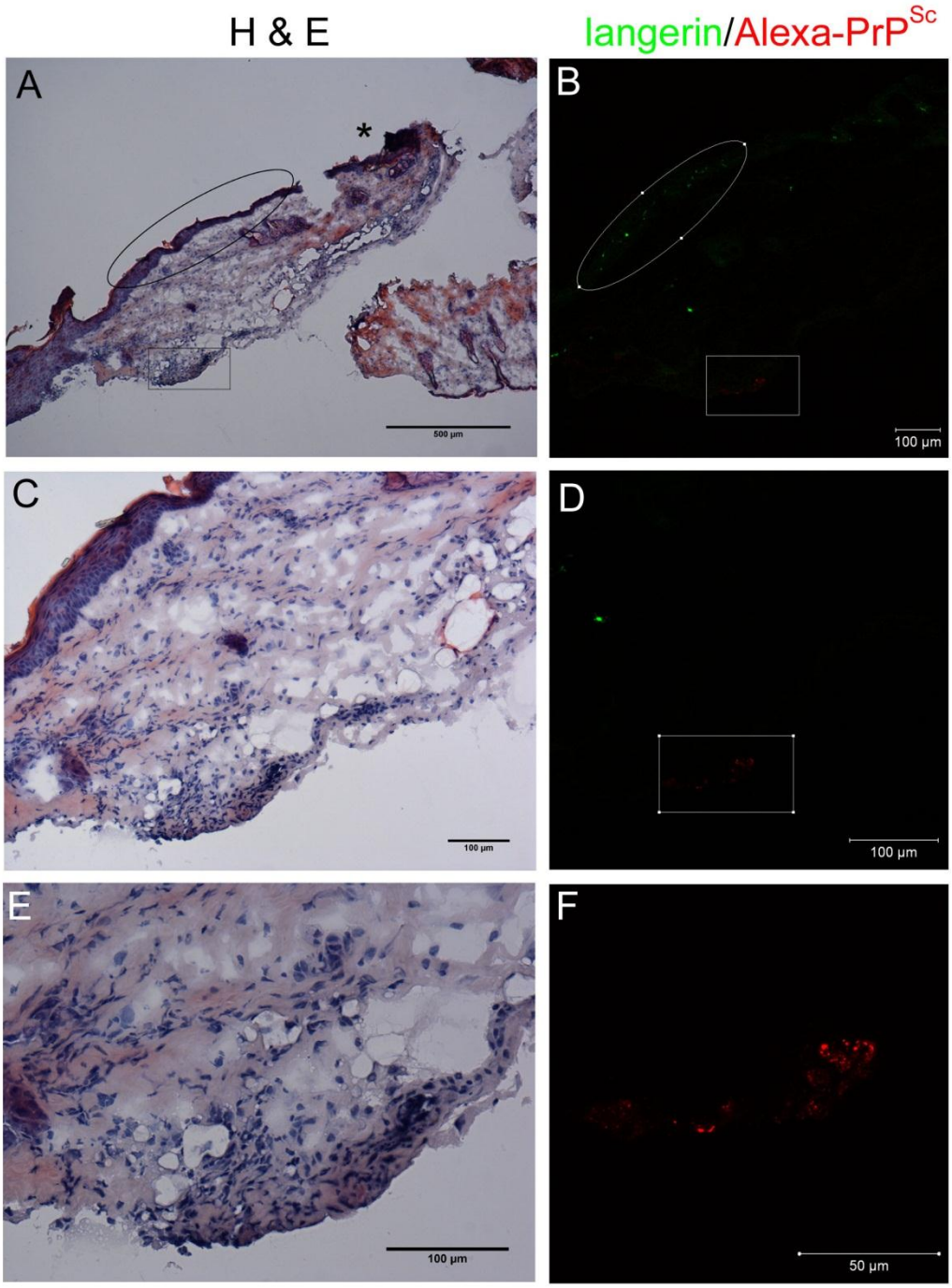

Figure 9.6. Alexa-PrP detected distal to the scarification site 72 hrs post infection. Mice were infected with Alexa-PrP^{Sc} inoculum via skin scarification. Thigh skin from the site of scarification was collected 72 hr post infection for histopathological and immunofluorescent analysis. **A**,**C**,**E**: H&E staining. **A**: The scarification site is denoted by ∗. Red fluorescence, indicative of Alexa-PrP^{Sc} (red) was not detected near the scarification site but was detected at the opposite end of the section, delineated by the box (A, B, D). Immunolabelling with the anti-langerin specific antibody (green) denotes epidermal LCs (elipse in A and B), distant from the Alexa-PrP^{Sc}. **C**,**E**: higher power images of site of Alexa-PrP^{Sc}. **D**,**F**: increased magnification of Alexa-PrP^{Sc}. Scale bar, left column: 500 µm, 100 µm, 100 µm; right column: 100 µm, 100 µm, 50 µm.

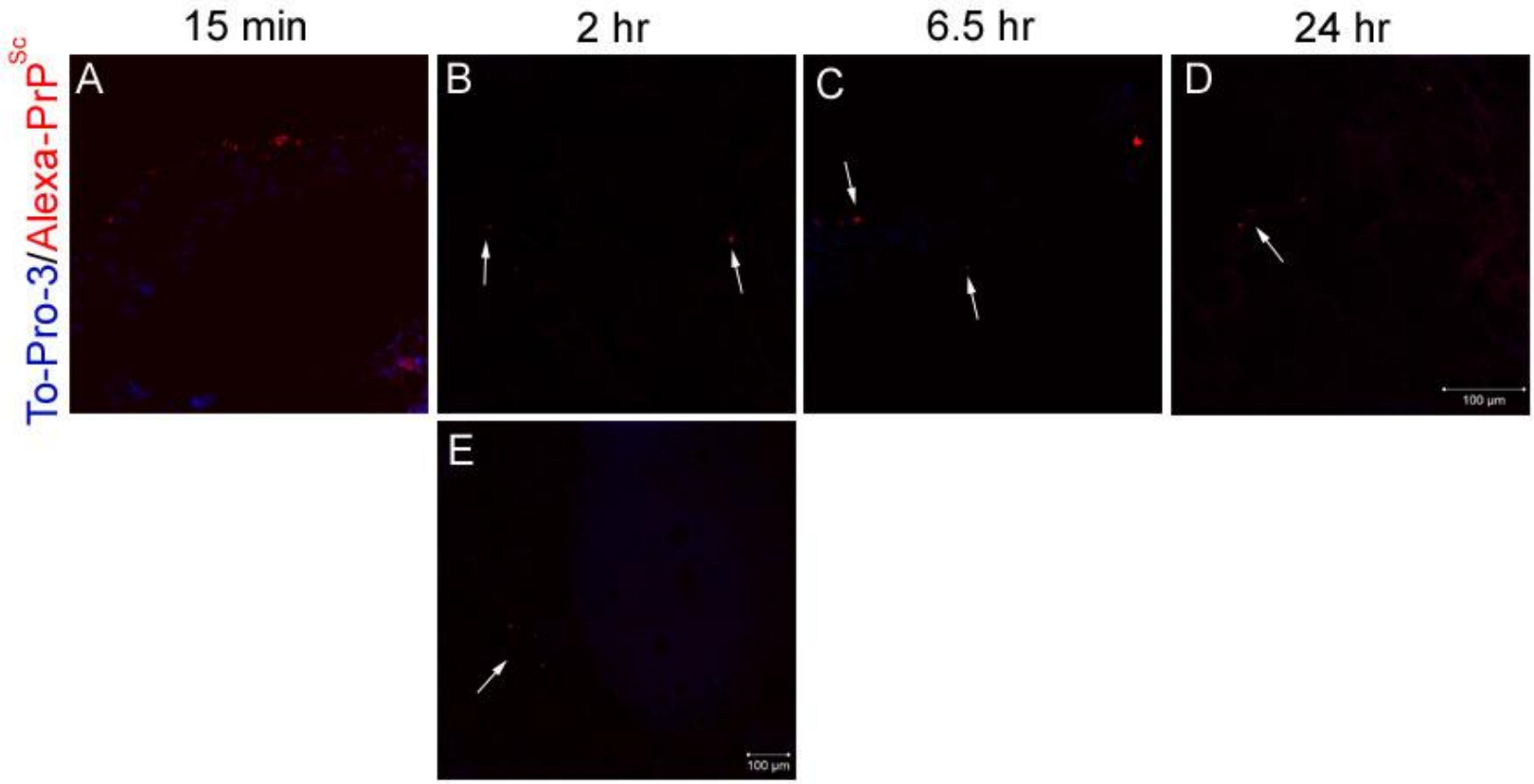

Figure 9.7. Detection of Alexa-PrP^{Sc} in the PAT of the draining iLN post exposure by scarification. Mice were infected with Alexa-PrP^{Sc} inoculum via skin scarification and draining iLNs collected from the above time points for immunofluorescent analysis, using TO-PRO®-3 iodide nuclear counterstain (blue). **A-E**: Red fluorescence, indicative of Alexa-PrP^{Sc} (red) was detected in the perinodal fat of the draining iLN from 15 min post infection. **E**: Alexa-PrP^{Sc} detected in the proximity of the iLN (blue). **D**,**F**: increased magnification of Alexa-PrP^{Sc}. Scale bar: 100 µm.

9.3.6. Alexa-PrP^{Sc} and other cell types

To further gain knowledge of whether PrP^{Sc} moves from the skin by a cell-dependent mechanism, immunofluorescence analysis was used to determine which, if any, cell types in the skin were associated with Alexa-PrP^{Sc} after exposure by via skin scarification. Immunolabelling with the anti-langerin specific antibody revealed the LCs in the epidermis of the skin (Fig. 9.8.), and some langerin^{+} dermal cells. The LCs were observed near the Alexa-PrP^{Sc}, usually under the crust formed at the site of scarification. Occasional cells were detected amongst the red fluorescence (Alexa-PrP^{Sc}) but there did not appear to be any direct interaction between the LCs and the Alexa-PrP^{Sc} inoculum between 15 min and 72 hr post scarification (Fig. 9.8.).

Immunofluorescence analysis was also used to determine the extent of neutrophil infiltration following scarification (Fig. 9.9.). Neutrophil infiltration was observed from 2 hrs post scarification, and from 6.5 hr post scarification were associated with a neutrophilic crust at the scarification site (Fig. 9.10.). By 48 and 72 hr post infection the intensity of neutrophil labelling had started to decrease compared to the earlier time points.

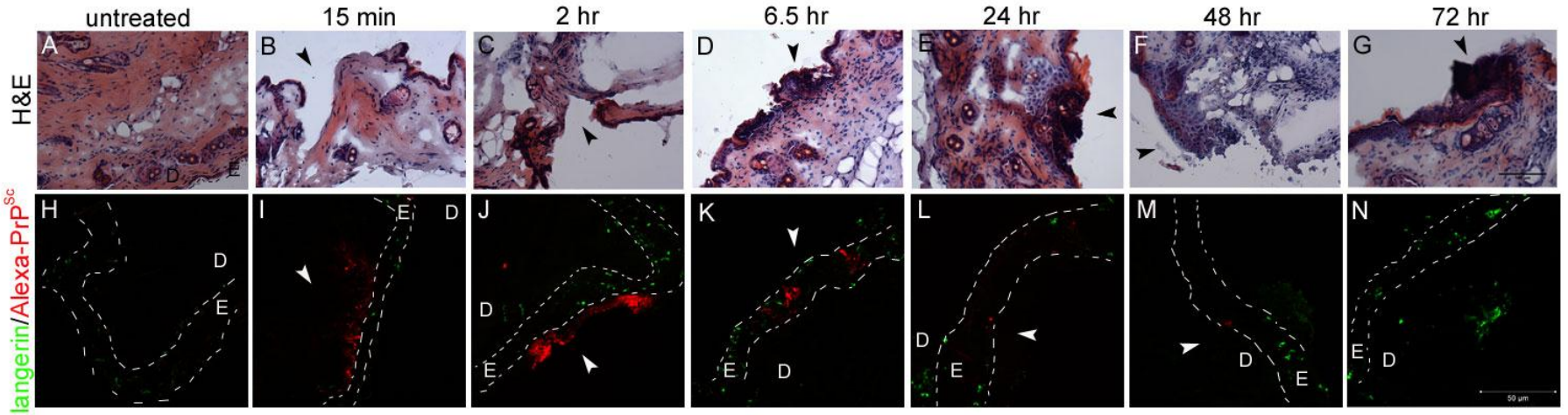

Figure 9.8. Alexa-PrP^{Sc} did not colocalise with epidermal LCs following infection via scarification. Mice were infected with Alexa-PrP^{Sc} inoculum via skin scarification. Thigh skin from the site of scarification was collected at the above time points for histopathological and immunofluorescent analysis. Arrowheads indicate site of scarification, and highlight the same areas between the light level and fluorescent images. Discontinuous lines delineate the epidermis: **E**; for orientation, the area of the dermis is denoted by **D**. **A-G**: H&E staining of the scarification sites. **H-N**: Adjacent sections confirmed that presence of Alexa-PrP^{Sc} (red) at or adjacent to the scarification sites, with the exception of 72 hr post infection. The anti-langerin specific antibody revealed the presence of LCs in the epidermis (green). These LCs appeared to be located below the layer of Alexa-PrP^{Sc}, occasional cells were detected interspersed within the Alexa-PrP^{Sc} but did not appear to be colocalised with this labelling. **G** shows the presence of LCs at the scarification site 72 hr post infection but no Alexa-PrP^{Sc} was detected at the site. Images are representative of observations in 4 animals/group. Scale bar: top row, 100 µm; bottom row, 50 µm.

untreated
15 min
2 hr
6.5 hr
24 hr
48 hr
72 hr
H&E
Alexa-PrP^Sc
neutrophil/Alexa-PrP^Sc
A
B
C
D
E
F
G
H
I
J
K
L
M
N
O
P
Q
R
S
T
U
V
W
X
Y
Z
AA
E
D
100 μm
20 μm

Figure 9.9. Neutrophil accumulation in the skin following exposure to Alexa-PrP^{Sc} by scarification. Mice were infected with Alexa-PrP^{Sc} inoculum via skin scarification. Thigh skin from the site of scarification was collected at the above time points for histopathological and immunofluorescent analysis. Discontinuous lines delineate the epidermis: **E**; for orientation, the area of the dermis is denoted by **D**. Arrowheads indicate sites of scarification, and highlight the same areas between the light level and fluorescent images. **A**-**G**: H&E staining of the scarification sites. **H**-**M**: Adjacent sections confirmed that presence of Alexa-PrP^{Sc} (red) at or adjacent to the scarification sites, with the exception of 72 hr post infection. Neutrophil infiltration (green) was observed from 2 hr post infection (**P**,**W**) and was associated with the scarification site. Formation of a neutrophillic crust was observed 6.5 hr (**Q**,**X**) and 24 hr (**R**,**Y**) post infection. Labelling was reduced from 48 hr post infection (**Z**). Images are representative of observations in 4 animals/group. Scale bar: top 3 rows, 100 µm; bottom row, 20 µm.

9.3.7. Alexa-PrP^{Sc} infection via scarification of the ear

To determine whether LCs might play a role in the degradation of PrP^{Sc} following inoculation via skin scarification, mice were infected with the Alexa-PrP^{Sc} via skin scarification of the ear. The pinna of the ear was selected as an appropriately flat surface, and allow for *en face* visualisation of both the epidermis and dermis, via separation of the dermal sheets. Ears were collected 15 min and 2 hrs after infection and separated into epidermal and dermal sheets. Sheets were labelled with the anti-langerin antibody to detect langerin^{+} cells. Z-stacks were obtained at areas where Alexa-PrP^{Sc} was detected, but no colocalisation was observed between the Alexa-PrP^{Sc} and LCs in the epidermis, or langerin^{+} dDCs in the dermis, at either time point (Fig. 9.10.). Some langerin^{+} dDCs are located near the site of scarification, it is unclear whether they have migrated towards the site or were positioned there when scarification was carried out.

Faint areas of red fluorescence were observed in areas of the epidermis that resembled the tight junctions described by Kubo *et al* (Kubo *et al.*, 2009) (Fig. 9.11.). These distinct structures were difficult to image as immunofluorescence faded quickly, but Figure 9.11. provides a very detailed example of what was observed.

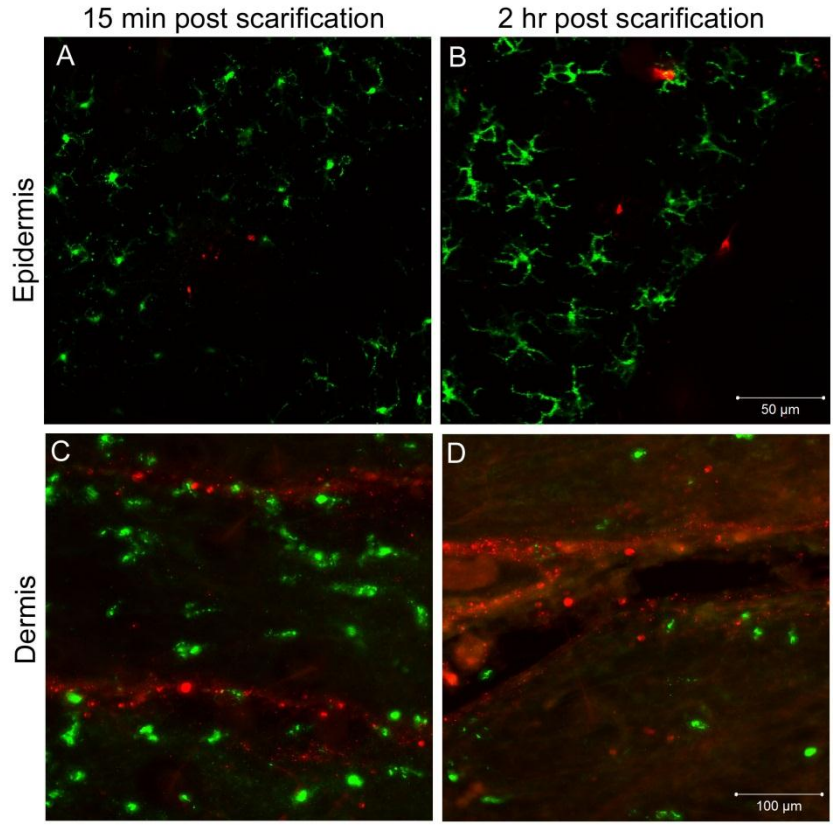

Figure 9.10. Alexa-PrP^{Sc} failed to colocalise with langerin^{+} cells in the skin following exposure to PrP^{Sc} via skin scarification. Mice were infected with Alexa-PrP^{Sc} inoculum (red) via skin scarification of the ventral side of the ear. Epidermal and dermal ear sheets collected 15 min and 2 hr post infection were immunolabelled with the anti-langerin specific antibody (green). **A**: 15 min post scarification Alexa-PrP^{Sc} was detected within epidermal sheets. Analysis of the Z-stacks showed that LCs did not appear interact to with Alexa-PrP^{Sc}. Similar results were observed 2 hr post scarification, **B**. **C** and **D**: Alexa-PrP^{Sc} was detected along the site of scarification in the dermis. A few langerin^{+} cells were detected in close proximity to the Alexa-PrP^{Sc} at both time points. Images are representative of observations in 4 animals/group. Scale bar: top row, 50 µm; bottom row, 100 µm.

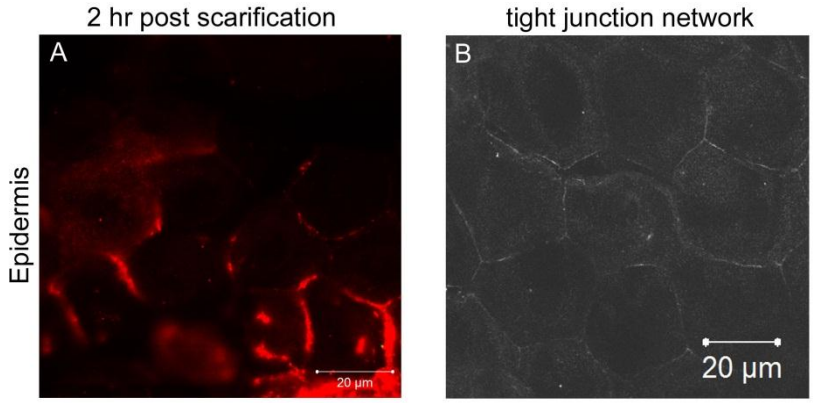

Figure 9.11. Alexa-PrP^{Sc} appears to associate with epidermal tight junctions. Mice were exposed to Alexa-PrP^{Sc} (red) via skin scarification of the ventral side of the ear, and epidermal ear sheets collected for immunofluorescent analysis 2 hr post scarification. **A**: Red fluorescence was detected in patterns that resembled epidermal tight junctions. **B**: Epidermal tight junctions detected with the anti-ZO-1 mAb. Scale bar: 20 µm.

9.4. Discussion

Research in this chapter has highlighted the immediate and longer term effects associated with scarification of the skin. Both neutrophils and $CD11b^{+}$ cells were shown to migrate to the site of scarification within a couple of hours. CD11b is a marker expressed by granulocytes, monocytes, NK cells, and tissues macrophages. This does not exclude the possibility of other cell types that migrate to the site at the time of scarification; they simply were not tested for here. However, these two markers cover the range of cells typically associated with inflammatory responses in the skin (Delavary *et al.*, 2011). These results were further supported by analysis of the trafficking of Alexa-PrP^{Sc} after exposure by skin scarification, where neutrophil infiltration was observed from 2 hr post infection, and neutrophils were further associated with the formation of a crust at the site of scarification. The epidermis in which the LCs reside is a relatively thin tissue, where *en face* visualisation of epidermal sheets clearly outlined the cellular network created by these LCs. While the cells are not on a single plane, they do organise themselves in several layers, fitting within the constraints of the epidermis. It is therefore difficult to determine whether scarification stimulated LC accumulation to the site of trauma, but data in this chapter suggest this was unlikely. It was possible to observe a hyperplastic epidermis from 6.5 hr after scarification, by histopathological analysis. This indicates the presence of too many cells within the epidermis, and is associated with a 'danger' signal, a response to scarification.

LCs did not appear to associate with Alexa-PrP^{Sc} following infection via skin scarification when observed in the epidermal sheets or in the skin cross sections.

These results do further support previous studies indicating that LCs do not play a role in TSE disease (Mohan *et al.*, 2005b; Mohan *et al.*, 2005c), and data in this thesis showing that disease incubation period was not affected in the absence of LCs at the time of scrapie infection (Chapter 8).

Studies have shown that Alexa-PrP^{Sc} could be transferred between DCs and neurons *in vitro* (Gousset *et al.*, 2009). Results observed in Chapter 4 point towards a role for DCs in early scrapie agent spread from the skin to the draining iLN. In contrast to the LCs of the epidermis, analysis of the dermal sheet from the ear scarified with Alexa-PrP^{Sc} indicate a possible interaction between langerin^{+} dDCs and the Alexa-PrP^{Sc} compound in the dermis as early as 15 min post scarification.

While a lot of research is focused on determining potential cell types involved in scrapie agent transmission from the skin, the possibility of a cell free mechanism cannot be excluded. Knight (Knight, 2008) highlighted the potential role of the PAT in stimulating immune cells found within the PAT. Phan *et al* demonstrated the movement of fluorescently tagged immune complexes from the skin to the draining LNs within 15 min of exposure (Phan *et al.*, 2007). In the current study, Alexa-PrP^{Sc} was detected in the PAT of the draining iLN as early as 15 min post scarification, thereby indicating that Alexa-PrP^{Sc} might travel to the draining iLN via a cell-free mechanism, as well as a cell-associated mechanism. The structure of the epidermis is maintained by a network of tight junctions between the cells within it (Kubo *et al.*, 2009). These tight junctions form a distinctive honeycomb structure, within which sit the LCs (Kubo *et al.*, 2009). The LCs were found to stretch their dendrites through

the tight junctions to pick up antigen in the extra-tight junction environment. Following scarification with Alexa-PrP^{Sc} in the ear, several areas of fluorescence were observed in a distinct honeycomb structure. Some of these areas were larger than others, but they were uniformly difficult to acquire images of. Fig. 9.11. is therefore just an example of what was observed, but clearly highlights the honeycomb structure associated with the tight junctions in the skin. These results point toward an alternative mechanism for the scrapie agent to potentially move from the surface of the skin following scarification.

Gene profile analysis and the information it provides can shed a lot of light on biological function during and as a result of different events. In this chapter, this meta-analysis was used to help understand how gene function was affected by several events that have been described in previous chapters: scarification and DTX-mediated depletion of $langerin^{+}$ or $CD11c^{+}$ cells. Previous data suggests no adverse/inflammatory response in the skin following DTX-mediated $langerin^{+}$ cell depletion (Kissenpfennig *et al.*, 2005b). Equally, no long-term defects or illness were associated with $CD11c^{+}$ cell depletion (Jung *et al.*, 2002). Microarray analysis carried out on skin samples from langerin-DTR or CD11c-DTR→WT mice support these findings. No inflammatory gene expression clusters were identified within DTX-treated tissues. No major gene profile changes were observed in CD11c-DTR→WT mice specifically treated with DTX. Some changes were observed across the mouse line (including untreated controls) suggesting a possible effect due to bone marrow reconstitution. In langerin-DTR mice, there was one cluster where genes were specifically upregulated following DTX treatment, which appeared to be

associated with transcription. As expected, scarification resulted in a much more specific response. The upregulated genes were mostly associated with expression clusters enriched for genes associated with inflammation and skin damage, and cluster 44 was associated with B lymphocytes. These data further support the results obtained through histopathological analysis of skin, demonstrating the effects of scarification in the skin.

Data in this chapter, from the analysis of the trafficking of Alexa-PrP^{Sc} after scarification, suggests a lack of LC involvement following scrapie infection from the skin. These data are congruent with data in Chapter 8, showing depletion of LCs did not delay TSE neurinvasion from the skin. Whether other cell types such as $langerin^{+}$ dDCs play a role in scrapie agent transport from the skin is uncertain, data in this chapter also imply the possibility of cell-free transport from the skin, for example as a complement-bound complex.

10

GENERAL DISCUSSION

10.1. The role of CD11c$^+$ cells in TSE transmission from skin

How prions are propagated from the skin to the draining LN after exposure via skin scarification is uncertain. Experimental TSE transmission had previously been established through scarification of the skin or in the mouth (Bartz *et al.*, 2003; Carp, 1982; Denkers *et al.*, 2011; Glaysher and Mabbott, 2007a; Mohan *et al.*, 2004; Mohan *et al.*, 2005b; Taylor *et al.*, 1996). Following experimental scrapie infection via scarification of the skin or tongue, PrP^{Sc} accumulated in the draining LNs prior to neuroinvasion (Bartz *et al.*, 2003; Glaysher and Mabbott, 2007a; Mohan *et al.*, 2004; Mohan *et al.*, 2005b). LCs and dDCs are immune cells which acquire antigen within the skin before migrating to the skin draining LNs (Bursch *et al.*, 2007; Ginhoux *et al.*, 2007; Kissenpfennig *et al.*, 2005b; Poulin *et al.*, 2007), where they present the antigen. Based on previous evidence linking CD11c$^+$ cells/DC subsets to PrP^{Sc} transport (Cordier-Dirikoc and Chabry, 2008; Gousset *et al.*, 2009; Huang *et al.*, 2002; Raymond *et al.*, 2007; Sethi *et al.*, 2007), the main aim of this thesis was to establish whether these cells might also play a role in the transport of PrP^{Sc} from the skin to the draining iLN following scrapie infection via skin scarification. To address this question, transgenic mice were used which express DTR on target cells, and where the target cells could be temporarily depleted through a single injection of DTX (Jung *et al.*, 2002). Following targeted cell depletion, these mice were infected with the ME7 strain of scrapie via skin scarification of the inner thigh.

In order to study the role of LCs and dDCs and other CD11c$^+$ MNP populations on scrapie transmission independently of each other, transgenic bone marrow chimeric mice were created where all the CD11c$^+$ cell subsets were depleted following DTX

treatment, with the exception of LCs (Chapters 3 and 5). Depletion of $CD11c^+$ cells prior to scrapie infection via the skin, delayed early stage PrP^{Sc} infection compared to control groups (Chapter 4). The data presented in this thesis show that depletion of $CD11c^+$ cells delays early PrP^{Sc} accumulation in the draining iLN following scrapie infection via the skin, although this did not affect disease susceptibility. Following infection via skin scarification in mice where $CD11c^+$ DCs had returned but $CD11c^+$ SCS macrophages remained partially depleted following DTX treatment, there was no effect on early stage PrP^{Sc} accumulation in the draining iLN or on disease susceptibility.

These results point towards a role for $CD11c^+$ DCs in the initial transport of PrP^{Sc} from the skin to the draining iLN. It is therefore likely that transport occurs via the lymphatics rather than blood, as DCs migrate via the lymph. Equally, if PrP^{Sc} were transported via the blood, it should reach all lymphoid tissues within a similar time frame, but following scrapie infection via scarification, PrP^{Sc} accumulates first in the draining lymphoid tissue before spreading to others (Glaysher and Mabbott, 2007a; Mohan *et al.*, 2005a). In contrast, the draining LN was only found to play a critical role in scrapie pathogenesis in a small cohort of hamsters infected with a low dose of inoculum following footpad injection (Kratzel *et al.*, 2007). Scrapie infection via skin scarification uses only a very small amount of inoculum (6 µl). Results from Chapter 9 point towards a lot of inoculum remaining on the skin or being lost in the crust. This route of infection may therefore result in similar findings to low dose infections in hamsters infected via the footpad (Kratzel *et al.*, 2007), as higher doses of infection appear to utilise other routes of spread than just the LRS (Kratzel *et al.*,

2007). DTX-mediated $CD11c^+$ cell depletion prior to oral scrapie challenge blocked early PrP^{Sc} accumulation in the gut associated lymphoid tissue, and reduced disease susceptibility (Raymond *et al.*, 2007). Incubation period differences were near 200 days in some mice, and the absence of these cells completely blocked early stage PrP^{Sc} accumulation compared to a delay following infection via the skin. This indicates that while $CD11c^+$ cells play a major role in oral scrapie pathogenesis; it is likely that PrP^{Sc} arrives in the draining iLN via more than one route or cell type.

Certain tissue macrophage populations such as those in the peritoneal cavity, the lamina propria of the intestine, the SCS and the splenic marginal zone also express low levels of CD11c. Accordingly, these macrophage populations are likewise depleted in CD11c-DTR mice (Bradford *et al.*, 2011; Probst *et al.*, 2005). The SCS macrophages are a distinct, poorly endocytic and degradative macrophage subset (Phan *et al.*, 2009; Phan *et al.*, 2007), and appear to be specialised to capture antigen-containing immune complexes arriving in the LN via their cell processes that extend into the lumen of the SCS (Carrasco and Batista, 2007; Junt *et al.*, 2007; Phan *et al.*, 2009; Phan *et al.*, 2007; Roozendaal *et al.*, 2009). In contrast to other macrophage subsets, SCS macrophages retain these immune complexes on their surfaces for rapid translocation through the SCS floor to underlying, follicular B cells. These B cells then acquire the immune complexes via their complement receptors and deliver them to FDC. The shuttling of immune complexes via the SCS macrophage-B cell cellular relay represents an efficient route through which antigens are delivered to FDC. Prions are also considered to be acquired by FDC as complement bound complexes (Klein *et al.*, 2001; Mabbott and Bruce, 2004; Mabbott *et al.*, 2001; Zabel *et al.*,

2007). This highlights the possibility that SCS macrophages in LNs (and their counterparts in the spleen) may also facilitate the delivery of complement-bound prions to FDC. Indeed, disease-specific PrP has been detected in association with SCS macrophages in the mesenteric LNs of prion-exposed sheep (Jeffrey *et al.*, 2006). PrP^{Sc} might therefore enter the draining LNs via the lymph without a cellular association. Studies in aged mice have determined that FDCs in these mice exhibited reduced immune complex trapping capacity, concurrent with a drop in cellular PrP^{c} expression, reducing the ability of older mice to accumulate PrP^{Sc} (Brown *et al.*, 2009), further highlighting the possibility of PrP^{Sc} association with immune complexes.

$CD11c^{+}CD169^{+}$ SCS macrophages were partially depleted following DTX treatment in CD11c-DTR bone marrow chimeric mice. These cells were absent at the time of scrapie infection along with $CD11c^{+}CD169^{-}$ classical DCs, in the experiment described in Chapter 4. It was therefore not possible to determine whether the delayed accumulation of PrP^{Sc} was a result of absent DCs or absent macrophages. In Chapter 6, scrapie infection was not carried out until 6 days after DTX treatment, when the classical DCs had mostly repopulated the tissues but the $CD11c^{+}CD169^{+}$ SCS macrophages remained partially depleted. If the $CD11c^{+}CD169^{+}$ cells played a direct role in the transport of the PrP^{Sc} from the lymph to the FDCs, one would expect PrP^{Sc} accumulation to be delayed in these mice. There was, however, no observable differences in PrP^{Sc} accumulation between the DTX treated and control group. These data suggest that the effects of DTX-treatment on the early accumulation of prions within the draining iLNs of CD11c-DTR→WT mice were

not due the depletion of $CD11c^{+}CD169^{+}$langerin^{-} SCS macrophages. Flow cytometric analysis of $CD169^{+}$ SCS macrophages has yielded both a $CD11c^{+}CD169^{+}$ and a $CD11c^{-}$ $CD169^{+}$ macrophage population (Asano *et al.*, 2011), situated within the cortical and paracortical sinus, and within the SCS respectively. Both cell types appeared to equally phagocytose subcutaneously injected antigen. The authors do not rule out the possibility that these $CD11c^{+}CD169^{+}$ cells are a subset of $CD8\alpha^{+}$ DCs (Asano *et al.*, 2011). These findings further emphasise the influence of minor subpopulations within tissues, as has previously been highlighted throughout this thesis. Analysis in this thesis focused on immunohistochemical detection, rather than flow cytometric analysis. It is therefore possible that the $CD11c^{-}CD169^{+}$ macrophages could play a role in the transport of PrP^{Sc} from the SCS of the LN to the FDCs, in addition to a cellular transport by $CD11c^{+}$ DCs. This would explain why despite $CD11c^{+}$ cell depletion, some PrP^{Sc} was still able to reach, and accumulate within, the draining iLN.

10.2. The role of langerin^{+} cells in TSE transmission from skin

The above studies could not exclude a role for LCs in TSE pathogenesis since these cells were unaffected in the DTX-treated CD11c-DTR→WT mice. LCs can be identified through their expression of langerin (Valladeau *et al.*, 2002; Valladeau *et al.*, 1999; Valladeau *et al.*, 2000), but more recently a subset of dermal DC, termed langerin^{+} dDCs, has also been described (Bursch *et al.*, 2007; Ginhoux *et al.*, 2007; Poulin *et al.*, 2007). To address the question of whether LCs play a role in the transport of the scrapie agent from the skin to the draining iLN, transgenic mice were used, which express DTR on langerin^{+} target cells (LCs and langerin^{+} dDCs in the

skin, and langerin^{+} cells in the skin draining LNs), and where these cells could be temporarily depleted through a single injection of DTX (Kissenpfennig *et al.*, 2005b). Following targeted cell depletion, these mice were infected with the ME7 strain of scrapie via skin scarification of the inner thigh.

Depletion of langerin^{+} cells in the skin prior to scrapie infection via skin scarification (Chapter 8) did not affect early stage PrP^{Sc} deposition in the draining iLN, 5 weeks post scarification (when a delay was observed following CD11c^{+} cell depletion). This implies that LCs are not involved in the initial delivery of the TSE agent to the draining LN. However, 7 weeks post infection, PrP^{Sc} accumulation and CD21/35 expression was greatly increased compared to the two control groups. Despite these results, no differences were observed between incubation periods of the different groups.

It is uncertain whether the observed increases in PrP^{Sc} and CD21/35 occurred simultaneously, as there was no indication of such changes two weeks prior to this. Evidence that PrP^{Sc} accumulation is dependent on CD21/35 expression on FDCs (Zabel *et al.*, 2007), suggests that response to the LC-depletion had enhanced the expression of PrP^{c} and/or CD21/35, which accelerated PrP^{Sc} accumulation in the draining iLN. Equally, a potential sudden influx of PrP^{Sc} to the iLN, after repopulation of the LCs in the epidermis, might trigger this response. It could be argued that the depletion of large cell subsets might trigger an immune response in affected tissues, but this was not observed following CD11c^{+} cell depletion, in the mice receiving DTX treatment prior to scarification with NB homogenate, or in

langerin-DTR/C57BL/6 bone marrow chimeric mice. Equally, gene profile analysis did not show any major inflammatory type (or other) responses in the skin as a result of DTX treatment.

Langerin causes the internalisation of antigen from the surface of LCs to the Birbeck granules (Merad *et al.*, 2008). Langerin has also been shown to degrade HIV. Previous work has demonstrated a degradative effect of LCs on PrP^{Sc} *in vitro* (Mohan *et al.*, 2005c). In addition, blocking the migration of LCs in $CD40L^{-/-}$ mice or via caspase-1 inhibition shortened TSE disease incubation time (Mohan *et al.*, 2005b). Following scarification with the Alexa-PrP^{Sc} (Chapter 9) there was no observable association between LCs and Alexa-PrP^{Sc}. Association between LCs and Alexa-PrP^{Sc} might be expected if LCs were degrading the protein (Mohan *et al.*, 2005c). The increase in PrP^{Sc} accumulation following LC depletion might suggest that LCs play a phagocytic role following scrapie infection via the skin, and therefore the absence of LCs accelerates this infection. One would then expect to observe accelerated PrP^{Sc} accumulation in the draining iLN even at the earlier 5 week time point.

The results presented in Chapter 9, where mice were scarified with Alexa-PrP^{Sc} did not show any direct interaction between LCs and PrP^{Sc} by 2 hr after exposure. There may be a closer interaction between the $langerin^{+}$ dDCs and fluorescent inoculum, but the results observed cannot determine whether these cells are migrating towards the site of scarification, or whether they were simply positioned there at the time of scarification. Small specks of Alexa-PrP^{Sc} were detected in the PAT as early as 15

min post scarification. These results point towards cell-free movement of at least a small portion of Alexa-PrP^{Sc} from the skin towards the draining iLN, as skin resident cells typically only start to appear in the draining LN 24 hr after initial stimulation (Kissenpfennig *et al.*, 2005b), compared to immune complexes which have been visualised in the draining LN as soon as 15min after exposure (Phan *et al.*, 2007).

The lack of incubation period effect after increased PrP^{Sc} accumulation in $langerin^{+}$ cell depleted mice, might be explained by the 'second wave' of PrP^{Sc} accumulation occurring after the start of neuroinvasion or spread to other lymphoid tissues, from the draining iLN. This correlates with previous data, where temporary blockade of the lymphotoxin-β receptor signalling pathway (causing FDC dedifferentiation) at early time points after scrapie infection via the skin significantly reduced disease susceptibility, but FDC dedifferentiation 42 days post infection failed to affect the incubation period (Mohan *et al.*, 2005a). Further support for the theory of a 'second wave' of PrP^{Sc} accumulation could be considered following the increased PrP^{Sc} accumulation observed in terminally scrapie affected mice, where $CD11c^{+}$ cells were depleted prior to infection (Chapter 4).

The structure of the epidermis is maintained by a network of tight junctions between the cells, which form a distinctive honeycomb structure, within which sit the LCs (Kubo *et al.*, 2009). One could argue that because LCs form such a tight network in the epidermis, their complete depletion may significantly damage the integrity of the epidermis. Several attempts were made to determine whether tight junction structure (Kubo *et al.*, 2009) was affected following DTX mediated $langerin^{+}$ cell depletion.

The results presented in Chapter 9 indicate that after scarification damage to the epidermis might enable Alexa-PrP^{Sc} to pass through the tight junctions of the skin. It is, therefore, plausible that any disruptions to the skin, as a consequence of scarification, may lead to significant penetrance of prions into the underlying tissue and their dissemination via afferent lymph to the draining LN. If this was the direct, 'cell-free' route of PrP^{Sc} from the skin towards the draining iLN, again, one would expect to see earlier increased PrP^{Sc} accumulation, as cell free transport from the skin is fairly rapid (Asano *et al.*, 2011; Junt *et al.*, 2007; Phan *et al.*, 2009; Phan *et al.*, 2007). The timing of the increase in PrP^{Sc} accumulation, between 5 and 7 weeks post infection, point towards a possible link with $langerin^{+}$ cell repopulation following DTX-mediated depletion. Under normal circumstances LCs might clear the scrapie inoculum from the site of scarification. However, in their absence, much of the PrP^{Sc} remains within the skin until LCs start to return, which then carry the agent to the draining LN. Another possibility is that the sudden return of LCs triggers an immune reaction, which enhances CD21/35 expression within the draining LNs. These results do point towards a potential role of LCs in scrapie transmission from the skin, although it is not yet clear what their exact function is.

10.3. Relevance of research for natural TSEs

When working with a murine disease research model, one is often questioned about the relevance of the research to natural disease, which inevitably occurs in species other than mice. Mice are not naturally infected with scrapie, but they have proven to be a very effective model for the disease in a laboratory setting, without requiring genetic manipulation. There have been issues with a species barrier with other forms

TSE, such as BSE, which have been genetically addressed (Cancellotti *et al.*, 2007). In addition, scrapie replication in the mouse follows similar patterns to those often observed in natural TSEs.

The skin and oral mucosa present a likely route of transmission in several TSE diseases. Natural TSE infections might occur via lesions in the mouth and gastrointestinal tract through consumption of rough feed or birth-associated lesions to the skin or mucus membranes. These routes has proven successful in experimental transmission of scrapie and CWD (Bartz *et al.*, 2003; Carp, 1982; Denkers *et al.*, 2011; Glaysher and Mabbott, 2007a; Mohan *et al.*, 2004; Mohan *et al.*, 2005b; Taylor *et al.*, 1996). As infectivity has been readily detected in excreta and bodily fluids of both natural and experimentally transmitted TSEs (Gough and Maddison, 2010; Haley *et al.*, 2011; Haley *et al.*, 2009; Kariv-Inbal *et al.*, 2006; Ligios *et al.*, 2011; Mathiason *et al.*, 2006; Saunders *et al.*, 2008; Seeger *et al.*, 2005), as well as infectivity being identified in the skin of TSE infected animals (Cunningham *et al.*, 2004; Notari *et al.*, 2010; Thomzig *et al.*, 2007), or even present in the environment (Gough and Maddison, 2010), these points highlight the potential risk of transmission via the skin that can occur.

Much of this thesis has focused on the accumulation of PrP^{Sc} in the draining iLN following scrapie infection via skin scarification. LRS involvement in TSE disease is widespread in non-experimental situations. Widespread LRS involvement can be observed in CWD-infected animals (Keane *et al.*, 2009; Keane *et al.*, 2008; Sigurdson *et al.*, 1999; Spraker *et al.*, 2004; Spraker *et al.*, 2009) and some

genotypes of scrapie-infected sheep (Andréoletti *et al.*, 2000; Heggebø *et al.*, 2002; Heggebø *et al.*, 2000). Agent accumulation in lymphoid tissues is also a feature of vCJD patients (Foster *et al.*, 2001; Hill *et al.*, 1997) or BSE-infected sheep (Jeffrey *et al.*, 2001c), even though BSE and scrapie pathogenesis display differently within sheep (Jeffrey *et al.*, 2001a).

In contrast, early LRS involvement is not a major feature of sCJD (Hill *et al.*, 1999), nor in VRQ-heterozygous sheep genotypes (Schreuder *et al.*, 1998). While little LRS involvement has been linked to BSE in cattle (Somerville *et al.*, 1997), PrP^{Sc} and infectivity has been detected in the PPs of BSE-infected cattle (Buschmann and Groschup, 2005 although differences have been observed between natural and experimental transmission {Iwata, 2006 #263; Terry *et al.*, 2003).

The ME7 scrapie strain that was used for the experiments described in this thesis has been well utilised in numerous experiments conducted at the Neurobiology Division, The Roslin Institute, and its pathogenesis within the lymphoid system has been well documented. Disease pathogenesis in the mouse models replicates a route that likely often occurs in natural transmission. As experimental scrapie transmission involves PrP^{Sc} accumulation in the LRS following peripheral infection at a number of different sites (Glaysher and Mabbott, 2007a; Kimberlin and Walker, 1989a; Kimberlin and Walker, 1989b; Mohan *et al.*, 2004; Mohan *et al.*, 2005a), confirming that disease could potentially be transmitted via a number of different routes.

The identification of disease infectivity in skin (Cunningham *et al.*, 2004; Notari *et al.*, 2010; Thomzig *et al.*, 2007), fat (Race *et al.*, 2008; Race *et al.*, 2009), and antler velvet (Angers *et al.*, 2009) of both naturally and experimentally TSE-infected animals draws attention to the potential risk this could pose to both animals and humans. Animals will always have altercations, and especially in the case of cervids, where reproductive dominance is often decided by clashing horns. Hunters are less likely to wear protective gloves when cutting up an animal (personal communication), and are more likely to be subjected to prolonged exposure to a potential source of infection by eating repeated meals from the same animals (Race *et al.*, 2009). It was discussed at the Prion 2011 conference (Montreal, Canada) that people who hunted in CWD-affected areas would often not wait to consume the meat even if samples had been sent for TSE testing. As yet, CWD has not been linked to any prion disease in humans, but clearly some individuals are at high risk of exposure. These issues serve to highlight the potential importance of the skin as a route of TSE transmission, and why research should continue in order to further uncover how disease transmission occurs from this site.

10.4. Future work

There are of course a multitude of different possibilities to investigate in order to fully understand the mechanisms of spread of this disease from the site of exposure, such as the skin. The following section attempts to highlight a couple of these potential investigative routes, which have come to light during the course of this thesis.

10.4.1. Neutrophils

The work produced in this thesis has demonstrated that both LCs and dDCs influence scrapie agent transmission from the skin, albeit with potentially opposing roles. Despite the depletion of $CD11c^+$ cells in the CD11c-DTR bone marrow chimeric mice prior to scrapie infection via the skin, PrP^{Sc} accumulation in the draining iLN was only delayed. In contrast, $CD11c^+$ cell depletion prior to oral scrapie challenge blocked early stage PrP^{Sc} accumulation in the PPs, mesenteric LNs, and spleen up to 15 weeks post scrapie challenge (Raymond *et al.*, 2007). The above study elicited a much greater effect on overall disease susceptibility following $CD11c^+$ cell depletion, compared to the results observed in Chapter 4. While $CD11c^+$ cells appear to play a role in the initial transport of PrP^{Sc} from the skin to the draining iLN, other mechanisms or cell types are also likely involved in the scrapie transmission from the skin.

The time course study described in Chapter 9 demonstrated a large influx of neutrophils to the site of scarification as early as 2 hr post scarification. Many of these neutrophils are associated with the crust that has formed at the site of scarification. A crust will likely fall off after a few days. However, a good number of macrophages are also found below the area of the crust within the skin. Following scrapie infection via skin scarification in sheep, the only cells that were associated with PrP^{Sc} following scarification, were neutrophils (Gossner *et al.*, 2006).

Neutrophils have been linked to transmission of Leishmaniasis from the skin following sand fly bites (Peters *et al.*, 2008). This process, like scarification,

produces local inflammatory response (Peters *et al.*, 2008), which was associated with a sustained infiltration of neutrophils into the skin, accompanied by substantial macrophage recruitment (Peters *et al.*, 2008). Once the neutrophils have served their purpose at the site of inflammation they are phagocytosed by macrophages, or expelled in the crust (Delavary *et al.*, 2011). If PrP^{Sc}-associated neutrophils were phagocytosed by macrophages following an inflammatory response, this highlights a potential role for neutrophils following scrapie infection via skin scarification. However, it has also been demonstrated that neutrophils can traffic to LNs following infection or immune stimulation (Appelberg, 2007; Maletto *et al.*, 2006; Pesce *et al.*, 2008) as well as after intradermal vaccination (Abadie *et al.*, 2005). Neutrophils may also transport PrP^{Sc} from the skin to the draining LN following scrapie infection via scarification. One of the sites of neutrophil accumulation in the draining LNs, is the SCS (Chtanova *et al.*, 2008). The potential relevance of the SCS in TSE disease was highlighted in Chapter 6. In light of these findings, it would be useful to further investigate the potential role of neutrophils in scrapie transmission from the skin.

10.4.2. Keratinocytes

Keratinocytes are cells located within the epidermis. LCs elongate their dendrites between keratinocytes to comprise a dense network within the skin (Kubo *et al.*, 2009). There is emerging evidence of their importance in skin immune responses. They are one of the many cell types which express PrP^{c} on their surface (Sugaya *et al.*, 2002). As PrP^{c} is essential for maintaining PrP^{Sc} infection, its presence on these cells could indicate their potential role in disease transmission from the skin. The skin is the body's first line of defence against infection. DCs are the main APCs

present in the skin, and it was therefore considered that DC subsets, including LCs, were key in presenting antigens from the skin in order to mount appropriate immune responses, either in the skin or the draining LNs which they migrate to. However, the identification of langerin^{+} dDCs has forced the re-evaluation of LC function in many aspects of skin immunity (Romani *et al.*, 2010). Langerin^{+} dDCs were found to carry out functions previously assigned to LCs (Romani *et al.*, 2010). For example, it has been shown that a subpopulation of langerin^{+} dDCs were able to cross-present antigen from keratinocytes in the absence of LCs (Henri *et al.*, 2010). In this sense it is important to remember that the increased PrP^{Sc} accumulation observed in the draining iLN following scrapie infection via the skin (Chapter 8) was only observed in the bone marrow chimeric mice where LCs alone were depleted. While it is likely that PrP^{Sc} from skin-associated infection has reached the draining iLN before 10 days (when langerin^{+} dDCs) had repopulated the dermis, Fluorescent tagging of PrP^{Sc} demonstrated that this was present in the skin up to 72 hr after scarification, and all of it is therefore not cleared from the skin within a matter of hours. Keratinocytes have also been found to possibly play a role in presenting antigen directly to skin-reactive T cells (Kim *et al.*, 2009). Whether this is a function they carry out all the time, or simply due to the absence of both LCs and langerin^{+} dDCs in these experiments, is yet to be determined. It is, however, possible that keratinocytes might play a role in scrapie transmission from the skin, and these cells should also be investigated. For example keratinocytes cultivated in Epidermal Keratinocyte 3D medium (Millipore, UK) might provide a useful *in vitro* system to determine whether and how these cells acquire and process PrP^{Sc}.

10.5. Conclusion

Data in this thesis point towards a role for $CD11c^+$ cells in the initial transport of PrP^{Sc} from the site of exposure to the draining LN after exposure via the skin. The skin is a very robust defence system, and topical application of TSE inoculum without scarification or injury does not result in disease. Scarification induces a localised inflammatory response. This sets infection via the skin apart from other routes of transmission. Studies of the role of $CD11c^+$ cells in oral TSE pathogenesis were investigated in the steady state. In contrast, as shown in this thesis, scarification elicits cellular migration to the site of exposure, which itself is likely to significantly influence the handling and processing of PrP^{Sc} and its delivery to the draining LN.

Classical DC were efficiently depleted in DTX-treated CD11c-DTR→WT mice, early PrP^{Sc} accumulation within the draining iLN was partially impaired, and the mice succumbed to clinical prion disease. This suggests that other CD11c-independent mechanisms contribute to the propagation of prions from the skin to the draining LN. By triggering an inflammatory response at the site of infection, scarification introduces a range of potential mechanisms that may aid the spread of the scrapie agent. Prions may also be delivered to the draining LN by other cell populations such as neutrophils. Data in this thesis shows that neutrophil infiltration is a prominent feature after skin scarification. Collectively, these results indicate that identification of the precise cellular and molecular mechanisms by which prions are propagated from the site of exposure to the draining lymphoid tissues in which they replicate before neuroinvasion, may identify novel factors which influence disease susceptibility or targets for intervention in peripherally-acquired infections.

BIBLIOGRAPHY

Abadie, V., Badell, E., Douillard, P., Ensergueix, D., Leenen, P. J. M., Tanguy, M., Fiette, L., Saeland, S., Gicquel, B. and Winter, N. (2005). Neutrophils rapidly migrate via lymphatics after Mycobacterium bovis BCG intradermal vaccination and shuttle live bacilli to the draining lymph nodes. *Blood,* **106,** 1843-1850.

Andréoletti, O., Berthon, P., Marc, D., Sarradin, P., Grosclaude, J., van Keulen, L., Schelcher, F., Elsen, J.-M. and Lantier, F. (2000). Early accumulation of PrPSc in gut-associated lymphoid and nervous tissues of susceptible sheep from a Romanov flock with natural scrapie. *Journal of General Virology,* **81,** 3115-3126.

Angers, R. C., Seward, T. S., Napier, D., Green, M., Hoover, E. A., Spraker, T., O'Rourke, K., Balachandran, A. and Telling, G. C. (2009). Chronic Wasting Disease Prions in Elk Antler Velvet. *Emerging Infectious Diseases,* **15,** 696-703.

Appelberg, R. (2007). Neutrophils and intracellular pathogens: beyond phagocytosis and killing. *Trends in Microbiology,* **15,** 87-92.

Asano, K., Nabeyama, A., Miyake, Y., Qiu, C.-H., Kurita, A., Tomura, M., Kanagawa, O., Fujii, S.-i. and Tanaka, M. (2011). CD169-Positive Macrophages Dominate Antitumor Immunity by Crosspresenting Dead Cell-Associated Antigens. *Immunity*.

Atarashi, R., Wilham, J. M., Christensen, L., Hughson, A. G., Moore, R. A., Johnson, L. M., Onwubiko, H. A., Priola, S. A. and Caughey, B. (2008). Simplified ultrasensitive prion detection by recombinant PrP conversion with shaking. *Nat Meth,* **5,** 211-212.

Aucouturier, P., Geissmann, F., Damotte, D., Saborio, G. P., Meeker, H. C., Kascsak, R., Kascsak, R., Carp, R. I. and Wisniewski, T. (2001). Infected splenic dendritic cells are sufficient for prion transmission to the CNS in mouse scrapie. *The Journal of clinical investigation,* **108,** 703-708.

Austin, J. M. (1999). Dendritic Cells in Spleen and Lymph Node. In: *Dendritic Cells Biology and Clinical Applications*, M. T. Lotze and A. W. Thomson, Eds, Academic Press, pp. 179-204.

Banks, P. R. and Paquette, D. M. (1995). Comparison of Three Common Amine Reactive Fluorescent Probes Used for Conjugation to Biomolecules by Capillary Zone Electrophoresis. *Bioconjugate Chemistry,* **6,** 447-458.

Bartz, J. C., Kincaid, A. E. and Bessen, R. A. (2003). Rapid Prion Neuroinvasion following Tongue Infection. *Journal of Virology,* **77,** 583-591.

Bedford, P. A., Todorovic, V., Westcott, E. D. A., Windsor, A. C. J., English, N. R., Al-Hassi, H. O., Raju, K. S., Mills, S. and Knight, S. C. (2006). Adipose tissue of human omentum is a major source of dendritic cells, which lose MHC Class II and stimulatory function in Crohn's disease. *Journal of Leukocyte Biology,* **80,** 546-554.

Bedoui, S., Whitney, P. G., Waithman, J., Eidsmo, L., Wakim, L., Caminschi, I., Allan, R. S., Wojtasiak, M., Shortman, K., Carbone, F. R., Brooks, A. G. and Heath, W. R. (2009). Cross-presentation of viral and self antigens by skin-derived $CD103^{+}$ dendritic cells. *Nat Immunol,* **10,** 488-495.

Bennett, C. L., van Rijn, E., Jung, S., Inaba, K., Steinman, R. M., Kapsenberg, M. L. and Clausen, B. E. (2005). Inducible ablation of mouse Langerhans cells diminishes but fails to abrogate contact hypersensitivity. *The Journal of Cell Biology,* **169,** 569-576.

Bergtold, A., Desai, D. D., Gavhane, A. and Clynes, R. (2005). Cell Surface Recycling of Internalized Antigen Permits Dendritic Cell Priming of B Cells. *Immunity,* **23,** 503-514.

Beringue, V., Demoy, M., Lasmézas, C. I., Gouritin, B., Weingarten, C., Deslys, J.-P., Andreux, J.-P., Couvreur, P. and Dormont, D. (2000). Role of spleen macrophages in the clearance of scrapie agent early in pathogenesis. *The Journal of Pathology,* **190,** 495-502.

Birbeck, M. S., Breathnach, A. S. and Everall, J. D. (1961). An Electron Microscope Study of Basal Melanocytes and High-Level Clear Cells (Langerhans Cells) in Vitiligo1. *The Journal of investigative dermatology,* **37,** 51-64.

Boche, D., Cunningham, C., Docagne, F., Scott, H. and Perry, V. H. (2006). TGFβ1 regulates the inflammatory response during chronic neurodegeneration. *Neurobiology of Disease,* **22,** 638-650.

Bolton, D. C., McKinley, M. P. and Prusiner, S. B. (1982). Identification of a protein that purifies with the scrapie prion. *Science,* **218,** 1309-1311.

Bolton, D. C., Meyer, R. K. and Prusiner, S. B. (1985). Scrapie PrP27-30 is a Sialoglycoprotein. *Journal of Virology,* **53,** 596-606.

Bradford, B. M., Sester, D. P., Hume, D. A. and Mabbott, N. A. (2011). Defining the anatomical localisation of subsets of the murine mononuclear phagocyte system using integrin alpha X (Itgax, CD11c) and colony stimulating factor 1 receptor (Csf1r, CD115) expression fails to discriminate dendritic cells from macrophages. *Immunobiology,* **216,** 1228-1237.

Brown, K. L., Ritchie, D. L., McBride, P. A. and Bruce, M. E. (2000). Detection of PrP in Extraneural Tissues. *Microscopy Research and Technique,* **50,** 40-45.

Brown, K. L., Stewart, K., Ritchie, D. L., Mabbott, N. A., Williams, A., Fraser, H., Morrison, W. I. and Bruce, M. E. (1999). Scrapie replication in lymphoid tissues depends on prion protein-expressing follicular dendritic cells. *Nature Medicine,* **5,** 1308-1312.

Brown, K. L., Wathne, G. J., Sales, J., Bruce, M. E. and Mabbott, N. A. (2009). The Effects of Host Age on Follicular Dendritic Cell Status Dramatically Impair Scrapie Agent Neuroinvasion in Aged Mice. *The Journal of Immunology,* **183,** 5199-5207.

Bruce, M. E. (1993). Scrapie strain variation and mutation. *British Medical Bulletin,* **49,** 822-838.

Bruce, M. E., Brown, K. L., Mabbott, N. A., Farquhar, C. F. and Jeffrey, M. (2000). Follicular dendritic cells in TSE pathogenesis. *Immunology Today,* **21,** 442-446.

Bruce, M. E. and Fraser, H. (1982). Focal and asymmetrical vacuolar lesions in the brains of mice infected with certain strains of scrapie. *Acta Neuropathologica,* **58,** 133-140.

Bruce, M. E., Will, R. G., Ironside, J. W., McConnell, I., Drummond, D., Suttie, A., McCardle, L., Chree, A., Hope, J., Birkett, C., Cousens, S., Fraser, H. and Bostock, C. J. (1997). Transmissions to mice indicate that `new variant' CJD is caused by the BSE agent. *Nature,* **389,** 498-501.

Büeler, H., Aguzzi, A., Sailer, A., Greiner, R. A., Autenried, P., Aguet, M. and Weissmann, C. (1993). Mice devoid of PrP are resistant to scrapie. *Cell,* **73,** 1339-1347.

Bueler, H., Fischer, M., Lang, Y., Bluethmann, H., Lipp, H.-P., DeArmond, S. J., Prusiner, S. B., Aguet, M. and Weissmann, C. (1992). Normal development and behaviour of mice lacking the neuronal cell-surface PrP protein. *Nature,* **356,** 577-582.

Bulloch, K., Miller, M. M., Gal-Toth, J., Milner, T. A., Gottfried-Blackmore, A., Waters, E. M., Kaunzner, U. W., Liu, K., Lindquist, R., Nussenzweig, M. C., Steinman, R. M. and McEwen, B. S. (2008). CD11c/EYFP transgene illuminates a discrete network of dendritic cells within the embryonic, neonatal, adult, and injured mouse brain. *The Journal of Comparative Neurology,* **508,** 687-710.

Bursch, L. S., Wang, L., Igyarto, B., Kissenpfennig, A., Malissen, B., Kaplan, D. H. and Hogquist, K. A. (2007). Identification of a novel population of Langerin^{+} dendritic cells. *The Journal of Experimental Medicine,* **204,** 3147-3156.

Burthem, J., Urban, B., Pain, A. and Roberts, D. J. (2001). The normal cellular prion protein is strongly expressed by myeloid dendritic cells. *Blood,* **98,** 3733-3738.

Buschmann, A. and Groschup, M. H. (2005). Highly Bovine Spongiform Encephalopathy–Sensitive Transgenic Mice Confirm the Essential Restriction of Infectivity to the Nervous System in Clinically Diseased Cattle. *Journal of Infectious Diseases,* **192,** 934-942.

Cancellotti, E., Barron, R. M., Bishop, M. T., Hart, P., Wiseman, F. and Manson, J. C. (2007). The role of host PrP in Transmissible Spongiform Encephalopathies. *Biochimica et Biophysica Acta (BBA) - Molecular Basis of Disease,* **1772,** 673-680.

Cardone, F., Thomzig, A., Schulz-Schaeffer, W., Valanzano, A., Sbriccoli, M., Abdel-Haq, H., Graziano, S., Pritzkow, S., Puopolo, M., Brown, P., Beekes, M. and Pocchiari, M. (2009). PrP^{TSE} in muscle-associated lymphatic tissue during the preclinical stage of mice infected orally with bovine spongiform encephalopathy. *Journal of General Virology,* **90,** 2563-2568.

Carp, R. I. (1982). Transmission of scrapie by oral route: effect of gingival scarification. *The Lancet,* **1(8264),** 170-171.

Carp, R. I. and Callahan, S. (1981). In vitro interaction of scrapie agent and mouse peritoneal macrophages. *Intervirology,* **16,** 8-13.

Carp, R. I. and Callahan, S. (1982). Effect of mouse peritoneal macrophages on scrapie infectivity during extended in vitro incubation. *Intervirology,* **17,** 201-207.

Carrasco, Y. R. and Batista, F. D. (2007). B Cells Acquire Particulate Antigen in a Macrophage-Rich Area at the Boundary between the Follicle and the Subcapsular Sinus of the Lymph Node. *Immunity,* **27,** 160-171.

Chandler, R. L. (1961). Encephalopathy in mice produced by inoculation with scrapie brain material. *The Lancet,* **277,** 1378-1379.

Chelle, P. L. (1945). Un cas de Tremblante chez la Chèvre. *Bulletin de l'Academie Veterinaire de France,* **15,** 294-295.

Chtanova, T., Schaeffer, M., Han, S.-J., van Dooren, G. G., Nollmann, M., Herzmark, P., Chan, S. W., Satija, H., Camfield, K., Aaron, H., Striepen, B. and Robey, E. A. (2008). Dynamics of Neutrophil Migration in Lymph Nodes during Infection. *Immunity,* **29,** 487-496.

Ciesielski-Treska, J., Grant, N. J., Ulrich, G., Corrotte, M., Bailly, Y., Haeberle, A.-M., Chasserot-Golaz, S. and Bader, M.-F. (2004). Fibrillar prion peptide (106–126) and scrapie prion protein hamper phagocytosis in microglia. *Glia,* **46,** 101-115.

Cordier-Dirikoc, S. and Chabry, J. (2008). Temporary depletion of $CD11c^+$ dendritic cells delays lymphoinvasion after intraperitonal scrapie infection. *Journal of Virology***,** JVI.02440-02407.

Crocker, P. R., Mucklow, S., Bouckson, V., McWilliam, A., Willis, A. C., Gordon, S., Milon, G., Kelm, S. and Bradfield, P. (1994). Sialoadhesin, a macrophage sialic acid binding receptor for haemopoietic cells with 17 immunoglobulin-like domains. *EMBO J,* **13,** 4490-4503.

Cuillé, J. and Chelle, P. L. (1936). La maladie dite *tremblante du mouton* est-elle inoculable? *Comptes Rendus de l'Académie des sciences,* **203,** 1552-1554.

Cunningham, A. A., Kirkwood, J. K., Dawson, M., Spencer, Y. I., Green, R. B. and Wells, G. A. H. (2004). Bovine spongiform encephalopathy infectivity in greater kudu (Tragelaphus strepsiceros). *Emerging Infectious Diseases,* **10,** 1044-1049.

de Jong, M. A. W. P. and Geijtenbeek, T. B. H. (2010). Langerhans cells in innate defense against pathogens. *Trends in Immunology,* **31,** 452-459.

Delamarre, L., Pack, M., Chang, H., Mellman, I. and Trombetta, E. S. (2005). Differential Lysosomal Proteolysis in Antigen-Presenting Cells Determines Antigen Fate. *Science,* **307,** 1630-1634.

Delavary, B. M., van der Veer, W. M., van Egmond, M., Niessen, F. B. and Beelen, R. H. J. (2011). Macrophages in skin injury and repair. *Immunobiology,* **216,** 753-762.

Denkers, N. D., Telling, G. C. and Hoover, E. A. (2011). Minor Oral Lesions Facilitate Transmission of Chronic Wasting Disease. *J. Virol.,* **85,** 1396-1399.

Dickinson, A. G., Bruce, M. E., Outram, G. W. and Kimberlin, R. H. (1984). Scrapie strain differences: the implication of stability and mutation. In: *Proceedings of Workshop on slow transmissible disease,* , J. Tateishi, Ed, Japanese Ministry of Health and Welfare, Tokyo, pp. 105-118.

Dickinson, A. G., Meikle, V. M. H. and Fraser, H. (1968). Identification of a gene which controls the incubation period of some strains of scrapie agent in mice. *Journal of Comparative Pathology,* **78,** 293-299.

Douillard, P., Stoitzner, P., Tripp, C. H., Clair-Moninot, V., Ait-Yahia, S., McLellan, A. D., Eggert, A., Romani, N. and Saeland, S. (2005). Mouse Lymphoid Tissue Contains Distinct Subsets of Langerin/$CD207^+$ Dendritic Cells, Only One of Which Represents Epidermal-Derived Langerhans Cells. *J Investig Dermatol,* **125,** 983-994.

Edwards, J. C., Moore, S. J., Hawthorn, J. A., Neale, M. H. and Terry, L. A. (2010). PrPSc is associated with B cells in the blood of scrapie-infected sheep. *Virology,* **405,** 110-119.

Eidsmo, L., Allan, R., Caminschi, I., van Rooijen, N., Heath, W. R. and Carbone, F. R. (2009). Differential Migration of Epidermal and Dermal Dendritic Cells during Skin Infection. *The Journal of Immunology,* **182,** 3165-3172.

Farquhar, C. F., Somerville, R. A. and Ritchie, L. A. (1989). Post-mortem immunodiagnosis of scrapie and bovine spongiform encephalopathy. *Journal of Virological Methods,* **24,** 215-222.

Flacher, V., Douillard, P., Ait-Yahia, S., Stoitzner, P., Clair-Moninot, V., Romani, N. and Saeland, S. (2008). Expression of Langerin/CD207 reveals dendritic cell heterogeneity between inbred mouse strains. *Immunology,* **123,** 339-347.

Flacher, V., Tripp, C. H., Stoitzner, P., Haid, B., Ebner, S., Del Frari, B., Koch, F., Park, C. G., Steinman, R. M., Idoyaga, J. and Romani, N. (2009). Epidermal Langerhans Cells Rapidly Capture and Present Antigens from C-Type Lectin-Targeting Antibodies Deposited in the Dermis. *J Invest Dermatol*.

Flores-Langarica, A., Sebti, Y., Mitchell, D. A., Sim, R. B. and MacPherson, G. G. (2009). Scrapie Pathogenesis: The Role of Complement C1q in Scrapie Agent Uptake by Conventional Dendritic Cells. *J Immunol,* **182,** 1305-1313.

Foster, J. D., Parnham, D. W., Hunter, N. and Bruce, M. (2001). Distribution of the prion protein in sheep terminally affected with BSE following experimental oral transmission. *Journal of General Virology,* **82,** 2319-2326.

Frappier, A. and Guy, R. (1950). A new and practical B.C.G. skin test (the B.C.G. scarification test) for the detection of the total tuberculous allergy. *Canadian Journal of Public Health,* **41,** 72-83.

Fraser, H., Brown, K. L., Stewart, K., McConnell, I., McBride, P. and Williams, A. (1996). Replication of scrapie in spleens of SCID mice follows reconstitution with wild-type mouse bone marrow. *The Journal of General Virology,* **77,** 1935-1940.

Fraser, H. and Dickinson, A. G. (1967). Distribution of experimentally induced scrapie lesions in the brain. *Nature,* **216,** 1310-1311.

Fraser, H. and Dickinson, A. G. (1968). The sequential development of the brain lesion of scrapie in three strains of mice. *Journal of Comparative Pathology,* **78,** 301-311.

Fraser, H. and Dickinson, A. G. (1978). Studies of the lymphoreticular system in the pathogenesis of scrapie: The role of spleen and thymus. *Journal of Comparative Pathology,* **88,** 563-573.

Freeman, T. C., Goldovsky, L., Brosch, M., van Dongen, S., Mazière, P., Grocock, R. J., Freilich, S., Thornton, J. and Enright, A. J. (2007). Construction, Visualisation, and Clustering of Transcription Networks from Microarray Expression Data. *PLoS Comput Biol,* **3,** e206.

Fukunaga, A., Khaskhely, N. M., Sreevidya, C. S., Byrne, S. N. and Ullrich, S. E. (2008). Dermal Dendritic Cells, and Not Langerhans Cells, Play an Essential Role in Inducing an Immune Response. *Journal of Immunology,* **180,** 3057-3064.

Gabliks, J. and Falconer, M. (1966). Interaction of diphtheria toxin with cell cultures from susceptible and resistant animals. *The Journal of Experimental Medicine,* **123,** 723-732.

Gadotti, V. and Zamponi, G. (2011). Cellular prion protein protects from inflammatory and neuropathic pain. *Molecular Pain,* **7,** 59.

Gajdusek, D. C. (1967). Slow-virus infections of the nervous system. *The New England Journal of Medicine,* **276,** 392-400.

Gimbel, D. A., Nygaard, H. B., Coffey, E. E., Gunther, E. C., Lauren, J., Gimbel, Z. A. and Strittmatter, S. M. (2010). Memory Impairment in Transgenic Alzheimer Mice Requires Cellular Prion Protein. *J. Neurosci.,* **30,** 6367-6374.

Ginhoux, F., Collin, M. P., Bogunovic, M., Abel, M., Leboeuf, M., Helft, J., Ochando, J., Kissenpfennig, A., Malissen, B., Grisotto, M., Snoeck, H., Randolph, G. and Merad, M. (2007). Blood-derived dermal langerin^{+} dendritic cells survey the skin in the steady state. *The Journal of Experimental Medicine,* **204,** 3133-3146.

Glaysher, B. R. and Mabbott, N. A. (2007a). Role of the draining lymph node in scrapie agent transmission from the skin. *Immunology Letters,* **109,** 64-71.

Glaysher, B. R. and Mabbott, N. A. (2007b). Role of the GALT in Scrapie Agent Neuroinvasion from the Intestine. *Journal of Immunology,* **178,** 3757-3766.

Gossner, A., Hunter, N. and Hopkins, J. (2006). Role of lymph-borne cells in the early stages of scrapie agent dissemination from the skin. *Veterinary Immunology and Immunopathology,* **109,** 267-278.

Gossner, A., Roupaka, S., Foster, J., Hunter, N. and Hopkins, J. (2011). Transcriptional profiling of peripheral lymphoid tissue reveals genes and networks linked to SSBP/1 scrapie pathology in sheep. *Veterinary Microbiology,* **153,** 218-228.

Gough, K. C. and Maddison, B. C. (2010). Prion transmission: Prion excretion and occurrence in the environment. *Prion,* **4,** 275-282.

Gousset, K., Schiff, E., Langevin, C., Marijanovic, Z., Caputo, A., Browman, D. T., Chenouard, N., de Chaumont, F., Martino, A., Enninga, J., Olivo-Marin, J.-C., Mannel, D. and Zurzolo, C. (2009). Prions hijack tunnelling nanotubes for intercellular spread. *Nat Cell Biol,* **11,** 328-336.

Haley, N. J., Mathiason, C. K., Carver, S., Zabel, M., Telling, G. C. and Hoover, E. A. (2011). Detection of Chronic Wasting Disease Prions in Salivary, Urinary, and Intestinal Tissues of Deer: Potential Mechanisms of Prion Shedding and Transmission. *Journal of Virology,* **85,** 6309-6318.

Haley, N. J., Seelig, D. M., Zabel, M. D., Telling, G. C. and Hoover, E. A. (2009). Detection of CWD Prions in Urine and Saliva of Deer by Transgenic Mouse Bioassay. *PLoS ONE,* **4,** e4848.

Halliday, S., Houston, F. and Hunter, N. (2005). Expression of PrPC on cellular components of sheep blood. *Journal of General Virology,* **86,** 1571-1579.

Heath, W. R. and Carbone, F. R. (2009). Dendritic cell subsets in primary and secondary T cell responses at body surfaces. *Nat Immunol*, **10,** 1237-1244.

Heggebø, R., Press, C. M., Gunnes, G., González, L. and Jeffrey, M. (2002). Distribution and accumulation of PrP in gut-associated and peripheral lymphoid tissue of scrapie-affected Suffolk sheep. *Journal of General Virology*, **83,** 479-489.

Heggebø, R., Press, C. M., Gunnes, G., Lie, K. I., Tranulis, M. A., Ulvund, M., Groschup, M. H. and Landsverk, T. (2000). Distribution of prion protein in the ileal Peyer's patch of scrapie-free lambs and lambs naturally and experimentally exposed to the scrapie agent. *Journal of General Virology*, **81,** 2327-2337.

Henri, S., Poulin, L. F., Tamoutounour, S., Ardouin, L., Guilliams, M., de Bovis, B., Devilard, E., Viret, C., Azukizawa, H., Kissenpfennig, A. and Malissen, B. (2010). $CD207^{+}$ $CD103^{+}$ dermal dendritic cells cross-present keratinocyte-derived antigens irrespective of the presence of Langerhans cells. *J. Exp. Med.*, **207,** 189-206.

Henri, S., Siret, C., Machy, P., Kissenpfennig, A., Malissen, B. and Leserman, L. (2007). Mature DC from skin and skin-draining LN retain the ability to acquire and efficiently present targeted antigen. *European Journal of Immunology*, **37,** 1184-1193.

Hill, A. F., Butterworth, R. J., Joiner, S., Jackson, G., Rossor, M. N., Thomas, D. J., Frosh, A., Tolley, N., Bell, J. E., Spencer, M., King, A., Al-Sarraj, S., Ironside, J. W., Lantos, P. L. and Collinge, J. (1999). Investigation of variant Creutzfeldt-Jakob disease and other human prion diseases with tonsil biopsy samples. *The Lancet*, **353,** 183-189.

Hill, A. F., Zeidler, M., Ironside, J. and Collinge, J. (1997). Diagnosis of new variant Creutzfeldt-Jakob disease by tonsil biopsy. *The Lancet*, **349,** 99-100.

Hilton, D. A., Fathers, E., Edwards, P., Ironside, J. W. and Zajicek, J. (1998). Prion immunoreactivity in appendix before clinical onset of variant Creutzfeldt-Jakob disease. *The Lancet*, **352,** 703-704.

Hilton, D. A., Ghani, A. C., Conyers, L., Edwards, P., McCardle, L., Ritchie, D., Penney, M., Hegazy, D. and Ironside, J. W. (2004). Prevalence of lymphoreticular prion protein accumulation in UK tissue samples. *The Journal of Pathology*, **203,** 733-739.

Hoffmann, C., Eiden, M., Kaatz, M., Keller, M., Ziegler, U., Rogers, R., Hills, B., Balkema-Buschmann, A., van Keulen, L., Jacobs, J. and Groschup, M. (2011). BSE infectivity in jejunum, ileum and ileocaecal junction of incubating cattle. *Veterinary Research*, **42,** 21.

Holmes, R. K. (2000). Biology and Molecular Epidemiology of Diphtheria Toxin and the tox Gene. *The Journal of Infectious Diseases*, **181,** S156-S167.

Horiuchi, M., Yamazaki, N., Ikeda, T., Ishiguro, N. and Shinagawa, M. (1995). A cellular form of prion protein (PrP^{C}) exists in many non-neuronal tissues of sheep. *Journal of General Virology*, **76,** 2583-2587.

Houston, F., Foster, J. D., Chong, A., Hunter, N. and Bostock, C. J. (2000). Transmission of BSE by blood transfusion in sheep. *The Lancet*, **356,** 999-1000.

Houston, F., McCutcheon, S., Goldmann, W., Chong, A., Foster, J., Sisó, S., González, L., Jeffrey, M. and Hunter, N. (2008). Prion diseases are efficiently transmitted by blood transfusion in sheep. *Blood*, **112,** 4739-4745.

Huang, F.-P., Farquhar, C. F., Mabbott, N. A., Bruce, M. E. and MacPherson, G. G. (2002). Migrating intestinal dendritic cells transport PrP^{Sc} from the gut. *The Journal of General Virology*, **83,** 267-271.

Hughes, M. M., Field, R. H., Perry, V. H., Murray, C. L. and Cunningham, C. (2010). Microglia in the degenerating brain are capable of phagocytosis of beads and of apoptotic cells, but do not efficiently remove PrPSc, even upon LPS stimulation. *Glia*, **58,** 2017-2030.

Hume, D. A. (2008). Macrophages as APC and the Dendritic Cell Myth. *The Journal of Immunology*, **181,** 5829-5835.

Isaacs, J. D., Jackson, G. S. and Altmann, D. M. (2006). The role of the cellular prion protein in the immune system. *Clinical & Experimental Immunology*, **146,** 1-8.

Itoh, M., Yonemura, S., Nagafuchi, A. and Tsukita, S. (1991). A 220-kD undercoat-constitutive protein: its specific localization at cadherin-based cell-cell adhesion sites. *The Journal of Cell Biology*, **115,** 1449-1462.

Iwata, N., Sato, Y., Higuchi, Y., Nohtomi, K., Nagata, N., Hasegawa, H., Tobiume, M., Nakamura, Y., Hagiwara, K., Furuoka, H., Horiuchi, M., Yamakawa, Y. and Sata, T. (2006). Distribibution of PrP^{Sc} in cattle with bovine spongiform encephalopathy slaughtered at abattoirs in Japan. *Japanese Journal of Infectious Diseases*, **59,** 100-107.

Jeffrey, M., González, L., Espenes, A., Press, C., Martin, S., Chaplin, M., Davis, L., Landsverk, T., MacAldowie, C., Eaton, S. and McGovern, G. (2006). Transportation of prion protein across the intestinal mucosa of scrapie-susceptible and scrapie-resistant sheep. *The Journal of Pathology,* **209,** 4-14.

Jeffrey, M., Martin, S., González, L., Ryder, S. J., Bellworthy, S. J. and Jackman, R. (2001a). Differential Diagnosis of Infections with the Bovine Spongiform Encephalopathy (BSE) and Scrapie Agents in Sheep. *Journal of Comparative Pathology,* **125,** 271-284.

Jeffrey, M., Martin, S., Thomson, J. R., Dingwall, W. S., Begara-McGorum, I. and González, L. (2001b). Onset and Distribution of Tissue PrP Accumulation in Scrapie-affected Suffolk Sheep as Demonstrated by Sequential Necropsies and Tonsillar Biopsies. *Journal of Comparative Pathology,* **125,** 48-57.

Jeffrey, M., McGovern, G., Goodsir, C. M., L Brown, K. and Bruce, M. E. (2000a). Sites of prion protein accumulation in scrapie-infected mouse spleen revealed by immuno-electron microscopy. *The Journal of Pathology,* **191,** 323-332.

Jeffrey, M., McGovern, G., Martin, S., Goodsir, C. M. and Brown, K. L. (2000b). Cellular and sub-cellular localisation of PrP in the lymphoreticular system of mice and sheep. *Archives of virology. Supplementum,* **16,** 23-28.

Jeffrey, M., Ryder, S., Martin, S., Hawkins, S. A. C., Terry, L., Berthelin-Baker, C. and Bellworthy, S. J. (2001c). Oral Inoculation of Sheep with the Agent of Bovine Spongiform Encephalopathy (BSE). 1. Onset and Distribution of Disease-specific PrP Accumulation in Brain and Viscera. *Journal of Comparative Pathology,* **124,** 280-289.

Jung, S., Unutmaz, D., Wong, P., Sano, G.-I., De los Santos, K., Sparwasser, T., Wu, S., Vuthoori, S., Ko, K., Zavala, F., Pamer, E. G., Littman, D. R. and Lang, R. A. (2002). In Vivo Depletion of $CD11c^{+}$ Dendritic Cells Abrogates Priming of $CD8^{+}$ T Cells by Exogenous Cell-Associated Antigens. *Immunity,* **17,** 211-220.

Junt, T., Moseman, E. A., Iannacone, M., Massberg, S., Lang, P. A., Boes, M., Fink, K., Henrickson, S. E., Shayakhmetov, D. M., Di Paolo, N. C., van Rooijen, N., Mempel, T. R., Whelan, S. P. and von Andrian, U. H. (2007). Subcapsular sinus macrophages in lymph nodes clear lymph-borne viruses and present them to antiviral B cells. *Nature,* **450,** 110-114.

Kaneider, N. C., Kaser, A., Dunzendorfer, S., Tilg, H. and Wiedermann, C. J. (2003). Sphingosine Kinase-Dependent Migration of Immature Dendritic Cells in Response to Neurotoxic Prion Protein Fragment. *Journal of Virology,* **77,** 5535-5539.

Kariv-Inbal, Z., Ben-Hur, T., Grigoriadis, N. C., Engelstein, R. and Gabizon, R. (2006). Urine from Scrapie-Infected Hamsters Comprises Low Levels of Prion Infectivity. *Neurodegenerative Diseases,* **3,** 123-128.

Kassim, S. H., Rajasagi, N. K., Zhao, X., Chervenak, R. and Jennings, S. R. (2006). In Vivo Ablation of CD11c-Positive Dendritic Cells Increases Susceptibility to Herpes Simplex Virus Type 1 Infection and Diminishes NK and T-Cell Responses. *Journal of Virology,* **80,** 3985-3993.

Keane, D., Barr, D., Osborn, R., Langenberg, J., O'Rourke, K., Schneider, D. and Bochsler, P. (2009). Validation of Use of Rectoanal Mucosa-Associated Lymphoid Tissue for Immunohistochemical Diagnosis of Chronic Wasting Disease in White-Tailed Deer (Odocoileus virginianus). *Journal of Clinical Microbiology,* **47,** 1412-1417.

Keane, D. P., Barr, D. J., Bochsler, P. N., Hall, S. M., Gidlewski, T., O'Rourke, K. I., Spraker, T. R. and Samuel, M. D. (2008). Chronic Wasting Disease in a Wisconsin White-Tailed Deer Farm. *Journal of Veterinary Diagnostic Investigation,* **20,** 698-703.

Kim, B. S., Miyagawa, F., Cho, Y.-H., Bennett, C. L., Clausen, B. E. and Katz, S. I. (2009). Keratinocytes Function as Accessory Cells for Presentation of Endogenous Antigen Expressed in the Epidermis. *J Invest Dermatol,* **129,** 2805-2817.

Kim, J.-I., Cali, I., Surewicz, K., Kong, Q., Raymond, G. J., Atarashi, R., Race, B., Qing, L., Gambetti, P., Caughey, B. and Surewicz, W. K. (2010). Mammalian Prions Generated from Bacterially Expressed Prion Protein in the Absence of Any Mammalian Cofactors. *Journal of Biological Chemistry,* **285,** 14083-14087.

Kimberlin, R. H. and Walker, C. A. (1979). Pathogenesis of mouse scrapie: Dynamics of agent replication in spleen, spinal cord and brain after infection by different routes. *Journal of Comparative Pathology,* **89,** 551-562.

Kimberlin, R. H. and Walker, C. A. (1989a). Pathogenesis of scrapie in mice after intragastric infection. *Virus Research,* **12,** 213-220.

Kimberlin, R. H. and Walker, C. A. (1989b). The role of the spleen in the neuroinvasion of scrapie in mice. *Virus Research,* **12,** 201-211.

Kissenpfennig, A., Ait-Yahia, S., Clair-Moninot, V., Stossel, H., Badell, E., Bordat, Y., Pooley, J. L., Lang, T., Prina, E., Coste, I., Gresser, O., Renno, T., Winter, N., Milon, G., Shortman, K., Romani, N., Lebecque, S., Malissen, B., Saeland, S. and Douillard, P. (2005a). Disruption of the langerin/CD207 Gene Abolishes Birbeck Granules without a Marked Loss of Langerhans Cell Function. *Mol. Cell. Biol.,* **25,** 88-99.

Kissenpfennig, A., Henri, S., Dubois, B., Laplace-Builhe, C., Perrin, P., Romani, N., Tripp, C. H., Douillard, P., Leserman, L., Kaiserlian, D., Saeland, S., Davoust, J. and Malissen, B. (2005b). Dynamics and Function of Langerhans Cells In Vivo: Dermal Dendritic Cells Colonize Lymph Node Areas Distinct from Slower Migrating Langerhans Cells. *Immunity,* **22,** 643-654.

Kissenpfennig, A. and Malissen, B. (2006). Langerhans cells - revisiting the paradigm using genetically engineered mice. *Trends in Immunology,* **27,** 132-139.

Klein, M. A., Kaeser, P. S., Schwarz, P., Weyd, H., Xenarios, I., Zinkernagel, R. M., Carroll, M. C., Verbeek, J. S., Botto, M., Walport, M. J., Molina, H., Kalinke, U., Acha-Orbea, H. and Aguzzi, A. (2001). Complement facilitates early prion pathogenesis. *Nat Med,* **7,** 488-492.

Knight, S. C. (2008). Specialized Perinodal Fat Fuels and Fashions Immunity. *Immunity,* **28,** 135-138.

Kosco-Vilbois, M. H. (2003). Are follicular dendritic cells really good for nothing? *Nat Rev Immunol,* **3,** 764-769.

Kovács, G. G., Preusser, M., Strohschneider, M. and Budka, H. (2005). Subcellular Localization of Disease-Associated Prion Protein in the Human Brain. *The American journal of pathology,* **166,** 287-294.

Kratzel, C., Kruger, D. and Beekes, M. (2007). Relevance of the regional lymph node in scrapie pathogenesis after peripheral infection of hamsters. *BMC Veterinary Research,* **3,** 22.

Kretlow, A., Wang, Q., Beekes, M., Naumann, D. and Miller, L. M. (2008). Changes in protein structure and distribution observed at pre-clinical stages of scrapie pathogenesis. *Biochimica et Biophysica Acta (BBA) - Molecular Basis of Disease,* **1782,** 559-565.

Kretzschmar, H. A., Prusiner, S. B., Stowring, L. E. and DeArmond, S. J. (1986). Scrapie prion protein are synthesized in neurons. *The American journal of pathology,* **122,** 1-5.

Krüger, D., Thomzig, A., Lenz, G., Kampf, K., McBride, P. and Beekes, M. (2009). Faecal shedding, alimentary clearance and intestinal spread of prions in hamsters fed with scrapie. *Vet. Res.,* **40,** 04.

Kubo, A., Nagao, K., Yokouchi, M., Sasaki, H. and Amagai, M. (2009). External antigen uptake by Langerhans cells with reorganization of epidermal tight junction barriers. *The Journal of Experimental Medicine,* **206,** 2937-2946.

Lai, L., Alaverdi, N., Maltais, L. and Morse, H. C., III. (1998). Mouse Cell Surface Antigens: Nomenclature and Immunophenotyping. *Journal of Immunology,* **160,** 3861-3868.

Lasmézas, C. I., Cesbron, J. Y., Deslys, J. P., Demaimay, R., Adjou, K. T., Rioux, R., Lemaire, C., Locht, C. and Dormont, D. (1996). Immune system-dependent and -independent replication of the scrapie agent. *Journal of Virology,* **70,** 1292-1295.

Lawson, V. A., Collins, S. J., Masters, C. L. and Hill, A. F. (2005). Prion protein glycosylation. *Journal of Neurochemistry,* **93,** 793-801.

Li, R., Liu, D., Zanusso, G., Liu, T., Fayen, J. D., Huang, J.-H., Petersen, R. B., Gambetti, P. and Sy, M.-S. (2001). The Expression and Potential Function of Cellular Prion Protein in Human Lymphocytes. *Cellular Immunology,* **207,** 49-58.

Ligios, C., Cancedda, M. G., Carta, A., Santucciu, C., Maestrale, C., Demontis, F., Saba, M., Patta, C., DeMartini, J. C., Aguzzi, A. and Sigurdson, C. J. (2011). Sheep with Scrapie and Mastitis Transmit Infectious Prions through the Milk. *Journal of Virology,* **85,** 1136-1139.

Llewelyn, C. A., Hewitt, P. E., Knight, R. S. G., Amar, K., Cousens, S., Mackenzie, J. and Will, R. G. (2004). Possible transmission of variant Creutzfeldt-Jakob disease by blood transfusion. *The Lancet,* **363,** 417-421.

Løvik, M., Alberg, T., Nygaard, U. C., Samuelsen, M., Groeng, E.-C. and Gaarder, P. I. (2007). Popliteal lymph node (PLN) assay to study adjuvant effects on respiratory allergy. *Methods,* **41,** 72-79.

Lucas, A. and MacPherson, G. (2002). Langerhans cells: immigrants or residents? *Nature Immunology,* **3,** 1125-1126.

Luhr, K. M., Wallin, R. P. A., Ljunggren, H.-G., Low, P., Taraboulos, A. and Kristensson, K. (2002). Processing and Degradation of Exogenous Prion Protein by $CD11c^{+}$ Myeloid Dendritic Cells In Vitro. *J. Virol.,* **76,** 12259-12264.

Mabbott, N. A. (2004). The complement system in prion diseases. *Current Opinion in Immunology,* **16,** 587-593.

Mabbott, N. A., Brown, K. L., Manson, J. and Bruce, M. E. (1997). T-lymphocyte activation and the cellular form of the prion protein. *Immunology,* **92,** 161-165.

Mabbott, N. A. and Bruce, M. E. (2001). The immunobiology of TSE diseases. *The Journal of General Virology,* **82,** 2307-2318.

Mabbott, N. A. and Bruce, M. E. (2004). Complement component C5 is not involved in scrapie pathogenesis. *Immunobiology,* **209,** 545-549.

Mabbott, N. A., Bruce, M. E., Botto, M., Walport, M. J. and Pepys, M. B. (2001). Temporary depletion of complement component C3 or genetic deficiency of C1q significantly delays onset of scrapie. *Nat Med,* **7,** 485-487.

Mabbott, N. A., Farquhar, C. F., Brown, K. L. and Bruce, M. E. (1998). Involvement of the immune system in TSE pathogenesis. *Immunology Today,* **19,** 201-203.

Mabbott, N. A., Kenneth Baillie, J., Hume, D. A. and Freeman, T. C. (2010). Meta-analysis of lineage-specific gene expression signatures in mouse leukocyte populations. *Immunobiology,* **215,** 724-736.

Mabbott, N. A., Kenneth Baillie, J., Kobayashi, A., Donaldson, D. S., Ohmori, H., Yoon, S.-O., Freedman, A. S., Freeman, T. C. and Summers, K. M. (2011). Expression of mesenchyme-specific gene signatures by follicular dendritic cells: insights from the meta-analysis of microarray data from multiple mouse cell populations. *Immunology,* **133,** 482-498.

Mabbott, N. A., Mackay, F., Minns, F. and Bruce, M. E. (2000). Temporary inactivation of follicular dendritic cells delays neuroinvasion of scrapie. *Nat Med,* **6,** 719-720.

Mabbott, N. A., Young, J., McConnell, I. and Bruce, M. E. (2003). Follicular Dendritic Cell Dedifferentiation by Treatment with an Inhibitor of the Lymphotoxin Pathway Dramatically Reduces Scrapie Susceptibility. *J. Virol.,* **77,** 6845-6854.

MacPherson, G., Kushnir, N. and Wykes, M. (1999). Dendritic cells, B cells and the regulation of antibody synthesis. *Immunological Reviews,* **172,** 325-334.

Maletto, B. A., Ropolo, A. S., Alignani, D. O., Liscovsky, M. V., Ranocchia, R. P., Moron, V. G. and Pistoresi-Palencia, M. C. (2006). Presence of neutrophil-bearing antigen in lymphoid organs of immune mice. *Blood,* **108,** 3094-3102.

Manson, J. C., Clarke, A. R., Hooper, M. L., Aitchison, L., McConnell, I. and Hope, J. (1994). 129/Ola mice carrying a null mutation in PrP that abolishes mRNA production are developmentally normal. *Molecular neurobiology,* **8,** 121-127.

Martins, V. R., Beraldo, F. H., Hajj, G. N., Lopes, M. H., Lee, K. S., Prado, M. M. and Linden, R. (2010). Prion protein:orchestrating neurotrophic activities. *Current Issues in Molecular Biology,* **12,** 63-86.

Mathiason, C. K., Powers, J. G., Dahmes, S. J., Osborn, D. A., Miller, K. V., Warren, R. J., Mason, G. L., Hays, S. A., Hayes-Klug, J., Seelig, D. M., Wild, M. A., Wolfe, L. L., Spraker, T. R., Miller, M. W., Sigurdson, C. J., Telling, G. C. and Hoover, E. A. (2006). Infectious Prions in the Saliva and Blood of Deer with Chronic Wasting Disease. *Science,* **314,** 133-136.

Mattei, V., Garofalo, T., Misasi, R., Circella, A., Manganelli, V., Lucania, G., Pavan, A. and Sorice, M. (2004). Prion protein is a component of the multimolecular signaling complex involved in T cell activation. *FEBS Letters,* **560,** 14-18.

McCulloch, L., Brown, K. L., Bradford, B. M., Hopkins, J., Bailey, M., Rajewsky, K., Manson, J. C. and Mabbott, N. A. (2011). Follicular Dendritic Cell-Specific Prion Protein (PrP^{c}) Expression Alone Is Sufficient to Sustain Prion Infection in the Spleen. *PLoS Pathog,* **7,** e1002402.

McCutcheon, S., Alejo Blanco, A. R., Houston, E. F., de Wolf, C., Tan, B. C., Smith, A., Groschup, M. H., Hunter, N., Hornsey, V. S., MacGregor, I. R., Prowse, C. V., Turner, M. and Manson, J. C. (2011). All Clinically-Relevant Blood Components Transmit Prion Disease following a Single Blood Transfusion: A Sheep Model of vCJD. *PLoS ONE,* **6,** e23169.

McGovern, G., Brown, K. L., Bruce, M. E. and Jeffrey, M. (2004). Murine Scrapie Infection Causes an Abnormal Germinal Centre Reaction in the Spleen. *Journal of Comparative Pathology,* **130,** 181-194.

McGovern, G., Mabbott, N. and Jeffrey, M. (2009). Scrapie Affects the Maturation Cycle and Immune Complex Trapping by Follicular Dendritic Cells in Mice. *PLoS ONE,* **4,** e8186.
McGowan, J. P. (1922). Scrapie in Sheep. *The Scottish Journal of Agriculture,* **5,** 365-375.
McKinley, M. P., Bolton, D. C. and Prusiner, S. B. (1983). A protease-resistant protein is a structural component of the Scrapie prion. *Cell,* **35,** 57-62.
Merad, M., Ginhoux, F. and Collin, M. (2008). Origin, homeostasis and function of Langerhans cells and other langerin-expressing dendritic cells. *Nat Rev Immunol,* **8,** 935-947.
Merad, M., Manz, M. G., Karsunky, H., Wagers, A., Peters, W., Charo, I., Weissman, I. L., Cyster, J. G. and Engleman, E. G. (2002). Langerhans cells renew in the skin throughout life under steady-state conditions. *Nature Immunology,* **3,** 1135-1141.
Merz, P. A., Somerville, R. A., Wisniewski, H. M. and Iqbal, K. (1981). Abnormal fibrils from scrapie-infected brain. *Acta Neuropathologica,* **54,** 63-74.
Mitamura, T., Higashiyama, S., Taniguchi, N., Klagsbrun, M. and Mekada, E. (1995). Diphtheria Toxin Binds to the Epidermal Growth Factor (EGF)-like Domain of Human Heparin-binding EGF-like Growth Factor/Diphtheria Toxin Receptor and Inhibits Specifically Its Mitogenic Activity. *Journal of Biological Chemistry,* **270,** 1015-1019.
Mohan, J., Brown, K. L., Farquhar, C. F., Bruce, M. E. and Mabbott, N. A. (2004). Scrapie transmission following exposure through the skin is dependent on follicular dendritic cells in lymphoid tissues. *Journal of Dermatological Science,* **35,** 101-111.
Mohan, J., Bruce, M. E. and Mabbott, N. A. (2005a). Follicular dendritic cell dedifferentiation reduces scrapie susceptibility following inoculation via the skin. *Immunology,* **114,** 225-234.
Mohan, J., Bruce, M. E. and Mabbott, N. A. (2005b). Neuroinvasion by Scrapie following Inoculation via the Skin Is Independent of Migratory Langerhans Cells. *Journal of Virology,* **79,** 1888-1897.
Mohan, J., Hopkins, J. and Mabbott, N. A. (2005c). Skin-derived dendritic cells acquire and degrade the scrapie agent following in vitro exposure. *Immunology,* **116,** 122-133.
Montrasio, F., Frigg, R., Glatzel, M., Klein, M. A., Mackay, F., Aguzzi, A. and Weissmann, C. (2000). Impaired Prion Replication in Spleens of Mice Lacking Functional Follicular Dendritic Cells. *Science,* **288,** 1257-1259.
Moore, R. C., Hope, J., McBride, P. A., McConnell, I., Selfridge, J., Melton, D. W. and Manson, J. C. (1998). Mice with gene targetted prion protein alterations show that Prnp, Sinc and Prni are congruent. *Nature Genetics,* **18,** 118-125.
Morris, R. E. and Saelinger, C. B. (1983). Diphtheria toxin does not enter resistant cells by receptor-mediated endocytosis. *Infection and Immunity,* **42,** 812-817.
Murayama, Y., Yoshioka, M., Okada, H., Takata, M., Yokoyama, T. and Mohri, S. (2007). Urinary excretion and blood level of prions in scrapie-infected hamsters. *Journal of General Virology,* **88,** 2890-2898.
Nagao, K., Ginhoux, F., Leitner, W. W., Motegi, S.-I., Bennett, C. L., Clausen, B. r. E., Merad, M. and Udey, M. C. (2009). Murine epidermal Langerhans cells and langerin-expressing dermal dendritic cells are unrelated and exhibit distinct functions. *Proceedings of the National Academy of Sciences,* **106,** 3312-3317.
Notari, S., Moleres, F. J., Hunter, S. B., Belay, E. D., Schonberger, L. B., Cali, I., Parchi, P., Shieh, W.-J., Brown, P., Zaki, S., Zou, W.-Q. and Gambetti, P. (2010). Multiorgan Detection and Characterization of Protease-Resistant Prion Protein in a Case of Variant CJD Examined in the United States. *PLoS ONE,* **5,** e8765.
O'Rourke, K. I., Huff, T. P., Leathers, C. W., Robinson, M. M. and Gorham, J. R. (1994). SCID mouse spleen does not support scrapie agent replication. *Journal of General Virology,* **75,** 1511-1514.
Oetke, C., Vinson, M. C., Jones, C. and Crocker, P. R. (2006). Sialoadhesin-Deficient Mice Exhibit Subtle Changes in B- and T-Cell Populations and Reduced Immunoglobulin M Levels. *Molecular and Cellular Biology,* **26,** 1549-1557.
Palucka, A. K. (2000). Dengue virus and dendritic cells. *Nat Med,* **6,** 748-749.
Pan, K. M., Baldwin, M., Nguyen, J., Gasset, M., Serban, A., Groth, D., Mehlhorn, I., Huang, Z., Fletterick, R. J. and Cohen, F. E. (1993). Conversion of alpha-helices into beta-sheets features in the formation of the scrapie prion proteins. *Proceedings of the National Academy of Sciences,* **90,** 10962-10966.
Pappenheimer, A. M. J. (1977). Diphtheria toxin. *Annual reviews of biochemistry,* **46,** 69-94.

Pattison, I. H., Gordon, W. S. and Millson, G. C. (1959). Experimental production of scrapie in goats. *Journal of Comparative Pathology,* **69,** 300-312.

Pattison, I. H. and Millson, G. C. (1961). Scrapie Produced Experimentally in Goats with Special Reference to the Clinical Syndrome. *Journal of Comparative Pathology,* **71,** 101-108.

Peden, A. H., Head, M. W., Diane, L. R., Jeanne, E. B. and James, W. I. (2004). Preclinical vCJD after blood transfusion in a PRNP codon 129 heterozygous patient. *The Lancet,* **364,** 527-529.

Perry, H. V., Cunningham, C. and Boche, D. (2002). Atypical inflammation in the central nervous system in prion disease. *Current Opinion in Neurology,* **15,** 349-354.

Perry, V. H., Cunningham, C. and Holmes, C. (2007). Systemic infections and inflammation affect chronic neurodegeneration. *Nat Rev Immunol,* **7,** 161-167.

Pesce, J. T., Liu, Z., Hamed, H., Alem, F., Whitmire, J., Lin, H., Liu, Q., Urban, J. F. and Gause, W. C. (2008). Neutrophils Clear Bacteria Associated with Parasitic Nematodes Augmenting the Development of an Effective Th2-Type Response. *The Journal of Immunology,* **180,** 464-474.

Peters, N. C., Egen, J. G., Secundino, N., Debrabant, A., Kimblin, N., Kamhawi, S., Lawyer, P., Fay, M. P., Germain, R. N. and Sacks, D. (2008). In Vivo Imaging Reveals an Essential Role for Neutrophils in Leishmaniasis Transmitted by Sand Flies. *Science,* **321,** 970-974.

Phan, T. G., Green, J. A., Gray, E. E., Xu, Y. and Cyster, J. G. (2009). Immune complex relay by subcapsular sinus macrophages and noncognate B cells drives antibody affinity maturation. *Nat Immunol,* **10,** 786-793.

Phan, T. G., Grigorova, I., Okada, T. and Cyster, J. G. (2007). Subcapsular encounter and complement-dependent transport of immune complexes by lymph node B cells. *Nat Immunol,* **8,** 992-1000.

Poulin, L. F., Henri, S., de Bovis, B., Devilard, E., Kissenpfennig, A. and Malissen, B. (2007). The dermis contains langerin^{+} dendritic cells that develop and function independently of epidermal Langerhans cells. *The Journal of Experimental Medicine,* **204,** 3119-3131.

Prinz, M., Huber, G., Macpherson, A. J. S., Heppner, F. L., Glatzel, M., Eugster, H.-P., Wagner, N. and Aguzzi, A. (2003). Oral Prion Infection Requires Normal Numbers of Peyer's Patches but Not of Enteric Lymphocytes. *The American journal of pathology,* **162,** 1103-1111.

Probst, H. C., Tschannen, K., Odermatt, B., Schwendener, R., Zinkernagel, R. M. and Van Den Broek, M. (2005). Histological analysis of CD11c-DTR/GFP mice after in vivo depletion of dendritic cells. *Clinical & Experimental Immunology,* **141,** 398-404.

Prusiner, S. B. (1982). Novel proteinaceous infectious particles cause scrapie. *Science,* **216,** 136-144.

Race, B., Meade-White, K., Oldstone, M. B. A., Race, R. and Chesebro, B. (2008). Detection of Prion Infectivity in Fat Tissues of Scrapie-Infected Mice. *PLoS Pathog,* **4,** e1000232.

Race, B., Meade-White, K., Race, R. and Chesebro, B. (2009). Prion Infectivity in Fat of Deer with Chronic Wasting Disease. *J. Virol.,* **83,** 9608-9610.

Raymond, C. R., Aucouturier, P. and Mabbott, N. A. (2007). In Vivo Depletion of CD11c^{+} Cells Impairs Scrapie Agent Neuroinvasion from the Intestine. *Journal of Immunology,* **179,** 7758-7766.

Raymond, C. R. and Mabbott, N. A. (2007). Assessing the involvement of migratory dendritic cells in the transfer of the scrapie agent from the immune to peripheral nervous systems. *Journal of Neuroimmunology,* **187,** 114-125.

Rezaie, P. and Al-Sarraj, S. (2007). Vacuolar degeneration affecting brain macrophages/microglia in variant CJD: a report on two cases. *Acta Neuropathologica,* **114,** 651-658.

Rezaie, P. and Lantos, P. L. (2001). Microglia and the pathogenesis of spongiform encephalopathies. *Brain Research Reviews,* **35,** 55-72.

Riesner, D. (2003). Biochemistry and structure of PrPC and PrPSc. *British Medical Bulletin,* **66,** 21-33.

Romani, N., Clausen, B. E. and Stoitzner, P. (2010). Langerhans cells and more: langerin-expressing dendritic cell subsets in the skin. *Immunological Reviews,* **234,** 120-141.

Roozendaal, R., Mempel, T. R., Pitcher, L. A., Gonzalez, S. F., Verschoor, A., Mebius, R. E., von Andrian, U. H. and Carroll, M. C. (2009). Conduits Mediate Transport of Low-Molecular-Weight Antigen to Lymph Node Follicles. *Immunity,* **30,** 264-276.

Ryder, S., Dexter, G., Heasman, L., Warner, R. and Moore, S. J. (2009). Accumulation and dissemination of prion protein in experimental sheep scrapie in the natural host. *BMC Veterinary Research,* **5,** 9.

Saborio, G. P., Permanne, B. and Soto, C. (2001). Sensitive detection of pathological prion protein by cyclic amplification of protein misfolding. *Nature,* **411,** 810-813.

Saito, M., Iwawaki, T., Taya, C., Yonekawa, H., Noda, M., Inui, Y., Mekada, E., Kimata, Y., Tsuru, A. and Kohno, K. (2001). Diphteria toxin receptor-mediated conditional and targeted cell ablation in transgenic mice. *Nature Biotechnology,* **19,** 746-750.

Sallusto, F., Cella, M., Danieli, C. and A, L. (1995). Dendritic cells use macropinocytosis and the mannose receptor to concentrate macromolecules in the major histocompatibility complex class II compartment: downregulation by cytokines and bacterial products. *The Journal of Experimental Medicine,* **182,** 283-288.

Sassa, Y., Inoshima, Y. and Ishiguro, N. (2010a). Bovine macrophage degradation of scrapie and BSE PrPSc. *Veterinary Immunology and Immunopathology,* **133,** 33-39.

Sassa, Y., Yamasaki, T., Horiuchi, M., Inoshima, Y. and Ishiguro, N. (2010b). The effects of lysosomal and proteasomal inhibitors on abnormal forms of prion protein degradation in murine macrophages. *Microbiology and immunology,* **54,** 763-768.

Saunders, S. E., Bartelt-Hunt, S. L. and Bartz, J. C. (2008). Prions in the environment: Occurrence, fate and mitigation. *Prion,* **2,** 162-169.

Schreuder, B. E., van Keulen, L. J., Vromans, M. E., Langeveld, J. P. and Smits, M. A. (1998). Tonsillar biopsy and PrP^{Sc} detection in the preclinical diagnosis of scrapie. *Veterinary Record,* **142,** 564-568.

Schröder, J. M., Reich, K., Kabashima, K., Liu, F., Romani, N., Metz, M., Kerstan, A., Lee, P. H. A., Loser, K., Schön, M. P., Maurer, M., Stoitzner, P., Beissert, S., Tokura, Y. and Gallo, R. L. (2006). Who is really in control of skin immunity under *phsyiological* circumstances – lymphocytes, dendritic cells or keratinocytes? *Experimental Dermatology,* **15,** 913-929.

Seeger, H., Heikenwalder, M., Zeller, N., Kranich, J., Schwarz, P., Gaspert, A., Seifert, B., Miele, G. and Aguzzi, A. (2005). Coincident Scrapie Infection and Nephritis Lead to Urinary Prion Excretion. *Science,* **310,** 324-326.

Sethi, S., Kerksiek, K. M., Brocker, T. and Kretzschmar, H. (2007). Role of the $CD8^{+}$ Dendritic Cell Subset in Transmission of Prions. *Journal of Virology,* **81,** 4877-4880.

Shklovskaya, E., Roediger, B. and Fazekas de St. Groth, B. (2008). Epidermal and Dermal Dendritic Cells Display Differential Activation and Migratory Behavior While Sharing the Ability to Stimulate CD4+ T Cell Proliferation In Vivo. *J Immunol,* **181,** 418-430.

Shyng, S.-L., Moulder, K. L., Lesko, A. and Harris, D. A. (1995). The N-terminal Domain of a Glycolipid-anchored Prion Protein Is Essential for Its Endocytosis via Clathrin-coated Pits. *Journal of Biological Chemistry,* **270,** 14793-14800.

Sigurdson, C. J. and Miller, M. W. (2003). Other animal prion diseases. *British Medical Bulletin,* **66,** 199-212.

Sigurdson, C. J., Williams, E. S., Miller, M. W., Spraker, T. R., O'Rourke, K. I. and Hoover, E. A. (1999). Oral transmission and early lymphoid tropism of chronic wasting disease PrP^{res} in mule deer fawns (Odocoileus hemionus). *Journal of General Virology,* **80,** 2757-2764.

Somerville, R. A., Birkett, C. R., Farquhar, C. F., Hunter, N., Goldmann, W., Dornan, J., Grover, D., Hennion, R. M., Percy, C., Foster, J. and Jeffrey, M. (1997). Immunodetection of PrP^{Sc} in spleens of some scrapie-infected sheep but not BSE-infected cows. *The Journal of General Virology,* **78,** 2389-2396.

Soto, C., Saborio, G. P. and Anderes, L. (2002). Cyclic amplification of protein misfolding: application to prion-related disorders and beyond. *Trends in Neurosciences,* **25,** 390-394.

Spraker, T. R., Balachandran, A., Zhuang, D. and O'Rourke, K. I. (2004). Variable patterns of distribution of $PrP^{(CWD)}$ in the obex and cranial lymphoid tissues of Rocky Mountain elk (Cervus elaphus nelsoni) with subclinical chronic wasting disease. *Veterinary Record,* **155,** 295-302.

Spraker, T. R., VerCauteren, K. C., Gidlewski, T., Schneider, D. A., Munger, R., Balachandran, A. and O'Rourke, K. I. (2009). Antemortem Detection of PrP^{CWD} in Preclinical, Ranch-Raised Rocky Mountain Elk (Cevvus Elaphus Nelsoni) by Biopsy of the Rectal Mucosa. *Journal of Veterinary Diagnostic Investigation,* **21,** 15-24.

Stahl, N., Borchelt, D. R., Hsiao, K. and Prusiner, S. B. (1987). Scrapie prion protein contains a phosphatidylinositol glycolipid. *Cell,* **51,** 229-240.

Steinman, R. M. (1991). The Dendritic Cell System and its Role in Immunogenicity. *Annual Review of Immunology,* **9,** 271-296.

Sugaya, M., Nakamura, K., Watanabe, T., Asahina, A., Yasaka, N., Koyama, Y.-i., Kusubata, M., Ushiki, Y., Kimura, K., Morooka, A., Irie, S., Yokoyama, T., Inoue, K., Itohara, S. and Tamaki, K. (2002). Expression of cellular prion-related protein by murine Langerhans cells and keratinocytes. *Journal of Dermatological Science,* **28,** 126-134.

Swartzendruber, D. C. and Congdon, C. C. (1963). Electron microscope observations on tingible body macrophages in mouse spleen. *The Journal of Cell Biology,* **19,** 641-646.

Takahara, K., Omatsu, Y., Yashima, Y., Maeda, Y., Tanaka, S., Iyoda, T., Clusen, B., Matsubara, K., Letterio, J., Steinman, R. M., Matsuda, Y. and Inaba, K. (2002). Identification and expression of mouse Langerin (CD207) in dendritic cells. *International Immunology,* **14,** 433-444.

Takakura, I., Miyazawa, K., Kanaya, T., Itani, W., Watanabe, K., Ohwada, S., Watanabe, H., Hondo, T., Rose, M. T., Mori, T., Sakaguchi, S., Nishida, N., Katamine, S., Yamaguchi, T. and Aso, H. (2011). Orally Administered Prion Protein Is Incorporated by M Cells and Spreads into Lymphoid Tissues with Macrophages in Prion Protein Knockout Mice. *The American journal of pathology,* **179,** 1301-1309.

Tateno, H., Ohnishi, K., Yabe, R., Hayatsu, N., Sato, T., Takeya, M., Narimatsu, H. and Hirabayashi, J. (2010). Dual Specificity of Langerin to Sulfated and Mannosylated Glycans via a Single C-type Carbohydrate Recognition Domain. *Journal of Biological Chemistry,* **285,** 6390-6400.

Taylor, D. M. (1993). Bovine spongiform encephalopathy and its association with the feeding of ruminant-derived protein. *Developments in Biological Standardization,* **80,** 215-224.

Taylor, D. M., McConnell, I. and Fraser, H. (1996). Scrapie infection can be established readily through skin scarification in immunocompetent but not immunodeficient mice. *The Journal of General Virology,* **77,** 1595-1599.

Taylor, D. M. and Woodgate, S. L. (1997). Bovine spongiform encephalopathy: the causal role of ruminant-derived protein in cattle diets. *Revue scientifique et technique,* **16,** 187-198.

Terry, L. A., Marsh, S., Ryder, S. J., Hawkins, S. A. C., Wells, G. A. H. and Spencer, Y. I. (2003). Detection of disease-specific PrP in the distal ileum of cattle exposed orally to the agent of bovine spongiform encephalopathy. *Veterinary Record,* **152,** 387-392.

Theocharidis, A., van Dongen, S., Enright, A. J. and Freeman, T. C. (2009). Network visualization and analysis of gene expression data using BioLayout Express3D. *Nat. Protocols,* **4,** 1535-1550.

Thomzig, A., Schulz-Schaeffer, W., Wrede, A., Wemheuer, W., Brenig, B., Kratzel, C., Lemmer, K. and Beekes, M. (2007). Accumulation of Pathological Prion Protein PrP^{Sc} in the Skin of Animals with Experimental and Natural Scrapie. *PLoS Pathogens,* **3,** e66.

Valladeau, J., Clair-Moninot, V., Dezutter-Dambuyant, C., Pin, J.-J., Kissenpfennig, A., Mattei, M.-G., Ait-Yahia, S., Bates, E. E. M., Malissen, B., Koch, F., Fossiez, F., Romani, N., Lebecque, S. and Saeland, S. (2002). Identification of Mouse Langerin/CD207 in Langerhans Cells and Some Dendritic Cells of Lymphoid Tissues. *Journal of Immunology,* **168,** 782-792.

Valladeau, J., Duvert-Frances, V., Pin, J.-J., Dezutter-Dambuyant, C., Vincent, C., Massacrier, C., Vincent, J., Yoneda, K., Banchereau, J., Caux, C., Davoust, J. and Saeland, S. (1999). The monoclonal antibody DCGM4 recognizes Langerin, a protein specific of Langerhans cells, and is rapidly internalized from the cell surface. *European Journal of Immunology,* **29,** 2695-2704.

Valladeau, J., Ravel, O., Dezutter-Dambuyant, C., Moore, K., Kleijmeer, M., Liu, Y., Duvert-Frances, V., Vincent, C., Schmitt, D., Davoust, J., Caux, C., Lebecque, S. and Saeland, S. (2000). Langerin, a Novel C-Type Lectin Specific to Langerhans Cells, Is an Endocytic Receptor that Induces the Formation of Birbeck Granules. *Immunity,* **12,** 71-81.

van den Berg, T. K., Yoshida, K. and Dijkstra, C. D. (1995). Mechanisms of immune complex trapping by follicular dendritic cells. *Current Topics in Microbiology and Immunology,* **201,** 49-67.

van den Berghe, L. and Chardome, M. (1951). An easier and more accurate diagnosis of malaria and filariasis through the use of the skin scarification smear. *American Journal of Tropical Medicine and Hygiene,* **31,** 411-413.

Waite, J. C., Leiner, I., Lauer, P., Rae, C. S., Barbet, G., Zheng, H., Portnoy, D. A., Pamer, E. G. and Dustin, M. L. (2011). Dynamic Imaging of the Effector Immune Response to *Listeria* Infection *In Vivo*. *PLoS Pathog,* **7,** e1001326.

Walz, R., Amaral, O. B., Rockenbach, I. C., Roesler, R., Izquierdo, I., Cavalheiro, E. A., Martins, V. R. and Brentani, R. R. (1999). Increased sensitivity to seizures in mice lacking cellular prion protein. *Epilepsia,* **40,** 1679-1682.

Wells, G. A., Dawson, M., Hawkins, S. A., Green, R. B., Dexter, I., Francis, M. E., Simmons, M. M., Austin, A. R. and Horigan, M. W. (1994). Infectivity in the ileum of cattle challenged orally with bovine spongiform encephalopathy. *Veterinary Record,* **135,** 40-41.

Will, R. G., Ironside, J. W., Zeidler, M., Estibeiro, K., Cousens, S. N., Smith, P. G., Alperovitch, A., Poser, S., Pocchiari, M. and Hofman, A. (1996). A new variant of Creutzfeldt-Jakob disease in the UK. *The Lancet,* **347,** 921-925.

Wolff, K. (1967). The fine structure of the langerhans cell granule. *The Journal of Cell Biology,* **35,** 468-473.

Wroe, S. J., Pal, S., Siddique, D., Hyare, H., Macfarlane, R., Joiner, S., Linehan, J. M., Brandner, S., Wadsworth, J. D. F., Hewitt, P. and Collinge, J. (2006). Clinical presentation and pre-mortem diagnosis of variant Creutzfeldt-Jakob disease associated with blood transfusion: a case report. *The Lancet,* **368,** 2061-2067.

Wu, S.-J. L., Grouard-Vogel, G., Sun, W., Mascola, J. R., Brachtel, E., Putvatana, R., Louder, M. K., Filgueira, L., Marovich, M. A., Wong, H. K., Blauvelt, A., Murphy, G. S., Robb, M. L., Innes, B. L., Birx, D. L., Hayes, C. G. and Schlessinger Frankel, S. (2000). Human skin Langerhans cells are targets of dengue virus infection. *Nature Medicine,* **6,** 816-820.

Wykes, M., Pombo, A., Jenkins, C. and MacPherson, G. G. (1998). Dendritic Cells Interact Directly with Naive B Lymphocytes to Transfer Antigen and Initiate Class Switching in a Primary T-Dependent Response. *The Journal of Immunology,* **161,** 1313-1319.

Zabel, M. D., Heikenwalder, M., Prinz, M., Arrighi, I., Schwarz, P., Kranich, J., von Teichman, A., Haas, K. M., Zeller, N., Tedder, T. F., Weis, J. H. and Aguzzi, A. (2007). Stromal Complement Receptor CD21/35 Facilitates Lymphoid Prion Colonization and Pathogenesis. *The Journal of Immunology,* **179,** 6144-6152.

Zlotnik, I. and Rennie, J. C. (1963). Further observations on the experimental transmission of scrapie from sheep and goats to laboratory mice. *The Journal of Comparative Pathology and Therapeutics,* **73,** 150-162.

APPENDICES

Appendix 1: Publications List

All publications are included at the end of this thesis.

Wathne, G. J., Kissenpfennig, A., Malissen, B., Zurzolo, C. and Mabbott, N. A. (2012). Determining the role of mononuclear phagocytes in prion neuroinvasion from the skin. *Journal of Leukocyte Biology*, **91**.

Wathne, G. J. and Mabbott, N. A. (2012). The diverse roles of mononuclear phagocytes in prion disease pathogenesis. *Prion*, **6,** 0-9.

Appendix 2: CD-ROM of microarray data

CD-ROM attached at back of thesis.